

Drivers of plant nutrient acquisition and allocation strategies and their influence
on plant responses to environmental change

by

Evan A. Perkowski, B.S.

A Dissertation

In

Biological Sciences

Submitted to the Graduate Faculty
of Texas Tech University in
Partial Fulfillment of
the Requirements for
the Degree of

Doctor of Philosophy

Approved

Nicholas G. Smith, Ph.D.
Chair of Committee

Aimée T. Classen, Ph.D.

Natasja van Gestel, Ph.D.

Lindsey C. Slaughter, Ph.D.

Dylan W. Schwilk, Ph.D.

Mark Sheridan, Ph.D.
Dean of the Graduate School

May 2023

Copyright 2023, Evan A. Perkowski

Acknowledgements

This dissertation was made possible by the mentorship, collaboration, and friendship of many people. I am so thankful to be surrounded by such supportive and helpful mentors, peers, and friends that have made navigating through graduate school and finishing this dissertation an enjoyable experience. Specifically, I am thankful for the incredible mentorship of my advisor and committee chair, Dr. Nick Smith, who provided invaluable insight and tools that have helped shape me into the plant ecophysiological I claim to be today. I am also indebted to my committee members, Drs. Aimée Classen, Natasja van Gestel, Dylan Schwilk, and Lindsey Slaughter, for useful feedback, invaluable support, and encouragement as I planned and implemented experiments.

I am also thankful for past and present members of the EcoHealth lab for encouragement, support, and extracurricular activities that made time inside and outside the lab enjoyable and memorable. Particular thanks go to Dr. Lizz Waring, Dr. Xiulin Gao, Helen Scott, and Risa McNellis, Billi Jean Petermann, and the late Dr. Kris Petterson, all of whom were invaluable to helping me navigate my first year. I am especially thankful for the mentorship and friendship of Dr. Lizz Waring, as our weekly coffee chats were instrumental for helping me feel welcome in Lubbock and acclimate to life as a graduate student. I am also grateful for the friendship of Billi Jean Petermann and the late Dr. Kris Petterson for their encouragement and willingness to discuss microbial symbioses over coffee on random Saturday mornings.

Additional thanks go out to Isa Beltran, Snehanjana Chatterjee, Jeff Chi-

eppa, Peter Eludini, Zinny Ezekannagha, Hannah German, Eve Gray, Monika Kelley, Azaj Mahmud, Jorge Ochoa, Brad Posch, Avery Schoenherr, Christine Vanginault, and Jose Villeda for help with experiments or for lending an ear over puzzling results. I am also thankful for collaborators Dr. Christy Goodale and Dave Frey, who provided invaluable insight for the second experimental chapter.

I would like to thank my undergraduate advisor, Dr. Janice Krumm, for continued mentorship and friendship and for insightful advice about navigating graduate school, but most of all for helping me realize my career aspirations and pushing me to pursue this endeavor. Additional thanks go out to my family, particularly my parents, partner, and dog for continued support and distractions outside the lab. The experiments included here would not have been possible without their emotional and monetary support.

This work was made possible from funding by the NSF, USDA, Braun and Gresham, PLLC., and was a contribution to the LEMONTREE (Land Ecosystem Models based On New Theory, obseRvations and ExperimEnts) project. The LEMONTREE project is funded through the generosity of Eric and Wendy Schmidt by recommendation of the Schmidt Futures programme and the Imperial College initiative on Grand Challenges in Ecosystems and the Environment. This work was also funded by graduate student research awards from Texas Tech University and the Botanical Society of America.

I have inevitably missed mentioning folks that were instrumental to the completion of these experiments and contributed to my development as a plant ecophysiological. Please know that I am grateful and appreciative of our interactions.

Table of Contents

Acknowledgements	ii
Abstract	ix
List of Tables	xi
List of Figures	xv
1. Introduction	1
2. Structural carbon costs to acquire nitrogen are determined by nitrogen and light availability in two species with different nitrogen acquisition strategies	7
2.1 Introduction	7
2.2 Methods	11
2.2.1 <i>Experiment setup</i>	11
2.2.2 <i>Plant measurements and calculations</i>	12
2.2.3 <i>Statistical analyses</i>	13
2.3 Results	15
2.3.1 <i>Carbon costs to acquire nitrogen</i>	15
2.3.2 <i>Whole plant nitrogen biomass</i>	18
2.3.3 <i>Root carbon biomass</i>	20
2.3.4 <i>Root nodule biomass</i>	22
2.4 Discussion	26
2.4.1 <i>Carbon costs to acquire nitrogen increase with light availability and decrease with fertilization</i>	26
2.4.2 <i>Modeling implications</i>	28
2.4.3 <i>Study limitations</i>	30
2.4.4 <i>Conclusions</i>	32
3. Soil nitrogen availability modifies leaf nitrogen economies in mature temperate deciduous forests: a direct test of photosynthetic least-cost theory	34
3.1 Introduction	34

3.2	Methods	38
3.2.1	<i>Study site description</i>	38
3.2.2	<i>Experimental design</i>	39
3.2.3	<i>Leaf gas exchange and trait measurements</i>	39
3.2.4	A_{net}/C_i curve-fitting and parameter estimation	42
3.2.5	<i>Proportion of leaf nitrogen allocated to photosynthesis and structure</i>	44
3.2.6	<i>Tradeoffs between nitrogen and water use</i>	45
3.2.7	<i>Soil nitrogen availability and pH</i>	46
3.2.8	<i>Statistical analyses</i>	48
3.3	Results	50
3.3.1	<i>Leaf nitrogen content</i>	50
3.3.2	<i>Net photosynthesis and leaf biochemistry</i>	53
3.3.3	<i>Leaf nitrogen allocation</i>	56
3.3.4	<i>Tradeoffs between nitrogen and water use</i>	59
3.4	Discussion	62
3.4.1	<i>Soil nitrogen availability modifies tradeoffs between nitrogen and water use</i>	63
3.4.2	<i>Soil pH did not modify tradeoffs between nitrogen and water usage</i>	65
3.4.3	<i>Species identity explains a large amount of variation in leaf and whole plant traits</i>	66
3.4.4	<i>Implications for photosynthetic least-cost theory model development</i>	67
3.4.5	<i>Conclusions</i>	69
4.	The relative cost of resource use for photosynthesis drives variance in leaf nitrogen content across a climate and soil resource availability gradient	70
4.1	Introduction	70
4.2	Methods	76
4.2.1	<i>Site descriptions and sampling methodology</i>	76

4.2.2 <i>Leaf trait measurements</i>	77
4.2.3 <i>Site climate data</i>	82
4.2.4 <i>Site edaphic characteristics</i>	82
4.2.5 <i>Plant functional group assignments</i>	84
4.2.6 <i>Data analysis</i>	85
4.3 Results	88
4.3.1 <i>Cost to acquire nitrogen relative to water</i>	88
4.3.2 <i>Leaf $C_i:C_a$</i>	91
4.3.3 <i>Leaf nitrogen content</i>	94
4.3.4 <i>Structural equation model</i>	98
4.4 Discussion	101
4.4.1 <i>Negative effects of leaf $C_i:C_a$ on N_{area} are driven by reductions in M_{area}, not N_{mass}</i>	101
4.4.2 <i>Soil nitrogen availability increases N_{area} through changes in β</i>	103
4.4.3 <i>Soil moisture increases N_{area} by facilitating increases in soil nitrogen availability</i>	104
4.4.4 <i>Indirect effects of climate on N_{area} are mediated through changes in leaf $C_i:C_a$ and β</i>	105
4.4.5 <i>Species identity traits modify effects of the environment on β, leaf $C_i:C_a$, and N_{area}</i>	106
4.4.6 <i>Next steps for optimality model development</i>	107
4.4.7 <i>Conclusions</i>	108
5. Optimal resource investment to photosynthetic capacity maximizes nutrient allocation to whole plant growth under elevated CO₂	110
5.1 Introduction	110
5.2 Methods	115
5.2.1 <i>Seed treatments and experimental design</i>	115
5.2.2 <i>Growth chamber conditions</i>	116
5.2.3 <i>Leaf gas exchange measurements</i>	118

5.2.4 <i>Leaf trait measurements</i>	119
5.2.5 <i>A/C_i curve fitting and parameter estimation</i>	121
5.2.6 <i>Stomatal limitation</i>	122
5.2.7 <i>Proportion of leaf nitrogen allocated to photosynthesis and structure</i>	122
5.2.8 <i>Whole plant traits</i>	124
5.2.9 <i>Statistical analyses</i>	126
5.3 Results	128
5.3.1 <i>Leaf nitrogen and chlorophyll content</i>	128
5.3.2 <i>Leaf biochemistry and stomatal conductance</i>	132
5.3.3 <i>Leaf nitrogen allocation</i>	136
5.3.4 <i>Whole plant traits</i>	140
5.3.5 <i>Nitrogen fixation</i>	144
5.4 Discussion	148
5.4.1 <i>Soil nitrogen fertilization has divergent effects on leaf and whole plant acclimation responses to CO₂</i>	149
5.4.2 <i>Implications for future model development</i>	152
5.4.3 <i>Study limitations and future directions</i>	154
5.4.4 <i>Conclusions</i>	155
6. Conclusions	157
References	167
Appendix A: Supplemental material for "Structural carbon costs to acquire nitrogen are determined by nitrogen and light availability in two species with different nitrogen acquisition strategies"	204
Appendix B: Supplemental material for "Soil nitrogen availability modifies leaf nitrogen economies in mature temperate deciduous forests: a direct test of photosynthetic least-cost theory"	208

Appendix C: Supplemental material for "The relative cost of resource use for photosynthesis drives variance in leaf nitrogen content across a climate and soil resource availability gradient"	213
Appendix D: Supplemental material for "Optimal resource investment to photosynthetic capacity maximizes nutrient allocation to whole plant growth under elevated CO₂" . .	219

Abstract

Photosynthesis is the largest carbon flux between the atmosphere and is constrained by ecosystem carbon and nutrient cycle dynamics, which causes terrestrial biosphere models to be sensitive to the formulation of photosynthetic processes. Terrestrial biosphere models exhibit high divergence in simulated carbon and nitrogen fluxes under future environmental conditions, which may be due to uncertainty in the acclimation response of photosynthetic processes to environmental change. Photosynthetic least-cost theory provides a promising framework for understanding effects of climatic and edaphic factors on photosynthetic acclimation responses to changing environments. Yet, empirical tests of the theory are rare, limiting our ability to assess whether the theory is suitable for implementation in next-generation terrestrial biosphere models.

Here, I present four experiments designed to test assumptions of photosynthetic least-cost theory. Experiment chapters are flanked by a general introduction chapter and conclusions chapter. The first experimental chapter quantifies structural carbon costs to acquire nitrogen in *Glycine max* and *Gossypium hirsutum* grown under four nitrogen fertilization levels and four light availability levels in a full factorial greenhouse experiment. I find that carbon costs to acquire nitrogen in both species increase with increasing light availability and decrease with increasing fertilization, though responses to fertilization in *G. max* were markedly less than *G. hirsutum*. The second experimental chapter quantifies leaf nitrogen and photosynthetic traits in upper canopy leaves of deciduous trees growing in a 9-year nitrogen-by-sulfur field manipulation experiment. I find strong evi-

dence for nitrogen-water use tradeoffs with increasing soil nitrogen availability, evidenced through a strong negative relationship between leaf nitrogen content and leaf $C_i:C_a$ and stronger increase in leaf nitrogen content with increasing soil nitrogen availability than leaf $C_i:C_a$. The third experiment investigates variance in leaf nitrogen content across a climate and soil resource availability gradient in Texan grasslands, showing that effects of soil resource availability and climate on leaf nitrogen content are driven by changes in leaf $C_i:C_a$. Finally, the fourth experiment quantifies leaf and whole plant acclimation responses in *G. max* grown under two atmospheric CO₂ levels, with and without inoculation with *Bradyrhizobium japonicum*, and across nine nitrogen fertilization treatments in a full factorial growth chamber experiment. I find that leaf acclimation responses to CO₂ were independent of soil nitrogen fertilization or inoculation treatment, though stimulations in whole plant growth under elevated CO₂ were enhanced with increasing soil nitrogen fertilization and in inoculated pots under low nitrogen fertilization.

Experiments included in this dissertation provide consistent support for patterns expected from photosynthetic least-cost theory. The use of multiple experimental approaches allowed me to examine mechanisms driving patterns expected from the theory and investigate whether these patterns occur in the field across environmental gradients. Findings from these chapters challenge common paradigms in plant ecophysiology, providing empirical evidence suggesting that including photosynthetic least-cost frameworks in terrestrial biosphere models may improve the longstanding observed divergence in simulated outcomes across terrestrial biosphere model products.

List of Tables

2.1	Analysis of variance results exploring species-specific effects of light availability, nitrogen fertilization, and their interactions on carbon costs to acquire nitrogen, whole-plant nitrogen biomass, and root carbon biomass	16
2.2	Analysis of variance results exploring effects of light availability, nitrogen fertilization, and their interactions on <i>G. max</i> root nodule biomass and the ratio of root nodule biomass to root biomass	23
2.3	Slopes of the regression line describing the relationship between each dependent variable and nitrogen fertilization at each light level	24
3.1	Effects of soil nitrogen availability, soil pH, and species on leaf nitrogen content per unit leaf area, leaf nitrogen content per unit leaf mass, and leaf mass per unit leaf area	51
3.2	Effects of soil nitrogen availability, soil pH, species, and N_{area} on net photosynthesis, the maximum rate of Rubisco carboxylation, the maximum rate of RuBP regeneration, and the ratio of the maximum rate of RuBP regeneration to the maximum rate of Rubisco carboxylation	54
3.3	Effects of soil nitrogen availability, soil pH, and species on the proportion of leaf nitrogen content allocated to photosynthesis, Rubisco, bioenergetics, and structure	57

3.4 Effects of soil nitrogen availability, soil pH, species, and N_{area} on χ , photosynthetic nitrogen use efficiency, leaf nitrogen content per unit χ , and maximum Rubisco carboxylation rate per unit χ	60
4.1 Site locality information, sampling year, 2006-2020 mean annual precipitation, mean annual temperature, and water holding capacity	80
4.2 Effects of soil moisture, soil nitrogen availability, and plant functional group on β	89
4.3 Effects of soil moisture, soil nitrogen availability, and plant functional group on leaf $C_i:C_a$	92
4.4 Effects of soil moisture, soil nitrogen availability, plant functional group, and leaf $C_i:C_a$ on leaf nitrogen content per unit leaf area, leaf nitrogen content per unit leaf biomass, and leaf biomass per unit leaf area	96
4.5 Structural equation model results investigating direct effects of climatic and soil resource availability on leaf nitrogen content	99
5.1 Effects of soil nitrogen fertilization, inoculation, and CO_2 treatments on leaf nitrogen content per unit leaf area, leaf nitrogen content per unit leaf mass, leaf mass per unit leaf area, and chlorophyll content per unit leaf area	130

5.2	Effects of soil nitrogen fertilization, inoculation, and CO ₂ on the maximum rate of Rubisco carboxylation, the maximum rate of RuBP regeneration, dark respiration, the ratio of the maximum rate of RuBP regeneration to the maximum rate of Rubisco carboxylation, stomatal conductance, and stomatal limitation	134
5.3	Effects of soil nitrogen fertilization, inoculation, and CO ₂ on the fraction of leaf nitrogen allocated to Rubisco, bioenergetics, light harvesting proteins, photosynthesis, and structure	138
5.4	Effects of CO ₂ , fertilization, and inoculation on total leaf area, whole plant biomass, carbon costs to acquire nitrogen, belowground carbon biomass, and whole plant nitrogen biomass	142
5.5	Effects of CO ₂ , fertilization, and inoculation on root nodule biomass, plant investments in symbiotic nitrogen fixation, and percent nitrogen fixed from the atmosphere	146
A1	Summary table containing volumes of compounds used to create modified Hoagland's solutions for each soil nitrogen fertilization treatment	204
A2	Analysis of variance results exploring species-specific effects of light availability, nitrogen fertilization, and their interactions on the ratio of whole plant biomass to pot volume	205
A3	Slopes of the regression line describing the relationship between each dependent variable and nitrogen fertilization at each light level	206

B1	Sample sizes of each species, abbreviated by their USDA NRCS PLANTS database code, within each plot at each site	208
B2	Analysis of variance results exploring the linear effect of leaf temperature on net photosynthesis rate and stomatal conductance measured at 400 $\mu\text{mol mol}^{-1}$ CO ₂	209
B3	Second order log-polynomial regression coefficients that described the effect of leaf temperature on net photosynthesis and stomatal conductance measured at 400 $\mu\text{mol mol}^{-1}$ CO ₂	210
B4	Mean, standard error, and 95% confidence interval ranges of soil nitrogen availability estimates across all measured plots	211
C1	List of sampled species and their plant functional group assignment	215
C2	List of sampled species and their plant functional group assignment (cont.)	216
C3	Model selection results for soil moisture and vapor pressure deficit	217
D1	Summary table containing volumes of compounds used to create modified Hoagland's solutions for each soil nitrogen fertilization treatment	219
D2	Summary of the daily growth chamber growing condition program	220
D3	Effects of CO ₂ , fertilization, and inoculation on whole plant biomass: pot volume	221

List of Figures

2.1 Relationships between soil nitrogen fertilization and light availability on carbon costs to acquire nitrogen in <i>G. hirsutum</i> and <i>G. max</i>	17
2.2 Relationships between soil nitrogen fertilization and light availability on whole-plant nitrogen biomass in <i>G. hirsutum</i> and <i>G. max</i>	19
2.3 Relationships between soil nitrogen fertilization and light availability on root carbon biomass in <i>G. hirsutum</i> and <i>G. max</i>	21
2.4 Effects of shade cover and nitrogen fertilization on root nodule biomass and the ratio of root nodule biomass to root biomass in <i>G. max</i>	25
3.1 Effects of soil nitrogen availability and species on leaf nitrogen content per unit leaf area, leaf nitrogen content per unit leaf biomass, and leaf mass per leaf area	52
3.2 Effects of soil nitrogen availability, species, and leaf nitrogen content on net photosynthesis, maximum Rubisco carboxylation rate, and maximum RuBP regeneration rate	55
3.3 Effects of soil nitrogen availability, species, and leaf nitrogen content on the fraction of leaf nitrogen allocated to photosynthesis and structure	58
3.4 Effects of soil N availability, species, and leaf N content on tradeoffs between nitrogen and water use	61

4.1	Site locations along 2006-2020 mean annual precipitation and mean annual temperature gradients in Texas, USA.	81
4.2	Effects of soil nitrogen availability and soil moisture on the cost of acquiring and using nitrogen	90
4.3	Effects of 4-day mean vapor pressure deficit, 2-day soil moisture (per water holding capacity), and soil nitrogen availability on leaf $C_i:C_a$	93
4.4	Effects of leaf $C_i:C_a$, soil nitrogen availability, and soil moisture on leaf nitrogen content per unit leaf area, leaf nitrogen content per unit leaf biomass, and leaf mass per area.	97
4.5	Structural equation model results exploring drivers of N_{area}	100
5.1	Effects of CO_2 , fertilization, and inoculation on leaf nitrogen per unit leaf area, leaf nitrogen content, leaf mass per unit leaf area, and chlorophyll content per unit leaf area	131
5.2	Effects of CO_2 , fertilization, and inoculation on maximum rate of Rubisco carboxylation, the maximum rate of RuBP regeneration, and the ratio of the maximum rate of RuBP regeneration to the maximum rate of Rubisco carboxylation leaf mass per unit leaf area, dark respiration, stomatal conductance, and stomatal limitation .	135
5.3	Effects of CO_2 , fertilization, and inoculation on the relative fraction of leaf nitrogen allocated to photosynthesis and the fraction of leaf nitrogen allocated to structure	139

5.4	Effects of CO ₂ , fertilization, and inoculation on total leaf area, total biomass, and structural carbon costs to acquire nitrogen	143
5.5	Effects of CO ₂ , fertilization, and inoculation on nodule biomass, nodule biomass: root biomass, and percent nitrogen fixed from the atmosphere	147
A1	Effects of shade cover and nitrogen fertilization on the ratio of plant biomass to rooting volume in <i>G. hirsutum</i> and <i>G. max</i>	207
B1	Effects of leaf temperature on net photosynthesis rate and stomatal conductance values when measured at 400 μmol mol ⁻¹ CO ₂ . . .	212
C1	Model selection results exploring relevant timescales for soil moisture and vapor pressure deficit	218
D1	Relationships between area-based leaf nitrogen content, mass-based leaf nitrogen content, and leaf mass per unit leaf area measured on the focal leaf used to generate A_{net}/C_i curves and leaf nitrogen content measured on the leaf used for chlorophyll extractions . . .	222
D2	Effects of CO ₂ , fertilization, and inoculation on the ratio of whole plant biomass to pot volume	223

1 Chapter 1

2 Introduction

3 Photosynthesis represents the largest carbon flux between the atmosphere
4 and biosphere, and is regulated by complex ecosystem carbon and nutrient cy-
5 cles (Hungate et al. 2003; IPCC 2021). As a result, the inclusion of robust,
6 empirically tested representations of photosynthetic processes is critical in order
7 for terrestrial biosphere models to accurately and reliably simulate carbon and
8 nutrient fluxes between the atmosphere and terrestrial biosphere (Oreskes et al.
9 1994; Smith and Dukes 2013; Prentice et al. 2015; Wieder et al. 2015). Despite
10 evidence that the inclusion of coupled carbon and nutrient cycles can improve
11 model uncertainty, widespread divergence in predicted carbon and nutrient fluxes
12 is still apparent across model products (Friedlingstein et al. 2014; Arora et al.
13 2020; Davies-Barnard et al. 2020). Divergence in predicted carbon and nutrient
14 fluxes across terrestrial biosphere models may be due to an incomplete under-
15 standing of how plants acclimate to changing environments (Smith and Dukes
16 2013; Davies-Barnard et al. 2020), as terrestrial biosphere models are sensitive to
17 the formulation of photosynthetic processes (Bonan et al. 2011; Ziehn et al. 2011;
18 Booth et al. 2012; Smith et al. 2016; Smith et al. 2017; Rogers et al. 2017).

Many terrestrial biosphere models predict leaf-level photosynthesis through linear relationships between area-based leaf nitrogen content and the maximum rate of Ribulose-1,5-bisphosphate carboxylase/oxygenase (“Rubisco”), following the idea that large fractions of leaf nitrogen content are allocated to the construction and maintenance of Rubisco and other photosynthetic enzymes (Evans

24 1989). The inclusion of coupled carbon and nutrient cycles in terrestrial bio-
25 sphere models (Shi et al. 2016; Braghieri et al. 2022) allows for the prediction
26 of leaf nitrogen content through soil nitrogen availability, which causes models to
27 indirectly predict photosynthetic processes through shifts in soil nitrogen avail-
28 ability (Smith et al. 2014; Lawrence et al. 2019). While these patterns are
29 commonly observed in ecosystems globally (Brix 1971; Evans 1989; Firn et al.
30 2019; Liang et al. 2020), this formulation does not allow for the prediction of
31 leaf and whole plant acclimation responses to changing environments (Smith and
32 Dukes 2013; Rogers et al. 2017; Harrison et al. 2021), and suggests that constant
33 leaf nitrogen-photosynthesis relationships are ubiquitous across ecosystems.

34 Photosynthetic least-cost theory (Prentice et al. 2014; Wang et al. 2017;
35 Smith et al. 2019; Paillassa et al. 2020; Scott and Smith 2022; Harrison et al.
36 2021) provides a contemporary framework for predicting leaf and whole plant ac-
37 climation responses to environmental change. The theory, which unifies optimal
38 coordination (Chen et al. 1993; Maire et al. 2012) and least-cost (Wright et al.
39 2003) theories, posits that plants optimize photosynthetic processes by minimizing
40 the summed cost of nutrient and water use (i.e., β). The summed cost of nutrient
41 and water use is predicted to be positively correlated with the ratio of intercellular
42 CO₂ to atmospheric CO₂ (leaf $C_i:C_a$). Leaf $C_i:C_a$ is determined by factors that
43 influence leaf nutrient demand, such as CO₂, temperature, vapor pressure deficit,
44 and light availability (Prentice et al. 2014; Wang et al. 2017; Smith et al. 2019;
45 Stocker et al. 2020), and may change in response to changing edaphic charac-
46 teristics through changes in β (Paillassa et al. 2020). Photosynthetic processes
47 are optimized such that nutrients and water are allocated to photosynthetic en-

48 zymes to allow net photosynthesis rates to be equally co-limited by the maximum
49 rate of Rubisco carboxylation and the maximum rate of Ribulose-1,5-bisphosphate
50 (RuBP) regeneration (Chen et al. 1993; Maire et al. 2012). The theory indicates
51 that costs of nutrient and water use are substitutable such that, in a given en-
52 vironment, optimal photosynthesis rates can be achieved by sacrificing inefficient
53 use of a relatively more abundant (and less costly to acquire) resource for more
54 efficient use of a relatively less abundant (and more costly to acquire) resource.

55 Optimality models leveraging patterns expected from photosynthetic least-
56 cost theory have been developed for both C₃ (Wang et al. 2017; Smith et al. 2019;
57 Stocker et al. 2020) and more recently for C₄ species (Scott and Smith 2022).
58 Such models show broad agreement with patterns observed across environmental
59 gradients (Smith et al. 2019; Stocker et al. 2020; Paillassa et al. 2020; Querejeta
60 et al. 2022; Westerband et al. 2023), and are capable of reconciling dynamic
61 leaf nitrogen-photosynthesis relationships and acclimation responses to elevated
62 CO₂, temperature, light availability, and vapor pressure deficit (Dong et al. 2017;
63 Dong et al. 2020; Smith and Keenan 2020; Luo et al. 2021; Peng et al. 2021;
64 Dong et al. 2022; Dong et al. 2022; Querejeta et al. 2022; Westerband et al.
65 2023). Current versions of optimality models that invoke patterns expected from
66 photosynthetic least-cost theory hold β constant across growing environments.
67 As growing evidence suggests that costs of nutrient use change across resource
68 availability and climatic gradients in species with different nutrient acquisition
69 strategies (Fisher et al. 2010; Brzostek et al. 2014; Terrer et al. 2018; Allen et al.
70 2020), one might expect that β should dynamically change across environments
71 and in species with different nutrient acquisition strategies.

72 Despite recent recognition that patterns expected from photosynthetic
73 least-cost theory occur across broad environmental gradients, a limited number
74 of studies have investigated how β varies across edaphic and climatic gradients
75 and how variance in β might scale to influence leaf nutrient-water use tradeoffs
76 (Lavergne et al. 2020; Paillassa et al. 2020). Furthermore, no previous study has
77 investigated whether β varies in species with different nutrient acquisition strate-
78 gies, or if changes in β due to changes in edaphic characteristics scale to influence
79 leaf or whole plant acclimation responses to changing environments. The lack of
80 such studies provided motivation for the experimental chapters included in this
81 dissertation.

82 In this dissertation, I use a combination of greenhouse, field manipulation,
83 environmental gradient, and growth chamber experiments to quantify leaf and
84 whole plant acclimation responses across various climatic and edaphic conditions
85 and different nutrient acquisition strategies. Together, these experiments eval-
86 uated patterns expected from photosynthetic least-cost theory and test mechanisms
87 predicted to drive responses expected from theory. The empirical data collected
88 in these experiments provide important information needed to refine existing opti-
89 mality models that include photosynthetic least-cost frameworks, and could help
90 determine whether such models are suitable for implementing in next-generation
91 terrestrial biosphere models. While theory suggests that plants acclimate across
92 environments by minimizing the summed cost of nutrients relative to water, I chose
93 to isolate effects of soil nitrogen availability on costs of nitrogen acquisition rela-
94 tive to water for the sake of brevity. I acknowledge that patterns expected from
95 theory may be modified by other nutrients (e.g., phosphorus) or other edaphic

96 characteristics (Smith et al. 2019; Paillassa et al. 2020; Westerband et al. 2023),
97 and, though not included here, should also be investigated.

98 In the first experimental chapter, I re-analyze data from a greenhouse ex-
99 periment that grew *Glycine max* and *Gossypium hirsutum* seedlings under full-
100 factorial combinations of four light treatments and four fertilization treatments
101 to examine effects of nitrogen and light availability on structural carbon costs to
102 acquire nitrogen. In the second experimental chapter, I measure leaf physiological
103 traits in the upper canopy of mature trees growing in a 9-year nitrogen-by-pH
104 field manipulation experiment to assess whether changes in soil nitrogen availabil-
105 ity or soil pH modify nitrogen-water use trade-offs expected from photosynthetic
106 least-cost theory. The third experimental chapter leverages a broad precipitation
107 and soil nitrogen availability gradient in Texan grasslands to investigate primary
108 drivers of leaf nitrogen content. In the fourth experimental chapter, I use growth
109 chambers to quantify leaf and whole plant acclimation responses to CO₂ across
110 a soil nitrogen fertilization gradient, while also manipulating nutrient acquisition
111 strategy by controlling whether seedlings were able to form associations with sym-
112 biotic nitrogen-fixing bacteria.

113 Across experiments, I find strong and consistent support for patterns ex-
114 pected from photosynthetic least-cost theory, showing that shifts in edaphic char-
115 acteristics predictably alter β , and that shifts in β facilitate changes in leaf
116 nitrogen-water use tradeoffs and leaf nitrogen-photosynthesis relationships. I also
117 show that costs of nitrogen acquisition vary in species with different nitrogen
118 acquisition strategies. Finally, I show strong evidence suggesting that leaf accli-
119 mation responses to elevated CO₂ are decoupled from soil nitrogen availability and

120 inoculation with symbiotic nitrogen-fixing bacteria. It is my hope that these ex-
121 periments will encourage future iterations of optimality models that adopt photo-
122 synthetic least-cost frameworks to consider frameworks for implementing dynamic
123 β values across soil resource availability gradients and in species with different nu-
124 trient acquisition strategies.

125 The four experimental chapters included in this dissertation are presented
126 either as previously published journal articles or as manuscript drafts currently
127 in preparation for journal submission. Specifically, the first experimental chapter
128 was published in *Journal of Experimental Botany* in 2021 and the second chapter
129 is currently in review, while the third and fourth chapters are each in preparation
130 for journal submission. The dissertation concludes with a sixth chapter that sum-
131 marizes experiment findings, briefly synthesizes common themes observed across
132 experiments, and provides some suggestions for future experimentation.

133

Chapter 2

134

Structural carbon costs to acquire nitrogen are determined by
135 nitrogen and light availability in two species with different nitrogen
136 acquisition strategies

137 Perkowski EA, EF Waring, NG Smith, "Root mass carbon costs to acquire nitro-
138 gen are determined by nitrogen and light availability in two species with different
139 nitrogen acquisition strategies", *Journal of Experimental Botany*, 2021, Volume
140 72, Issue 15, Pages 5766-5776, by permission of Oxford University Press

141 2.1 Introduction

142 Carbon and nitrogen cycles are tightly coupled in terrestrial ecosystems. This
143 tight coupling influences photosynthesis (Walker et al. 2014; Rogers et al. 2017),
144 net primary productivity (LeBauer and Treseder 2008; Thomas et al. 2013), de-
145 composition (Cornwell et al. 2008; Bonan et al. 2013; Sulman et al. 2019), and
146 plant resource competition (Gill and Finzi 2016; Xu-Ri and Prentice 2017). Ter-
147 restrial biosphere models are beginning to include connected carbon and nitrogen
148 cycles to improve the realism of their simulations (Fisher et al. 2010; Brzostek
149 et al. 2014; Wieder et al. 2015; Shi et al. 2016; Zhu et al. 2019). Simula-
150 tions from these models indicate that coupling carbon and nitrogen cycles can
151 drastically influence future biosphere-atmosphere feedbacks under global change,
152 such as elevated carbon dioxide or nitrogen deposition (Thornton et al. 2007;
153 Goll et al. 2012; Wieder et al. 2015; Wieder et al. 2019). Nonetheless, there
154 are still limitations in our quantitative understanding of connected carbon and
155 nitrogen dynamics (Thomas et al. 2015; Meyerholt et al. 2016; Rogers et al.
156 2017; Exbrayat et al. 2018; Shi et al. 2019), forcing models to make potentially
157 unreliable assumptions.

158 Plant nitrogen acquisition is a process in terrestrial ecosystems by which
159 carbon and nitrogen are tightly coupled (Vitousek and Howarth 1991; Delaire
160 et al. 2005; Brzostek et al. 2014). Plants must allocate photosynthetically de-
161 rived carbon belowground to produce and maintain root systems or exchange with
162 symbiotic soil microbes in order to acquire nitrogen (Högberg et al. 2008; Hög-
163 berg et al. 2010). Thus, plants have an inherent carbon cost associated with
164 acquiring nitrogen, which can include both direct energetic costs associated with
165 nitrogen acquisition and indirect costs associated with building structures that
166 support nitrogen acquisition (Gutschick 1981; Rastetter et al. 2001; Vitousek
167 et al. 2002; Menge et al. 2008). Model simulations (Fisher et al. 2010; Brzostek
168 et al. 2014; Shi et al. 2016; Allen et al. 2020) and meta-analyses (Terrer et al.
169 2018) suggest that these carbon costs vary between species, particularly those
170 with different nitrogen acquisition strategies. For example, simulations using iter-
171 ations of the Fixation and Uptake of Nitrogen (FUN) model indicate that species
172 that acquire nitrogen from non-symbiotic active uptake pathways (e.g. mass flow)
173 generally have larger carbon costs to acquire nitrogen than species that acquire
174 nitrogen through symbiotic associations with nitrogen-fixing bacteria (Brzostek
175 et al. 2014; Allen et al. 2020).

176 Carbon costs to acquire nitrogen likely vary in response to changes in soil
177 nitrogen availability. For example, if the primary mode of nitrogen acquisition
178 is through non-symbiotic active uptake, then nitrogen availability could decrease
179 carbon costs to acquire nitrogen as a result of increased per-root nitrogen up-
180 take (Franklin et al. 2009; Wang et al. 2018). However, if the primary mode of
181 nitrogen acquisition is through symbiotic active uptake, then nitrogen availabil-

182 ity may incur additional carbon costs to acquire nitrogen if it causes microbial
183 symbionts to shift toward parasitism along the parasitism–mutualism continuum
184 (Johnson et al. 1997; Hoek et al. 2016; Friel and Friesen 2019) or if it reduces
185 the nitrogen acquisition capacity of a microbial symbiont (van Diepen et al. 2007;
186 Soudzilovskaia et al. 2015; Muñoz et al. 2016). Species may respond to shifts in
187 soil nitrogen availability by switching their primary mode of nitrogen acquisition
188 to a strategy with lower carbon costs to acquire nitrogen in order to maximize
189 the magnitude of nitrogen acquired from a belowground carbon investment and
190 outcompete other individuals for soil resources (Rastetter et al. 2001; Menge et al.
191 2008).

192 Environmental conditions that affect demand to acquire nitrogen to sup-
193 port new and existing tissues could also be a source of variance in plant carbon
194 costs to acquire nitrogen. For example, an increase in plant nitrogen demand could
195 increase carbon costs to acquire nitrogen if this increases the carbon that must be
196 allocated belowground to acquire a proportional amount of nitrogen (Kulmatiski
197 et al. 2017; Noyce et al. 2019). This could be driven by a temporary state of
198 diminishing return associated with investing carbon toward building and main-
199 taining structures that are necessary to support enhanced nitrogen uptake, such
200 as fine roots (Matamala and Schlesinger 2000; Norby et al. 2004; Arndal et al.
201 2018), mycorrhizal hyphae (Saleh et al. 2020), or root nodules (Parvin et al.
202 2020). Alternatively, if the environmental factor that increases plant nitrogen de-
203 mand causes nitrogen to become more limiting in the system (e.g. atmospheric
204 CO₂) (Luo et al. 2004; LeBauer and Treseder 2008; Vitousek et al. 2010; Liang
205 et al. 2016), species might switch their primary mode of nitrogen acquisition to

206 a strategy with lower relative carbon costs to acquire nitrogen in order to gain a
207 competitive advantage over species with either different or more limited modes of
208 nitrogen acquisition (Ainsworth and Long 2005; Taylor and Menge 2018).

209 Using a plant economics approach, I examined the influence of plant ni-
210 trogen demand and soil nitrogen availability on plant carbon costs to acquire
211 nitrogen. This was done by growing a species capable of forming associations
212 with nitrogen-fixing bacteria (*Glycine max* L. (Merr)) and a species not capable
213 of forming these associations (*Gossypium hirsutum* L.) under four levels of light
214 availability (plant nitrogen demand proxy) and four levels of soil nitrogen fertil-
215 ization (soil nitrogen availability proxy) in a full-factorial, controlled greenhouse
216 experiment. I used this experimental set-up to test the following hypotheses:

- 217 1. An increase in plant nitrogen demand due to increasing light availability will
218 increase carbon costs to acquire nitrogen through a proportionally larger
219 increase in belowground carbon than whole-plant nitrogen acquisition. This
220 will be the result of an increased investment of carbon toward belowground
221 structures that support enhanced nitrogen uptake, but at a lower nitrogen
222 return.
- 223 2. An increase in soil nitrogen availability will decrease carbon costs to acquire
224 nitrogen as a result of increased per root nitrogen uptake in *G. hirsutum*.
225 However, soil nitrogen availability will not affect carbon costs to acquire
226 nitrogen in *G. max* because of the already high return of nitrogen supplied
227 through nitrogen fixation.

228 2.2 Methods

229 2.2.1 *Experiment setup*

230 *Gossypium hirsutum* and *G. max* were planted in individual 3 liter pots (NS-300; **231** Nursery Supplies, Orange, CA, USA) containing a 3:1 mix of unfertilized potting **232** mix (Sungro Sunshine Mix #2, Agawam, MA, USA) to native soil extracted from **233** an agricultural field most recently planted with *G. max* at the USDA-ARS Lab-**234** oratory in Lubbock, TX, USA (33.59°N, -101.90°W). The field soil was classified **235** as Amarillo fine sandy loam (75% sand, 10% silt, 15% clay). Upon planting, **236** all *G. max* pots were inoculated with *Bradyrhizobium japonicum* (Verdesian N-**237** Dure™ Soybean, Cary, NC, USA) to stimulate root nodulation. Individuals of **238** both species were grown under similar, unshaded, ambient greenhouse conditions **239** for 2 weeks to germinate and begin vegetative growth.

240 Three blocks were set up in the greenhouse, each containing four light **241** treatments created using shade cloth that reduced incoming radiation by either 0 **242** (full sun), 30, 50, or 80%. Two weeks post-germination, individuals were randomly **243** placed in the four light treatments in each block. Individuals received one of four **244** nitrogen fertilization doses as 100mL of a modified Hoagland solution (Hoagland **245** and Arnon 1950) equivalent to either 0, 70, 210, or 630 ppm N twice per week **246** within each light treatment. Nitrogen fertilization doses were received as topical **247** agents to the soil surface. Each Hoagland solution was modified to keep concen-**248** trations of other macro- and micronutrients equivalent (Table A1). Plants were **249** routinely well watered to eliminate water stress.

250 2.2.2 *Plant measurements and calculations*

251 Each individual was harvested after 5 weeks of treatment, and biomass was sepa-
252 rated by organ type (leaves, stems, and roots). Nodules on *G. max* roots were also
253 harvested. Except for the 0% shade cover and 630 ppm N treatment combination,
254 all treatment combinations in both species had lower average dry biomass:pot vol-
255 ume ratios than the 1:1 ratio recommended by Poorter et al. (2012) to minimize
256 the likelihood of pot volume-induced growth limitation (Table A2, A3; Fig. A1).

257 All harvested material was dried, weighed, and ground by organ type.
258 Carbon and nitrogen content (g g^{-1}) was determined by subsampling from ground
259 and homogenized biomass of each organ type using an elemental analyzer (Costech
260 4010; Costech, Inc., Valencia, CA, USA). I scaled these values to total leaf, stem,
261 and root carbon and nitrogen biomass (g) by multiplying dry biomass of each
262 organ type by carbon or nitrogen content of each corresponding organ type. Whole
263 plant nitrogen biomass (g) was calculated as the sum of total leaf (g), stem (g),
264 and root (g) nitrogen biomass. Root nodule carbon biomass was not included in
265 the calculation of root carbon biomass; however, relative plant investment toward
266 root or root nodule standing stock was estimated as the ratio of root biomass to
267 root nodule biomass (g g^{-1}), following similar metrics to those adopted by Dovrat
268 et al. (2018) and Dovrat et al. (2020).

269 Carbon costs to acquire nitrogen (N_{cost} ; gC gN^{-1}) were estimated as the
270 ratio of total root carbon biomass (C_{bg} ; gC) to whole-plant nitrogen biomass
271 (N_{wp} ; gN). This calculation quantifies the relationship between carbon spent on
272 nitrogen acquisition and whole plant nitrogen acquisition by using root carbon
273 biomass as a proxy for estimating the magnitude of carbon allocated toward ni-

274 trogen acquisition. This calculation therefore assumes that the magnitude of root
275 carbon standing stock is proportional to carbon transferred to root nodules or my-
276 corrhizae, or lost through root exudation or turnover. The assumption has been
277 supported in species that associate with ectomycorrhizal fungi (Hobbie 2006; Hob-
278 bie and Hobbie 2008), but is less clear in species that acquire nitrogen through
279 non-symbiotic active uptake or symbiotic nitrogen fixation. It is also unclear
280 whether relationships between root carbon standing stock and carbon transfer to
281 root nodules are similar in magnitude to carbon lost through exudation or when
282 allocated toward other active uptake pathways. Thus, because of the way mea-
283 surements were calculated, proximal values of carbon costs to acquire nitrogen are
284 underestimates.

285 2.2.3 *Statistical analyses*

286 I explored the effects of light and nitrogen availability on carbon costs to acquire
287 nitrogen using separate linear mixed-effects models for each species. Models in-
288 cluded shade cover, nitrogen fertilization, and interactions between shade cover
289 and nitrogen fertilization as continuous fixed effects, and also included block as a
290 random intercept term. Three separate models for each species were built with
291 this independent variable structure for three different dependent variables: (i)
292 carbon costs to acquire nitrogen (gC gN^{-1}); (ii) whole plant nitrogen biomass
293 (denominator of carbon cost to acquire nitrogen; gN); and (iii) belowground car-
294 bon biomass (numerator of carbon cost to acquire nitrogen; gC). I constructed two
295 additional models for *G. max* with the same model structure described above to
296 investigate the effects of light availability and nitrogen fertilization on root nodule

297 biomass (g) and the ratio of root nodule biomass to root biomass (unitless).

298 I used Shapiro–Wilk tests of normality to determine whether species spe-
299 cific linear mixed-effects model residuals followed a normal distribution. Zero
300 models satisfied residual normality assumptions when models were fit using un-
301 transformed data (Shapiro–Wilk: $p < 0.05$ in all cases). I attempted to satisfy
302 residual normality assumptions by first fitting models using dependent variables
303 that were natural-log transformed. If residual normality assumptions were still
304 not met (Shapiro–Wilk: $p > 0.05$), then models were fit using dependent variables
305 that were square root transformed. All residual normality assumptions were satis-
306 fied when models were fit with either a natural-log or square root transformation
307 (Shapiro–Wilk: $p > 0.05$ in all cases). Specifically, I natural-log transformed *G.*
308 *hirsutum* carbon costs to acquire nitrogen and *G. hirsutum* whole-plant nitrogen
309 biomass. I also square root transformed *G. max* carbon costs to acquire nitrogen,
310 *G. max* whole-plant nitrogen biomass, root carbon biomass in both species, *G.*
311 *max* root nodule biomass, and the *G. max* ratio of root nodule biomass to root
312 biomass. I used the ‘lmer’ function in the ‘lme4’ R package (Bates et al. 2015) to
313 fit each model and the ‘Anova’ function in the ‘car’ R package (Fox and Weisberg
314 2019) to calculate Wald’s χ^2 to determine the significance ($\alpha = 0.05$) of each fixed
315 effect coefficient. Finally, I used the ‘emmeans’ R package (Lenth 2019) to conduct
316 post-hoc comparisons of our treatment combinations using Tukey’s tests. Degrees
317 of freedom for all Tukey’s tests were approximated using the Kenward–Roger ap-
318 proach (Kenward and Roger 1997). All analyses and plots were conducted in R
319 version 4.0.1 (R Core Team 2021).

320 2.3 Results

321 2.3.1 *Carbon costs to acquire nitrogen*

322 Carbon costs to acquire nitrogen in *G. hirsutum* increased with increasing light
323 availability ($p<0.001$; Table 2.1; Fig. 2.1) and decreased with increasing nitrogen
324 fertilization ($p<0.001$; Table 2.1; Fig. 2.1). There was no interaction between
325 light availability and nitrogen fertilization ($p=0.486$, Table 2.1; Fig. 2.1).

326 Carbon costs to acquire nitrogen in *G. max* also increased with increasing
327 light availability ($p<0.001$, Table 2.1; Fig. 2.1) and decreased with increasing
328 nitrogen fertilization ($p<0.001$; Table 2.1; Fig. 2.1). There was no interaction
329 between light availability and nitrogen fertilization ($p=0.261$, Table 2.1; Fig. 2.1).

Table 2.1. Analysis of variance results exploring species-specific effects of light availability, nitrogen fertilization, and their interactions on carbon costs to acquire nitrogen (N_{cost} ; gC gN $^{-1}$), whole plant nitrogen biomass (N_{wp} ; gN), and root carbon biomass (C_{bg} ; gC)

	N_{cost}			N_{wp}			C_{bg}			
	df	Coefficient	χ^2	p	Coefficient	χ^2	p	Coefficient	χ^2	p
<i>G. hirsutum</i>										
Intercept		1.594	-	-	-3.232	-	-	0.432	-	-
Light (L)	1	-1.09E-02	56.494	<0.001	-6.41E-03	91.275	<0.001	-2.62E-03	169.608	<0.001
Nitrogen (N)	1	-1.34E-03	54.925	<0.001	1.83E-03	118.784	<0.001	1.15E-04	2.901	0.089
L*N	1	3.88E-06	0.485	0.486	-1.34E-05	10.721	0.001	-1.67E-06	3.140	0.076
<i>G. max</i>										
Intercept		1.877	-	-	0.239	-	-	0.438	-	-
Light (L)	1	-7.67E-03	174.156	<0.001	-6.72E-04	39.799	<0.001	-2.55E-03	194.548	<0.001
Nitrogen (N)	1	-2.35E-04	21.948	<0.001	1.55E-04	70.771	<0.001	2.52E-04	19.458	<0.001
L*N	1	-2.89E-06	1.262	0.261	-6.32E-07	1.435	0.231	-3.16E-06	10.803	0.001

16

330 *Significance determined using Wald's χ^2 tests ($p=0.05$). P -values less than 0.05 are in bold and p -values between
 331 0.05 and 0.1 are italicized. Negative coefficients for light treatments indicate a positive effect of increasing light
 332 availability on all response variables, as light availability is treated as percent shade cover in all linear mixed-effects
 333 models.

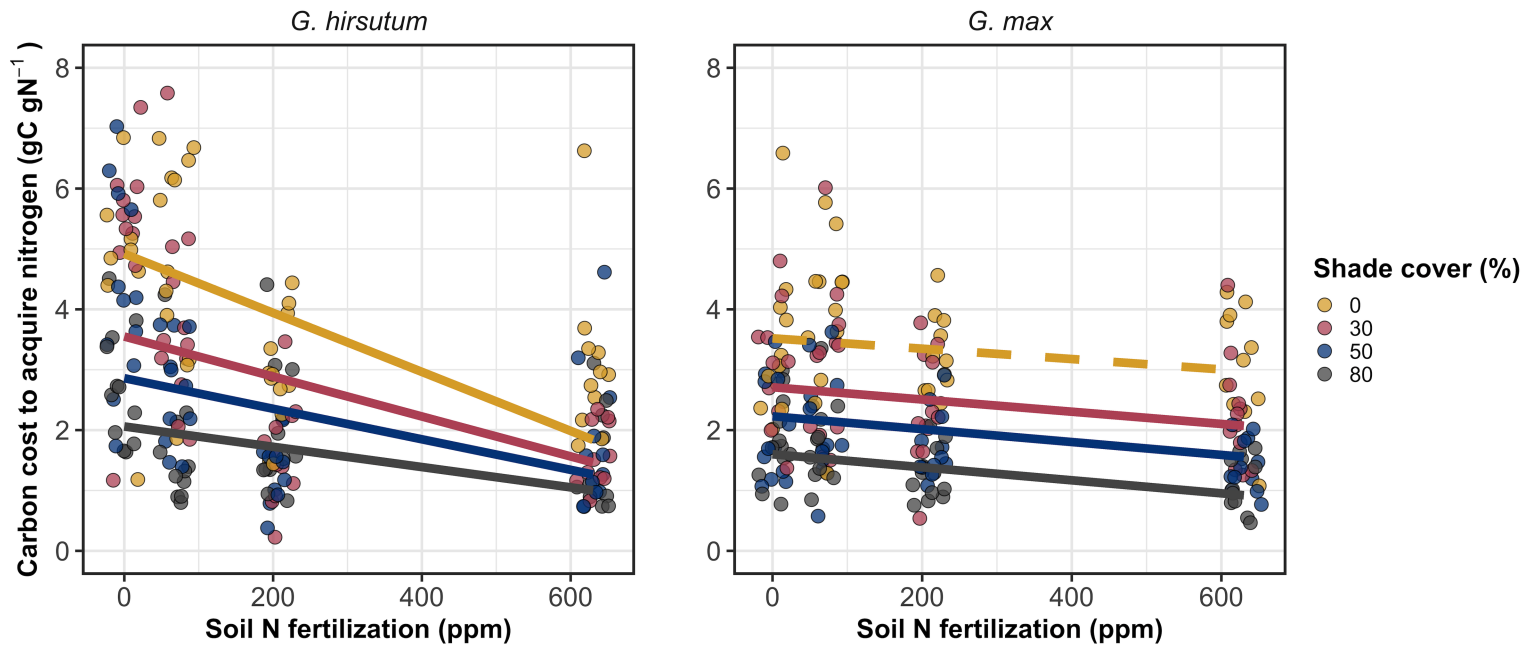


Figure 2.1. Relationships between soil nutrient fertilization and light availability on carbon costs to acquire nitrogen in *G. hirsutum* and *G. max*. Nitrogen fertilization treatments are represented on the x-axis. Shade cover treatments are represented through colored points and trendlines. Trendlines were created by back-transforming marginal mean slopes and intercepts from species-specific linear mixed-effects models. These values were calculated using the ‘emtrends’ and ‘emmeans’ functions in the ‘emmeans’ R package (Lenth, 2019). Yellow points and trendlines represent the 0% shade cover treatment, red points and trendlines represent the 30% shade cover treatment, blue points and trendlines represent the 50% shade cover treatment, and gray points and trendlines represent the 80% shade cover treatment. Solid trendlines indicate slopes that are significantly different from zero (Tukey: $p < 0.05$), while dashed trendlines indicate slopes that are not statistically different from zero.

334 2.3.2 *Whole plant nitrogen biomass*

335 Whole plant nitrogen biomass in *G. hirsutum* was driven by an interaction between
336 light availability and nitrogen fertilization ($p=0.001$; Table 2.1; Fig. 2.2). This
337 interaction indicated a greater stimulation of whole-plant nitrogen biomass by
338 nitrogen fertilization as light levels increased (Table 2.1; Fig. 2.2).

339 Whole plant nitrogen biomass in *G. max* increased with increasing light
340 availability ($p<0.001$) and nitrogen fertilization ($p<0.001$), with no interaction
341 between light availability and nitrogen fertilization ($p=0.231$; Table 2.1; Fig. 2.2).

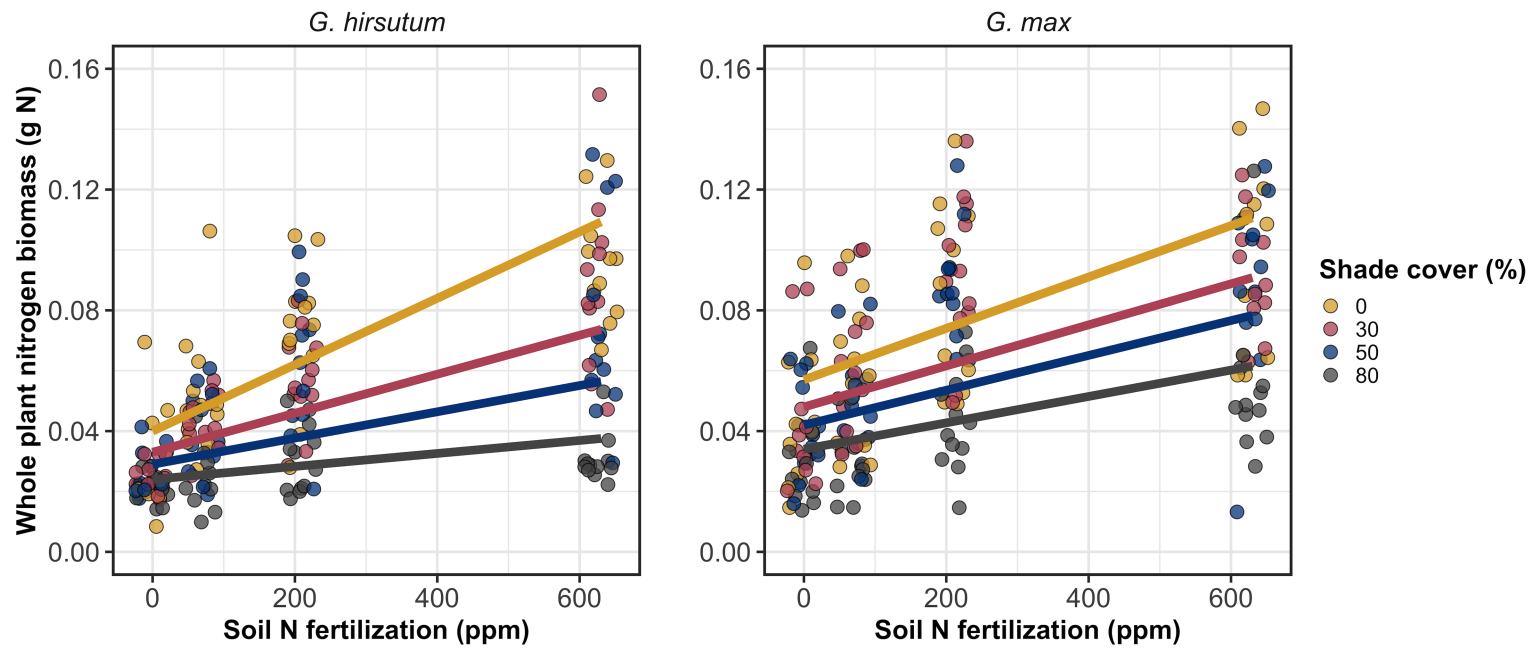


Figure 2.2. Relationships between soil nutrient fertilization and light availability on whole-plant nitrogen biomass in *G. hirsutum* and *G. max*. Whole-plant nitrogen biomass is the denominator of the carbon cost to acquire nitrogen calculation. Nitrogen fertilization treatments are represented on the x-axis. Shade cover treatments are represented through colored points and trendlines. Trendlines were created by back-transforming marginal mean slopes and intercepts from species-specific linear mixed-effects models. These values were calculated using the ‘emtrends’ and ‘emmeans’ functions in the ‘emmeans’ R package (Lenth 2019). Points are jittered for visibility. Colored points and trendlines are as explained in Fig. 2.1. Solid trendlines indicate slopes that are significantly different from zero (Tukey: $p < 0.05$), while dashed trendlines indicate slopes that are not statistically different from zero.

342 2.3.3 *Root carbon biomass*

343 Root carbon biomass in *G. hirsutum* significantly increased with increasing light availability ($p<0.001$; Table 2.1; Fig. 2.3) and marginally increased with nitrogen fertilization ($p=0.089$; Table 2.1; Fig. 2.3). There was also a marginal interaction between light availability and nitrogen fertilization ($p=0.076$; Table 2.1), driven by an increase in the positive response of root carbon biomass to increasing nitrogen fertilization as light availability increased (Table 2.3). This resulted in significantly positive trends between root carbon biomass and nitrogen fertilization in the two highest light treatments (Tukey: $p<0.05$ in both cases; Table 2.3; Fig. 2.3) and no effect of nitrogen fertilization in the two lowest light treatments (Tukey: $p>0.05$ in both cases; Table 2.3; Fig. 2.3).

353 There was an interaction between light availability and nitrogen fertilization on root carbon biomass in *G. max* ($p=0.001$; Table 2.1; Fig. 2.3). Post-hoc analyses indicated that the positive effects of nitrogen fertilization on *G. max* root carbon biomass increased with increasing light availability (Table 2.3; Fig. 2.3). There were also positive individual effects of increasing nitrogen fertilization ($p<0.001$; Table 2.3) and light availability ($p<0.001$; Table 2.3) on *G. max* root carbon biomass (Table 2.1; Fig. 2.3).

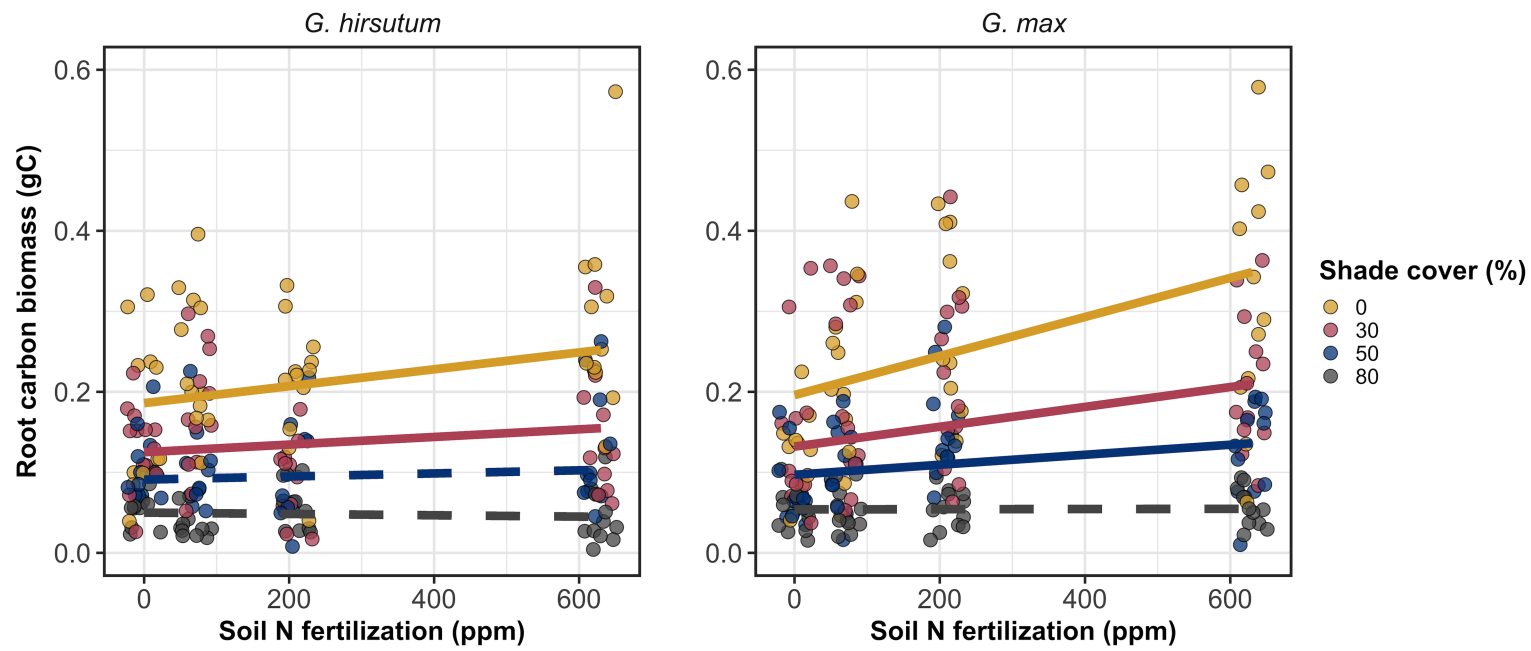


Figure 2.3. Relationships between soil nutrient fertilization and light availability on root carbon biomass in *G. hirsutum* and *G. max*. Root carbon biomass is the numerator of the carbon cost to acquire nitrogen calculation. Nitrogen fertilization treatments are represented on the x-axis. Colored points and trendlines are as explained in Fig. 2.1. Trendlines were created by back-transforming marginal mean slopes and intercepts from species-specific linear mixed-effects models. These values were calculated using the ‘emtrends’ and ‘emmeans’ functions in the ‘emmeans’ R package (Lenth 2019). Points are jittered for visibility. Colored points and trendlines are as explained in Fig. 2.1.

360 2.3.4 *Root nodule biomass*

361 Root nodule biomass in *G. max* increased with increasing light availability ($p <$
362 0.001; Table 2.2; Fig. 2.4a) and decreased with increasing nitrogen fertilization
363 ($p < 0.001$; Table 2.2; Fig. 2.4a). There was no interaction between nitrogen
364 fertilization and light availability ($p = 0.133$; Table 2.2; Fig. 2.4a). The ratio of
365 root nodule biomass to root biomass did not change in response to light availability
366 ($p = 0.481$; Table 2.2; Fig. 2.4b) but decreased with increasing nitrogen fertilization
367 ($p < 0.001$; Table 2.2; Fig. 2.4b). There was no interaction between nitrogen
368 fertilization and light availability on the ratio of root nodule biomass to root
369 biomass ($p = 0.621$; Table 2.2; Fig. 2.4b).

Table 2.2. Analysis of variance results exploring effects of light availability, nitrogen fertilization, and their interactions on *G. max* root nodule biomass (g) and the ratio of root nodule biomass to root biomass (g g⁻¹)*

	Nodule biomass			Nodule biomass: root biomass			<i>p</i>
	df	Coefficient	χ^2	<i>p</i>	Coefficient	χ^2	
(Intercept)		0.302	-	-	0.448	-	-
Light (L)	1	-1.81E-03	72.964	<0.001	-8.76E-05	0.496	0.481
Nitrogen (N)	1	-2.83E-04	115.377	<0.001	-5.09E-04	156.476	<0.001
L*N	1	1.14E-06	2.226	0.133	-7.30E-07	0.244	0.621

370 *Significance determined using Wald's χ^2 tests ($\alpha=0.05$). *P*-values less than 0.05 are in bold. Negative coefficients for
 371 light treatments indicate a positive effect of increasing light availability on all response variables, as light availability
 372 is treated as percent shade cover in all linear mixed-effects models. Root nodule biomass and nodule biomass: root
 373 biomass models were only constructed for *G. max* because *G. hirsutum* was not inoculated with *B. japonicum* and
 374 is not capable of forming root nodules.

Table 2.3. Slopes of the regression line describing the relationship between each dependent variable and nitrogen fertilization at each light level*

Shade cover	Carbon cost to acquire nitrogen	Whole plant nitrogen biomass	Belowground carbon biomass	Root nodule biomass	Nodule biomass: root biomass
<i>G. hirsutum</i>					
0%	-1.34E-03^a	1.83E-03^a	1.15E-04^b	-	-
30%	-1.22E-03^a	1.43E-03^a	1.17E-04^b	-	-
50%	-1.14E-03^a	1.17E-03^a	3.12E-05 ^b	-	-
80%	-1.02E-03^a	7.66E-04^a	-1.89E-06 ^b	-	-
<i>G. max</i>					
0%	-2.35E-04 ^b	1.55E-05^b	2.51E-04^b	-2.83E-04^b	-5.09E-04^b
30%	-3.22E-04^b	1.35E-05^b	1.57E-04^b	-2.49E-04^b	-5.31E-04^b
50%	-3.80E-04^b	1.23E-05^b	9.37E-05^b	-2.26E-04^b	-5.45E-04^b
80%	-4.66E-04^b	1.04E-05^b	-9.95E-07 ^b	-1.92E-04^b	-5.67E-04^b

24

375 * Slopes represent estimated marginal mean slopes from linear mixed-effects models described in the Methods. Slopes
 376 were calculated using the ‘emmeans’ R package (Lenth 2019). Superscripts indicate slopes fit to natural-log (^a) or
 377 square root (^b) transformed data. Slopes statistically different from zero (Tukey: $p<0.05$) are indicated in bold.
 378 Marginally significant slopes (Tukey: $0.05< p<0.1$) are italicized.

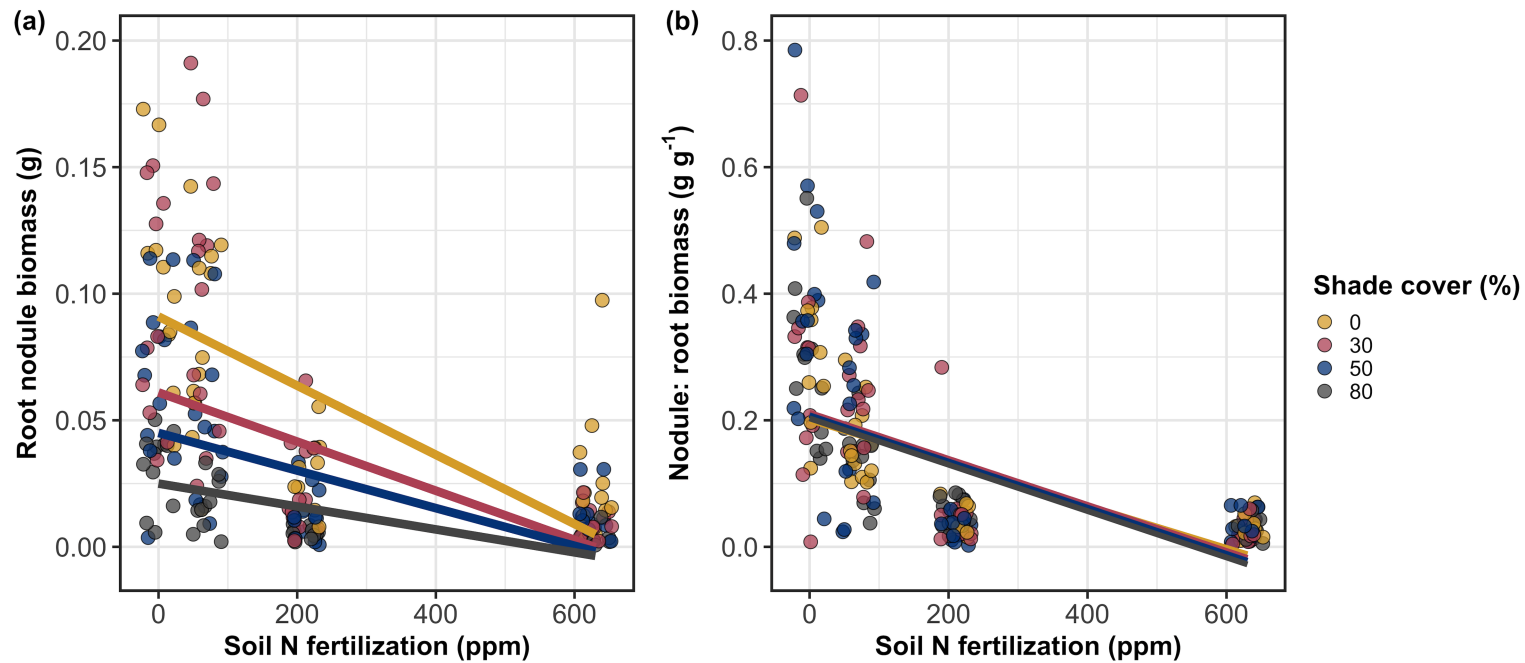


Figure 2.4. Effects of shade cover and nitrogen fertilization on root nodule biomass (a) and the ratio of root nodule biomass to root biomass (b) in *G. max*. Nitrogen fertilization treatments are represented on the x-axis. Shade cover treatments are represented through colored points and trendlines. Trendlines were created by back-transforming marginal mean slopes and intercepts from species-specific linear mixed-effects models. These values were calculated using the ‘emtrends’ and ‘emmeans’ functions in the ‘emmeans’ R package (Lenth 2019). Points are jittered for visibility. Yellow points and trendlines represent the 0% shade cover treatment, blue points and trendlines represent the 30% shade cover treatment, green points and trendlines represent the 50% shade cover treatment, and purple points and trendlines represent the 80% shade cover treatment. Solid trendlines indicate slopes that are significantly different from zero (Tukey: $p < 0.05$), while dashed trendlines indicate slopes that are not statistically different from zero.

379 2.4 Discussion

380 In this chapter, I determined the effects of light availability and soil nitrogen
381 fertilization on root mass carbon costs to acquire nitrogen in *G. hirsutum* and *G.*
382 *max*. In support of my hypotheses, I found that carbon costs to acquire nitrogen
383 generally increased with increasing light availability and decreased with increasing
384 soil nitrogen fertilization in both species. These findings suggest that carbon costs
385 to acquire nitrogen are determined by factors that influence plant nitrogen demand
386 and soil nitrogen availability. In contrast to my second hypothesis, root nodulation
387 data suggested that *G. max* and *G. hirsutum* achieved similar directional carbon
388 cost responses to nitrogen fertilization despite a likely shift in *G. max* allocation
389 from nodulation to root biomass along the nitrogen fertilization gradient.

390 2.4.1 *Carbon costs to acquire nitrogen increase with light availability and*
391 *decrease with fertilization*

392 Both *G. max* and *G. hirsutum* experienced an increase in carbon costs to ac-
393 quire nitrogen due to increasing light availability. These patterns were driven by
394 a larger increase in root carbon biomass than whole-plant nitrogen biomass. In-
395 creases in root carbon biomass due to factors that increase plant nitrogen demand
396 are a commonly observed pattern, as carbon allocated belowground provides sub-
397 strate needed to produce and maintain structures that satisfy aboveground plant
398 nitrogen demand (Nadelhoffer and Raich 1992; Giardina et al. 2005; Raich et al.
399 2014). Findings suggest that plants allocate relatively more carbon for acquiring
400 nitrogen when demand increases over short temporal scales, which may cause a
401 temporary state of diminishing return due to asynchrony between belowground

402 carbon and whole-plant nitrogen responses to plant nitrogen demand (Kulmatiski
403 et al. 2017; Noyce et al. 2019). These responses might be attributed to a temporal
404 lag associated with producing structures that enhance nitrogen acquisition. For
405 example, fine roots (Matamala and Schlesinger 2000; Norby et al. 2004; Arndal
406 et al. 2018) and root nodules (Parvin et al. 2020) take time to build and first
407 require the construction of coarse roots. Thus, full nitrogen returns from these
408 investments may not occur immediately (Kayler et al. 2010; Kayler et al. 2017),
409 and may vary by species acquisition strategy. I speculate that increases in ni-
410 trogen acquisition from a given carbon investment may occur beyond the 5-week
411 scope of this experiment. A similar study conducted over a longer temporal scale
412 would address this.

413 Increasing soil nitrogen fertilization generally decreased carbon costs to
414 acquire nitrogen in both species. These patterns were driven by a larger increase
415 in whole-plant nitrogen biomass than root carbon biomass. In *G. hirsutum*, re-
416 ductions in carbon costs to acquire nitrogen may have been due to an increase in
417 per-root nitrogen uptake, allowing individuals to maximize the amount of nitro-
418 gen acquired from a belowground carbon investment. Interestingly, increased soil
419 nitrogen fertilization increased whole-plant nitrogen biomass in *G. max* despite
420 reductions in root nodule biomass that likely reduced the nitrogen-fixing capac-
421 ity of *G. max* (Andersen et al. 2005; Muñoz et al. 2016). While reductions in
422 root nodulation due to increased soil nitrogen availability are commonly observed
423 (Gibson and Harper 1985; Fujikake et al. 2003), root nodulation responses were
424 observed in tandem with increased root carbon biomass, implying that *G. max*
425 shifted relative carbon allocation from nitrogen fixation to soil nitrogen acquisition

426 (Markham and Zekveld 2007; Dovrat et al. 2020). This was likely because there
427 was a reduction in the carbon cost advantage of acquiring fixed nitrogen relative
428 to soil nitrogen, and suggests that species capable of associating with symbiotic
429 nitrogen-fixing bacteria shift their relative nitrogen acquisition pathway to opti-
430 mize nitrogen uptake (Rastetter et al. 2001). Future studies should investigate
431 these patterns with a larger quantity of phylogenetically related species, or differ-
432 ent varieties of a single species that differ in their ability to form associations with
433 symbiotic nitrogen-fixing bacteria to more directly test the impact of nitrogen
434 fixation on the patterns observed in this study.

435 2.4.2 *Modeling implications*

436 Carbon costs to acquire nitrogen are subsumed in the general discussion of eco-
437 nomic analogies to plant resource uptake (Bloom et al. 1985; Rastetter et al.
438 2001; Vitousek et al. 2002; Phillips et al. 2013; Terrer et al. 2018; Henneron
439 et al. 2020). Despite this, terrestrial biosphere models rarely include costs of
440 nitrogen acquisition within their framework for predicting plant nitrogen uptake.
441 There is currently one plant resource uptake model, FUN, that quantitatively
442 predicts carbon costs to acquire nitrogen within a framework for predicting plant
443 nitrogen uptake for different nitrogen acquisition strategies (Fisher et al. 2010;
444 Brzostek et al. 2014). Iterations of FUN are currently coupled to two terrestrial
445 biosphere models: the Community Land Model 5.0 and the Joint UK Land En-
446 vironment Simulator (Clark et al. 2011; Shi et al. 2016; Lawrence et al. 2019).
447 Recent work suggests that coupling FUN to CLM 5.0 caused a large overpredic-
448 tion of plant nitrogen uptake associated with nitrogen fixation (Davies-Barnard

449 et al. 2020) compared to other terrestrial biosphere model products. Thus, em-
450 pirical data from manipulative experiments that explicitly quantify carbon costs
451 to acquire nitrogen in species capable of associating with nitrogen-fixing bacteria
452 across different environmental contexts is an important step toward identifying
453 potential biases in models such as FUN.

454 These findings broadly support the FUN formulation of carbon costs to
455 acquire nitrogen in response to soil nitrogen availability. FUN calculates carbon
456 costs to acquire nitrogen based on the sum of carbon costs to acquire nitrogen
457 via nitrogen fixation, mycorrhizal active uptake, non-mycorrhizal active uptake,
458 and retranslocation (Fisher et al. 2010; Brzostek et al. 2014). Carbon costs to
459 acquire nitrogen via mycorrhizal or non-mycorrhizal active uptake pathways are
460 derived as a function of nitrogen availability, root biomass, and two parameterized
461 values based on nitrogen acquisition strategy (Brzostek et al. 2014). Due to this,
462 FUN simulates a net decrease in carbon costs to acquire nitrogen with increasing
463 nitrogen availability for mycorrhizal and non-mycorrhizal active uptake pathways,
464 assuming constant root biomass. This was a pattern I observed in *G. hirsutum* re-
465 gardless of light availability. In contrast, FUN would not simulate a net change in
466 carbon costs to acquire nitrogen via nitrogen fixation due to nitrogen availability.
467 This is because carbon costs to acquire nitrogen via nitrogen fixation are derived
468 from a well established function of soil temperature, which is independent of soil
469 nitrogen availability (Houlton et al. 2008; Fisher et al. 2010). I observed a net
470 reduction in carbon costs to acquire nitrogen in *G. max*, except when individu-
471 als were grown under 0% shade cover. While a net reduction of carbon costs in
472 response to nitrogen fertilization runs counter to nitrogen fixation carbon costs

473 simulated by FUN, these patterns were likely because *G. max* individuals switched
474 their primary mode of nitrogen acquisition from symbiotic nitrogen fixation to a
475 non-symbiotic active uptake pathway.

476 2.4.3 *Study limitations*

477 It should be noted that the metric used in this study to determine carbon costs
478 to acquire nitrogen has several limitations. Most notably, this metric uses root
479 carbon biomass as a proxy for estimating the amount of carbon spent on nitrogen
480 acquisition. While it is true that most carbon allocated belowground has at least
481 an indirect structural role in acquiring soil resources, it remains unclear whether
482 this assumption holds true for species that acquire nitrogen via symbiotic nitro-
483 gen fixation. I also cannot quantify carbon lost through root exudates or root
484 turnover, which may increase due to factors that increase plant nitrogen demand
485 (Tingey et al. 2000; Phillips et al. 2011), and can increase the magnitude of
486 available nitrogen from soil organic matter through priming effects on soil micro-
487 bial communities (Uselman et al. 2000; Bengtson et al. 2012). It is also not
488 clear whether these assumptions hold under all environmental conditions, such
489 as those that shift belowground carbon allocation toward a different mode of ni-
490 trogen acquisition (Taylor and Menge 2018; Friel and Friesen 2019) or between
491 species with different acquisition strategies. In this study, increasing soil nitrogen
492 fertilization increased carbon investment to roots relative to carbon transferred to
493 root nodules. By assuming that carbon allocated to root carbon was proportional
494 to carbon allocated to root nodules across all treatment combinations, these ob-
495 served responses to soil nitrogen fertilization were likely to be overestimated in *G.*

496 *max*. I encourage future research to quantify these carbon fates independently.

497 Researchers conducting pot experiments must carefully choose pot volume
498 to minimize the likelihood of growth limitations induced by pot volume (Poorter
499 et al. 2012). Poorter et al. (2012) indicate that researchers are likely to avoid
500 growth limitations associated with pot volume if measurements are collected when
501 the plant biomass:pot volume ratio is less than 1 g L^{-1} . In this experiment, all
502 treatment combinations in both species had biomass:pot volume ratios less than
503 1 g L^{-1} except for *G. max* and *G. hirsutum* that were grown under 0% shade
504 cover and had received 630 ppm N. Specifically, *G. max* and *G. hirsutum* had
505 average respective biomass:pot volume ratios of $1.24 \pm 0.07 \text{ g L}^{-1}$ and 1.34 ± 0.13
506 g L^{-1} , when grown under 0% shade cover and received 630 ppm N (Table A2,
507 A3; Fig. A1). If growth in this treatment combination was limited by pot vol-
508 ume, then individuals may have had larger carbon costs to acquire nitrogen than
509 would be expected if they were grown in larger pots. This pot volume induced
510 growth limitation could cause a reduction in per-root nitrogen uptake associated
511 with more densely packed roots, which could reduce the positive effect of nitro-
512 gen fertilization on whole-plant nitrogen biomass relative to root carbon biomass
513 (Poorter et al. 2012).

514 Growth limitation associated with pot volume provides a possible expla-
515 nation for the marginally insignificant effect of increasing nitrogen fertilization on
516 *G. max* carbon costs to acquire nitrogen when grown under 0% shade cover. This
517 is because the regression line describing the relationship between carbon costs to
518 acquire nitrogen and nitrogen fertilization in *G. max* grown under 0% shade cover
519 would have flattened if growth limitation had caused larger than expected carbon

520 costs to acquire nitrogen in the 0% shade cover, 630 ppm N treatment combi-
521 nation. This may have been exacerbated by the fact that *G. max* likely shifted
522 relative carbon allocation from nitrogen fixation to soil nitrogen acquisition, which
523 could have increased the negative effect of more densely packed roots on nitrogen
524 uptake. These patterns could have also occurred in *G. hirsutum* grown under 0%
525 shade cover; however, there was no change in the effect of nitrogen fertilization on
526 *G. hirsutum* carbon costs to acquire nitrogen grown under 0% shade cover relative
527 to other shade cover treatments. Regardless, the possibility of growth limitation
528 due to pot volume suggests that effects of increasing nitrogen fertilization on car-
529 bon costs to acquire nitrogen in both species grown under 0% shade cover could
530 have been underestimated. Follow-up studies using a similar experimental design
531 with a larger pot volume would be necessary in order to determine whether these
532 patterns were impacted by pot volume-induced growth limitation.

533 2.4.4 *Conclusions*

534 In conclusion, this chapter provides empirical evidence that carbon costs to ac-
535 quire nitrogen are influenced by light availability and soil nitrogen fertilization
536 in a species capable of acquiring nitrogen via symbiotic nitrogen fixation and a
537 species not capable of forming such associations. We show that carbon costs to
538 acquire nitrogen generally increase with increasing light availability and decrease
539 with increasing nitrogen fertilization. This chapter provides important empirical
540 data needed to evaluate the formulation of carbon costs to acquire nitrogen in
541 terrestrial biosphere models, particularly carbon costs to acquire nitrogen that
542 are associated with symbiotic nitrogen fixation. Findings broadly support the

543 general formulation of these carbon costs in the FUN biogeochemical model in
544 response to shifts in nitrogen availability. However, there is a need for future
545 studies to explicitly quantify carbon costs to acquire nitrogen under different en-
546 vironmental contexts, over longer temporal scales, and using larger selections of
547 phylogenetically related species. In addition, I suggest that future studies mini-
548 mize the limitations associated with the metric used here by explicitly measuring
549 belowground carbon fates independently.

550

Chapter 3

551 Soil nitrogen availability modifies leaf nitrogen economies in mature
552 temperate deciduous forests: a direct test of photosynthetic least-cost
553 theory

554 3.1 Introduction

555 Photosynthesis represents the largest carbon flux between the atmosphere and
556 land surface (IPCC 2021), and plays a central role in biogeochemical cycling at
557 multiple spatial and temporal scales (Vitousek and Howarth 1991; LeBauer and
558 Treseder 2008; Kaiser et al. 2015; Wieder et al. 2015). Therefore, carbon and
559 energy fluxes simulated by terrestrial biosphere models are sensitive to the formu-
560 lation of photosynthetic processes (Ziehn et al. 2011; Bonan et al. 2011; Booth
561 et al. 2012; Smith et al. 2016; Smith et al. 2017) and must be represented using
562 robust, empirically tested processes (Prentice et al. 2015; Wieder et al. 2019).
563 Current formulations of photosynthesis vary across terrestrial biosphere models
564 (Smith and Dukes 2013; Rogers et al. 2017), which causes variation in modeled
565 ecosystem processes (Knorr 2000; Knorr and Heimann 2001; Bonan et al. 2011;
566 Friedlingstein et al. 2014) and casts uncertainty on the ability of these models to
567 accurately predict terrestrial ecosystem responses and feedbacks to global change
568 (Zaehle et al. 2005; Schaefer et al. 2012; Davies-Barnard et al. 2020).

569 Terrestrial biosphere models commonly represent C₃ photosynthesis th-
570 rough variants of the Farquhar et al. (1980) biochemical model (Smith and Dukes
571 2013; Rogers 2014; Rogers et al. 2017). This well-tested photosynthesis model
572 estimates leaf-level carbon assimilation, or photosynthetic capacity, as a function
573 of the maximum rate of Ribulose-1,5-bisphosphate carboxylase-oxygenase (Ru-

574 bisco) carboxylation (V_{cmax}) and the maximum rate of Ribulose-1,5-bisphosphate
575 (RuBP) regeneration (J_{max}) (Farquhar et al. 1980). Many terrestrial biosphere
576 models predict these model inputs based on plant functional group specific lin-
577 ear relationships between leaf nutrient content and V_{cmax} (Smith and Dukes 2013;
578 Rogers 2014; Rogers et al. 2017) under the tenet that a large fraction of leaf nutri-
579 ents, and nitrogen in particular, are partitioned toward building and maintaining
580 enzymes that support photosynthetic capacity, such as Rubisco (Brix 1971; Gul-
581 mon and Chu 1981; Evans 1989; Kattge et al. 2009; Walker et al. 2014). Terres-
582 trial biosphere models predict leaf nutrient content from soil nutrient availability
583 based on the assumption that increasing soil nutrients generally increases leaf nu-
584 trients (Firn et al. 2019; Li et al. 2020; Liang et al. 2020) which, in the case of
585 nitrogen, generally corresponds with an increase in photosynthetic processes (Li
586 et al. 2020; Liang et al. 2020).

587 Recent work calls the generality of relationships between soil nutrient avail-
588 ability, leaf nutrient content, and photosynthetic capacity into question, suggest-
589 ing instead that leaf nutrients and photosynthetic capacity are better predicted as
590 an integrated product of aboveground climate, leaf traits, and soil nutrient avail-
591 ability, rather than soil nutrient availability alone (Dong et al. 2017; Dong et al.
592 2020; Dong et al. 2022; Firn et al. 2019; Smith et al. 2019; Peng et al. 2021).
593 It has been reasoned that this result is because plants allocate added nutrients to
594 growth and storage rather than alterations in leaf chemistry (Smith et al. 2019),
595 perhaps as a result of nutrient limitation of primary productivity (LeBauer and
596 Treseder 2008; Fay et al. 2015). Additionally, recent work suggests that relation-
597 ships between leaf nutrient content and photosynthesis vary across environments,

598 and that the proportion of leaf nutrient content allocated to photosynthetic tis-
599 sue varies over space and time with plant acclimation and adaptation responses
600 to light availability, vapor pressure deficit, soil pH, soil nutrient availability, and
601 environmental factors that influence leaf mass per area (Pons and Pearcy 1994;
602 Niinemets and Tenhunen 1997; Evans and Poorter 2001; Hikosaka and Shigeno
603 2009; Ghimire et al. 2017; Onoda et al. 2017; Luo et al. 2021). The use of linear
604 relationships between leaf nutrient content and V_{cmax} to predict photosynthetic
605 capacity, as commonly used in terrestrial biosphere models (Rogers 2014), is not
606 capable of detecting such responses.

607 Photosynthetic least-cost theory provides an alternative framework for un-
608 derstanding relationships between soil nutrient availability, leaf nutrient content,
609 and photosynthetic capacity (Harrison et al. 2021). Leveraging a two-input mi-
610 croeconomics approach (Wright et al. 2003), the theory posits that plants accli-
611 mate to a given environment by optimizing leaf photosynthesis rates at the lowest
612 summed cost of using nutrients and water (Prentice et al. 2014; Wang et al. 2017;
613 Smith et al. 2019; Paillassa et al. 2020). Across resource availability gradients,
614 the theory predicts that optimal photosynthetic rates can be achieved by trading
615 less efficient use of a resource that is less costly to acquire (or more abundant)
616 for more efficient use of a resource more costly to acquire (or less abundant). For
617 example, an increase in soil nutrient availability should reduce the cost of acquir-
618 ing and using nutrients (Bae et al. 2015; Eastman et al. 2021; Perkowski et al.
619 2021), which could increase leaf nutrient investments in photosynthetic proteins to
620 allow similar photosynthetic rates to be achieved with higher nutrient use (lower
621 nutrient use efficiency) but lower water use (greater water use efficiency). The

622 theory suggests similar tradeoffs in response to increasing soil pH (Paillassa et al.
623 2020), specifically, that increasing soil pH should reduce the cost of acquiring soil
624 nutrients due to an increase in plant-available nutrient concentration (Paillassa
625 et al. 2020; Dong et al. 2022). The theory is also capable of reconciling dynamic
626 leaf nutrient-photosynthesis relationships at global scales (Luo et al. 2021).

627 Patterns expected from photosynthetic least-cost theory have recently re-
628 ceived empirical support both in global environmental gradient (Smith et al.
629 2019; Paillassa et al. 2020; Luo et al. 2021; Querejeta et al. 2022; Wester-
630 band et al. 2023) and local manipulative invasion (Bialic-Murphy et al. 2021)
631 studies. However, nutrient addition experiments that directly examine nutrient-
632 water use tradeoffs expected from the theory are rare (but see Guerrieri et al.
633 2011), and only global gradient studies testing the theory have considered soil pH
634 in their analyses. As a result, there is a need to use nutrient addition and soil pH
635 manipulation experiments to test mechanisms driving responses predicted by the
636 theory.

637 In this study, I measured leaf responses to soil nitrogen availability in five
638 deciduous tree species growing in the upper canopy of mature closed canopy tem-
639 perate forests in the northeastern United States. Soil nitrogen availability and pH
640 were manipulated through a nitrogen-by-pH field manipulation experiment with
641 treatments applied since 2011, eight years prior to measurement. Two different soil
642 nitrogen treatments were applied to increase nitrogen availability with opposing
643 effects on soil pH. An additional nitrogen-free acidifying treatment was expected
644 to decrease soil pH. I hypothesized that increased soil nitrogen availability would
645 enable plants to increase nutrient uptake and create more photosynthetic enzymes

646 per leaf, allowing similar photosynthetic rates achieved with lower leaf C_i:C_a and
647 increased leaf nitrogen content allocated to photosynthetic leaf tissue. I expected
648 that this response would be driven by a reduction in the cost of acquiring nitrogen,
649 which would cause trees to sacrifice efficient nitrogen use to enable more efficient
650 use of other limiting resources (i.e., water). Finally, I hypothesized similar leaf
651 responses to increasing soil pH.

652 3.2 Methods

653 3.2.1 *Study site description*

654 I conducted this study in summer 2019 at three stands located within a 20-km ra-
655 dius of Ithaca, NY, USA (42.444 °N, 76.502 °W). All stands contain mature,
656 closed-canopy forests dominated by deciduous tree species. Stands contained
657 abundant sugar maple (*Acer saccharum* Marshall), American beech (*Fagus gran-*
658 *difolia* Ehrh.), and white ash (*Fraxinus americana* L.), accounting for 43%, 15%,
659 and 17% of the total aboveground biomass across the three stands, respectively,
660 with less frequent red maple (*Acer rubrum* L.; 9% of total aboveground biomass)
661 and red oak occurrences (*Quercus rubra* L.; 10% of total aboveground biomass).
662 Soils at each site were broadly classified as a channery silt loam Inceptisols using
663 the USDA NRCS Web Soil Survey data product (Soil Survey Staff 2022). Between
664 2006 and 2020, study sites averaged 972 mm of precipitation per year and had an
665 average temperature of 7.9 °C per a weather station located near the Cornell Uni-
666 versity campus (42.449 °N, 76.449 °W) part of the NOAA NCEI Global Historical
667 Climatology Network (Menne et al. 2012).

668 3.2.2 *Experimental design*

669 Four 40 m x 40 m plots were set up at each site in 2009, each with an additional
670 10 m buffer along plot perimeters (60 m x 60 m total). The plots were set up as a
671 nitrogen-by-pH field manipulation experiment, with one each of four treatments
672 at each site. Two nitrogen treatments were applied, both at $50 \text{ kg N ha}^{-1} \text{ yr}^{-1}$, as
673 either sodium nitrate (NaNO_3) to raise soil pH, or ammonium sulfate ($(\text{NH}_4)_2\text{SO}_4$)
674 to acidify; an elemental sulfur treatment was selected to acidify without nitrogen,
675 applied at the same rate of S addition ($57 \text{ kg S ha}^{-1} \text{ yr}^{-1}$); and control plots
676 received no additions. All amendments were added in pelletized form using hand-
677 held fertilizer spreaders to both the main plots and buffers. Amendments were
678 divided into three equal doses distributed across the growing season from 2011-
679 2017 and added as a single dose from 2018 onward. During 2019, plots were
680 fertilized during the week of May 20.

681 3.2.3 *Leaf gas exchange and trait measurements*

682 I sampled one leaf each from 6 to 10 individuals per plot between June 25 and July
683 12, 2019 for gas exchange measurements (Table B1). Leaves were collected from
684 deciduous broadleaf trees represented across all sites and plots and were replicated
685 in efforts to mimic the species abundance of each plot at each site. I attempted
686 to collect leaves from the upper canopy to reduce differential shading effects on
687 leaf physiology. Leaves were accessed by pulling down small branches using an
688 arborist's slingshot and weighted beanbag attached to a throw line. Branches
689 were immediately recut under deionized water and remained submerged to reduce
690 stomatal closure and avoid xylem embolism, as done in Smith and Dukes (2018),

691 until gas exchange data were collected.

692 Randomly selected leaves with little to no visible external damage were
693 attached to a Li-COR LI-6800 (Li-COR Bioscience, Lincoln, Nebraska, USA)
694 portable photosynthesis machine to measure net photosynthesis (A_{net} ; $\mu\text{mol m}^{-2}$
695 s^{-1}), stomatal conductance (g_{sw} ; $\text{mol m}^{-2} \text{s}^{-1}$), and intercellular CO_2 concentra-
696 tion (C_i ; $\mu\text{mol mol}^{-1}$) at different reference CO_2 concentrations (C_a ; $\mu\text{mol mol}^{-1}$)
697 concentrations (i.e., an A_{net}/C_i curve) under saturating light conditions (2,000
698 $\mu\text{mol m}^{-2} \text{s}^{-1}$). Reference CO_2 concentrations followed the sequence: 400, 300,
699 200, 100, 50, 400, 400, 600, 800, 1000, 1200, 1500, and 2000 $\mu\text{mol mol}^{-1} \text{CO}_2$. Leaf
700 temperatures were not controlled in the cuvette and ranged from 21.8 °C to 31.7
701 °C (mean±SD: 27.2±2.2 °C). A linear and second order log-polynomial nonlinear
702 regression suggested no effect of temperature on stomatal conductance measured
703 at 400 $\mu\text{mol mol}^{-1} \text{CO}_2$ or net photosynthesis measured at 400 $\mu\text{mol mol}^{-1} \text{CO}_2$
704 (Table B2, B3; Fig. B1). All A_{net}/C_i curves were generated within one hour of
705 branch severance.

706 Leaf morphological and chemical traits were collected on the same leaf used
707 to generate each A_{net}/C_i curve. Images of each leaf were taken using a flat-bed
708 scanner to determine fresh leaf area using the ‘LeafArea’ R package (Katabuchi
709 2015), which automates leaf area calculations using ImageJ software (Schneider
710 et al. 2012). Each leaf was dried at 65°C for at least 48 hours, weighed, and
711 ground using a Retsch MM200 ball mill grinder (Verder Scientific, Inc., Newtown,
712 PA, USA) until homogenized. Leaf mass per unit leaf area (M_{area} , g m^{-2}) was
713 calculated as the ratio of dry leaf biomass to fresh leaf area. Using a subsample
714 of ground and homogenized leaf biomass, leaf nitrogen content (N_{mass} ; gN g^{-1})

715 and leaf $\delta^{13}\text{C}$ (‰, relative to Vienna Pee Dee Belemnite international reference
 716 standard) were measured at the Cornell Stable Isotope Lab with an elemental
 717 analyzer (NC 2500, CE Instruments, Wigan, UK) interfaced to an isotope ratio
 718 mass spectrometer (Delta V Isotope Ratio Mass Spectrometer, ThermoFisher Sci-
 719 entific, Waltham, MA, USA). Leaf nitrogen content per unit leaf area (N_{area} ; g N
 720 m^{-2}) was calculated by multiplying N_{mass} by M_{area} .

721 I used leaf $\delta^{13}\text{C}$ values to estimate χ (unitless), which is an isotope-derived
 722 estimate of the leaf $C_i:C_a$ ratio. While intercellular and atmospheric CO_2 concen-
 723 trations were directly measured during each A_{net}/C_i curve, deriving χ from $\delta^{13}\text{C}$
 724 provides a more integrative estimate of the leaf $C_i:C_a$ over an individual leaf's
 725 lifespan. I derived χ following the approach of Farquhar et al. (1989) described
 726 in Cernusak et al. (2013):

$$\chi = \frac{\Delta^{13}\text{C} - a}{b - a} \quad (3.1)$$

727 where $\Delta^{13}\text{C}$ represents the relative difference between leaf $\delta^{13}\text{C}$ (‰) and air $\delta^{13}\text{C}$
 728 (‰), and is calculated from the following equation:

$$\Delta^{13}\text{C} = \frac{\delta^{13}\text{C}_{\text{air}} - \delta^{13}\text{C}_{\text{leaf}}}{1 + \delta^{13}\text{C}_{\text{leaf}}} \quad (3.2)$$

729 where $\delta^{13}\text{C}_{\text{air}}$ is assumed to be -8‰ (Keeling et al. 1979; Farquhar et al. 1989), a
 730 represents the fractionation between ^{12}C and ^{13}C due to diffusion in air, assumed
 731 to be 4.4‰, and b represents the fractionation caused by Rubisco carboxylation,
 732 assumed to be 27‰ (Farquhar et al. 1989).

733 3.2.4 A_{net}/C_i curve-fitting and parameter estimation

734 I fit A_{net}/C_i curves of each individual using the ‘fitaci’ function in the ‘plante-
735 cophys’ R package (Duursma 2015). This function estimates the maximum rate
736 of Rubisco carboxylation (V_{cmax} ; $\mu\text{mol m}^{-2} \text{s}^{-1}$) and maximum rate of electron
737 transport for RuBP regeneration (J_{max} ; $\mu\text{mol m}^{-2} \text{s}^{-1}$) based on the Farquhar,
738 von Caemmerer, and Berry biochemical model of C₃ photosynthesis (Farquhar
739 et al. 1980). For each curve fit, I included triose phosphate utilization (TPU)
740 limitation to avoid underestimating J_{max} (Gregory et al. 2021). Curves were
741 visually examined to confirm the likely presence of TPU limitation.

742 I determined Michaelis-Menten coefficients for Rubisco affinity to CO₂ (K_c ;
743 $\mu\text{mol mol}^{-1}$) and O₂ (K_o ; $\mu\text{mol mol}^{-1}$), and the CO₂ compensation point (Γ^* ;
744 $\mu\text{mol mol}^{-1}$) using leaf temperature and equations described in Medlyn et al.
745 (2002) and derived in Bernacchi et al. (2001). Specifically, K_c and K_o were
746 calculated as:

$$K_c = 404.9 * \exp^{\frac{79430(T_k - 298)}{298RT_k}} \quad (3.3)$$

747 and

$$K_o = 278.4 * \exp^{\frac{36380(T_k - 298)}{298RT_k}} \quad (3.4)$$

748 while Γ^* was calculated as:

$$\Gamma^* = 42.75 * \exp^{\frac{37830(T_k - 298)}{298RT_k}} \quad (3.5)$$

749 In all three equations, T_k is the leaf temperature (in Kelvin) during each A_{net}/C_i

750 curve and R is the universal gas constant ($8.314 \text{ J mol}^{-1} \text{ K}^{-1}$).

751 I standardized V_{cmax} and J_{max} estimates to 25°C using a modified Arrhe-

752 nius equation (Kattge and Knorr 2007):

$$k_{25} = \frac{k_{\text{obs}}}{e^{\frac{H_a(T_{\text{obs}} - T_{\text{ref}})}{T_{\text{ref}}RT_{\text{obs}}}} * \frac{1+e^{\frac{T_{\text{ref}}\Delta S - H_d}{T_{\text{obs}}\Delta S - H_d}}}{1+e^{\frac{T_{\text{obs}}\Delta S - H_d}{T_{\text{obs}}}}}} \quad (3.6)$$

753 k_{25} represents the standardized V_{cmax} or J_{max} rate at 25°C , k_{obs} represents the

754 V_{cmax} or J_{max} estimate at the average leaf temperature measured inside the cuvette

755 during the A_{net}/C_i curve. H_a is the activation energy of V_{cmax} ($71,513 \text{ J mol}^{-1}$)

756 Kattge and Knorr (2007) or J_{max} ($49,884 \text{ J mol}^{-1}$) (Kattge and Knorr 2007).

757 H_d represents the deactivation energy of both V_{cmax} and J_{max} ($200,000 \text{ J mol}^{-1}$)

758 (Medlyn et al. 2002), and R represents the universal gas constant (8.314 J mol^{-1}

759 K^{-1}). T_{ref} represents the standardized temperature of 298.15 K (25°C) and T_{obs}

760 represents the mean leaf temperature (in K) during each A_{net}/C_i curve. ΔS is an

761 entropy term that (Kattge and Knorr 2007) derived as a linear relationship with

762 average growing season temperature (T_g ; $^\circ\text{C}$), where:

$$\Delta S_{v_{\text{cmax}}} = -1.07 T_g + 668.39 \quad (3.7)$$

763 and

$$\Delta S_{j_{\text{max}}} = -0.75 T_g + 659.70 \quad (3.8)$$

764 I estimated T_g in Equations 3.7 and 3.8 based on mean daily (24-hour) air tem-
765 perature of the 30 days leading up to the day of each sample collection using the
766 same weather station reported in the site description. I used V_{cmax25} and J_{max25}
767 estimates to calculate the ratio of J_{max25} to V_{cmax25} ($J_{max25}:V_{cmax25}$; unitless).

768 3.2.5 *Proportion of leaf nitrogen allocated to photosynthesis and structure*

769 I used equations from Niinemets and Tenhunen (1997) to estimate the proportion
770 of leaf nitrogen content allocated to Rubisco and bioenergetics. The proportion of
771 leaf nitrogen allocated to Rubisco ($\rho_{rubisco}$; gN gN⁻¹) was calculated as a function
772 of V_{cmax25} and N_{area} :

$$\rho_{rubisco} = \frac{V_{cmax25} N_r}{V_{cr} N_{area}} \quad (3.9)$$

773 where N_r is the amount of nitrogen in Rubisco, set to 0.16 gN (gN in Rubisco)⁻¹
774 and V_{cr} is the maximum rate of RuBP carboxylation per unit Rubisco protein,
775 set to 20.5 μmol CO₂ (g Rubisco)⁻¹. The proportion of leaf nitrogen allocated to
776 bioenergetics (ρ_{bioe} ; gN gN⁻¹) was similarly calculated as a function of J_{max25} and
777 N_{area} :

$$\rho_{bioe} = \frac{J_{max25} N_b}{J_{mc} N_{area}} \quad (3.10)$$

778 where N_b is the amount of nitrogen in cytochrome f, set to 0.12407 gN (μmol
779 cytochrome f)⁻¹ assuming a constant 1: 1: 1.2 cytochrome f: ferredoxin NADP
780 reductase: coupling factor molar ratio (Evans and Seemann 1989; Niinemets and
781 Tenhunen 1997), and J_{mc} is the capacity of electron transport per cytochrome f,

782 set to 156 μmol electron (μmol cytochrome f) $^{-1}\text{s}^{-1}$.

783 I estimated the proportion of leaf nitrogen content allocated to photosynthetic tissue (ρ_{photo} ; gN gN^{-1}) as the sum of ρ_{rubisco} and ρ_{bioe} . This calculation
784 is an underestimate of the proportion of leaf nitrogen allocated to photosynthetic
785 tissue because it does not include nitrogen allocated to light harvesting proteins.
786 This leaf nitrogen pool was not included because I did not perform chlorophyll
787 extractions on focal leaves. However, the proportion of leaf nitrogen content al-
788 located to light harvesting proteins tends to be small relative to ρ_{rubisco} and ρ_{bioe} ,
789 and may scale with changes in ρ_{rubisco} and ρ_{bioe} (Niinemets and Tenhunen 1997).

791 Finally, the proportion of leaf nitrogen content allocated to structural tissue
792 ($\rho_{\text{structure}}$; gN gN^{-1}) was estimated as:

$$\rho_{\text{structure}} = \frac{N_{\text{cw}}}{N_{\text{area}}} \quad (3.11)$$

793 where N_{cw} is the leaf nitrogen content allocated to cell walls (gN m^{-2}), calculated
794 as a function of M_{area} using an empirical equation from Onoda et al. (2017):

$$N_{\text{cw}} = 0.000355 * M_{\text{area}}^{1.39} \quad (3.12)$$

795 3.2.6 *Tradeoffs between nitrogen and water use*

796 Photosynthetic nitrogen use efficiency (PNUE; $\mu\text{mol CO}_2 \text{ mol}^{-1} \text{ N s}^{-1}$) was cal-
797 culated by dividing A_{net} by N_{area} , first converting N_{area} to mol N m^{-2} using the
798 molar mass of nitrogen (14 g mol^{-1}). I used χ as an indicator of water use effi-
799 ciency, which exploratory analyses suggest had similar responses to soil nitrogen

800 availability and pH as intrinsic water use efficiency measured from gas exchange
801 ($A_{\text{net}}/g_{\text{sw}}$). Tradeoffs between nitrogen and water use were determined by cal-
802 culating the ratio of N_{area} to χ ($N_{\text{area}}:\chi$; gN m⁻²) and V_{cmax25} to χ ($V_{\text{cmax25}}:\chi$;
803 $\mu\text{mol m}^{-2} \text{ s}^{-1}$). This approach is similar to tradeoff calculations in which nitrogen-
804 water use tradeoffs are measured as the ratio of N_{area} or V_{cmax25} to g_{sw} (Paillassa
805 et al. 2020; Bialic-Murphy et al. 2021). In this chapter, I quantify these rela-
806 tionships using χ in lieu of g_{sw} because g_{sw} rapidly changes with environmental
807 conditions and therefore may have been altered by recent tree branch severance
808 and/or placement in the cuvette.

809 3.2.7 *Soil nitrogen availability and pH*

810 To characterize soil nitrogen availability at the time of our leaf gas exchange
811 measurements, I used mixed bed resin bags to quantify mobile ammonium-N and
812 nitrate-N concentrations in each plot. Lycra mesh bags were filled with 5 g of
813 Dowex® Marathon MR-3 hydrogen and hydroxide form resin (MilliporeSigma,
814 Burlington, MA USA) and sealed with a zip tie. Each bag was activated by
815 soaking in 0.5 M HCl for 20 minutes, then in 2 M NaCl until pH of the saline
816 solution stabilized, as described in Allison et al. (2008). Five resin bags were
817 inserted about 10 cm below the soil surface at each plot on June 25, 2019: one
818 near each of the four plot corners and one near the plot center. All resin bags
819 were collected 24 days later on July 19, 2019 and were frozen until extracted.

820 Prior to anion and cation extraction, each resin bag was rinsed with ul-
821 trapure water (MilliQ IQ 7000; Millipore Sigma, Burlington, MA) to remove any
822 surface soil residues. Anions and cations were extracted from surface-cleaned

823 resin bags by individually soaking and shaking each bag in 100 mL of a 0.1 M
824 HCl/2.0 M NaCl matrix for one hour. Using a microplate reader (Biotek Synergy
825 H1; Biotek Instruments, Winooski, VT USA), I quantified nitrate-N concentra-
826 tions spectrophotometrically at 540 nm with the end product of a single reagent
827 vanadium (III) chloride reaction (Doane and Horwáth 2003), and ammonium-N
828 concentrations quantified at 650 nm with the end product of a modified phenol-
829 hypochlorite reaction (Weatherburn 1967; Rhine et al. 1998). Both the single
830 reagent vanadium (III) chloride and modified phenol-hypochlorite methodologies
831 are well established for determining nitrate-N and ammonium-N concentrations
832 in resin bag extracts (Arnone 1997; Allison et al. 2008). I used a series of nega-
833 tive and positive controls throughout each well plate to verify the accuracy and
834 precision of our measurements, assaying each resin bag extract and control in
835 triplicate. Soil nitrogen availability was estimated as the sum of the nitrate-N
836 and ammonium-N concentration in each resin bag, normalized per g of resin and
837 duration in the field ($\mu\text{g N g}^{-1} \text{ resin d}^{-1}$), then subsequently averaged across all
838 resin bags in a plot for a plot-level mean.

839 Soil pH was measured on 0-10 cm mineral soil samples collected prior to
840 fertilization in 2019. Near each of the four plot corners, three 5.5 cm diameter soil
841 cores were collected after first removing the forest floor where present. Each set
842 of three cores was placed in a plastic bag, and later composited by hand mixing
843 and sieved to 4mm. Soil pH was determined for a 1:2 soil:water slurry (10 g field-
844 moist soil to 20 mL DI water) of each sample using an Accumet AB15 pH meter
845 with flushable junction probe (Fisher Scientific; Hampton, NH, USA), and was
846 estimated at the plot level as the mean soil pH within each plot.

847 3.2.8 *Statistical analyses*

848 I built two separate series of linear mixed-effects models to explore effects of soil
849 nitrogen availability, soil pH, species, and leaf nitrogen content on leaf physiolog-
850 ical traits. In the first series of linear mixed-effects models, I explored the effect
851 of soil nitrogen availability, soil pH, and species on leaf nitrogen content, leaf
852 photosynthesis, stomatal conductance, and nitrogen-water use tradeoffs. Models
853 included plot-level soil nitrogen availability and plot-level soil pH as continuous
854 fixed effects, species as a categorical fixed effect, and site as a categorical ran-
855 dom intercept term. Interaction terms between fixed effects were not included
856 due to the small number of experimental plots. I built a series of separate mod-
857 els with this independent variable structure to quantify individual effects of soil
858 nitrogen availability, soil pH, and species on N_{area} , M_{area} , N_{mass} , A_{net} , V_{cmax25} ,
859 J_{max25} , $J_{\text{max25}}:V_{\text{cmax25}}$, ρ_{rubisco} , $\rho_{\text{bioenergetics}}$, ρ_{photo} , $\rho_{\text{structure}}$, χ , PNUE, $N_{\text{area}}:\chi$, and
860 $V_{\text{cmax25}}:\chi$.

861 A second series of linear mixed-effects models were built to investigate
862 relationships between leaf nitrogen content and photosynthetic parameters. Sta-
863 tistical models included N_{area} as a single continuous fixed effect with species and
864 site designated as individual random intercept terms. I used this independent
865 variable structure to quantify individual effects of leaf nitrogen content on A_{net} ,
866 V_{cmax25} , J_{max25} , $J_{\text{max25}}:V_{\text{cmax25}}$, and χ .

867 For all linear mixed-effects models, I used Shapiro-Wilk tests of normality
868 to determine whether linear mixed-effects models satisfied residual normality as-
869 sumptions. If residual normality assumptions were not met, then models were fit
870 using dependent variables that were natural log transformed. If residual normal-

871 ity assumptions were still not met (Shapiro-Wilk: $p<0.05$), then models were fit
872 using dependent variables that were square root transformed. All residual nor-
873 mality assumptions for both sets of models that did not originally satisfy residual
874 normality assumptions were met with either a natural log or square root data
875 transformation (Shapiro-Wilk: $p>0.05$ in all cases).

876 In the first series of models, models for N_{area} , M_{area} , N_{mass} , V_{cmax25} , J_{max25} ,
877 χ , $N_{\text{area}}:\chi$, and $V_{\text{cmax25}}:\chi$, ρ_{rubisco} , $\rho_{\text{bioenergetics}}$, ρ_{photo} , $\rho_{\text{structure}}$ satisfied residual
878 normality assumptions without data transformations (Shapiro-Wilk: $p>0.05$ in
879 all cases). The model for $J_{\text{max25}}:V_{\text{cmax25}}$ satisfied residual normality assumptions
880 with a natural log data transformation, while models for A_{net} and PNUE each
881 satisfied residual normality assumptions with square root data transformations.
882 In the second series of models, models for V_{cmax25} , J_{max25} , χ , and $V_{\text{cmax25}}:\chi$ satis-
883 fied residual normality assumptions without data transformations (Shapiro-Wilk:
884 $p>0.05$ in all cases). The model for $J_{\text{max25}}:V_{\text{cmax25}}$ required a natural log data
885 transformation and the model for A_{net} required a square root data transformation
886 (Shapiro-Wilk: $p>0.05$ in both cases).

887 In all models, I used the ‘lmer’ function in the ‘lme4’ R package (Bates
888 et al. 2015) to fit each model and the ‘Anova’ function in the ‘car’ R package
889 (Fox and Weisberg 2019) to calculate Type II Wald’s χ^2 and determine the signif-
890 icance level ($\alpha=0.05$) of each fixed effect coefficient. Finally, I used the ‘emmeans’
891 R package (Lenth, 2019) to conduct post-hoc comparisons using Tukey’s tests,
892 where degrees of freedom were approximated using the Kenward-Roger approach
893 (Kenward and Roger 1997). All analyses and plots were conducted in R version
894 4.1.1 (R Core Team 2021). All figure regression lines and associated 95% confi-

895 dence interval error bars were plotted using predictions generated across the soil
896 nitrogen availability gradient using the ‘emmeans’ R package (Lenth 2019).

897 3.3 Results

898 3.3.1 *Leaf nitrogen content*

899 Increasing soil nitrogen availability generally increased N_{area} (Table 3.1; Fig. 3.1a).
900 This pattern was driven by an increase in N_{mass} (Table 3.1; Fig. 3.1c) and a
901 marginal increase in M_{area} (Table 3.1; Fig. 3.1e) with increasing soil nitrogen
902 availability. There was no effect of soil pH on N_{area} , N_{mass} , or M_{area} (Table 3.1);
903 however, I also observed strong differences in N_{area} (Fig. 3.1b), N_{mass} (Fig. 3.1d),
904 and M_{area} (Fig. 3.1e) between species (Table 3.1).

Table 3.1. Effects of soil nitrogen availability, soil pH, and species on leaf nitrogen content per unit leaf area (N_{area} ; gN m⁻²), leaf nitrogen content per unit leaf mass (N_{mass} ; gN g⁻¹), and leaf mass per unit leaf area (M_{area} ; g m⁻²)*

	N_{area}			N_{mass}			M_{area}			
	df	Coefficient	χ^2	p	Coefficient	χ^2	p	Coefficient	χ^2	p
Intercept	-	9.03E-01	-	-	1.68E+00	-	-	4.60E+01	-	-
Soil N	1	1.68E-02	11.990	0.001	1.25E-02	6.902	0.009	4.87E-01	4.143	0.042
Soil pH	1	9.28E-02	0.836	0.361	8.08E-02	0.663	0.415	4.05E+00	0.653	0.419
Species	4	-	72.128	<0.001	-	35.074	<0.001	-	29.869	<0.001

905 *Significance determined using Type II Wald χ^2 tests ($\alpha=0.05$). P-values<0.05 are in bold.

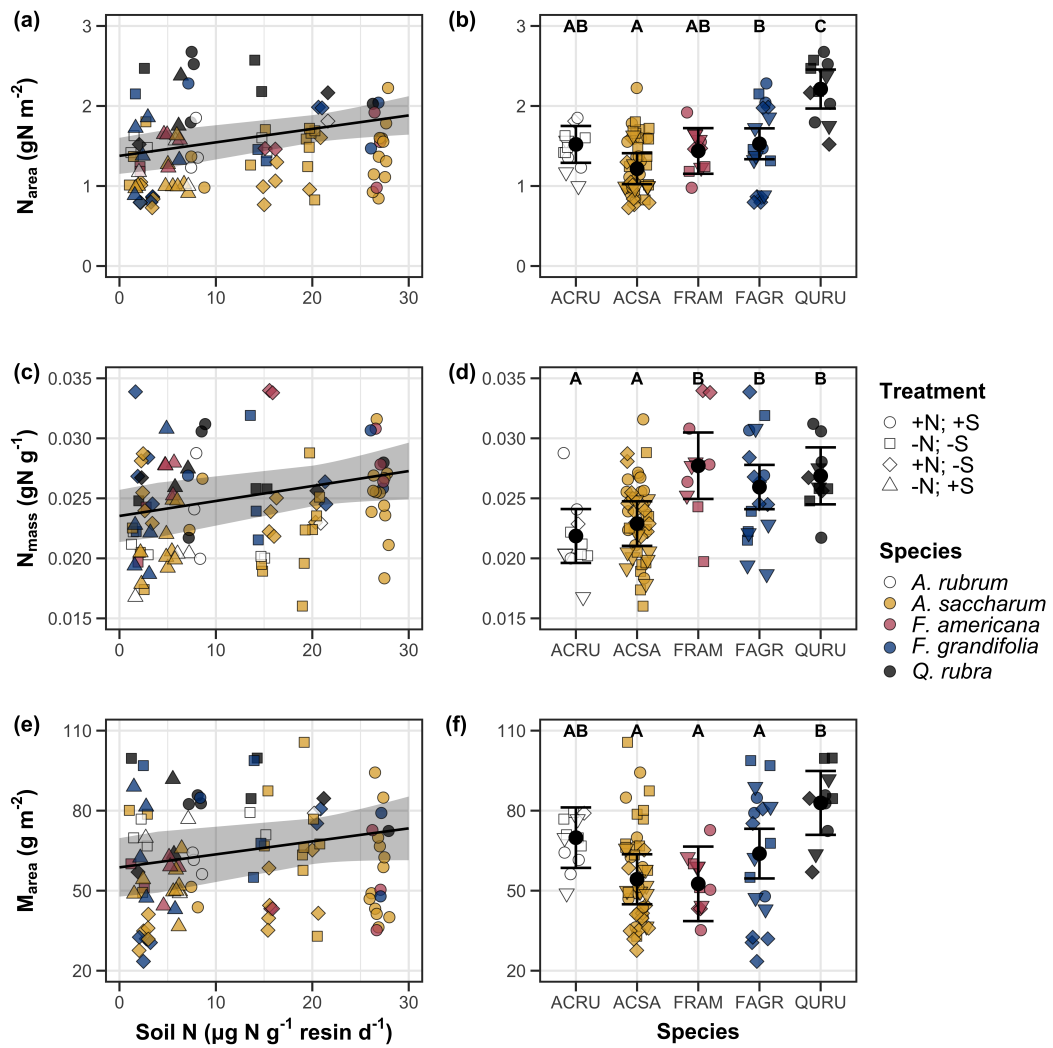


Figure 3.1. Effects of soil N availability and species on leaf nitrogen content per unit leaf area (a-b), leaf nitrogen content per unit leaf biomass (c-d), and leaf mass per unit leaf area (e-f). Soil nitrogen availability is represented on the x-axis in the left column of panels, while species is represented on the x-axis in the right column of panels. Tree species are represented as colored points and treatment plots are represented as shaped points, jittered for visibility. Species are abbreviated in the right column of panels through their assigned NRCS PLANTS Database symbol (USDA NRCS 2022), grouped along the x-axis per common mycorrhizal association, where the first three species commonly associate with arbuscular mycorrhizae (ACRU, ASCA, FAGR) and the second two species with ectomycorrhizae (FAGR, QURU). Trendlines are only included when the regression slope is statistically different from zero ($p < 0.05$).

906 3.3.2 *Net photosynthesis and leaf biochemistry*

907 Increasing soil nitrogen availability generally had no effect on A_{net} , V_{cmax25} , J_{max25} ,
908 or $J_{\text{max25}}:V_{\text{cmax25}}$ (Table 3.2, Figs. 3.2a, 3.2d, 3.2g). I also observed strong species
909 effects on all measured leaf photosynthetic traits (Table 3.2; Figs. 3.2b, 3.2e, 3.2h).
910 Increasing soil pH had a marginal negative effect on A_{net} , but had no effect on
911 V_{cmax25} , J_{max25} , or $J_{\text{max25}}:V_{\text{cmax25}}$ (Table 3.2). There was a weak positive effect of
912 increasing N_{area} on A_{net} (Fig. 3.2c), but quite strong positive effects of increasing
913 N_{area} on V_{cmax25} and J_{max25} (Table 3.2; Fig. 3.2f and 3.2i).

Table 3.2. Effects of soil nitrogen availability, soil pH, species, and N_{area} on net photosynthesis (A_{net} ; $\mu\text{mol m}^{-2} \text{s}^{-1}$), the maximum rate of Rubisco carboxylation (V_{cmax25} ; $\mu\text{mol m}^{-2} \text{s}^{-1}$), the maximum rate of RuBP regeneration (J_{max25} ; $\mu\text{mol m}^{-2} \text{s}^{-1}$), and the ratio of the maximum rate of RuBP regeneration to the maximum rate of Rubisco carboxylation ($J_{\text{max25}}:V_{\text{cmax25}}$; unitless)*

	A_{net}			V_{cmax25}			J_{max25}			
	df	Coefficient	χ^2	p	Coefficient	χ^2	p	Coefficient	χ^2	p
(Intercept)	-	3.29E+00 ^b	-	-	6.38E+01	-	-	1.12E+02	-	-
Soil N	1	-1.23E-03 ^b	1.798	0.180	-3.84E-01	1.745	0.187	-6.70E-01	2.172	0.141
Soil pH	1	-3.09E-01 ^b	3.312	0.069	-4.91E+00	0.655	0.418	-8.18E+00	0.742	0.389
Species	4	-	11.838	0.019	-	31.748	<0.001	-	27.291	<0.001
(N_{area} int.)	-	6.59E-01 ^b	-	-	1.45E-01	-	-	2.86E+01	-	-
N_{area}	4	3.13E-01 ^b	4.790	0.029	2.43E+01	22.616	<0.001	4.04E+01	28.259	<0.001

	$J_{\text{max25}}:V_{\text{cmax25}}$			
	df	Coefficient	χ^2	p
(Intercept)	-	6.59E-01 ^a	-	-
Soil N	1	7.04E-04 ^a	0.088	0.767
Soil pH	1	-7.84E-03 ^a	0.025	0.874
Species	4	-	12.745	0.013
(N_{area} int.)	-	6.69E-01 ^a	-	-
N_{area}	4	-4.69E-02 ^a	1.142	0.285

54

914 *Significance determined using Type II Wald χ^2 tests ($\alpha=0.05$). P-values less than 0.05 are in bold, while p-values
 915 between 0.05 and 0.1 are italicized. Superscript letters indicate model coefficients fit to natural-log (^a) or square-root
 916 (^b) transformed data. Relationships between N_{area} and each response variable were fit using the second series of
 917 bivariate mixed-effects models, so model coefficients and results are independent of model coefficients and results
 918 reported for relationships between soil nitrogen, soil pH, and species for each response variable.

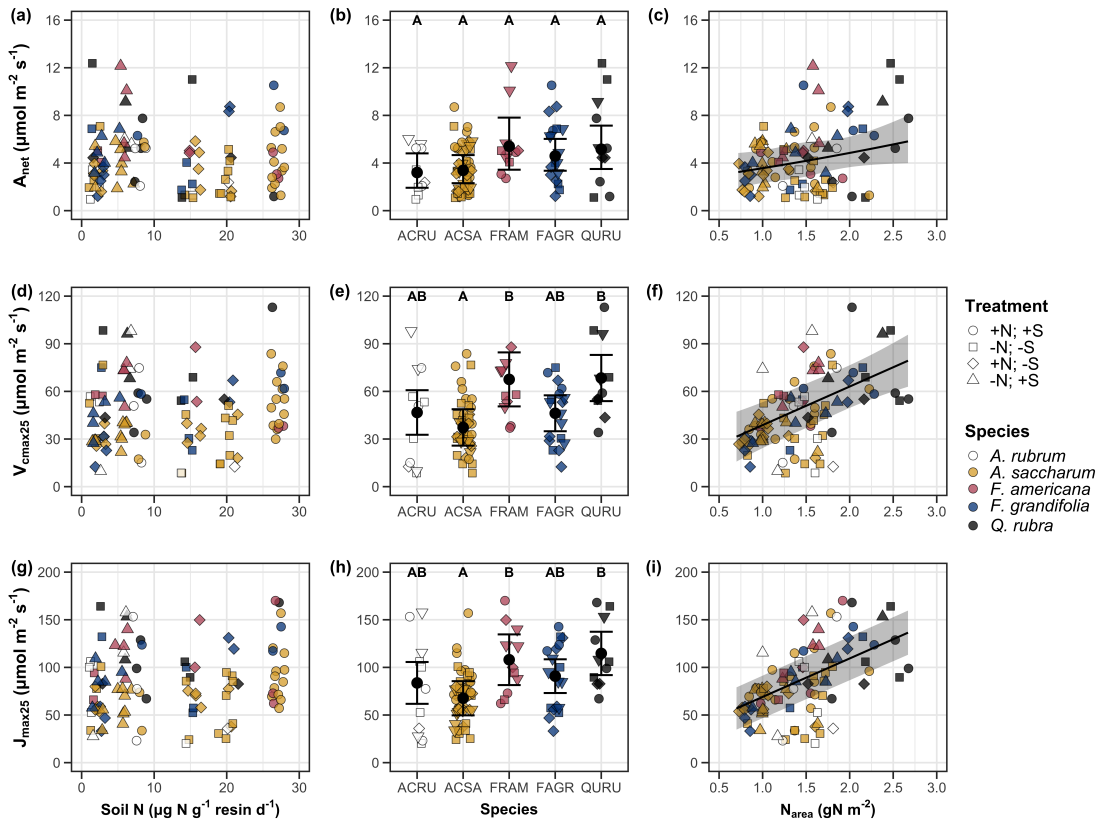


Figure 3.2. Effects of soil nitrogen availability (left column of panels), species (middle column of panels), and leaf nitrogen content per unit leaf area (right column of panels) on net photosynthesis (a-c), maximum Rubisco carboxylation rate (d-f), and maximum RuBP regeneration rate (g-i). Soil nitrogen availability is represented on the x-axis in the left column of panels, species is represented on the x-axis in the middle column of panels, and leaf nitrogen content per unit leaf area is represented continuously on the x-axis in the right column of panels. Species abbreviations and position along the x-axis in the middle column of panels, colored points, shapes, and trendlines are as explained in Figure 3.1.

919 3.3.3 *Leaf nitrogen allocation*

920 Neither soil nitrogen availability nor soil pH affected the proportion of leaf nitrogen
921 allocated to Rubisco or bioenergetics (Table 3.3; Fig. 3.3a, Fig. 3.3c). There was
922 also no effect of soil nitrogen availability or soil pH on the proportion of leaf
923 nitrogen allocated to photosynthesis (Table 3.3; Fig. 3.3f). I found no effect of
924 soil nitrogen availability or soil pH on the proportion of leaf nitrogen allocated to
925 structure (Table 3.3; Fig 3.3g). Species varied in the proportion of leaf nitrogen
926 allocated to Rubisco, photosynthesis, and structure (Fig 3.3b, Fig. 3.3f, Fig 3.3h),
927 with no detectable species effect on the proportion of leaf nitrogen allocated to
928 bioenergetics (Table 3.3, Fig. 3.3d).

Table 3.3. Effects of soil nitrogen availability, soil pH, and species on the proportion of leaf nitrogen content allocated to photosynthesis (ρ_{photo} ; gN gN⁻¹), Rubisco (ρ_{rubisco} ; gN gN⁻¹), bioenergetics (ρ_{bioe} ; gN gN⁻¹), and structure ($\rho_{\text{structure}}$; gN gN⁻¹)*

	ρ_{photo}			ρ_{rubisco}			ρ_{bioe}			
	df	Coefficient	χ^2	p	Coefficient	χ^2	p	Coefficient	χ^2	p
Intercept	-	4.93E-01	-	-	4.17E-01	-	-	7.64E-02	-	-
Soil N	1	-1.23E-03	0.521	0.470	-1.04E-03	0.501	0.479	-1.77E-04	0.557	0.455
Soil pH	1	-4.37E-02	1.581	0.209	-3.70E-02	1.511	0.219	-6.84E-03	1.941	0.164
Species	4	-	13.106	0.011	-	14.152	0.007	-	7.300	0.121

	$\rho_{\text{structure}}$			
	df	Coefficient	χ^2	p
Intercept	-	9.77E-02	-	-
Soil N	1	-2.29E-04	1.165	0.280
Soil pH	1	-1.87E-03	0.179	0.672
Species	4	-	16.428	0.002

929 *Significance determined using Type II Wald χ^2 tests ($\alpha=0.05$). P-values less than 0.05 are in bold.

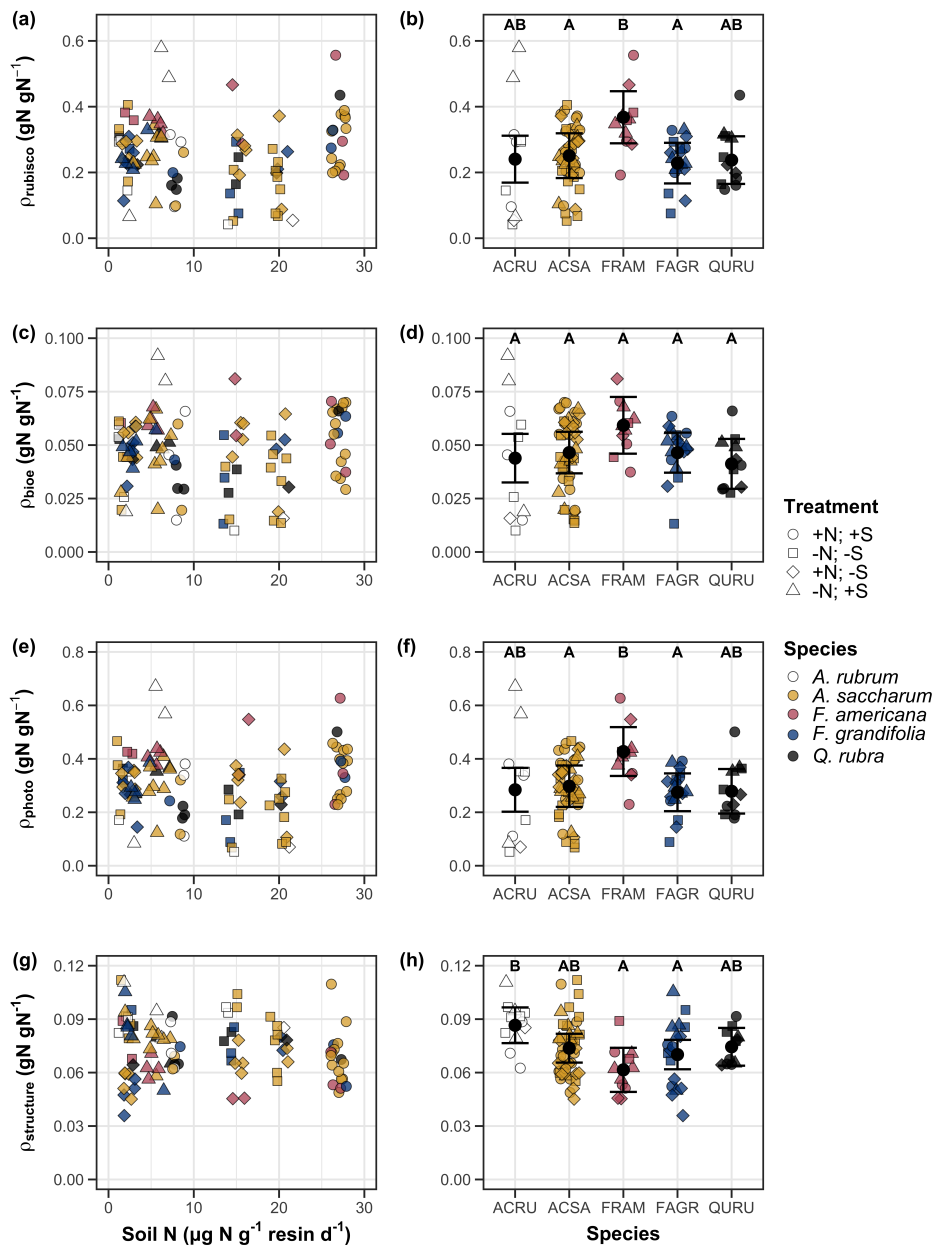


Figure 3.3. Effects of soil nitrogen availability and species on the proportion of leaf nitrogen content allocated to Rubisco (a-b), bioenergetics (c-d), photosynthesis (e-f), and structure (g-h). Soil nitrogen availability is represented on the x-axis in the left column of panels and species are represented on the x-axis in the right column of panels. Species abbreviations and position along the x-axis in the middle column of panels, colored points, shapes, trendlines, error bars, and compact lettering are as explained in Figure 3.1.

930 3.3.4 *Tradeoffs between nitrogen and water use*

931 Although soil nitrogen availability did not affect χ (Table 3.4; Fig. 3.4a), increasing
932 soil nitrogen availability decreased PNUE (Table 3.4; Fig. 3.4d) and increased
933 the ratio of $N_{\text{area}}:\chi$ (Table 3.4; Fig. 3.4f). Specifically, this response yielded a
934 26% reduction in PNUE and 37% stimulation in $N_{\text{area}}:\chi$ across the soil nitrogen
935 availability gradient. There was no apparent effect of soil nitrogen availability on
936 $V_{\text{cmax25}}:\chi$ (Table 3.4; Fig. 3.4h). Increasing soil pH had a weak marginal nega-
937 tive effect on PNUE, but did not influence χ , $N_{\text{area}}:\chi$, or $V_{\text{cmax25}}:\chi$ (Table 3.4). I
938 observed differences in χ (Fig. 3.4b), PNUE (Fig. 3.4e), $N_{\text{area}}:\chi$ (Fig. 3.4g), and
939 $V_{\text{cmax25}}:\chi$ (Fig. 3.4i) between species (Table 3.4). Finally, increasing N_{area} had a
940 strong negative effect on χ (Table 3.4; Fig. 3.4c) and a strong positive effect on
941 $V_{\text{cmax25}}:\chi$ (Table 3.4; Fig. 3.4j).

Table 3.4. Effects of soil nitrogen availability, soil pH, species, and N_{area} on χ (unitless), photosynthetic nitrogen use efficiency (PNUE; $\mu\text{mol CO}_2 \text{ mol}^{-1} \text{ N s}^{-1}$), leaf nitrogen content per unit χ ($N_{\text{area}}:\chi$; gN m^{-2}), and maximum Rubisco carboxylation rate per unit χ ($V_{\text{cmax25}}:\chi$; $\mu\text{mol m}^{-2} \text{ s}^{-1}$)^{*}

	χ			PNUE			$N_{\text{area}}:\chi$			
	df	Coefficient	χ^2	p	Coefficient	χ^2	p	Coefficient	χ^2	p
(Intercept)	-	8.12E-01	-	-	9.57E+00 ^b	-	-	9.19E-01	-	-
Soil N	1	-1.14E-03	1.698	0.193	-6.63E-02 ^b	6.396	0.011	2.60E-02	9.533	0.002
Soil pH	1	-1.91E-02	1.087	0.297	-9.25E-01 ^b	2.843	<i>0.092</i>	2.03E-01	1.321	0.250
Species	4	-	18.843	0.001	-	13.454	0.009	-	52.983	<0.001
(N_{area} int.)	-	8.93E-01	-	-	-	-	-	-	-	-
N_{area}	1	-1.11E-01	80.606	<0.001	-	-	-	-	-	-

	$V_{\text{cmax25}}:\chi$			
	df	Coefficient	χ^2	p
(Intercept)	-	7.20E+01	-	-
Soil N	1	3.99E-01	0.963	0.326
Soil pH	1	-3.12E+00	0.138	0.711
Species	4	-	31.450	<0.001
(N_{area} int.)	-	1.18E+01	-	-
N_{area}	4	3.87E+01	32.797	<0.001

60

942 *Significance determined using Type II Wald χ^2 tests ($\alpha = 0.05$). P -values less than 0.05 are in bold, while p -values
 943 between 0.05 and 0.1 are italicized. Superscript letters indicate model coefficients fit to natural-log (^a) or square-root
 944 (^b) transformed data. Relationships between N_{area} and each response variable were fit using the second series of
 945 bivariate mixed-effects models, so model coefficients and results are independent of model coefficients and results
 946 reported for relationships between soil nitrogen, soil pH, and species for each response variable.

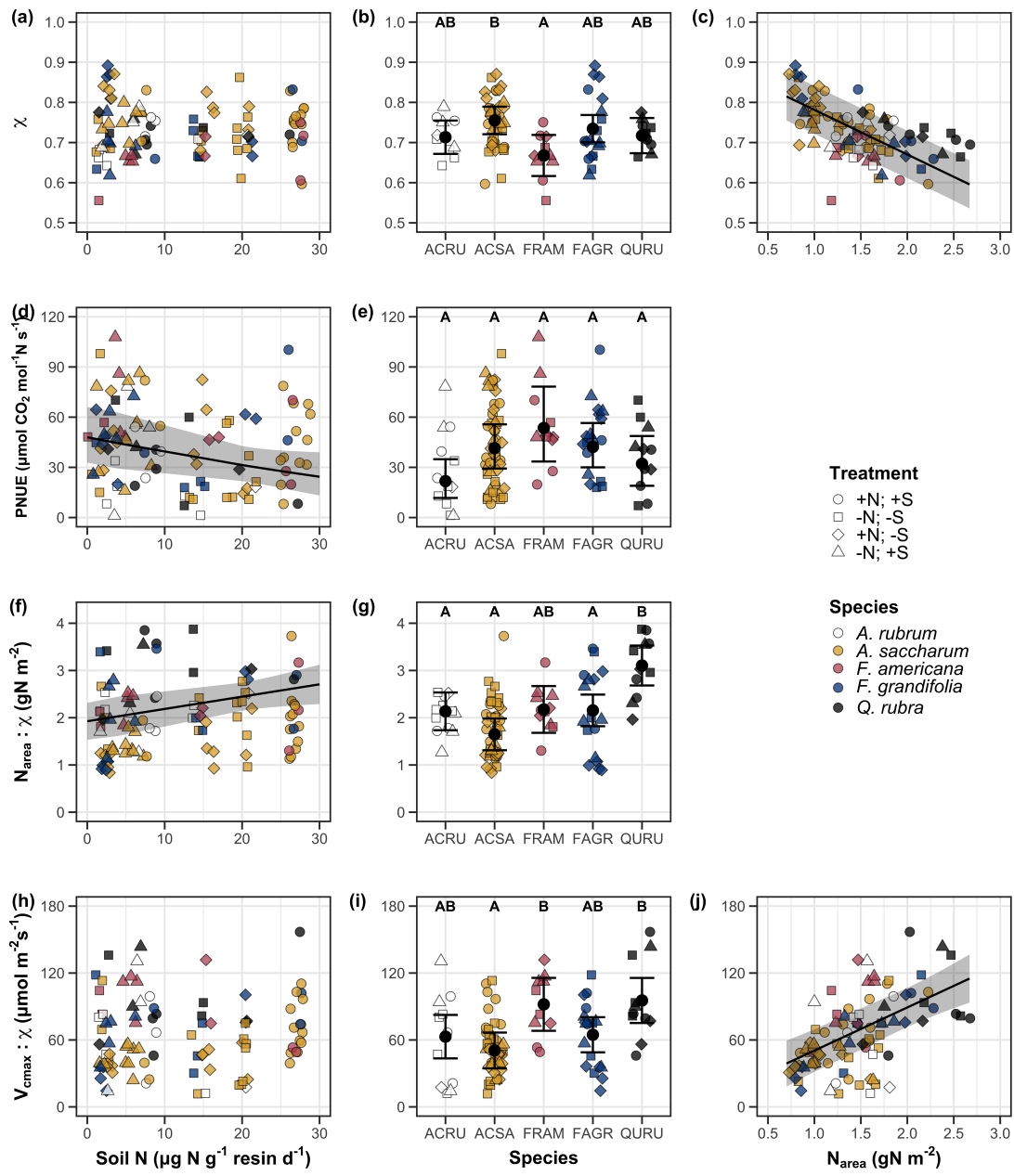


Figure 3.4. Effects of soil nitrogen availability and species on the proportion of leaf nitrogen content allocated to Rubisco (a-b), bioenergetics (c-d), photosynthesis (Rubisco + bioenergetics; e-f), and structure (g-h). Soil nitrogen availability is represented on the x-axis in the left column of panels and species are represented on the x-axis in the right column of panels. Species abbreviations and position along the x-axis in the middle column of panels, colored points, shapes, trendlines, error bars, and compact lettering are as explained in Figure 3.1.

947 3.4 Discussion

948 Photosynthetic least-cost theory provides an explanation for understanding rela-
949 tionships between soil nutrient availability, leaf nutrient allocation, and photosyn-
950 thetic capacity. The theory suggests that plants acclimate to a given environment
951 by optimizing leaf photosynthesis rates at the lowest summed cost of using nu-
952 trients and water (Prentice et al. 2014; Wang et al. 2017; Smith et al. 2019;
953 Paillassa et al. 2020). The theory predicts that an increase in soil nutrient avail-
954 ability should allow similar photosynthesis rates to be achieved with increased leaf
955 nutrient content and photosynthetic capacity (i.e., V_{cmax25} and J_{max25}) at lower
956 leaf $C_i:C_a$ (χ), resulting in an increase in water use efficiency, decrease in nutri-
957 ent use efficiency, and increase in both leaf nutrient content and photosynthetic
958 capacity per unit χ . The theory predicts similar leaf responses to increasing soil
959 pH under acidic conditions, presumably due to generally faster nutrient cycle dy-
960 namics and consequent reductions in the cost of acquiring nutrients relative to
961 water with increasing soil pH (Wang et al. 2017; Paillassa et al. 2020; Dong et al.
962 2020).

963 Supporting the theory, increasing soil nitrogen availability was associated
964 with increased leaf nitrogen content, a pattern that reduced photosynthetic nitro-
965 gen use efficiency and increased leaf nitrogen content per unit χ . Increasing soil
966 nitrogen coincided with slight, but non-significant decreases in χ and increases
967 in V_{cmax25} and J_{max25} ($p<0.2$, Table 3.2). The positive trend between soil ni-
968 trogen availability and photosynthetic capacity was supported by the concurrent
969 strong increase in leaf nitrogen content with increasing soil nitrogen availability,
970 which resulted in no change in the proportion of leaf nitrogen content allocated to

971 photosynthesis across the soil nitrogen availability gradient. Additionally, leaf ni-
972 trogen content exhibited a strong negative correlation with χ , indicative of strong
973 nitrogen-water use tradeoffs at the leaf level. Responses tended to vary more due
974 to soil nitrogen availability than soil pH. Overall, these findings are consistent
975 with the nutrient-water use tradeoffs predicted from theory.

976 3.4.1 *Soil nitrogen availability modifies tradeoffs between nitrogen and water use*
977 In support of expected least-cost outcomes and past environmental gradient stud-
978 ies (Dong et al. 2017; Paillassa et al. 2020), increasing soil nitrogen availability
979 was associated with increased leaf nitrogen content. Soil nitrogen availability had
980 smaller impacts on measures of net photosynthesis and χ , which led to reductions
981 in PNUE and increases in leaf nitrogen content per unit χ , as expected from the-
982 ory. Photosynthetic least-cost theory suggests that reductions in PNUE should
983 be driven by an increase in the proportion of leaf nitrogen allocated to photosyn-
984 thetic tissue, a pattern that should allow plants to achieve optimal photosynthetic
985 rates with greater photosynthetic capacity to make better use of available light.
986 Contrasting theory predictions, I found no effect of soil nitrogen availability on
987 photosynthetic capacity. However, photosynthetic capacity did tend to increase
988 with increasing soil nitrogen availability ($p<0.20$; Table 3.2) resulting in no effect
989 of soil nitrogen availability on the relative fraction of leaf nitrogen allocated to
990 photosynthesis, Rubisco, or bioenergetics. These lines of evidence support the
991 idea that trees use additional nitrogen to support increased leaf nitrogen alloca-
992 tion toward photosynthetic tissue and enhance photosynthetic capacity (Wright
993 et al. 2003).

994 Soil nitrogen availability had a stronger effect on leaf nitrogen than photo-
995 synthetic capacity. This pattern suggests that additional plant nitrogen up-
996 take due to increased soil nitrogen availability was also being used to support
997 non-photosynthetic nitrogen pools, possibly to structural tissue or stress-induced
998 amino acid and polyamine synthesis (Minocha et al. 2000; Onoda et al. 2004;
999 Bubier et al. 2011). While I found no change in the proportion of leaf nitrogen
1000 allocated to leaf structural tissue, the overall stimulation in leaf nitrogen content
1001 with increasing soil nitrogen availability suggests an increase in the net amount of
1002 nitrogen invested in leaf structural tissue along the nitrogen availability gradient.
1003 Importantly, leaf nitrogen allocated to structure was calculated using an empiri-
1004 cal relationship between M_{area} and the amount of leaf nitrogen allocated to cell
1005 walls (Onoda et al. 2017). As the generality of relationships between M_{area} and
1006 the amount of leaf nitrogen allocated to cell walls has been called into question
1007 (Harrison et al. 2009), future work should consider explicitly measuring nitrogen
1008 allocation to cell wall tissue and stress-induced amino acid synthesis to confirm
1009 these patterns.

1010 In opposition to patterns expected from least-cost theory, increasing soil
1011 nitrogen availability had no apparent effect on χ . Interestingly, despite the null
1012 effect of soil nitrogen availability on χ , I observed a strong negative effect of in-
1013 creasing N_{area} on χ , consistent with the nitrogen-water use tradeoffs expected from
1014 theory. The null response of χ to increasing soil nitrogen availability may have
1015 been due to a lack of water limitation in the system, given that the area received
1016 approximately 20% more precipitation (1167 mm) during the 12-month period
1017 leading up to our measurement period than normally expected (972 mm). How-

1018 ever, droughts can and do occur in temperate forests of the northeastern United
1019 States (Sweet et al. 2017), so the observed increase in leaf nitrogen content with
1020 increasing soil nitrogen availability could be a strategy that allows trees to hedge
1021 bets against drier than normal growing seasons (Onoda et al. 2004; Onoda et al.
1022 2017; Hallik et al. 2009). As was suggested in Paillassa et al. (2020), and more
1023 recently by Querejeta et al. (2022), negative effects of soil nitrogen availabil-
1024 ity on χ may increase with increasing aridity. This strategy would be especially
1025 advantageous if it allows individuals growing in arid regions to maintain carbon
1026 assimilation rates with reduced water loss. Future work should attempt to quan-
1027 tify interactive roles of climate and soil nitrogen availability on nitrogen-water use
1028 tradeoffs, which could be done by leveraging coordinated and multifactor nutrient
1029 (Borer et al. 2014) and water (Knapp et al. 2017) manipulation experiments
1030 across broad climatic gradients.

1031 3.4.2 *Soil pH did not modify tradeoffs between nitrogen and water usage*

1032 While the primary purpose of this study was to examine the role of soil nitrogen
1033 availability on nitrogen-water use tradeoffs, this experimental design manipulated
1034 both soil nitrogen and pH, providing an opportunity to isolate the roles of these
1035 variables. Previous correlational studies along environmental gradients have iden-
1036 tified soil pH as a particularly important factor that can modify tradeoffs between
1037 nutrient and water use (Smith et al. 2019; Paillassa et al. 2020; Westerband et al.
1038 2023) and the proportion of leaf nitrogen allocated to photosynthesis (Luo et al.
1039 2021). Such studies implied that these patterns may be driven by reductions in
1040 the cost of acquiring nutrients relative to water with increasing pH, which may

1041 be exacerbated in acidic soils.

1042 Consistent with theory (Wright et al. 2003; Prentice et al. 2014), results
1043 indicate that increasing soil pH was negatively associated with PNUE. However,
1044 there was no effect of soil pH on leaf nitrogen content, χ , or leaf nitrogen content
1045 per unit χ , most likely because the experimental nitrogen additions increased soil
1046 nitrogen supply while both increasing (sodium nitrate) and decreasing (ammo-
1047 nium sulfate) soil pH. These results suggest that soil pH did not play a major
1048 role in modifying expected photosynthetic least-cost theory patterns, contrasting
1049 findings from Paillassa et al. (2020) and other gradient studies that note positive
1050 effects of increasing soil pH on leaf nitrogen content, Rubisco carboxylation, and
1051 χ (Viet et al. 2013; Cornwell et al. 2018; Luo et al. 2021). Instead, null responses
1052 to soil pH show that leaf photosynthetic parameters depend more on soil nitrogen
1053 availability than pH per se, and that inferences from gradient studies might be
1054 confounding covariation between nitrogen availability and soil acidity.

1055 3.4.3 *Species identity explains a large amount of variation in leaf and whole*
1056 *plant traits*

1057 Species generally explained a larger amount of variation in measured leaf traits
1058 than soil nitrogen availability or soil pH. Interspecies variation is an important
1059 factor to consider when deducing mechanisms that drive photosynthetic least-
1060 cost theory, particularly for species that form distinct mycorrhizal associations or
1061 have different photosynthetic pathways, growth forms, or leaf habit (Espelta et al.
1062 2005; Adams et al. 2016; Bialic-Murphy et al. 2021; Scott and Smith 2022). The
1063 need to consider species may also be important when comparing nutrient-water

1064 use tradeoffs in early and late successional species, or in species with different
1065 resource economic strategies (Abrams and Mostoller 1995; Ellsworth and Reich
1066 1996; Wright et al. 2004; Reich 2014; Onoda et al. 2017; Ziegler et al. 2020).

1067 A strength of the study design and sampling effort is that it controls for
1068 many species differences that should modify nitrogen-water use tradeoffs expected
1069 from theory. All tree species measured in this study shared the leaf habit of de-
1070 ciduous broadleaves, were growing in forests of similar successional stage, but
1071 differed in mycorrhizal association and consequent resource economic strategies.
1072 As stands tended to be dominated by trees that associate with arbuscular myc-
1073 orrhizae (*Fraxinus* and both *Acer* species made up roughly 70% of total above-
1074 ground biomass across stands), ecosystem biogeochemical cycle dynamics may be
1075 more closely aligned to the inorganic nutrient economy proposed in Phillips et al.
1076 (2013), which may promote stronger nitrogen-water use tradeoffs in tree species
1077 that associate with arbuscular mycorrhizae. This result was not observed here,
1078 as photosynthetic properties varied as much within as across the two mycorrhizal
1079 associations represented. Given the high variability in measured photosynthetic
1080 traits within and across species, effects of mycorrhizal association likely require
1081 more intensive sampling efforts to detect than were possible here.

1082 3.4.4 *Implications for photosynthetic least-cost theory model development*

1083 In the field, soil nutrient availability is heterogeneous across time and space (Ta-
1084 ble B4). Unaccounted within-plot heterogeneity may have contributed to the low
1085 amount of variation explained by soil nitrogen availability in statistical models,
1086 as resin bags are a coarse surrogate for soil nitrogen availability. Despite this, I

1087 still observed evidence for nutrient-water use tradeoffs, suggesting that observed
1088 responses reported here may be an underestimate toward the net effect of soil ni-
1089 trogen availability on these tradeoffs. While I urge caution in the interpretation of
1090 these results, they do provide a promising baseline for future studies investigating
1091 patterns expected from photosynthetic least-cost theory at finer spatiotemporal
1092 resolutions.

1093 The general stronger relationship between leaf nitrogen content and photo-
1094 synthetic parameters versus between leaf nitrogen content and soil nitrogen avail-
1095 ability suggests that leaf nitrogen content is more directly tied to photosynthesis
1096 than soil nitrogen availability. While this could be due to the high spatiotemporal
1097 heterogeneity of soil nitrogen availability, principles from photosynthetic least-
1098 cost theory suggest that leaf nitrogen content is the downstream product of leaf
1099 nutrient demand to build and maintain photosynthetic machinery, which is set by
1100 aboveground environmental conditions such as light availability, CO₂, tempera-
1101 ture, or vapor pressure deficit (Smith et al. 2019; Paillassa et al. 2020; Peng et al.
1102 2021; Westerband et al. 2023). The stronger relationship between leaf nitrogen
1103 and photosynthetic parameters, paired with the strong negative relationship be-
1104 tween leaf nitrogen and χ , could indicate a relatively stronger effect of climate on
1105 leaf nitrogen-photosynthesis relationships than soil resource availability. However,
1106 the short distance between plots and across sites limited my ability to test this
1107 mechanism.

1108 Variation in soil pH affected least cost responses less than variations in soil
1109 nitrogen availability, in part because experimental treatments directly increased
1110 soil nitrogen and affected soil pH in opposite directions. While soil pH has been

1111 shown to drive nitrogen-water tradeoffs in global gradient analyses (Viet et al.
1112 2013; Paillassa et al. 2020), these responses may be due to covariations between
1113 soil pH and nutrient cycling rather than a role of pH per se. The direct manipula-
1114 tions of soil pH and soil nitrogen availability in this study partly disentangle these
1115 factors and show that variation in nitrogen availability matters more for least-cost
1116 tradeoffs than pH alone.

1117 3.4.5 *Conclusions*

1118 Increasing soil nitrogen availability generally increased leaf nitrogen content (both
1119 area- and mass-based), but did not significantly influence χ . This shift in leaf ni-
1120 trogen led to a reduction in PNUE, and an increase in leaf nitrogen per unit
1121 χ with increasing soil nitrogen availability. Despite null effects of soil nitrogen
1122 availability on χ , I observed a strong negative relationship between leaf nitrogen
1123 content and χ . These results provide empirical support for the nutrient-water use
1124 tradeoffs expected from photosynthetic least-cost theory in response to increas-
1125 ing soil nutrient availability, but suggest that all tenets of the theory may not
1126 hold in every environment. These results experimentally test previous work sug-
1127 gesting that leaf nitrogen-water economies vary across gradients of soil nutrient
1128 availability and pH, and show that variations in nutrient availability matter more
1129 for determining variation in leaf photosynthetic traits than soil pH.

1130

Chapter 4

1131 The relative cost of resource use for photosynthesis drives variance in
1132 leaf nitrogen content across a climate and soil resource availability
1133 gradient

1134 4.1 Introduction

1135 Terrestrial biosphere models, which comprise the land surface component of Earth
1136 system models, are sensitive to the formulation of photosynthetic processes (Knorr
1137 and Heimann 2001; Ziehn et al. 2011; Booth et al. 2012; Walker et al. 2021).
1138 This is because photosynthesis is the largest carbon flux between the atmosphere
1139 and terrestrial biosphere (IPCC 2021), and is constrained by ecosystem carbon
1140 and nutrient cycles (Hungate et al. 2003; LeBauer and Treseder 2008; Fay et al.
1141 2015). Many terrestrial biosphere models formulate photosynthesis by parame-
1142 terizing photosynthetic capacity within plant functional groups through empiri-
1143 cal linear relationships between area-based leaf nitrogen content (N_{area}) and the
1144 maximum carboxylation rate of Ribulose-1,5-bisphosphate carboxylase/oxygenase
1145 (V_{cmax}) (Kattge et al. 2009; Rogers 2014; Rogers et al. 2017). Models are also
1146 beginning to include connected carbon-nitrogen cycles (Wieder et al. 2015; Shi
1147 et al. 2016; Davies-Barnard et al. 2020; Braghieri et al. 2022), which allows leaf
1148 photosynthesis to be predicted directly through changes in N_{area} and indirectly
1149 through changes in soil nitrogen availability (e.g., LPJ-GUESS, CLM5.0) (Smith
1150 et al. 2014; Lawrence et al. 2019). Despite recent model developments, open
1151 questions remain regarding the generality of ecological relationships between soil
1152 nitrogen availability, leaf nitrogen content, and leaf photosynthesis across edaphic
1153 and climatic gradients.

1154 Empirical support for positive relationships between soil nitrogen availabil-
1155 ity and N_{area} is abundant (Firn et al. 2019; Liang et al. 2020), and is a result
1156 often attributed to the high nitrogen cost of building and maintaining Rubisco
1157 (Evans 1989; Evans and Seemann 1989; Onoda et al. 2004; Walker et al. 2014;
1158 Onoda et al. 2017; Dong et al. 2020). Such patterns imply that positive relation-
1159 ships between soil nitrogen availability and N_{area} should increase leaf photosyn-
1160 thesis and photosynthetic capacity by increasing the maximum rate of Rubisco
1161 carboxylation through increased investments to Rubisco construction and mainte-
1162 nance. This integrated N_{area} -photosynthesis response to soil nitrogen availability
1163 has been observed both in manipulative experiments and across environmental
1164 gradients (Field and Mooney 1986; Evans 1989; Walker et al. 2014; Li et al.
1165 2020), and is thought to be driven by ecosystem nitrogen limitation, which lim-
1166 its primary productivity globally (LeBauer and Treseder 2008; Fay et al. 2015).
1167 However, this response is not consistently observed, as recent studies note variable
1168 N_{area} -photosynthesis relationships across edaphic and climatic gradients (Liang
1169 et al. 2020; Luo et al. 2021) and that aboveground growing conditions (e.g., light
1170 availability, temperature, vapor pressure deficit) or species identity traits (e.g.,
1171 photosynthetic pathway, nitrogen acquisition strategy) may be more important
1172 for explaining variance in N_{area} and photosynthetic capacity across environmental
1173 gradients (Adams et al. 2016; Dong et al. 2017; Smith et al. 2019; Dong et al.
1174 2020; Peng et al. 2021; Dong et al. 2022; Westerband et al. 2023).

1175 One hypothesized mechanism to explain variance in N_{area} across environ-
1176 mental gradients has been proposed via photosynthetic least-cost theory (Wright
1177 et al. 2003; Prentice et al. 2014; Paillassa et al. 2020; Harrison et al. 2021).

1178 The theory predicts that plants acclimate to environments by optimizing photo-
1179 synthetic assimilation rates at the lowest summed cost of nitrogen and water use
1180 (Wright et al. 2003; Prentice et al. 2014). In a given environment, the theory
1181 suggests that nitrogen and water use can be substituted for each other to maintain
1182 the lowest summed cost of resource use, such that optimal photosynthetic rates
1183 are achieved with less efficient use of the more abundant and less costly resource
1184 to acquire in exchange for more efficient use of the less abundant and more costly
1185 resource to acquire.

1186 Photosynthetic least-cost theory predicts that, all else equal, an increase in
1187 soil nitrogen availability should decrease the cost of acquiring and using nitrogen
1188 relative to water (a ratio referred to herein as β), resulting in optimal photosyn-
1189 thetic rates achieved with greater N_{area} at lower stomatal conductance and lower
1190 leaf $C_i:C_a$ (Wright et al. 2003; Prentice et al. 2014; Paillassa et al. 2020). Alter-
1191 natively, an increase in soil moisture should reduce costs of water acquisition and
1192 use, increasing β (Lavergne et al. 2020), stomatal conductance, and leaf $C_i:C_a$, re-
1193 sulting in optimal photosynthetic rates achieved with decreased N_{area} . The theory
1194 also predicts variability in stomatal conductance and N_{area} in response to climatic
1195 factors, suggesting that the optimal response to increased vapor pressure deficit
1196 should be a reduction in stomatal conductance and leaf $C_i:C_a$ that is counter-
1197 balanced by an increase in N_{area} to support the greater photosynthetic capacity
1198 needed to maintain high assimilation at lower conductance (Grossiord et al. 2020;
1199 Dong et al. 2020; López et al. 2021; Westerband et al. 2023).

1200 Leaf nitrogen allocation responses to changing climates or soil resource
1201 availability may also depend on their mode of nutrient acquisition or photo-

1202 synthetic pathway. For example, species that form associations with symbiotic
1203 nitrogen-fixing bacteria (referred as “N-fixing species” from this point forward)
1204 should, in theory, have access to less finite nitrogen supply than species not capa-
1205 ble of forming such associations (referred as “non-fixing species” from this point
1206 forward), which may result in lower β values in N-fixing species than non-fixing
1207 species. This result was previously shown in a greenhouse experiment, where a
1208 leguminous species generally had lower costs of nitrogen acquisition compared to a
1209 non-leguminous species, although these differences were generally stronger under
1210 increased nitrogen limitation (Perkowski et al. 2021). Lower β values could be an
1211 explanation for why N-fixing species commonly have greater leaf nitrogen content
1212 than non-fixing species (Adams et al. 2016; Dong et al. 2017).

1213 Similarly, leaf nitrogen allocation patterns across environmental gradients
1214 may be dependent on photosynthetic pathway. Lower leaf $C_i:C_a$ values in C₄
1215 species suggests that C₄ species should have lower β values than C₃ species (Scott
1216 and Smith 2022), a pattern that could be the result of increased costs associated
1217 with water acquisition and use or reduced costs of nitrogen acquisition and use
1218 relative to C₃ species. Theory predicts that this response in C₄ species will cause
1219 C₄ species to have higher leaf nitrogen content on average compared to C₃ species,
1220 though ample evidence exists documenting general lower leaf nitrogen content in
1221 C₄ species (Schmitt and Edwards 1981; Sage and Pearcy 1987; Ghannoum et al.
1222 2011). No study to date has directly quantified β in C₄ species aside from the
1223 initial parameterization of β in an optimality model for C₄ species (Scott and
1224 Smith 2022) using a global dataset of leaf $\delta^{13}\text{C}$ values (Cornwell et al. 2018).

1225 While photosynthetic least-cost theory provides a unified framework for

1226 understanding integrated effects of climate and soil resource availability on N_{area} ,
1227 empirical tests of the theory are sparse. Previous work shows that increasing
1228 soil nitrogen availability decreases costs of acquiring nutrients (Bae et al. 2015;
1229 Perkowski et al. 2021; Lu et al. 2022), which can induce predictable nutrient-
1230 water use tradeoffs expected from the theory across broad environmental gradients
1231 (Paillassa et al. 2020; Querejeta et al. 2022; Westerband et al. 2023) and in
1232 manipulation experiments (Bialic-Murphy et al. 2021). Additionally, increasing
1233 vapor pressure deficit has been shown to have a positive effect on N_{area} , which is
1234 commonly associated with reduced leaf $C_i:C_a$ (Dong et al. 2017; Dong et al. 2020;
1235 Firn et al. 2019; López et al. 2021).

1236 Despite evidence for patterns expected from photosynthetic least-cost the-
1237 ory, studies have been restricted to exploring these patterns in C₃ species and,
1238 while variance in N_{area} across environmental gradients has been shown to be driven
1239 by strong negative relationships with leaf $C_i:C_a$ (Dong et al. 2017; Paillassa et al.
1240 2020; Westerband et al. 2023), no study has explicitly investigated effects of soil
1241 resource availability or species identity on N_{area} using β as a direct predictor of
1242 leaf $C_i:C_a$. Furthermore, as N_{area} can be broken down into structural (leaf mass
1243 per area; M_{area} ; g m⁻²) and metabolic (mass-based leaf nitrogen content; N_{mass} ;
1244 gN g⁻¹) components (Dong et al. 2017), no study has investigated which compo-
1245 nent of N_{area} drives the hypothesized response of N_{area} to leaf $C_i:C_a$, which limits
1246 our ability to assess whether changes in N_{area} across environmental gradients are
1247 driven by changes in leaf morphology (i.e. M_{area}), leaf stoichiometry (i.e. N_{mass}),
1248 or both.

1249 In this study, I measured N_{area} , N_{mass} , M_{area} , leaf $\delta^{13}\text{C}$ -derived estimates

1250 of leaf $C_i:C_a$, and leaf $\delta^{13}\text{C}$ -derived estimates of β in 504 individuals spanning
1251 52 species scattered across 24 grassland sites in Texas, USA. The state of Texas
1252 contains a diverse climatic gradient, indicated by 2006-2020 mean annual precipi-
1253 tation totals ranging from 204 to 1803 mm and 2006-2020 mean annual tempera-
1254 ture ranging from 11.8° to 24.6°C within state boundaries (Fig. 4.1). Variability
1255 in soil nitrogen availability and soil moisture was expected across sites, owing to
1256 differences in soil texture and aboveground climate that would drive differential
1257 rates of water retention and nitrogen transformations to plant-available nitrogen
1258 substrate. I leveraged the expected climatic and soil resource variability across
1259 sites to test the following hypotheses:

- 1260 1. Soil nitrogen availability will decrease β through a reduction in costs of
1261 nitrogen acquisition and use, while soil moisture will increase β through a
1262 reduction in costs of water acquisition and use. Following previous results, I
1263 expected that N-fixing species would have lower β values and that C_4 species
1264 would have lower β values.
- 1265 2. Leaf $C_i:C_a$ will be positively related to β , a pattern that will result in a
1266 negative indirect effect of increasing soil nitrogen availability on leaf $C_i:C_a$,
1267 a positive indirect effect of increasing soil moisture on leaf $C_i:C_a$, and lower
1268 leaf $C_i:C_a$ in both N-fixing species and C_4 species. I expected that leaf
1269 $C_i:C_a$ would be negatively related to vapor pressure deficit, as increasing
1270 atmospheric dryness would cause plants to close stomata to minimize water
1271 loss.
- 1272 3. N_{area} will be negatively related to leaf $C_i:C_a$. This response will result in an
1273 indirect positive and negative effect of increasing soil nitrogen availability

1274 and soil moisture, respectively, on N_{area} , and larger N_{area} values in N-fixing
1275 species. While theory predicts that lower β values in C₄ species should
1276 yield larger N_{area} in C₄ species, I expected that C₄ species would have lower
1277 N_{area} than C₃ species due to greater nitrogen use efficiency in C₄ species.
1278 Additionally, I expected vapor pressure deficit to increase N_{area} , a pattern
1279 that would be directly mediated through the reduction in leaf $C_i:C_a$ with
1280 increasing vapor pressure deficit.

1281 4.2 Methods

1282 4.2.1 *Site descriptions and sampling methodology*

1283 Leaf and soil samples were collected from 24 open canopy grassland sites scattered
1284 across central and eastern Texas in summer 2020 and summer 2021 (Fig. 4.1).
1285 Twelve sites were visited between June and July 2020 and 14 sites (11 unique from
1286 2020) were visited between May and June 2021 (Table 4.1). Sites were chosen to
1287 maximize precipitation and edaphic variability across sites (Table 4.1). No site
1288 with personally communicated or anecdotal evidence of grazing or disturbance
1289 (e.g., mowing, feral hog activity, etc.) was used. Leaf material was collected
1290 from three individuals each of the five most abundant species at random locations
1291 at each site, only selecting species that were broadly classified as graminoid or
1292 forb/herb growth habits per the USDA PLANTS database (USDA NRCS 2022).
1293 All collected leaves were fully expanded with no visible herbivory or other external
1294 damage and also free from shading by nearby shrubs or trees. Five soil samples
1295 were collected from 0-15 cm below the soil surface at each site near the leaf
1296 collection sample locations. Soil samples were mixed together by hand to create

1297 one composite soil sample per site.

1298 4.2.2 *Leaf trait measurements*

1299 Images of each leaf were taken immediately following each site visit using a flat-
1300 bed scanner. Fresh leaf area was determined from each image using the ‘LeafArea’
1301 R package (Katabuchi 2015), which automates leaf area calculations using ImageJ
1302 software (Schneider et al. 2012). Each leaf was dried at 65°C for at least 48 hours
1303 to a constant mass, weighed, and manually ground in a mortar and pestle until
1304 homogenized. Leaf mass per area (M_{area} ; g m⁻²) was calculated as the ratio of
1305 dry leaf biomass to fresh leaf area. Subsamples of dried and homogenized leaf
1306 tissue were used to measure leaf nitrogen content (N_{mass} ; gN g⁻¹) through ele-
1307 mental combustion analysis (Costech-4010, Costech Instruments, Valencia, CA).
1308 Leaf nitrogen content per unit leaf area (N_{area} ; gN m⁻²) was calculated as the
1309 product of N_{mass} and M_{area} .

1310 Subsamples of dried and homogenized leaf tissue were sent to the University
1311 of California-Davis Stable Isotope Facility to determine leaf $\delta^{13}\text{C}$. Leaf $\delta^{13}\text{C}$ values
1312 were determined using an elemental analyzer (PDZ Europa ANCA-GSL; Sercon
1313 Ltd., Chestshire, UK) interfaced to an isotope ratio mass spectrometer (PDZ
1314 Europa 20-20 Isotope Ratio Mass Spectrometer, Sercon Ltd., Chestshire, UK).
1315 I used leaf $\delta^{13}\text{C}$ values (‰; relative to Vienna Pee Dee Belemnite international
1316 reference standard) to estimate the ratio of intercellular (C_i) to extracellular (C_a)
1317 CO₂ ratio (leaf $C_i:C_a$; unitless) following the approach of Farquhar et al. (1989)
1318 described in Cernusak et al. (2013). Specifically, I derived leaf $C_i:C_a$ as:

$$C_i : C_a = \frac{\Delta^{13}C - a}{b - a} \quad (4.1)$$

1319 where $\Delta^{13}C$ represents the relative difference between leaf $\delta^{13}\text{C}$ (\textperthousand) and air $\delta^{13}\text{C}$
1320 (\textperthousand), calculated as:

$$\Delta^{13}C = \frac{\delta^{13}C_{air} - \delta^{13}C_{leaf}}{1 + \delta^{13}C_{leaf}} \quad (4.2)$$

1321 $\delta^{13}\text{C}_{air}$, which is commonly assumed to be $-8\text{\textperthousand}$ (Keeling et al. 1979; Farquhar
1322 et al. 1989), was calculated as a function of calendar year t using an empirical
1323 equation derived in Feng (1999):

$$\delta^{13}C_{air} = -6.429 - 0.006e^{0.0217(t-1740)} \quad (4.3)$$

1324 Using this equation, $\delta^{13}\text{C}_{air}$ values were set to $-9.04\text{\textperthousand}$ and $-9.09\text{\textperthousand}$ for 2020 and
1325 2021, respectively. The parameter a represents the fractionation between ^{12}C
1326 and ^{13}C due to diffusion in air, assumed to be $4.4\text{\textperthousand}$, while b represents the
1327 fractionation caused by Rubisco carboxylation, assumed to be $27\text{\textperthousand}$ (Farquhar
1328 et al. 1989). For C_4 species, b in Eqn. 4.1 was set to $6.3\text{\textperthousand}$, and was derived from:

$$b = c + (d \cdot \phi) \quad (4.4)$$

1329 Where c was set to $-5.7\text{\textperthousand}$ and d was set to $30\text{\textperthousand}$ (Farquhar et al. 1989). ϕ , which
1330 is the bundle sheath leakiness term, was set to 0.4. All leaf $C_i:C_a$ values less than
1331 0.1 and greater than 0.95 were assumed to be incorrect and removed from the

1332 analysis.

1333 I derived the unit cost of resource use (β) using leaf $C_i:C_a$ and site climate

1334 data using equations first described in Prentice et al. (2014) and simplified in

1335 Lavergne et al. (2020):

$$\beta = 1.6\eta^*VPD \frac{\chi - (\frac{\Gamma^*}{C_a})^2}{(1 - \chi)^2(K_m + \Gamma^*)} \quad (4.5)$$

1336 where η^* is the viscosity of water relative to 25°C, calculated using elevation and

1337 mean air temperature of the seven days leading up to each site visit following equa-

1338 tions in Huber et al. (2009). VPD (Pa) was set to the mean vapor pressure deficit

1339 of the seven days leading up to each site visit, C_a represents atmospheric CO₂

1340 concentration, arbitrarily set to 420 $\mu\text{mol mol}^{-1}$ CO₂. K_m (Pa) is the Michaelis-

1341 Menten coefficient for Rubisco affinity to CO₂ and O₂, calculated as:

$$K_m = K_c \cdot \left(1 + \frac{O_i}{K_o}\right) \quad (4.6)$$

1342 where K_c (Pa) and K_o (Pa) are the Michaelis-Menten coefficients for Rubisco

1343 affinity to CO₂ and O₂, respectively, and O_i is the intercellular O₂ concentration.

1344 Γ^* (Pa) is the CO₂ compensation point in the absence of dark respiration. K_c , K_o ,

1345 and Γ^* were determined using equations described in Medlyn et al. (2002) and

1346 derived in Bernacchi et al. (2001), invoking an elevation correction for atmospheric

1347 pressure as explained in Stocker et al. (2020).

Table 4.1. Site locality information, sampling year, 2006-2020 mean annual precipitation (MAP; mm), mean annual temperature (MAT; °C), and water holding capacity (WHC; mm)*

Site	Latitude	Longitude	Sampling year	MAP	MAT	WHC
Edwards_2019_17	29.95	-100.36	2020	563.5	19.0	224.7
Uvalde_2020_02	29.59	-100.09	2020, 2021	648.5	19.5	224.7
Menard_2020_01	30.91	-99.59	2020	641.9	18.3	220.2
Kerr_2020_03	30.06	-99.34	2021	672.4	18.3	237.5
Bandera_2020_03	29.85	-99.30	2021	789.4	18.8	235.1
Sansaba_2020_01	31.29	-98.62	2020	733.0	18.8	234.3
Comal_2020_21	29.79	-98.43	2020	878.5	19.9	220.7
Blanco_2019_16	29.99	-98.43	2020	833.0	19.2	222.2
Bexar_2019_13	29.24	-98.43	2020	759.3	21.5	206.0
Burnet_2020_14	30.84	-98.34	2021	763.3	19.5	217.8
Comal_2020_19	30.01	-98.32	2021	845.0	19.3	220.4
Hays_2020_54	29.96	-98.17	2021	861.3	20.0	225.6
Burnet_2020_12	30.82	-98.06	2021	815.1	19.4	245.3
Williamson_2019_09	30.71	-97.86	2020	867.7	19.7	270.2
Williamson_2019_10	30.54	-97.77	2020	819.5	19.9	239.8
Bell_2021_08	31.06	-97.55	2021	937.3	19.6	232.3
Fayette_2021_12	29.86	-97.21	2021	985.7	20.4	165.6
Fayette_2019_04	30.09	-96.78	2020	1017.4	20.6	226.9
Fayette_2020_09	29.86	-96.71	2021	1002.7	20.8	187.6
Washington_2020_08	30.28	-96.41	2021	1077.4	20.4	203.9
Austin_2020_03	29.78	-96.24	2021	1108.7	20.6	253.0
Brazos_2020_16	30.93	-96.23	2021	1078.0	20.1	202.2
Brazos_2020_18	30.52	-96.21	2020, 2021	1099.4	20.4	233.5
Harris_2020_03	29.88	-95.31	2020, 2021	1492.0	21.6	265.6

1348 * Rows are arranged by longitude to visualize precipitation variability across sites

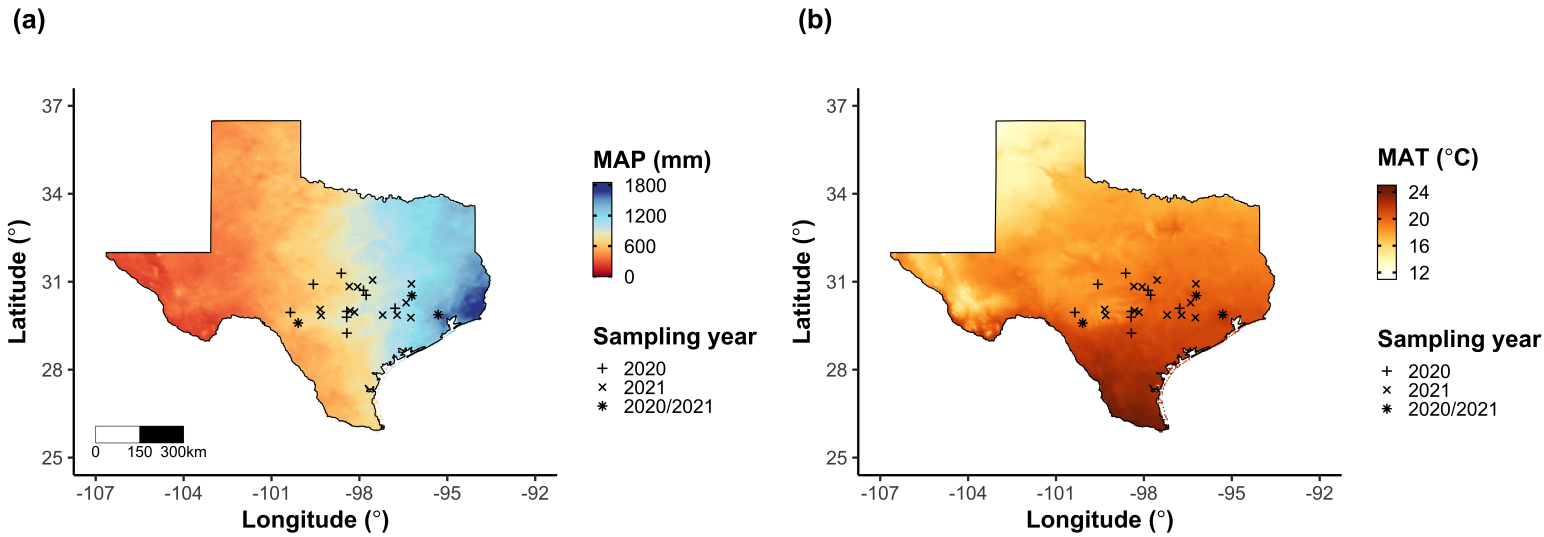


Figure 4.1. Site locations along 2006-2020 mean annual precipitation (a) and mean annual temperature (b) gradients in Texas, USA. Precipitation and temperature data were plotted using PRISM data at a 4-km grid resolution and are masked to include only grid cells that occur within the Texas state boundary of the United States. In both panels, addition signs refer to sites visited in 2020, multiplication signs to sites visited in 2021, and asterisks to sites visited in 2020 and 2021. The scale bar in (a) also applies to (b).

1349 4.2.3 *Site climate data*

1350 I used the Parameter elevation Regressions on Independent Slopes Model (PRISM)
1351 (Daly et al. 2008) climate product to access gridded daily temperature and precip-
1352 itation data for the coterminous United States at a 4-km grid resolution between
1353 January 1, 2006 and July 31, 2021 (PRISM Climate Group, Oregon State Uni-
1354 versity, <https://prism.oregonstate.edu>, data created 4 Feb 2014, accessed 24
1355 Mar 2022). Mean daily air temperature, mean daily vapor pressure deficit, and
1356 total daily precipitation data were extracted from the grid cell that contained the
1357 latitude and longitude of each property using the ‘extract’ function in the ‘terra’
1358 R package (Hijmans 2022). PRISM data were used in lieu of local weather sta-
1359 tion data because several rural sites did not have a local weather station present
1360 within a 20-km radius of the site. Daily site climate data were used to estimate
1361 mean annual precipitation and mean annual temperature for each site between
1362 2006 and 2020 (Table 4.1). I calculated total precipitation and mean daily vapor
1363 pressure deficit for the prior 1, 2, 3, 4, 5, 6, 7, 8, 9, 10, 15, 20, 25, 30, 60, and 90
1364 days leading up to each site visit. Temperature was not included in any analy-
1365 sis due to the close range in mean annual temperature between sites (mean±SD:
1366 $19.8 \pm 0.9^\circ\text{C}$; Table 4.1).

1367 4.2.4 *Site edaphic characteristics*

1368 Composted soil samples were sent to the Texas A&M Soil, Water and Forage
1369 Laboratory to quantify soil nitrate concentration ($\text{NO}_3\text{-N}$; ppm). Soil $\text{NO}_3\text{-N}$
1370 was determined by extracting composite soil samples in 1 M KCl, measuring
1371 absorbance values of extracts at 520 nm using the end product of a $\text{NO}_3\text{-N}$ to

1372 NO₂-N cadmium reduction reaction (Kachurina et al. 2000; Keeney and Nelson
1373 1983). Soil texture data from 0-15 cm below the soil surface were accessed using
1374 the SoilGrids2.0 data product (Poggio et al. 2021) through the ‘fetchSoilGrids’
1375 function in the ‘soilDB’ R package (Beaudette et al. 2022). I used SoilGrids2.0
1376 to access soil texture data in lieu of analyses using the composite soil sample due
1377 to a lack of soil material from some sites after sending samples for soil NO₃-N.

1378 Soil moisture was not measured in the field, but was estimated using the
1379 ‘Simple Process-Led Algorithms for Simulating Habitats’ model (SPLASH) (Davis
1380 et al. 2017). This model, derived from the STASH model (Cramer and Prentice
1381 1988), spins up a bucket model using Priestley-Taylor equations (Priestley and
1382 Taylor 1972) to calculate daily soil moisture (W_n ; mm) as a function of the previous
1383 day’s soil moisture (W_{n-1} ; mm), daily precipitation (P_n ; mm), condensation (C_n ;
1384 mm), actual evapotranspiration (E_n^a ; mm), and runoff (RO; mm):

$$W_n = W_{n-1} + P_n + C_n - E_n^a - RO \quad (4.7)$$

1385 Models were spun up by equilibrating the previous day’s soil moisture using succes-
1386 sive model iterations with daily mean air temperature, daily precipitation total,
1387 the number of daily sunlight hours, and latitude as model inputs (Davis et al.
1388 2017). Daily sunlight hours were estimated for each day at each site using the
1389 ‘getSunlightTimes’ function in the ‘suncalc’ R package, which estimated sunrise
1390 and sunset times of each property using date and site coordinates (Thieurmel and
1391 Elmarhraoui 2019). Water holding capacity (mm), or bucket size, was estimated
1392 as a function of soil texture using pedotransfer equations explained in Saxton and

1393 Rawls (2006), as done in Stocker et al. (2020) and Bloomfield et al. (2023). A
1394 summary of these equations is included in Appendix C.1.

1395 Daily soil moisture outputs from the SPLASH model for each site were
1396 used to calculate mean daily soil moisture for the prior 1, 2, 3, 4, 5, 6, 7, 8, 9,
1397 10, 15, 20, 25, 30, 60, and 90 days leading up to each site visit. Mean daily
1398 soil moisture values were then expressed as a fraction of water holding capacity
1399 to normalize across sites with different bucket depths, as done in Stocker et al.
1400 (2018). Site water holding capacity values are referenced in Table 4.1.

1401 4.2.5 *Plant functional group assignments*

1402 Plant functional group was assigned to each species and used as the primary de-
1403 scriptor of species identity. Specifically, plant functional groups were assigned
1404 based on photosynthetic pathway (C_3 , C_4) and ability to form associations with
1405 symbiotic nitrogen-fixing bacteria (N-fixer, non-fixer). The ability to form asso-
1406 ciations with symbiotic nitrogen-fixing bacteria was assigned based on whether
1407 species were in the *Fabaceae* family, and photosynthetic pathway of each species
1408 was determined from past literature and confirmed through leaf $\delta^{13}C$ values. I
1409 chose these plant functional groups based on *a priori* hypotheses regarding the
1410 functional role of nitrogen fixation and photosynthetic pathway on the sensitivity
1411 of plant nitrogen uptake and leaf nitrogen allocation to soil nitrogen availability
1412 and aboveground growing conditions. These plant functional group classifications
1413 resulted in three distinct plant functional groups within our dataset: C_3 N-fixers
1414 (n=53), C_3 non-fixers (n=334), and C_4 non-fixers (n=117).

1415 4.2.6 *Data analysis*

1416 All analyses and plotting were conducted in R version 4.1.1 (R Core Team 2021).

1417 I constructed a series of separate linear mixed-effects models to investigate en-

1418 vironmental drivers of β , leaf $C_i:C_a$, N_{area} , N_{mass} , and M_{area} , followed by a path

1419 analysis using a piecewise structural equation model to investigate direct and

1420 indirect effects of climate and soil resource availability on N_{area} .

1421 To explore environmental drivers of β , I built a linear mixed-effects model

1422 that included soil moisture, soil nitrogen availability, and plant functional group

1423 as fixed effect coefficients. Species were designated as a random intercept term.

1424 Interaction coefficients between all possible combinations of the three fixed effect

1425 coefficients were also included. β was natural log transformed to linearize data.

1426 I used an information-theoretic model selection approach to determine whether

1427 90-, 60-, 30-, 20-, 15-, 10-, 9-, 8-, 7-, 6-, 5-, 4-, 3-, 2-, or 1-day mean daily soil

1428 moisture conferred the best model fit for β . To do this, I constructed 16 separate

1429 linear mixed-effects models where log-transformed β was included as the response

1430 variable and each soil moisture time step was separately included as a single

1431 continuous fixed effect. Species were included as a random intercept term for all

1432 models. I used corrected Akaike Information Criterion (AICc) to select the soil

1433 moisture timescale that conferred the best model fit, indicated by the model with

1434 the lowest AICc score (Table C3; Fig. C1).

1435 To explore environmental drivers of leaf $C_i:C_a$, I constructed a second lin-

1436 ear mixed effects model that included vapor pressure deficit, soil moisture, soil

1437 nitrogen availability, and plant functional group as fixed effect coefficients. Two-

1438 way interactions between plant functional group and vapor pressure deficit, soil

1439 nitrogen availability, or soil moisture were included as additional fixed effect coef-
1440 ficients, in addition to a three-way interaction between soil moisture, soil nitrogen
1441 availability, and plant functional group. Species were included as a random inter-
1442 cept term. I used an information-theoretic model selection approach to determine
1443 whether 90-, 60-, 30-, 20-, 15-, 10-, 9-, 8-, 7-, 6-, 5-, 4-, 3-, 2-, or 1-day mean daily
1444 vapor pressure deficit conferred the best model fit for leaf $C_i:C_a$ using the same
1445 approach explained above for the soil moisture effect on β . The soil moisture
1446 timescale was set to the same timescale that conferred the best fit for β .

1447 To explore environmental drivers of N_{area} , N_{mass} , and M_{area} , I constructed
1448 a linear mixed effects model for each trait, including leaf $C_i:C_a$, soil nitrogen
1449 availability, soil moisture, and plant functional group as fixed effect coefficients
1450 for each model. Two-way interactions between plant functional group and β , leaf
1451 $C_i:C_a$, soil nitrogen availability, or soil moisture were included as additional fixed
1452 effect coefficients, in addition to a three-way interaction between soil nitrogen
1453 availability, soil moisture, and plant functional group. Species were included as a
1454 random intercept term, with the soil moisture timescale set to the same timescale
1455 that conferred the best fit for β .

1456 In all linear mixed-effects models explained above, including those to select
1457 relevant timescales, I used the ‘lmer’ function in the ‘lme4’ R package (Bates et al.
1458 2015) to fit each model and the ‘Anova’ function in the ‘car’ R package (Fox and
1459 Weisberg 2019) to calculate Type II Wald’s χ^2 and determine the significance
1460 level ($\alpha=0.05$) of each fixed effect coefficient. I used the ‘emmeans’ R package
1461 (Lenth 2019) to conduct post-hoc comparisons using Tukey’s tests, where degrees
1462 of freedom were approximated using the Kenward-Roger approach (Kenward and

1463 Roger 1997). Trendlines and error ribbons for all plots were drawn using a series
1464 of ‘emmeans’ outputs across the range in plotted x-axis values.

1465 Finally, I conducted a path analysis using a piecewise structural equation
1466 model to examine direct and indirect pathways that determined variance in N_{area} .
1467 Six separate linear mixed effects models were loaded into the piecewise structural
1468 equation model. Models were constructed per *a priori* hypotheses following pat-
1469 terns expected from photosynthetic least-cost theory. The first model regressed
1470 N_{area} against N_{mass} and M_{area} . The second model regressed M_{area} against leaf
1471 $C_i:C_a$ and soil nitrogen availability. The third model regressed N_{mass} against
1472 leaf $C_i:C_a$ and M_{area} (Dong et al. 2017; Dong et al. 2020). The fourth model re-
1473 gressed leaf $C_i:C_a$ against β and vapor pressure deficit. The fifth model regressed β
1474 against soil nitrogen availability, soil moisture, ability to associate with symbiotic
1475 nitrogen-fixing bacteria, and photosynthetic pathway. The sixth model regressed
1476 soil nitrogen availability against soil moisture. All models included the relevant
1477 timescale selected in the individual linear mixed effect models explained above.
1478 Models included species as a random intercept term, were built using the ‘lme’
1479 function in the ‘nlme’ R package (Pinheiro and Bates 2022), and subsequently
1480 loaded into the piecewise structural equation model using the ‘psem’ function in
1481 the ‘piecewiseSEM’ R package (Lefcheck 2016).

1482 4.3 Results

1483 4.3.1 *Cost to acquire nitrogen relative to water*

1484 Model selection indicated that 90-day mean soil moisture conferred the best model

1485 fit for β (AICc=1387.54; Table C3; Fig. C1).

1486 Increasing soil nitrogen availability generally decreased β ($p<0.001$; Table

1487 4.2; Fig. 4.2a), a pattern driven by a negative effect of increasing soil nitrogen on β

1488 in C₃ non-fixers (Tukey: $p=0.005$) and C₃ N-fixers (Tukey: $p=0.035$) despite a null

1489 effect of increasing soil nitrogen on β in C₄ non-fixers (Tukey: $p=0.856$). There

1490 was no effect of soil moisture on β ($p=0.872$; Table 4.2; Fig. 4.2b). A functional

1491 group effect ($p<0.001$; Table 4.2) indicated that C₄ non-fixers generally had lower

1492 β values than both C₃ N-fixers and C₃ non-fixers (Tukey: $p<0.001$ in both cases),

1493 while β values in C₃ N-fixers did not differ from C₃ non-fixers (Tukey: $p=0.854$).

Table 4.2. Effects of soil moisture, soil nitrogen availability, and plant functional group on β (unitless)*

	df	Coefficient	χ^2	p
Intercept	-	3.39E+00	-	-
Soil moisture (SM ₉₀)	1	-1.96E-01	0.026	0.872
Soil N (N)	1	-1.42E-02	12.031	<0.001
PFT	2	-	199.617	<0.001
SM ₉₀ *N	1	-3.02E-03	1.000	0.317
SM ₉₀ *PFT	2	-	0.623	0.732
N*PFT	2	-	5.271	0.072
SM ₉₀ *N*PFT	2	-	5.271	0.182

1494 *Significance determined using Type II Wald χ^2 tests ($\alpha=0.05$). P-values<0.05
1495 are in bold. Model coefficients are expressed on the natural-log scale and are only
1496 included for continuous fixed effects. Key: df=degrees of freedom; χ^2 =Wald Type
1497 II chi-square test statistic

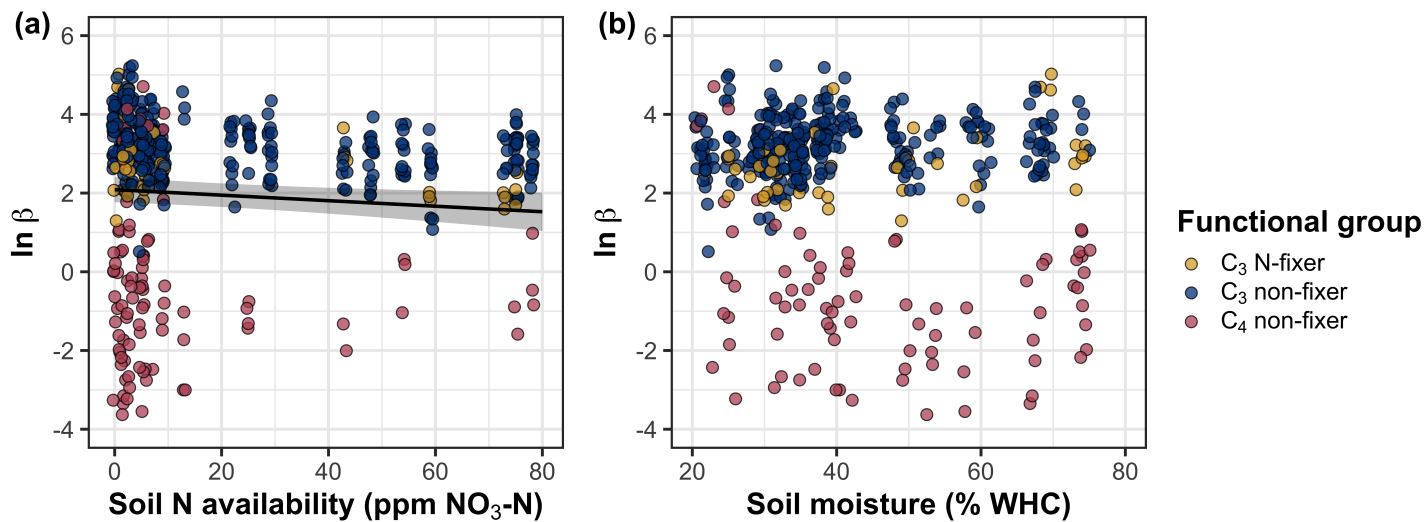


Figure 4.2. Effects of soil nitrogen availability (a) and soil moisture (b) on the cost of acquiring and using nitrogen (β ; unitless). Soil nitrogen availability is represented on the x-axis in (a), soil moisture is represented on the x-axis in (b) as a percent of site water holding capacity, and natural-log transformed β is represented on the y-axis for both panels. Yellow points represent C₃ N-fixers, blue points represent C₃ non-fixers, and red points represent C₄ non-fixers. Throughout, points are jittered for visibility. A black solid trendline is drawn to denote bivariate relationships where the slope is different from zero ($p<0.05$), with error ribbons representing the upper and lower 95% confidence intervals.

1498 4.3.2 *Leaf C_i:C_a*

1499 Model selection indicated that 4-day mean vapor pressure deficit was the timescale

1500 that conferred the best model fit for leaf $C_i:C_a$ (AICc=-755.81; Table C3; Fig. C1).

1501 Model results revealed that increasing vapor pressure deficit generally de-

1502 creased leaf $C_i:C_a$ ($p<0.001$; Table 4.3; Fig. 4.3a). There was no effect of soil mois-

1503 ture ($p=0.549$; Table 4.3; Fig. 4.3b) or soil nitrogen availability ($p=0.549$; Table

1504 4.3; Fig. 4.3c) on leaf $C_i:C_a$. A strong plant functional group effect ($p<0.001$; Ta-

1505 ble 4.3) indicated that C₄ non-fixers had lower leaf $C_i:C_a$ than C₃ N-fixers and C₃

1506 non-fixers (Tukey: $p<0.001$ in both cases), with no difference between C₃ N-fixers

1507 and C₃ non-fixers (Tukey: $p=0.866$).

Table 4.3. Effects of soil moisture, soil nitrogen availability, and plant functional group on leaf $C_i:C_a$ (unitless)*

	df	Coefficient	χ^2	<i>p</i>
Intercept	-	1.32E+00	-	-
Vapor pressure deficit (VPD_4)	1	-4.53E-01	10.987	<0.001
Soil moisture (SM_{90})	1	-1.71E-01	0.039	0.843
Soil N (N)	1	-1.71E-03	0.043	0.549
PFT	2	-	205.274	<0.001
SM_{90}^*N	1	7.29E-03	2.266	0.132
VPD_4^*PFT	2	-	0.887	0.642
SM_{90}^*PFT	2	-	0.814	0.666
N^*PFT	2	-	4.158	0.125
$SM_{90}^*N^*PFT$	2	-	3.465	0.177

1508 *Significance determined using Type II Wald χ^2 tests ($\alpha=0.05$). *P*-values less
1509 than 0.05 are in bold and *p*-values where $0.05 < p < 0.1$ are italicized. Leaf $C_i:C_a$
1510 was not transformed prior to model fitting, so model coefficients are reported
1511 on the response scale. Model coefficients are only included for continuous fixed
1512 effects. Key: df=degrees of freedom; χ^2 =Wald Type II chi-square test statistic

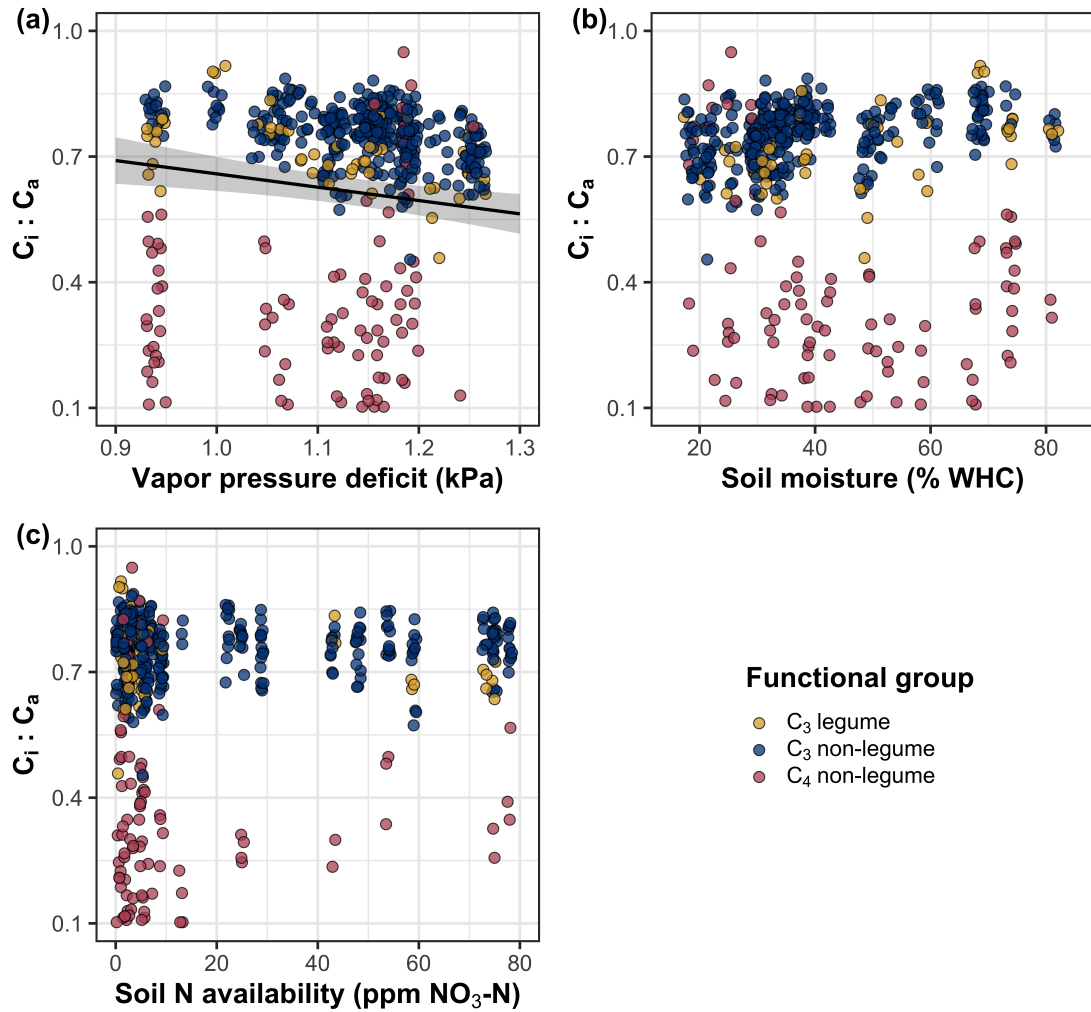


Figure 4.3. Effects of 4-day mean vapor pressure deficit (a), 90-day soil moisture (per water holding capacity; b), and soil nitrogen availability (c) on leaf $C_i:C_a$. Shading and trendlines are as explained in Figure 4.2. Points are jittered for visibility. Variably colored trendlines are only included if there is an interaction between the x-axis and plant functional group, where solid trendlines indicate slopes that are different from zero ($p < 0.05$) and dashed trendlines indicate slopes that are not different from zero ($p > 0.05$). Error ribbons represent the upper and lower 95% confidence intervals of each fitted trendline.

1513 4.3.3 *Leaf nitrogen content*

1514 An interaction between leaf $C_i:C_a$ and plant functional group ($p<0.001$; Table
1515 4.4) revealed that the negative effect of increasing leaf $C_i:C_a$ on N_{area} ($p<0.001$;
1516 Table 4.4) was driven by a negative effect of increasing leaf $C_i:C_a$ on N_{area} in
1517 C_3 non-fixers and C_3 N-fixers (Tukey: $p<0.001$ in both cases), but not C_4 non-
1518 fixers (Tukey: $p=0.786$; Fig. 4.4a). A marginal interaction between soil nitrogen
1519 availability and plant functional group ($p=0.057$; Table 4.4) indicated that the
1520 positive effect of increasing soil nitrogen ($p=0.007$; Table 4.4) was only apparent
1521 in C_3 N-fixers (Tukey: $p<0.001$; Table 4.4; Fig. 4.4d), but not C_3 non-fixers
1522 (Tukey: $p=0.329$) or C_4 non-fixers (Tukey: $p=0.682$). Increasing soil moisture
1523 increased N_{area} ($p=0.011$, Table 4.4). A plant functional group effect ($p<0.001$;
1524 Table 4.4) indicated that C_4 non-fixers had lower N_{area} compared to C_3 N-fixers
1525 and C_3 non-fixers (Tukey: $p<0.001$ in both cases), while C_3 N-fixers had lower
1526 N_{area} compared to C_3 non-fixers (Tukey: $p=0.024$).

1527 Leaf $C_i:C_a$ had no effect on N_{mass} ($p=0.455$; Table 4.4; Fig. 4.4b). Increas-
1528 ing soil nitrogen availability and soil moisture each had a positive effect on N_{mass}
1529 ($p<0.001$ in both cases; Table 4.4; Fig. 4.4h). A plant functional group effect
1530 ($p<0.001$; Table 4.4) indicated that C_4 non-fixers had lower N_{mass} compared to
1531 C_3 N-fixers and C_3 non-fixers (Tukey: $p=0.001$ in both cases), while N_{mass} did
1532 not differ between C_3 N-fixers and C_3 non-fixers (Tukey: $p=0.323$).

1533 Variance in M_{area} was driven by a three-way interaction between soil nitro-
1534 gen availability, soil moisture, and plant functional group ($p=0.018$; Table 4.4).
1535 This interaction indicated that increasing soil moisture increased the positive effect
1536 of increasing soil nitrogen availability on M_{area} in C_3 N-fixers (Tukey: $p=0.028$)

1537 but did not modify the negative effect of increasing soil nitrogen availability on
1538 M_{area} in C₄ non-fixers (Tukey: $p=0.806$) or C₃ non-fixers (Tukey: $p=0.998$). There
1539 was otherwise no effect of soil moisture on M_{area} ($p=0.436$; Table 4.4). An inter-
1540 action between leaf $C_i:C_a$ and plant functional group ($p<0.001$; Table 4.4; Fig.
1541 4.4c) indicated that the negative effect of increasing leaf $C_i:C_a$ on M_{area} ($p<0.001$;
1542 Table 4.4) was driven by a negative effect of increasing leaf $C_i:C_a$ on M_{area} in
1543 C₃ N-fixers (Tukey: $p<0.001$) and C₃ non-fixers(Tukey: $p=0.003$), but not C₄
1544 non-fixers (Tukey: $p=0.257$; Fig. 4.4c).

Table 4.4. Effects of soil moisture, soil nitrogen availability, plant functional group, and leaf $C_i:C_a$ on leaf nitrogen content per unit leaf area (N_{area} ; gN m $^{-2}$), leaf nitrogen content per unit leaf biomass (N_{mass} ; gN g $^{-1}$), and leaf biomass per unit leaf area (M_{area} ; g m $^{-2}$)

		N_{area}			N_{mass}			M_{area}		
	df	Coefficient	χ^2	p	Coefficient	χ^2	p	Coefficient	χ^2	p
(Intercept)	-	2.41E+00	-	-	7.72E-02	-	-	6.91E+00	-	-
$C_i:C_a$	1	-2.32E+00	6.841	0.009	7.91E-01	0.558	0.455	-3.13E+00	15.913	<0.001
Soil N (N)	1	1.26E-02	7.072	0.011	1.21E-02	87.457	<0.001	-2.66E-02	41.791	<0.001
Soil moisture (SM ₉₀)	1	5.60E-01	6.493	0.011	7.94E-01	10.889	<0.001	-2.54E-01	0.605	0.437
PFT	1	-	49.273	<0.001	-	21.786	<0.001	-	6.673	0.036
SM ₉₀ *N	1	5.45E-02	0.482	0.488	-2.18E-02	2.606	0.106	8.16E-02	0.791	0.374
$C_i:C_a$ *PFT	1	-	24.380	<0.001	-	5.367	0.068	-	30.073	<0.001
N*PFT	1	-	5.713	0.057	-	1.286	0.526	-	19.405	<0.001
SM ₉₀ *PFT	1	-	3.487	0.175	-	0.889	0.641	-	2.998	0.223
SM ₉₀ *N*PFT	1	-	3.523	0.172	-	0.161	0.923	-	7.996	0.018

96

1545 *Significance determined using Type II Wald χ^2 tests ($\alpha=0.05$). P-values less than 0.05 are in bold and p-values
 1546 where $0.05 < p < 0.1$ are italicized. Coefficients are reported on the natural-log scale for all traits and are only included
 1547 for continuous fixed effects. Key: df=degrees of freedom; χ^2 =Wald Type II chi-square test statistic

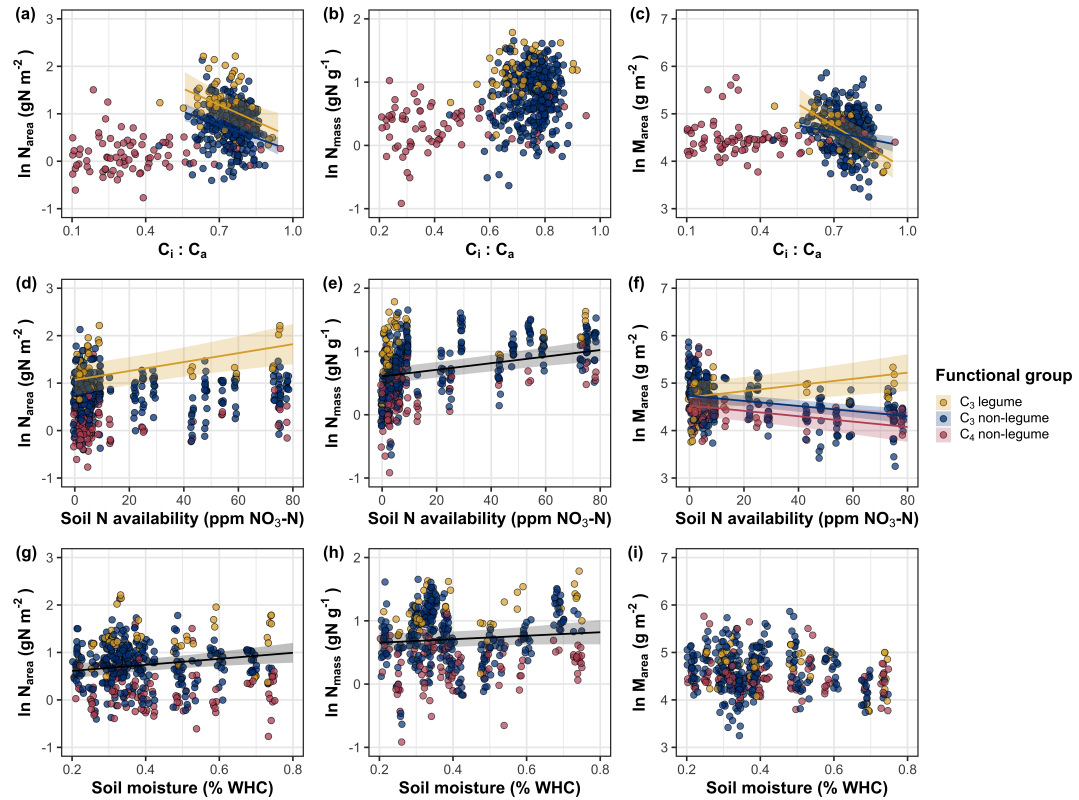


Figure 4.4. Effects of leaf $C_i:C_a$ (a-c), soil nitrogen availability (d-f), and soil moisture (g-i) on leaf nitrogen content per unit leaf area (a, d, g), leaf nitrogen content per unit leaf biomass (b, e, h), and leaf mass per area (c, f, i). Yellow points and trendlines indicate C₃ N-fixers, blue points and trendlines indicate C₃ non-fixers, and red points and trendlines indicate C₄ non-fixers. Points are jittered for visibility. Variably colored trendlines are only included if there is an interaction between plant functional group and the x-axis. Black solid trendlines denote bivariate slopes that are different from zero ($p < 0.05$) where there is no apparent interaction between plant functional group and the x-axis.

1548 4.3.4 *Structural equation model*

1549 The piecewise structural equation model explained 89%, 55%, 56%, 82%, and
1550 38% of variance in N_{area} , N_{mass} , M_{area} , leaf $C_i:C_a$, and β , respectively (Table
1551 4.5; Fig. 4.5). Increasing N_{mass} and M_{area} were each positively related to N_{area}
1552 ($p<0.001$ in both cases; Table 4.5; Fig. 4.5). N_{mass} increased with increasing
1553 soil nitrogen availability ($p<0.001$; Table 4.5) and leaf $C_i:C_a$ ($p=0.040$; Table
1554 4.5), and was generally larger in N-fixing species ($p<0.001$; Table 4.5), but was
1555 negatively related to increasing M_{area} ($p<0.001$; Table 4.5). M_{area} decreased with
1556 increasing leaf $C_i:C_a$ and soil nitrogen availability ($p<0.001$ in both cases; Table
1557 4.5). Leaf $C_i:C_a$ declined with increasing vapor pressure deficit, but was positively
1558 related to β ($p<0.001$ in both cases; Table 4.5). β decreased with increasing soil
1559 nitrogen availability and was higher in C₃ species ($p<0.001$ in both cases; Table
1560 4.5), but did not change with soil moisture ($p=0.895$; Table 4.5) or with ability
1561 to acquire nitrogen via symbiotic nitrogen fixation ($p=0.519$; Table 4.5). Finally,
1562 soil nitrogen availability was positively associated with increasing soil moisture
1563 ($p=0.003$; Table 4.5; Fig. 4.5).

Table 4.5. Structural equation model results investigating direct effects of climatic and soil resource availability on leaf nitrogen content (N_{area} ; g m⁻²)*

Predictor	Coefficient	<i>p</i>
N_{area} ($R^2_c=0.89$)		
M_{area}	0.714	<0.001
N_{mass}	0.778	<0.001
N_{mass} ($R^2_c=0.55$)		
Leaf $C_i:C_a$	0.113	0.040
M_{area}	-0.201	<0.001
Soil N	0.246	<0.001
N-fixing ability	0.326	<0.001
M_{area} ($R^2_c=0.56$)		
Leaf $C_i:C_a$	-0.224	<0.001
Soil N	-0.199	<0.001
Leaf $C_i:C_a$ ($R^2_c=0.82$)		
β	0.308	<0.001
VPD_4	-0.111	<0.001
β ($R^2_c=0.38$)		
Soil N	-0.207	<0.001
SM_{90}	-0.006	0.895
Photo. pathway	0.446	<0.001
N-fixing ability	-0.059	0.519
Soil N ($R^2_c=0.35$)		
SM_{90}	-0.148	0.003

1564 *Coefficients are standardized across the structural equation model. *P*-values less
 1565 than 0.05 are noted in bold. Positive coefficients for photosynthetic pathway
 1566 indicate generally larger values in C₃ species, while positive coefficients for N-
 1567 fixing ability indicate generally larger values in N-fixing species. Key: df=degrees
 1568 of freedom; χ^2 =Wald Type II chi-square test statistic; R^2_c =conditional R² value;
 1569 N_{mass} =leaf nitrogen content per unit leaf biomass (gN g⁻¹); M_{area} =leaf mass per
 1570 unit leaf biomass (g m⁻²); β =cost of acquiring nitrogen relative to water (unitless);
 1571 VPD_4 =4-day mean vapor pressure deficit (kPa); SM_{90} =90-day mean soil moisture
 1572 (mm)

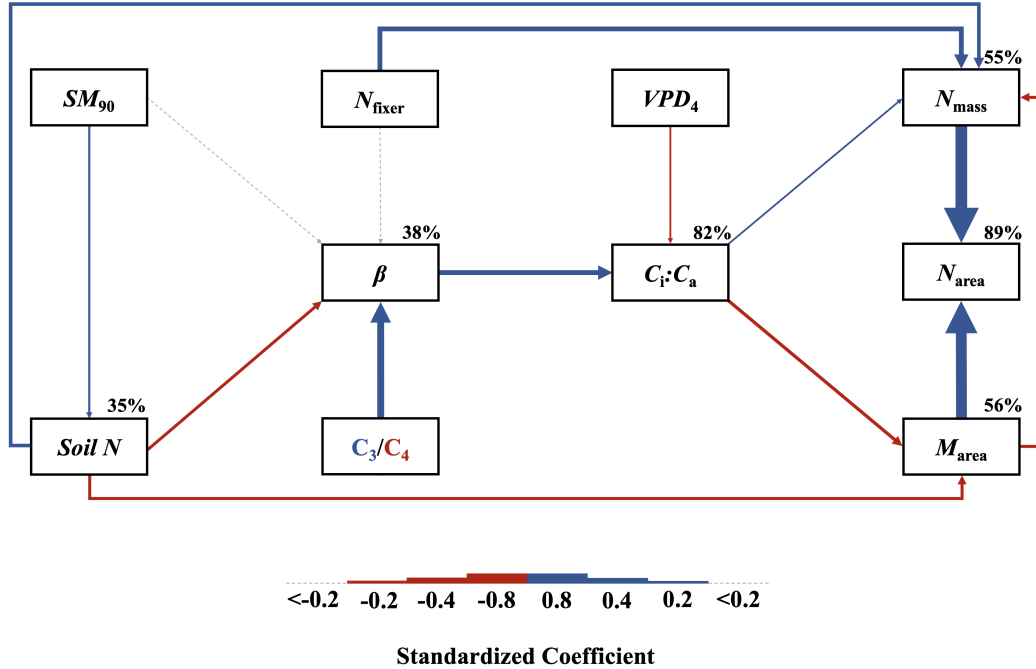


Figure 4.5. Structural equation model results exploring drivers of N_{area} . Boxes indicate measured edaphic factors, climatic factors, and leaf traits. Solid arrows indicate bivariate relationships where $p < 0.05$, while dashed arrows indicate relationships where $p > 0.05$. Positive model coefficients are indicated through blue arrows, negative model coefficients are indicated through red arrows, and insignificant coefficients are indicated through gray dashed arrows. Arrow thickness scales with the standardized model coefficient of each bivariate relationship. A positive coefficient for photosynthetic pathway indicates larger values in C₃ species, while a positive coefficient for N_{fixer} indicates larger values in N-fixing species. Standardized model coefficients and associated p -values are reported in Table 4.5, with conditional R² values for each response variable reported on the top right of each box.

1573 4.4 Discussion

1574 In this study, direct and indirect effects of edaphic and climatic characteristics on
1575 N_{area} and components of N_{area} (N_{mass} and M_{area}) were quantified in 504 individuals
1576 spanning across a soil resource availability and climate gradient in Texas, USA.
1577 Consistent patterns emerged in support of those expected from photosynthetic
1578 least-cost theory, a result driven by a strong direct negative relationship between
1579 leaf $C_i:C_a$ and N_{area} mediated through changes in M_{area} . In further support of
1580 patterns expected from theory, increasing soil nitrogen availability had a nega-
1581 tive effect on β , resulting in an indirect stimulation in N_{area} mediated through
1582 a positive relationship between β and $C_i:C_a$. Increasing vapor pressure deficit
1583 also indirectly increased N_{area} through a direct negative effect of increasing vapor
1584 pressure deficit on leaf $C_i:C_a$, following hypotheses and patterns expected from
1585 theory. Interestingly, a positive association between soil moisture and N_{area} was
1586 driven by covariance between soil moisture and soil nitrogen availability and was
1587 not associated with a direct effect of soil moisture on β . Overall, results provide
1588 strong and consistent support for patterns expected from photosynthetic least-cost
1589 theory, showing that both soil resource availability and climate drive variance in
1590 N_{area} through changes in leaf $C_i:C_a$.

1591 4.4.1 *Negative effects of leaf $C_i:C_a$ on N_{area} are driven by reductions in M_{area} ,*
1592 *not N_{mass}*

1593 The negative response of N_{area} to increasing leaf $C_i:C_a$ is consistent with pre-
1594 vious environmental gradient (Dong et al. 2017; Querejeta et al. 2022) and
1595 manipulation experiments (3.4c), showing strong support for the nitrogen-water

1596 use tradeoffs expected from photosynthetic least cost theory (Wright et al. 2003;
1597 Prentice et al. 2014). Negative effects of increasing leaf $C_i:C_a$ on N_{area} were driven
1598 by negative effect of increasing leaf $C_i:C_a$ on M_{area} coupled with a weak positive
1599 effect of increasing leaf $C_i:C_a$ on N_{mass} , suggesting that changes in N_{area} across
1600 the environmental gradient were driven more strongly by changes in leaf morphol-
1601 ogy than leaf chemistry. Interestingly, the negative relationship between M_{area}
1602 and N_{mass} suggested that stimulations in N_{mass} were often associated with larger,
1603 thinner leaves (i.e., lower M_{area}). These results are consistent with patterns re-
1604 ported from previous studies indicating that variance in N_{area} is driven by changes
1605 in M_{area} across environmental gradients, and that part of this response is due to
1606 negative covariance between M_{area} and N_{mass} (Dong et al. 2017; Dong et al. 2020).
1607 Negative covariance between M_{area} and N_{mass} could be a response associated with
1608 tradeoffs between leaf longevity and leaf productivity (Wright et al. 2004; Dong
1609 et al. 2017; Dong et al. 2022; Querejeta et al. 2022; Wang et al. 2023).

1610 The negative relationship between leaf $C_i:C_a$ and M_{area} could be indicative
1611 of tradeoffs between leaf longevity and leaf productivity. Tradeoffs between leaf
1612 longevity and leaf productivity are commonly observed and are included in a
1613 continuum of coordinated leaf traits that position individuals along a fast- or
1614 slow-growing leaf economics spectrum (Wright et al. 2003; Onoda et al. 2004;
1615 Reich 2014; Onoda et al. 2017; Wang et al. 2023). Negative relationships between
1616 leaf $C_i:C_a$ and M_{area} indicate that increased stomatal conductance and reduced
1617 water use efficiency were associated with thinner, larger leaves (i.e., lower M_{area}).
1618 Combined with the negative covariance between M_{area} and N_{mass} mentioned above,
1619 these responses may have allowed individuals to maximize light interception and

1620 productivity by exploiting high light environments at the expense of increased
1621 water loss and decreased water-use efficiency. This strategy may be especially
1622 advantageous for fast-growing species in open canopy systems. In this study, C₃
1623 N-fixers and C₃ non-fixers dominated the dataset (77% of total sampling effort),
1624 of which 23% (17% of total sampling effort) were classified as annual species with
1625 short growing seasons. We observed no effect of leaf $C_i:C_a$ on N_{area} or M_{area} in C₄
1626 non-fixers, which made up 23% of the sampling effort and were generally classified
1627 as warm season graminoid species with slower growth rates and longer growing
1628 seasons. These patterns indicate that stronger tradeoffs between nitrogen and
1629 water use may be more apparent in fast-growing species with high demand for
1630 building and maintaining productive leaf tissues.

1631 4.4.2 *Soil nitrogen availability increases N_{area} through changes in β*
1632 The structural equation model indicated multiple pathways where increasing soil
1633 nitrogen availability increased N_{area} . First, N_{area} increased with increasing soil
1634 nitrogen availability due to larger positive direct effects of increasing soil nitrogen
1635 availability on N_{mass} than the corresponding negative direct effect of increasing
1636 soil nitrogen availability on M_{area} . These patterns corroborate those observed in
1637 the individual linear mixed effect models and previous work. Second, soil nitrogen
1638 availability increased N_{area} indirectly through reductions in β , which increased leaf
1639 $C_i:C_a$ and stimulated N_{area} through a stronger negative effect of increasing leaf
1640 $C_i:C_a$ on M_{area} than corresponding positive effect of increasing leaf $C_i:C_a$ on N_{mass} .
1641 Reductions in β with increasing soil nitrogen availability were likely driven by re-
1642 ductions in the cost of acquiring and using nitrogen, following patterns observed

1643 in previous experiments (Bae et al. 2015; Eastman et al. 2021; Perkowski et al.
1644 2021; Lu et al. 2022). These pathways indicate that soil nitrogen availability can
1645 have direct positive effects on N_{area} by increasing leaf nitrogen concentration, fol-
1646 lowing previous work (Firn et al. 2019; Liang et al. 2020), or can alternatively have
1647 indirect positive effects on N_{area} through changes in leaf morphology associated
1648 with a reduction in the cost of acquiring nitrogen, following patterns expected
1649 from photosynthetic least-cost theory. Results reported here indicate that pho-
1650 tosynthetic least-cost frameworks are capable of detecting predictable variance in
1651 N_{area} and tradeoffs between nitrogen and water use across soil nitrogen availability
1652 gradients.

1653 4.4.3 *Soil moisture increases N_{area} by facilitating increases in soil nitrogen
1654 availability*

1655 Increasing soil moisture had a positive effect on N_{area} , though this response was
1656 associated with a null effect of soil moisture on β . These results contrast patterns
1657 expected from theory, where increasing soil moisture is expected to indirectly
1658 decrease N_{area} through an increase in β due to a reduction in costs associated
1659 with water acquisition and use (Wright et al. 2003; Prentice et al. 2014; Lavergne
1660 et al. 2020). Interestingly, structural equation model results revealed a strong
1661 positive association between soil moisture and soil nitrogen availability, indicating
1662 an indirect positive effect of increasing soil moisture on N_{area} mediated by the
1663 negative effect of increasing soil nitrogen availability on β . In Texan grasslands,
1664 productivity and nutrient uptake are often co-limited by precipitation and nutrient
1665 availability (Yahdjian et al. 2011; Wang et al. 2017). Thus, increases in soil
1666 moisture may have facilitated more favorable and productive environments for
1667 soil microbial communities (Reichman et al. 1966; Stark and Firestone 1995;

1668 Paul et al. 2003), or alternatively greater nitrogen mobility in soil solution. As
1669 discussed above, the positive indirect response of N_{area} to increasing soil nitrogen
1670 availability as mediated through reductions in β follow patterns expected from
1671 theory.

1672 4.4.4 *Indirect effects of climate on N_{area} are mediated through changes in leaf*
1673 $C_i:C_a$ *and β*

1674 In support of hypotheses and patterns expected from theory, increasing vapor
1675 pressure deficit indirectly increased N_{area} , mediated through the negative effect
1676 of increasing vapor pressure deficit on leaf $C_i:C_a$. These responses are consistent
1677 with previous work noting strong reductions in stomatal conductance with increas-
1678 ing vapor pressure deficit (Oren et al. 1999; Novick et al. 2016; Sulman et al.
1679 2016; Grossiord et al. 2020; López et al. 2021), a response that allows plants
1680 to minimize water loss as a result of high atmospheric water demand. Results
1681 also support findings from previous experiments across environmental gradients,
1682 where increasing vapor pressure deficit generally increases N_{area} at lower stomatal
1683 conductance across environmental gradients (Dong et al. 2017; Dong et al. 2022;
1684 Paillassa et al. 2020; Westerband et al. 2023). The increase in N_{area} with increas-
1685 ing vapor pressure deficit could allow plants to maximize photosynthetic capacity
1686 under reduced stomatal conductance (Dong et al. 2022), though this pattern con-
1687 trasts previous work suggesting that long-term increases in vapor pressure deficit
1688 are associated with increased plant mortality, reduced net primary productivity,
1689 and perhaps reductions in net photosynthesis rates over time due to prolonged
1690 stomatal closure (Eamus et al. 2013; Yuan et al. 2019; Grossiord et al. 2020).
1691 Importantly, such negative effects of increasing vapor pressure deficit often occur
1692 along much broader timescales compared to the timescale used here. Responses

1693 observed here suggest that variance in N_{area} across environmental gradients is
1694 a deterministic acclimation response to changing aboveground climate, allowing
1695 plants to satisfy demand to build and maintain photosynthetic enzymes and op-
1696 timize photosynthetic processes by maximizing resource use efficiency (Paillassa
1697 et al. 2020; Peng et al. 2021; Dong et al. 2022; Westerband et al. 2023).

1698 4.4.5 *Species identity traits modify effects of the environment on β , leaf $C_i:C_a$,*
1699 *and N_{area}*

1700 N-fixing species had greater N_{area} values on average compared to non-fixing species,
1701 a pattern driven by a stronger stimulation in N_{mass} in N-fixing species coupled with
1702 no change in M_{area} between species with different N-fixation ability. There was
1703 no evidence to suggest that N-fixing species had different β or leaf $C_i:C_a$ values
1704 compared to non-fixing species across the environmental gradient. These results
1705 follow patterns from previous environmental gradient experiments that investi-
1706 gate variance in leaf nitrogen allocation in N-fixing species (Adams et al. 2016;
1707 Dong et al. 2017; Dong et al. 2020), and that increases in N_{mass} and N_{area} in
1708 N-fixing species are not necessarily correlated to increases in water use efficiency
1709 or reductions in leaf $C_i:C_a$ (Adams et al. 2016). While results are consistent with
1710 results from previous environmental gradient experiments, they do not support
1711 hypotheses presented here or patterns expected from theory, which predicts that
1712 stimulations in N_{area} by N-fixing species should be driven by a reduction in β
1713 relative to non-fixing species, and that this response should decrease stomatal
1714 conductance and leaf $C_i:C_a$.

1715 C₄ species had reduced β , leaf $C_i:C_a$, and N_{area} than C₃ species. Reduced
1716 β and leaf $C_i:C_a$ values in C₄ species follow hypotheses listed above, a pattern

1717 that could be the result of either reduced costs of nitrogen acquisition and use,
1718 increased costs of water acquisition and use, or both (Wright et al. 2003; Prentice
1719 et al. 2014). Results also indicate that β in C₄ non-fixers was unresponsive to
1720 changes in soil nitrogen availability despite an apparent negative effect of increas-
1721 ing soil nitrogen availability on β in C₃ N-fixers and C₃ non-fixers. Combined
1722 with a general null response of β to soil moisture regardless of plant functional
1723 group, these patterns imply that reduced β values in C₄ species may be the re-
1724 sult of lower costs of nitrogen acquisition and use relative to C₃ species. While
1725 lower β values in C₄ species provides a possible explanation for why C₄ species
1726 often have lower leaf $C_i:C_a$ and greater water use efficiency, theory predicts that
1727 this response should cause C₄ species to have greater N_{area} values compared to
1728 C₃ species, though C₄ species commonly exhibit lower N_{area} and higher nitrogen
1729 use efficiency than C₃ species (Schmitt and Edwards 1981; Sage and Pearcy 1987;
1730 Ghannoum et al. 2011). We speculate that lowered costs of nitrogen acquisition
1731 and use in C₄ species could be driven by more efficient Rubisco carboxylation effi-
1732 ciency in C₄ species associated with CO₂ concentrating mechanisms that eliminate
1733 photorespiration (Ghannoum et al. 2011), which could reduce or eliminate the
1734 need to sacrifice inefficient nitrogen use for efficient water use to achieve optimal
1735 photosynthesis rates.

1736 4.4.6 *Next steps for optimality model development*

1737 Optimality models for both C₃ and C₄ species have been developed using principles
1738 from photosynthetic least-cost theory (Prentice et al. 2014; Wang et al. 2017;
1739 Smith et al. 2019; Stocker et al. 2020; Scott and Smith 2022). In both C₃ and C₄
1740 model variants, β values are held constant using global datasets of leaf $\delta^{13}\text{C}$ (Wang

1741 et al. 2017; Cornwell et al. 2018). Specifically, the C₃ optimality model initially
1742 assumed a constant β value of 240 (Wang et al. 2017), later corrected to 146
1743 (Stocker et al. 2020), while the C₄ optimality model assumes a constant β value of
1744 166 (Scott and Smith 2022). These results, which build on findings from Paillassa
1745 et al. (2020) and Lavergne et al. (2020), demonstrate high variability in calculated
1746 β values across the environmental gradient. Specifically, β values in C₃ species
1747 ranged from 1.7 to 188.0 (mean: 30.2; median: 23.1; standard deviation: 25.4),
1748 while ranged from 0.1 to 110.6 in C₄ species (mean: 7.2; median: 0.7; standard
1749 deviation: 18.6). Mean β values in both C₃ and C₄ species were consistently lower
1750 than values currently implemented in optimality models, though this was likely
1751 the result of increased water limitation across sites relative to global averages.
1752 Regardless, the high degree of β variability across this environmental gradient,
1753 together with findings from Lavergne et al. (2020) and Paillassa et al. (2020),
1754 suggests that the use of constant β values may contribute to erroneous errors when
1755 conducting optimality model simulations. Results from this experiment build
1756 on suggestions from Wang et al. (2017), suggesting that future photosynthetic
1757 least-cost optimality model developments should consider adopting frameworks
1758 for dynamically calculating β .

1759 4.4.7 *Conclusions*

1760 To summarize, variability in N_{area} across an environmental gradient in Texan
1761 grasslands was driven by indirect effects of climate and soil resource availability
1762 mediated by changes in β and leaf $C_i:C_a$. Results from this experiment provide
1763 strong and consistent support for patterns expected from photosynthetic least-

1764 cost theory, demonstrating that negative relationships between $C_i:C_a$ and N_{area}
1765 unify expected effects of climatic and edaphic characteristics on N_{area} across en-
1766 vironmental gradients. Results reported here also demonstrate a need to consider
1767 the dynamic nature of the relative cost of nitrogen versus water uptake (β) across
1768 environmental gradients in optimality models that leverage principles of photo-
1769 synthetic least-cost theory.

1770

Chapter 5

1771 Optimal resource investment to photosynthetic capacity maximizes
1772 nutrient allocation to whole plant growth under elevated CO₂

1773 5.1 Introduction

1774 Terrestrial ecosystems are regulated by complex carbon and nitrogen cycles. As
1775 a result, terrestrial biosphere models, which are beginning to include coupled
1776 carbon and nitrogen cycles (Shi et al. 2016; Davies-Barnard et al. 2020; Braghieri
1777 et al. 2022), must accurately represent these cycles under different environmental
1778 scenarios to reliably simulate carbon and nitrogen atmosphere-biosphere fluxes
1779 (Hungate et al. 2003; Prentice et al. 2015). While the inclusion of coupled carbon
1780 and nitrogen cycles tends to reduce model uncertainty (Arora et al. 2020), large
1781 uncertainty in role of soil nitrogen availability and nitrogen acquisition strategy
1782 on leaf and whole plant acclimation responses to CO₂ remains (Smith and Dukes
1783 2013; Terrer et al. 2018; Smith and Keenan 2020). This source of uncertainty
1784 likely contributes to the widespread divergence in future carbon and nitrogen flux
1785 simulations across terrestrial biosphere models (Friedlingstein et al. 2014; Zaehle
1786 et al. 2014; Meyerholt et al. 2020).

1787 Plants grown under elevated CO₂ generally have less leaf nitrogen content
1788 than those grown under ambient CO₂, a response that often corresponds with
1789 reductions in photosynthetic capacity and stomatal conductance at the leaf-level
1790 and biomass stimulation over time at the whole plant level (Curtis 1996; Drake
1791 et al. 1997; Ainsworth et al. 2002; Makino 2003; Morgan et al. 2004; Ainsworth
1792 and Long 2005; Ainsworth and Rogers 2007; Smith and Dukes 2013; Poorter et al.
1793 2022). As net primary productivity is generally limited by nitrogen availability

1794 (Vitousek and Howarth 1991; LeBauer and Treseder 2008; Fay et al. 2015), and
1795 soil nitrogen availability is often positively correlated with leaf nitrogen content
1796 and photosynthetic capacity (Field and Mooney 1986; Evans and Seemann 1989;
1797 Evans 1989; Walker et al. 2014; Firn et al. 2019; Liang et al. 2020), some
1798 have hypothesized that leaf and whole plant acclimation responses to CO₂ are
1799 constrained by soil nitrogen availability.

1800 The progressive nitrogen limitation hypothesis predicts that elevated CO₂
1801 will increase plant nitrogen demand, which will increase plant nitrogen uptake and
1802 progressively deplete soil nitrogen if soil nitrogen supply does not exceed plant
1803 nitrogen demand (Luo et al. 2004). The hypothesis predicts that this response
1804 should result in strong acute stimulations in whole plant growth and primary
1805 productivity that diminish over time as nitrogen becomes more limiting. Assuming
1806 a positive relationship between soil nitrogen availability, leaf nitrogen content, and
1807 photosynthetic capacity, this hypothesis also implies that progressive reductions in
1808 soil nitrogen availability should be the mechanism that drives the downregulation
1809 of leaf nitrogen content and photosynthetic capacity under elevated CO₂. This
1810 hypothesis has received some support from free air CO₂ enrichment experiments
1811 (Reich et al. 2006; Norby et al. 2010), although is not consistently observed across
1812 experiments (Finzi et al. 2006; Moore et al. 2006; Liang et al. 2016).

1813 While possible that progressive nitrogen limitation may determine leaf and
1814 whole plant acclimation responses to CO₂, growing evidence indicates that leaf ni-
1815 trogen and photosynthetic capacity are more strongly determined through above-
1816 ground growing conditions than by soil resource availability (Dong et al. 2017;
1817 Dong et al. 2020; Dong et al. 2022; Smith et al. 2019; Smith and Keenan 2020;

1818 Paillassa et al. 2020; Peng et al. 2021; Querejeta et al. 2022; Westerband et al.
1819 2023), and satellite-derived chlorophyll fluorescence data indicate that increasing
1820 atmospheric CO₂ may decrease leaf and canopy demand for nitrogen (Dong et al.
1821 2022). Together, results from these studies suggest that the downregulation in
1822 leaf nitrogen content and photosynthetic capacity due to increasing CO₂ may not
1823 be as tightly linked to progressive nitrogen limitation as previously hypothesized.

1824 A unification of optimal coordination and least-cost theories predicts that
1825 leaves acclimate to elevated CO₂ by downregulating nitrogen allocation to Ribulose-
1826 1,5-bisphosphate (RuBP) carboxylase/oxygenase (Rubisco) to optimize resource
1827 use efficiencies at the leaf level, which allows for greater resource allocation to
1828 whole plant growth (Drake et al. 1997; Wright et al. 2003; Prentice et al. 2014;
1829 Smith et al. 2019). The theory predicts that the downregulation in nitrogen
1830 allocation to Rubisco results in a stronger downregulation in the maximum rate
1831 of Rubisco carboxylation (V_{cmax}) than the maximum rate of RuBP regeneration
1832 (J_{max}), which maximizes photosynthetic efficiency by allowing net photosynthesis
1833 rates to be equally co-limited by Rubisco carboxylation and RuBP regeneration
1834 (Chen et al. 1993; Maire et al. 2012). This acclimation response allows plants to
1835 make more efficient use of available light while avoiding overinvestment in Rubisco,
1836 which has high nitrogen and energetic costs of building and maintaining (Evans
1837 1989; Evans and Clarke 2019). Instead, additional acquired resources not needed
1838 to optimize leaf photosynthesis are allocated to the maintenance of structures that
1839 support whole plant growth (e.g., total leaf area, whole plant biomass, etc.) or
1840 to allocation processes not related to leaf photosynthesis or growth, such as plant
1841 defense mechanisms. Regardless, optimized resource allocation at the leaf level

1842 should allow for greater resource allocation to whole plant growth. The theory
1843 indicates that leaf acclimation responses to CO₂ should be independent of changes
1844 in soil nitrogen availability. While this leaf acclimation response maximizes nitro-
1845 gen allocation to structures that support whole plant growth, the theory suggests
1846 that the positive effect of elevated CO₂ on whole plant growth may be further
1847 stimulated by soil nitrogen availability through reductions in the cost of acquiring
1848 nitrogen (Bae et al. 2015; Perkowski et al. 2021; Lu et al. 2022).

1849 Plants acquire nitrogen by allocating photosynthetically derived carbon be-
1850 lowground in exchange for nitrogen through different nitrogen acquisition strate-
1851 gies. These nitrogen acquisition strategies can include direct uptake pathways
1852 such as mass flow or diffusion (Barber 1962), symbioses with mycorrhizal fungi or
1853 symbiotic nitrogen-fixing bacteria (Vance and Heichel 1991; Marschner and Dell
1854 1994; Smith and Read 2008; Udvardi and Poole 2013), or through the release
1855 of root exudates that prime free-living soil microbial communities (Phillips et al.
1856 2011; Wen et al. 2022). Plants cannot acquire nitrogen without first allocating
1857 carbon belowground, which implies an inherent carbon cost to the plant for acquir-
1858 ing nitrogen regardless of nitrogen acquisition strategy. Carbon costs to acquire
1859 nitrogen often vary in species with different nitrogen acquisition strategies and
1860 are dependent on external environmental factors such as atmospheric CO₂, light
1861 availability, and soil nitrogen availability (Brzostek et al. 2014; Terrer et al. 2016;
1862 Terrer et al. 2018; Allen et al. 2020; Perkowski et al. 2021; Lu et al. 2022). These
1863 patterns suggest that acquisition strategy may at least partially determine the net
1864 effect of soil nitrogen availability on leaf and whole plant acclimation responses to
1865 elevated CO₂.

1866 A recent meta-analysis using data across 20 grassland and forest CO₂ en-
1867 richment experiments suggested that species which acquire nitrogen from sym-
1868 biotic nitrogen-fixing bacteria had reduced costs of nitrogen acquisition under
1869 elevated CO₂ (Terrer et al. 2018). Though these analyses only included data
1870 from two experimental sites, findings from this meta-analysis indicated that re-
1871 ductions in costs of nitrogen acquisition in species that form associations with
1872 symbiotic nitrogen-fixing bacteria under elevated CO₂ may drive stronger stim-
1873 ulations in whole plant growth and downregulations in V_{cmax} than species that
1874 associate with arbuscular mycorrhizal fungi (Smith and Keenan 2020), which gen-
1875 erally have greater costs of nitrogen acquisition under elevated CO₂ (Terrer et al.
1876 2018). However, plant investments in symbiotic nitrogen fixation generally de-
1877 cline with increasing nitrogen availability (Dovrat et al. 2018; Perkowski et al.
1878 2021), a response that has been previously inferred to be the result of a shift in
1879 the dominant mode of nitrogen acquisition to direct uptake pathways as costs of
1880 direct uptake decrease with increasing soil nitrogen availability (Rastetter et al.
1881 2001; Perkowski et al. 2021). Thus, effects of symbiotic nitrogen fixation on plant
1882 acclimation responses to CO₂ should decline with increasing soil nitrogen avail-
1883 ability, although manipulative experiments that directly test these patterns are
1884 rare.

1885 Here, I conducted a 7-week growth chamber experiment using *Glycine max*
1886 L. (Merr.) to examine the effects of soil nitrogen fertilization and inoculation with
1887 symbiotic nitrogen-fixing bacteria on leaf and whole plant acclimation responses
1888 to elevated CO₂. Following patterns expected from theory, I hypothesized that in-
1889 dividual leaves should acclimate to elevated CO₂ by more strongly downregulating

1890 V_{cmax} relative to J_{max} , allowing leaf photosynthesis to approach optimal coordi-
1891 nation. I expected this response to correspond with a stronger downregulation in
1892 leaf nitrogen content than V_{cmax} and J_{max} , which would increase the fraction of
1893 leaf nitrogen content allocated to photosynthesis and photosynthetic nitrogen use
1894 efficiency. At the whole-plant level, I hypothesized that plants would acclimate
1895 to elevated CO₂ by stimulating whole plant growth and productivity, a response
1896 that would be driven by a strong positive response of total leaf area and above-
1897 ground biomass to elevated CO₂. I predicted that leaf acclimation responses to
1898 elevated CO₂ would be independent of soil nitrogen fertilization and inoculation
1899 with symbiotic nitrogen-fixing bacteria; however, I expected that increasing soil
1900 nitrogen fertilization would increase the positive effect of elevated CO₂ on mea-
1901 sures of whole plant growth due to a stronger reduction in the cost of acquiring
1902 nitrogen under elevated CO₂ with increasing fertilization. I also expected stronger
1903 stimulations in whole plant growth due to inoculation, but that this effect would
1904 only be apparent under low fertilization due to a reduction in root nodulation
1905 with increasing fertilization.

1906 5.2 Methods

1907 5.2.1 *Seed treatments and experimental design*

1908 *Glycine max* L. (Merr) seeds were planted in 144 6-liter surface sterilized pots (NS-
1909 600, Nursery Supplies, Orange, CA, USA) containing a steam-sterilized 70:30 v:v
1910 mix of Sphagnum peat moss (Premier Horticulture, Quakertown, PA, USA) to
1911 sand (Pavestone, subsidiary of Quikrete Companies, Atlanta, GA, USA). Before
1912 planting, all *G. max* seeds were surface sterilized in 2% sodium hypochlorite for 3

1913 minutes, followed by three separate 3-minute washes with ultrapure water (MilliQ
1914 7000; MilliporeSigma, Burlington, MA USA). A subset of surface sterilized seeds
1915 were inoculated with *Bradyrhizobium japonicum* (Verdesian N-DureTM Soybean,
1916 Cary, NC, USA) in a slurry following manufacturer recommendations (3.12 g
1917 inoculant and 241 g deionized water per 1 kg seed).

1918 Seventy-two pots were randomly planted with surface-sterilized seeds inoc-
1919 ulated with *B. japonicum*, while the remaining 72 pots were planted with surface-
1920 sterilized uninoculated seeds. Thirty-six pots within each inoculation treatment
1921 were randomly placed in one of two atmospheric CO₂ treatments (ambient and
1922 1000 $\mu\text{mol mol}^{-1}$ CO₂). Pots within each unique inoculation-by-CO₂ treatment
1923 combination randomly received one of nine soil nitrogen fertilization treatments
1924 equivalent to 0, 35, 70, 105, 140, 210, 280, 350, or 630 ppm N. Nitrogen fertil-
1925 ization treatments were created using a modified Hoagland solution (Hoagland
1926 and Arnon 1950) designed to keep concentrations of other macronutrients and
1927 micronutrients equivalent across treatments (Table D1). Pots received the same
1928 fertilization treatment throughout the entire duration experiment, which were ap-
1929 plied twice per week in 150 mL doses as topical agents to the soil surface. This
1930 experimental design yielded a fully factorial experiment with four replicates per
1931 unique fertilization-by-inoculation-by-CO₂ combination.

1932 5.2.2 *Growth chamber conditions*

1933 Upon experiment initiation, pots were randomly placed in one of six Percival
1934 LED-41L2 growth chambers (Percival Scientific Inc., Perry, IA, USA) over two
1935 experimental iterations due to chamber space limitation. Two iterations were

1936 conducted such that one iteration included all elevated CO₂ pots and the second
1937 iteration included all ambient CO₂ pots. Mean (\pm SD) CO₂ concentrations across
1938 chambers throughout the experiment were $439 \pm 5 \mu\text{mol mol}^{-1}$ CO₂ for the ambient
1939 CO₂ treatment and $989 \pm 4 \mu\text{mol mol}^{-1}$ CO₂ for the elevated CO₂ treatment.

1940 Daytime growing conditions were simulated using a 16-hour photoperiod,
1941 with incoming light radiation set to chamber maximum (mean \pm SD: 1240 ± 32
1942 $\mu\text{mol m}^{-2} \text{s}^{-1}$ across chambers), air temperature set to 25°C, and relative humid-
1943 ity set to 50%. The remaining 8 hours simulated nighttime growing conditions,
1944 with incoming light radiation set to 0 $\mu\text{mol m}^{-2} \text{s}^{-1}$, chamber temperature set
1945 to 17°C, and relative humidity set to 50%. Transitions between daytime and
1946 nighttime growing conditions were simulated by ramping incoming light radiation
1947 in 45-minute increments and temperature in 90-minute increments over a 3-hour
1948 period (Table D2).

1949 Including the two, 3-hour ramping periods, pots grew under average (\pm SD)
1950 daytime light intensity of $1049 \pm 27 \mu\text{mol m}^{-2} \text{s}^{-1}$. In the elevated CO₂ iteration,
1951 pots grew under $24.0 \pm 0.2^\circ\text{C}$ during the day, $16.4 \pm 0.8^\circ\text{C}$ during the night, and
1952 51.6 \pm 0.4% relative humidity. In the ambient CO₂ iteration, pots grew under
1953 $23.9 \pm 0.2^\circ\text{C}$ during the day, $16.0 \pm 1.4^\circ\text{C}$ during the night, and 50.3 \pm 0.2% relative
1954 humidity. I accounted for any climatic differences across the six chambers by
1955 shuffling the same group of pots daily throughout the growth chambers. This
1956 process was done by iteratively moving the group of pots on the top rack of a
1957 chamber to the bottom rack of the same chamber, while simultaneously moving
1958 the group of pots on the bottom rack of a chamber to the top rack of the adjacent
1959 chamber. I moved pots within and across chambers every day throughout the

1960 course of each experiment iteration.

1961 5.2.3 *Leaf gas exchange measurements*

1962 Gas exchange measurements were collected for all individuals on the seventh week

1963 of development. All gas exchange measurements were collected on the center leaf

1964 of the most recent fully expanded trifoliate leaf set. Specifically, I measured net

1965 photosynthesis (A_{net} ; $\mu\text{mol m}^{-2} \text{s}^{-1}$), stomatal conductance (g_{sw} ; $\text{mol m}^{-2} \text{s}^{-1}$),

1966 and intercellular CO_2 (C_i ; $\mu\text{mol mol}^{-1}$) concentrations across a range of atmo-

1967 spheric CO_2 concentrations (i.e., an A_{net}/C_i curve) using the Dynamic Assimila-

1968 tion TechniqueTM. The Dynamic Assimilation TechniqueTM has been shown to

1969 correspond well with traditional steady-state CO_2 response curves in *G. max*

1970 (Saathoff and Welles 2021). A_{net}/C_i curves were generated along a reference CO_2

1971 ramp down from $420 \mu\text{mol mol}^{-1} \text{CO}_2$ to $20 \mu\text{mol mol}^{-1} \text{CO}_2$, followed by a ramp

1972 up from $420 \mu\text{mol mol}^{-1} \text{CO}_2$ to $1620 \mu\text{mol mol}^{-1} \text{CO}_2$ after a 90-second wait

1973 period at $420 \mu\text{mol mol}^{-1} \text{CO}_2$. The ramp rate for each curve was set to 200

1974 $\mu\text{mol mol}^{-1} \text{min}^1$, logging every five seconds, which generated 96 data points per

1975 response curve. All A_{net}/C_i curves were generated after A_{net} and g_{sw} stabilized

1976 in a LI-6800 cuvette set to a 500 mol s^{-1} , 10,000 rpm mixing fan speed, 1.5 kPa

1977 vapor pressure deficit, 25°C leaf temperature, $2000 \mu\text{mol m}^{-2} \text{s}^{-1}$ incoming light

1978 radiation, and initial reference CO_2 set to $420 \mu\text{mol mol}^{-1}$.

1979 With the same focal leaf used to generate A_{net}/C_i curves, I measured dark

1980 respiration (R_{d25} ; $\mu\text{mol m}^{-2} \text{s}^{-1}$) following at least a 30-minute period of darkness.

1981 Measurements were collected on a 5-second log interval for 60 seconds after stabi-

1982 lizing in a LI-6800 cuvette set to a 500 mol s^{-1} , 10,000 rpm mixing fan speed, 1.5

1983 kPa vapor pressure deficit, 25°C leaf temperature, and 420 $\mu\text{mol mol}^{-1}$ reference
1984 CO₂ concentration (for both CO₂ concentrations), with incoming light radiation
1985 set to 0 $\mu\text{mol m}^{-2} \text{s}^{-1}$. A single dark respiration value was determined for each
1986 focal leaf by calculating the mean dark respiration value (i.e. the absolute value
1987 of A_{net} during the logging period) across the logging interval.

1988 5.2.4 *Leaf trait measurements*

1989 The focal leaf used to generate A_{net}/C_i curves and dark respiration was harvested
1990 immediately following gas exchange measurements. Images of each focal leaf were
1991 curated using a flat-bed scanner to determine wet leaf area using the ‘LeafArea’ R
1992 package (Katabuchi 2015), which automates leaf area calculations using ImageJ
1993 software (Schneider et al. 2012). Each leaf was dried at 65°C for at least 48
1994 hours, and subsequently weighed and ground until homogenized. Leaf mass per
1995 area (M_{area} ; g m^{-2}) was calculated as the ratio of dry leaf biomass to fresh leaf
1996 area. Using subsamples of ground and homogenized leaf tissue, I measured leaf
1997 nitrogen content (N_{mass} ; gN g^{-1}) through elemental combustion analysis (Costech-
1998 4010, Costech, Inc., Valencia, CA, USA). Leaf nitrogen content per unit leaf area
1999 (N_{area} ; gN m^{-2}) was calculated by multiplying N_{mass} and M_{area} . Subsamples of
2000 ground and homogenized leaf tissue were also sent to the UC-Davis Stable Isotope
2001 Facility to quantify leaf $\delta^{15}\text{N}$, later used to estimate the fraction of leaf nitrogen
2002 derived from the atmosphere.

2003 I extracted chlorophyll content from a second leaf in the same trifoliolate
2004 leaf set as the focal leaf used to generate A_{net}/C_i curves. Prior to chlorophyll
2005 extraction, I used a cork borer to punch between 3 and 5 0.6 cm² disks from the

2006 leaf. Separate images of each punched leaf and set of leaf disks were curated using
2007 a flat-bed scanner to determine wet leaf area, again quantified using the ‘LeafArea’
2008 R package (Katabuchi 2015). The punched leaf was dried and weighed after at
2009 least 65°C in the drying oven to determine M_{area} of the chlorophyll leaf.

2010 Leaf disks were shuttled into a test tube containing 10mL dimethyl sulfoxide, vortexed, and incubated at 65°C for 120 minutes (Barnes et al. 1992). Incubated test tubes were vortexed again before loaded in 150 μL triplicate aliquots to
2013 a 96-well plate. Dimethyl sulfoxide was also loaded in a 150 μL triplicate aliquot
2014 as a blank. Absorbance measurements at 649.1 nm ($A_{649.1}$) and 665.1 nm ($A_{665.1}$)
2015 were read in each well using a plate reader (Bioteck Synergy H1; Bioteck Instruments, Winooski, VT USA) (Wellburn 1994), with triplicates subsequently averaged and corrected by the mean of the blank absorbance value. Blank-corrected
2018 absorbance values were used to estimate Chl_a ($\mu\text{g mL}^{-1}$) and Chl_b ($\mu\text{g mL}^{-1}$)
2019 following equations from Wellburn (1994):

$$Chl_a = 12.47A_{665.1} - 3.62A_{649.1} \quad (5.1)$$

2020 and

$$Chl_b = 25.06A_{665.1} - 6.50A_{649.1} \quad (5.2)$$

2021 Chl_a and Chl_b were converted to mmol mL^{-1} using the molar mass of chlorophyll a
2022 (893.51 g mol^{-1}) and the molar mass of chlorophyll b (907.47 g mol^{-1}), then added
2023 together to calculate total chlorophyll content in the dimethyl sulfoxide extractant
2024 (mmol mL^{-1}). Total chlorophyll content was multiplied by the volume of the
2025 dimethyl sulfoxide extractant (10 mL) and converted to area-based chlorophyll

2026 content by dividing by the total area of the leaf disks (Chl_{area} ; mmol m⁻²). Mass-
2027 based chlorophyll content (Chl_{mass} ; mmol g⁻¹) was calculated by dividing Chl_{area}
2028 by the leaf mass per area of the punched leaf.

2029 5.2.5 *A/C_i curve fitting and parameter estimation*

2030 I fit A_{net}/C_i curves of each individual using the ‘fitaci’ function in the ‘plante-
2031 cophys’ R package (Duursma 2015). This function estimates the maximum rate
2032 of Rubisco carboxylation (V_{cmax} ; $\mu\text{mol m}^{-2} \text{s}^{-1}$) and maximum rate of electron
2033 transport for RuBP regeneration (J_{max} ; $\mu\text{mol m}^{-2} \text{s}^{-1}$) based on the Farquhar
2034 biochemical model of C₃ photosynthesis (Farquhar et al. 1980). Triose phosphate
2035 utilization (TPU) limitation was included in all curve fits, and all curve fits in-
2036 cluded measured dark respiration values. As A_{net}/C_i curves were generated using
2037 a common leaf temperature, curves were fit using Michaelis-Menten coefficients
2038 for Rubisco affinity to CO₂ (K_c ; $\mu\text{mol mol}^{-1}$) and O₂ (K_o ; $\mu\text{mol mol}^{-1}$), and the
2039 CO₂ compensation point (Γ^* ; $\mu\text{mol mol}^{-1}$) reported in Bernacchi et al. (2001).
2040 Specifically, K_c was set to 404.9 $\mu\text{mol mol}^{-1}$, K_o was set to 278.4 $\mu\text{mol mol}^{-1}$,
2041 and Γ^* was set to 42.75 $\mu\text{mol mol}^{-1}$. All curve fits were visually examined for
2042 goodness-of-fit. The use of a common leaf temperature across curves and dark
2043 respiration measurements eliminated the need to temperature standardize rate
2044 estimates. For clarity, I reference V_{cmax} , J_{max} , and R_d estimates throughout the
2045 rest of the chapter as V_{cmax25} , J_{max25} , and R_{d25} .

2046 5.2.6 *Stomatal limitation*

2047 I quantified the extent by which stomatal conductance limited photosynthesis (l ;

2048 unitless) following equations originally described in Farquhar and Sharkey (1982).

2049 Stomatal limitation was calculated as:

$$l = 1 - \frac{A_{net}}{A_{mod}} \quad (5.3)$$

2050 where A_{mod} represents the photosynthetic rate where $C_i = C_a$. A_{mod} was calculated

2051 as:

$$A_{mod} = V_{cmax25} - \frac{420 - \Gamma^*}{420 + K_m} - R_{d25} \quad (5.4)$$

2052 K_m is the Michaelis-Menten coefficient for Rubisco-limited photosynthesis, calcu-

2053 lated as:

$$K_m = K_c \cdot \left(1 + \frac{O_i}{K_o}\right) \quad (5.5)$$

2054 where O_i refers to leaf intercellular O_2 concentrations, set to $210 \mu\text{mol mol}^{-1}$.

2055 5.2.7 *Proportion of leaf nitrogen allocated to photosynthesis and structure*

2056 I used equations from Niinemets and Tenhunen (1997) to estimate the proportion

2057 of leaf nitrogen content allocated to Rubisco, bioenergetics, and light harvesting

2058 proteins. The proportion of leaf nitrogen allocated to Rubisco ($\rho_{rubisco}$; gN g^{-1})

2059 was calculated as a function of V_{cmax25} and N_{area} :

$$\rho_{rubisco} = \frac{V_{cmax25} N_r}{V_{cr} N_{area}} \quad (5.6)$$

2060 where N_r is the amount of nitrogen in Rubisco, set to 0.16 gN (gN in Rubisco) $^{-1}$
2061 and V_{cr} is the maximum rate of RuBP carboxylation per unit Rubisco protein,
2062 set to 20.5 $\mu\text{mol CO}_2$ (g Rubisco) $^{-1}$. The proportion of leaf nitrogen allocated to
2063 bioenergetics (ρ_{bioe} ; gN gN $^{-1}$) was similarly calculated as a function of J_{max25} and
2064 N_{area} :

$$\rho_{bioe} = \frac{J_{max25} N_b}{J_{mc} N_{area}} \quad (5.7)$$

2065 where N_b is the amount of nitrogen in cytochrome f, set to 0.12407 gN (μmol
2066 cytochrome f) $^{-1}$ assuming a constant 1: 1: 1.2 cytochrome f: ferredoxin NADP
2067 reductase: coupling factor molar ratio (Evans and Seemann 1989; Niinemets and
2068 Tenhunen 1997), and J_{mc} is the capacity of electron transport per cytochrome f,
2069 set to 156 $\mu\text{mol electron}$ ($\mu\text{mol cytochrome f}$) $^{-1}\text{s}^{-1}$.

2070 The proportion of leaf nitrogen allocated to light harvesting proteins (ρ_{light} ;
2071 gN gN $^{-1}$) was calculated as a function of Chl_{mass} and N_{mass} :

$$\rho_{light} = \frac{Chl_{mass}}{N_{mass} c_b} \quad (5.8)$$

2072 where c_b is the stoichiometry of the light-harvesting chlorophyll complexes of
2073 photosystem II, set to 2.75 mmol chlorophyll (gN in chlorophyll) $^{-1}$. I used the
2074 N_{mass} value of the focal leaf used to generate A_{net}/C_i curves instead of the leaf
2075 used to extract chlorophyll content, as the two leaves are from the same trifoliolate
2076 leaf set and are highly correlated (Figure D1).

2077 The proportion of leaf nitrogen content allocated to photosynthetic tissue
2078 (ρ_{photo} ; gN gN $^{-1}$) was estimated as the sum of $\rho_{rubisco}$, ρ_{bioe} , and ρ_{light} . Finally,
2079 the proportion of leaf nitrogen content allocated to structural tissue ($\rho_{structure}$; gN

2080 gN^{-1}) was estimated as:

$$\rho_{structure} = \frac{N_{cw}}{N_{area}} \quad (5.9)$$

2081 where N_{cw} is the leaf nitrogen content allocated to cell walls (gN m^{-2}), calculated

2082 as a function of M_{area} using an empirical equation from Onoda et al. (2017):

$$N_{cw} = 0.000355 * M_{area}^{1.39} \quad (5.10)$$

2083 5.2.8 *Whole plant traits*

2084 Seven weeks after experiment initiation and immediately following gas exchange
2085 measurements, I harvested all experimental individuals and separated biomass of
2086 each experimental individual into major organ types (leaves, stems, roots, and
2087 nodules when present). Fresh leaf area of all harvested leaves was measured using
2088 an LI-3100C (Li-COR Biosciences, Lincoln, Nebraska, USA). Total fresh leaf area
2089 (cm^2) was calculated as the sum of all leaf areas, including the focal leaf used to
2090 collect gas exchange data and the focal leaf used to extract chlorophyll content. All
2091 harvested material was dried in an oven set to 65°C for at least 48 hours, weighed,
2092 and ground to homogeneity. Leaves and nodules were manually ground with a
2093 mortar and pestle, while stems and roots were ground using a Wiley mill (E3300
2094 Mini Mill; Eberbach Corp., MI, USA). Total dry biomass (g) was calculated as
2095 the sum of dry leaf (including focal leaf for both the A_{net}/C_i curve and leaf used
2096 to extract chlorophyll content), stem, root, and root nodule biomass. I quantified
2097 carbon and nitrogen content of each respective organ type through elemental
2098 combustion (Costech-4010, Costech, Inc., Valencia, CA, USA) using subsamples
2099 of ground and homogenized organ tissue.

2100 Following the approach explained in the first experimental chapter, I calcu-
 2101 lated structural carbon costs to acquire nitrogen as the ratio of total belowground
 2102 carbon biomass to whole plant nitrogen biomass (N_{cost} ; gC gN⁻¹). Belowground
 2103 carbon biomass (C_{bg} ; gC) was calculated as the sum of root carbon biomass
 2104 and root nodule carbon biomass. Root carbon biomass and root nodule carbon
 2105 biomass was calculated as the product of the organ biomass and the respective
 2106 organ carbon content. Whole plant nitrogen biomass (N_{wp} ; gN) was similarly
 2107 calculated as the sum of total leaf, stem, root, and root nodule nitrogen biomass,
 2108 including the focal leaf used for A_{net}/C_i curve and chlorophyll extractions. Leaf,
 2109 stem, root, and root nodule nitrogen biomass was calculated as the product of
 2110 the organ biomass and the respective organ nitrogen content. This calculation
 2111 only quantifies plant structural carbon costs to acquire nitrogen and does not
 2112 include any additional costs of nitrogen acquisition associated with respiration,
 2113 root exudation, or root turnover. An explicit explanation of the limitations for
 2114 interpreting this calculation can be found in Perkowski et al. (2021) and Terrer
 2115 et al. (2018).

2116 Finally, plant investments in nitrogen fixation were calculated as the ratio
 2117 of root nodule biomass to root biomass, where increasing values indicate an in-
 2118 crease in plant investments to nitrogen fixation (Dovrat et al. 2018; Dovrat et al.
 2119 2020; Perkowski et al. 2021). I also calculated the percent of leaf nitrogen ac-
 2120 quired from the atmosphere (% N_{dfa} ; %) using leaf $\delta^{15}\text{N}$ and the following equation
 2121 from Andrews et al. (2011):

$$\%N_{\text{dfa}} = \frac{\delta^{15}N_{\text{reference}} - \delta^{15}N_{\text{sample}}}{\delta^{15}N_{\text{reference}} - B} \quad (5.11)$$

2122 where $\delta^{15}\text{N}_{\text{reference}}$ refers to a reference plant that exclusively acquires nitrogen via
2123 direct uptake, $\delta^{15}\text{N}_{\text{sample}}$ refers to an individual's leaf $\delta^{15}\text{N}$, and B refers to individuals
2124 that are entirely reliant on nitrogen fixation. Within each unique nitrogen
2125 fertilization treatment-by-CO₂ treatment combination, I calculated the mean leaf
2126 $\delta^{15}\text{N}$ for individuals growing in the non-inoculated treatment for $\delta^{15}\text{N}_{\text{reference}}$. Any
2127 individuals with visual confirmation of root nodule formation were omitted from
2128 the calculation of $\delta^{15}\text{N}_{\text{reference}}$. Following recommendations from Andrews et al.
2129 (2011) I calculated B within each CO₂ treatment using the mean leaf $\delta^{15}\text{N}$ of
2130 inoculated individuals that received 0 ppm N. I did not calculate B within each
2131 unique soil nitrogen-by-CO₂ treatment combination, as previous studies suggest
2132 decreased reliance on nitrogen fixation with increasing soil nitrogen availability
2133 (Perkowski et al. 2021).

2134 5.2.9 *Statistical analyses*

2135 Uninoculated pots that had substantial root nodule formation (nodule biomass:
2136 root biomass values greater than 0.05 g g⁻¹) were removed from all analyses, as
2137 pots were assumed to have been colonized by symbiotic nitrogen-fixing bacteria
2138 from outside sources. This decision resulted in the removal of sixteen pots from
2139 analyses: two pots in the elevated CO₂ treatment that received 35 ppm N, three
2140 pots in the elevated CO₂ treatment that received 70 ppm N, one pot in the elevated
2141 CO₂ treatment that received 210 ppm N, two pots in the elevated CO₂ treatment
2142 that received 280 ppm N, two pots in the ambient CO₂ treatment that received
2143 0 ppm N, three pots in the ambient CO₂ treatment that received 70 ppm N, two
2144 pots in the ambient CO₂ treatment that received 105 ppm N, and one pot in the

2145 ambient CO₂ treatment that received 280 ppm N.

2146 I built a series of linear mixed effects models to investigate the impacts of
2147 CO₂ concentration, soil nitrogen fertilization, and inoculation with *B. japonicum*
2148 on *G. max* gas exchange, tradeoffs between nitrogen and water use, whole plant
2149 growth, and investment in nitrogen fixation. All models included CO₂ treatment
2150 as a categorical fixed effect, inoculation treatment as a categorical fixed effect,
2151 soil nitrogen fertilization as a continuous fixed effect, with interaction terms be-
2152 tween all three fixed effects. All models also accounted for climatic difference
2153 between chambers across experiment iterations by including a random intercept
2154 term that nested starting chamber rack by CO₂ treatment. Models with this
2155 independent variable structure were created for each of the following dependent
2156 variables: N_{area} , M_{area} , N_{mass} , Chl_{area} , V_{cmax25} , J_{max25} , $J_{\text{max25}}:V_{\text{cmax25}}$, R_{d25} , g_{sw} ,
2157 stomatal limitation, ρ_{rubisco} , ρ_{bioe} , ρ_{light} , ρ_{photo} , $\rho_{\text{structure}}$, total biomass, total leaf
2158 area, N_{cost} , C_{bg} , N_{wp} , nodule biomass, the ratio of nodule biomass to root biomass,
2159 and % N_{dfa} .

2160 I used Shapiro-Wilk tests of normality to determine whether linear mixed
2161 effects models satisfied residual normality assumptions. If residual normality as-
2162 sumptions were not met (Shapiro-Wilk: $p < 0.05$), then models were fit using de-
2163 pendent variables that were natural log transformed. If residual normality as-
2164 sumptions were still not met (Shapiro-Wilk: $p < 0.05$), then models were fit using
2165 dependent variables that were square root transformed. All residual normality
2166 assumptions that did not originally satisfy residual normality assumptions were
2167 met with either a natural log or square root data transformation (Shapiro-Wilk:
2168 $p > 0.05$ in all cases). Specifically, models for N_{area} , N_{mass} , Chl_{area} , V_{cmax25} , J_{max25} ,

2169 $J_{\max25}$: $V_{\text{cmax}25}$, R_{d25} , g_{sw} , stomatal limitation, ρ_{rubisco} , ρ_{bioe} , ρ_{light} , ρ_{photo} , total leaf
2170 area, N_{cost} satisfied residual normality assumptions without data transformation.
2171 Models for M_{area} , $\rho_{\text{structure}}$, C_{bg} , and total biomass satisfied residual normality as-
2172 sumptions with a natural log data transformation, while models for N_{wp} , nodule
2173 biomass, nodule biomass: root biomass, and $\%N_{dfa}$ satisfied residual normality
2174 assumptions with a square root data transformation.

2175 In all statistical models, I used the ‘lmer’ function in the ‘lme4’ R package
2176 (Bates et al. 2015) to fit each model and the ‘Anova’ function in the ‘car’ R
2177 package (Fox and Weisberg 2019) to calculate Type II Wald’s χ^2 and determine
2178 the significance ($\alpha=0.05$) of each fixed effect coefficient. I used the ‘emmeans’
2179 R package (Lenth 2019) to conduct post-hoc comparisons using Tukey’s tests,
2180 where degrees of freedom were approximated using the Kenward-Roger approach
2181 (Kenward and Roger 1997). All analyses and plots were conducted in R version
2182 4.2.0 (R Core Team 2021).

2183 5.3 Results

2184 5.3.1 Leaf nitrogen and chlorophyll content

2185 Elevated CO₂ reduced N_{area} , N_{mass} , and Chl_{area} by 29%, 50%, and 31%, respec-
2186 tively, and stimulated M_{area} by 44% ($p<0.001$ in all cases; Table 5.1). An inter-
2187 action between fertilization and CO₂ (CO₂-by-fertilization interaction: $p_{N_{\text{area}}}=$
2188 0.017, $p_{N_{\text{mass}}}<0.001$, $p_{Chl_{\text{area}}}=0.083$; Table 5.1) indicated that the positive effect
2189 of increasing fertilization on N_{area} , N_{mass} , and Chl_{area} ($p<0.001$ in all cases; Table
2190 5.1) was stronger under ambient CO₂ (Tukey _{N_{area}} : $p=0.026$; Tukey _{N_{mass}} : $p<0.001$;
2191 Tukey _{Chl_{area}} : $p=0.065$; Table 5.1; Figs. 5.1a, 5.1b, 5.1d). An interaction between

2192 fertilization and CO₂ on M_{area} (CO₂-by-fertilization interaction: $p=0.006$; Ta-
2193 ble 5.1) indicated that the positive effect of increasing fertilization on M_{area} was
2194 stronger under elevated CO₂ (Tukey: $p=0.009$; Fig. 5.1c). Overall, interactions
2195 between fertilization and CO₂ resulted in stronger reductions in N_{area} , N_{mass} , and
2196 Chl_{area} , and a stronger stimulation in M_{area} under elevated CO₂ with increasing
2197 fertilization.

2198 An interaction between inoculation and CO₂ on N_{area} (CO₂-by-inoculation
2199 interaction: $p=0.030$; Table 5.1) indicated that the positive effect of inoculation
2200 on N_{area} ($p<0.001$; Table 5.1) was stronger under elevated CO₂ (45% increase;
2201 Tukey: $p<0.001$) than under ambient CO₂ (18% increase; Tukey: $p<0.001$), a
2202 result that increased the reduction in N_{area} in inoculated pots under elevated
2203 CO₂. Inoculation treatment did not modify the downregulation in N_{mass} (CO₂-
2204 by-inoculation interaction: $p=0.148$; Table 5.1) and Chl_{area} ($p = 0.147$; Table
2205 5.1) or the stimulation in M_{area} ($p=0.866$; Table 5.1) under elevated CO₂. How-
2206 ever, interactions between fertilization and inoculation on N_{area} , N_{mass} , M_{area} ,
2207 and Chl_{area} (fertilization-by-inoculation interaction: $p_{N_{\text{area}}}<0.001$, $p_{N_{\text{mass}}}=0.001$,
2208 $p_{M_{\text{area}}}=0.025$, $p_{Chl_{\text{area}}}=0.083$; Table 5.1) indicated that the positive effect of in-
2209 creasing fertilization on each trait was stronger in uninoculated pots (Tukey _{N_{area}} :
2210 $p<0.001$; Tukey _{N_{mass}} : $p=0.001$; Tukey _{M_{area}} : $p=0.031$; Tukey _{Chl_{area}} : $p<0.001$;
2211 Figs. 5.1a-d).

Table 5.1. Effects of soil nitrogen fertilization, inoculation, and CO₂ treatments on leaf nitrogen content per unit leaf area (N_{area} ; gN m⁻²), leaf nitrogen content per unit leaf mass (N_{mass} , gN g⁻¹), leaf mass per unit leaf area (M_{area} ; g m⁻²), and chlorophyll content per unit leaf area (Chl_{area} ; mmol m⁻²)^{*}

	N_{area}			N_{mass}			M_{area}^a			
	df	Coefficient	χ^2	p	Coefficient	χ^2	p	Coefficient	χ^2	p
(Intercept)	-	1.10E+00	-	-	3.05E-02	-	-	3.64E+00	-	-
CO ₂	1	-5.67E-01	155.908	<0.001	-1.80E-02	272.362	<0.001	3.04E-01	151.319	<0.001
Inoculation (I)	1	6.21E-01	86.029	<0.001	7.54E-03	15.576	<0.001	1.81E-01	19.158	<0.001
Fertilization (N)	1	3.06E-03	316.408	<0.001	5.78E-05	106.659	<0.001	3.10E-04	21.440	<0.001
CO ₂ *I	1	2.63E-01	4.729	0.030	3.96E-03	2.025	0.155	-3.37E-02	0.029	0.866
CO ₂ *N	1	-3.68E-04	5.723	0.017	-2.85E-05	22.542	<0.001	2.80E-04	7.619	0.006
I*N	1	-1.36E-03	43.381	<0.001	-2.00E-05	11.137	0.001	-3.36E-04	5.022	0.025
CO ₂ *I*N	1	-3.23E-04	0.489	0.484	-2.59E-06	0.041	0.839	1.15E-04	0.208	0.649
Chl _{area}										
	df	Coefficient	χ^2	p						
(Intercept)	-	2.13E-02	-	-						
CO ₂	1	-1.33E-02	69.233	<0.001						
Inoculation (I)	1	1.24E-01	136.341	<0.001						
Fertilization (N)	1	3.35E-04	163.111	<0.001						
CO ₂ *I	1	-3.18E-02	2.102	0.147						
CO ₂ *N	1	-8.79E-05	2.999	0.083						
I*N	1	-2.65E-04	75.769	<0.001						
CO ₂ *I*N	1	7.68E-05	2.144	0.147						

2212 *Significance determined using Type II Wald χ^2 tests ($\alpha=0.05$). P-values less than 0.05 are in bold, while p-values
 2213 between 0.05 and 0.1 are italicized. A superscript “a” is included after trait labels to indicate if models were fit with
 2214 natural log transformed response variables. Key: df=degrees of freedom, χ^2 =Wald Type II chi-square test statistic.

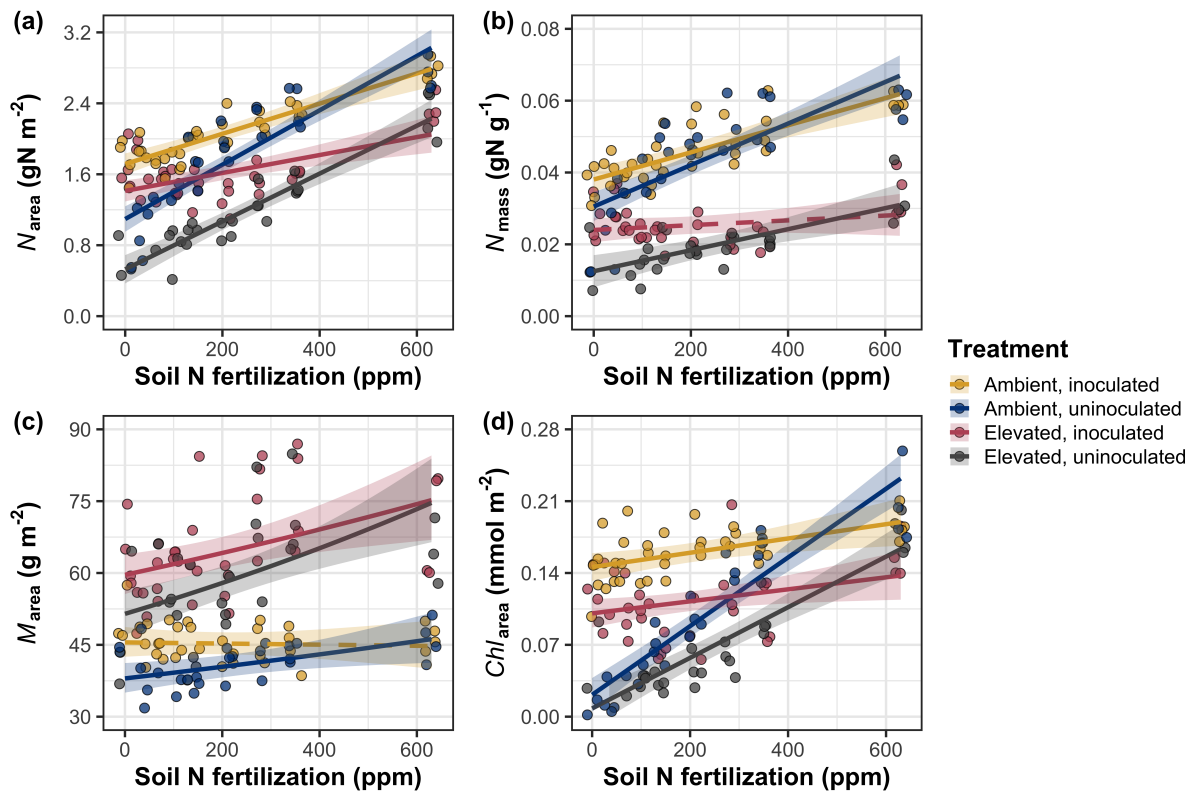


Figure 5.1. Effects of CO_2 , fertilization, and inoculation on leaf nitrogen per unit leaf area (a), leaf nitrogen content (b), leaf mass per unit leaf area (c), and chlorophyll content per unit leaf area (d). Soil nitrogen fertilization is represented on the x-axis in all panels. Yellow points and trendlines indicate inoculated individuals grown under ambient CO_2 , blue points and trendlines indicate uninoculated individuals grown under ambient CO_2 , red points and trendlines indicate inoculated individuals grown under elevated CO_2 , and grey points indicate uninoculated individuals grown under elevated CO_2 . Solid trendlines indicate regression slopes that are different from zero ($p < 0.05$), while dashed trendlines indicate slopes that are not distinguishable from zero ($p > 0.05$).

2215 5.3.2 *Leaf biochemistry and stomatal conductance*

2216 Elevated CO₂ resulted in plants with 16% lower V_{cmax25} ($p<0.001$; Table 5.2) and
2217 10% lower J_{max25} ($p=0.014$; Table 5.2) compared to those grown under ambient
2218 CO₂. However, CO₂ concentration did not influence R_{d25} ($p=0.613$; Table 5.2;
2219 Fig. 5.2d). A relatively stronger downregulation in V_{cmax25} than J_{max25} resulted
2220 in an 8% stimulation in $J_{max25}:V_{cmax25}$ under elevated CO₂ ($p<0.001$; Table 5.2).
2221 The downregulatory effect of CO₂ on V_{cmax25} and J_{max25} was not modified across
2222 the fertilization gradient (CO₂-by-fertilization interaction: $p=0.185$ and $p=0.389$
2223 for V_{cmax25} and J_{max25} , respectively; Table 5.2; Figs. 5.2a, 5.2b) or between in-
2224 oculation treatments (CO₂-by-inoculation interaction: $p=0.799$ and $p=0.714$ for
2225 V_{cmax25} and J_{max25} , respectively; Table 5.2). However, a strong interaction between
2226 fertilization and inoculation (fertilization-by-inoculation interaction: $p\leq0.001$ in
2227 all cases; Table 5.2) indicated that the positive effect of increasing fertilization
2228 on V_{cmax25} ($p<0.001$; Table 5.2), J_{max25} ($p<0.001$; Table 5.2), and R_{d25} ($p=0.015$;
2229 Table 5.2) was only observed in uninoculated pots (Tukey: $p\leq0.001$ in all cases;
2230 Figs. 5.2a, 5.2b). A stronger positive effect of increasing fertilization on V_{cmax25}
2231 than J_{max25} resulted in a reduction in $J_{max25}:V_{cmax25}$ with increasing fertilization
2232 ($p<0.001$; Table 5.2), though this pattern was only observed in uninoculated pots
2233 (fertilization-by-inoculation interaction: $p=0.002$; Table 5.2; Fig. 5.2c).
2234 Elevated CO₂ reduced stomatal conductance by 20% ($p<0.001$; Table 5.2;
2235 Fig. 5.2e), but this downregulation did not influence stomatal limitation of pho-
2236 tosynthesis ($p=0.355$; Table 5.2; Fig. 5.2f). As with V_{cmax25} and J_{max25} , the down-
2237 regulation of stomatal conductance due to elevated CO₂ was not modified across
2238 the fertilization gradient (CO₂-by-fertilization interaction: $p=0.141$; Table 5.2) or

2239 between inoculation treatments (CO_2 -by-inoculation interaction: $p=0.179$; Table
2240 5.2). Fertilization also did not modify the null effect of CO_2 on stomatal limitation
2241 (CO_2 -by-fertilization interaction: $p=0.554$; Table 5.2), although an interaction
2242 between CO_2 and inoculation (CO_2 -by-inoculation interaction: $p=0.043$; Table
2243 5.2) indicated that inoculation increased stomatal limitation under ambient CO_2
2244 (Tukey: $p=0.021$), but not under elevated CO_2 (Tukey: $p>0.999$). An interaction
2245 between inoculation and fertilization on stomatal conductance (fertilization-by-
2246 inoculation interaction: $p<0.001$; Table 5.2) indicated that increasing fertilization
2247 increased stomatal conductance in uninoculated pots (Tukey: $p=0.003$) but de-
2248 creased stomatal conductance in inoculated pots (Tukey: $p=0.021$). The similar
2249 in magnitude, but opposite direction, trend in the effect of increasing fertiliza-
2250 tion on stomatal conductance between inoculation treatments likely drove a null
2251 response of stomatal conductance to increasing fertilization ($p=0.642$; Table 5.2).

Table 5.2. Effects of soil nitrogen fertilization, inoculation, and CO₂ on the maximum rate of Rubisco carboxylation ($V_{\text{cmax}25}$; $\mu\text{mol m}^{-2} \text{s}^{-1}$), the maximum rate of RuBP regeneration ($J_{\text{max}25}$; $\mu\text{mol m}^{-2} \text{s}^{-1}$), dark respiration ($R_{\text{d}25}$; $\mu\text{mol m}^{-2} \text{s}^{-1}$), the ratio of the maximum rate of RuBP regeneration to the maximum rate of Rubisco carboxylation ($J_{\text{max}25}:V_{\text{cmax}25}$; unitless), stomatal conductance (g_{sw} ; $\text{mol m}^{-2} \text{s}^{-1}$), and stomatal limitation (unitless)*

	$V_{\text{cmax}25}$			$J_{\text{max}25}$			$R_{\text{d}25}$			
	df	Coefficient	χ^2	p	Coefficient	χ^2	p	Coefficient	χ^2	p
(Intercept)	-	4.36E+01	-	-	8.30E+01	-	-	1.69E+00	-	-
CO ₂	1	-7.05E+00	18.039	<0.001	-9.11E+00	6.042	0.014	4.53E-01	0.256	0.613
Inoculation (I)	1	5.87E+01	98.579	<0.001	9.62E+01	85.064	<0.001	1.04E+00	3.094	0.079
Fertilization (N)	1	1.32E-01	37.053	<0.001	2.09E-01	25.356	<0.001	2.86E-03	5.965	0.015
CO ₂ *I	1	-4.65E+00	0.065	0.799	7.84E-01	0.667	0.414	-5.71E-01	2.563	0.109
CO ₂ *N	1	-3.58E-02	1.758	0.185	-4.33E-02	0.742	0.389	-1.55E-03	2.675	0.102
I*N	1	-1.35E-01	60.394	<0.001	-2.30E-01	57.410	<0.001	-2.84E-03	12.083	0.001
CO ₂ *I*N	1	2.73E-02	0.748	0.387	3.46E-02	0.377	0.539	7.21E-04	0.244	0.622

134

	$J_{\text{max}25}:V_{\text{cmax}25}$			g_{sw}			Stomatal limitation			
	df	Coefficient	χ^2	p	Coefficient	χ^2	p	Coefficient	χ^2	p
(Intercept)	-	1.92E+00	-	-	1.95E-01	-	-	2.12E-01	-	-
CO ₂	1	5.71E-02	92.010	<0.001	-6.23E-02	9.718	0.002	3.91E-02	0.856	0.355
Inoculation (I)	1	-1.79E-01	27.768	<0.001	1.30E-01	22.351	<0.001	7.87E-02	4.582	0.032
Fertilization (N)	1	-4.61E-04	28.147	<0.001	2.50E-04	0.066	0.797	2.60E-04	32.218	<0.001
CO ₂ *I	1	8.94E-02	2.916	0.088	6.69E-02	1.810	0.179	-7.84E-02	4.093	0.043
CO ₂ *N	1	2.35E-04	3.210	0.073	-8.50E-05	2.165	0.141	-1.24E-04	0.350	0.554
I*N	1	3.27E-04	9.607	0.002	-3.09E-04	14.696	<0.001	-1.67E-04	2.547	0.110
CO ₂ *I*N	1	-1.66E-04	1.102	0.294	-8.89E-05	0.234	0.629	1.67E-04	2.231	0.135

2252 *Significance determined using Type II Wald χ^2 tests ($\alpha=0.05$). P-values less than 0.05 are in bold, while p-values between 0.05 and 0.1 are italicized. Key: df=degrees of freedom; χ^2 =Wald Type II chi-square test statistic.

2253

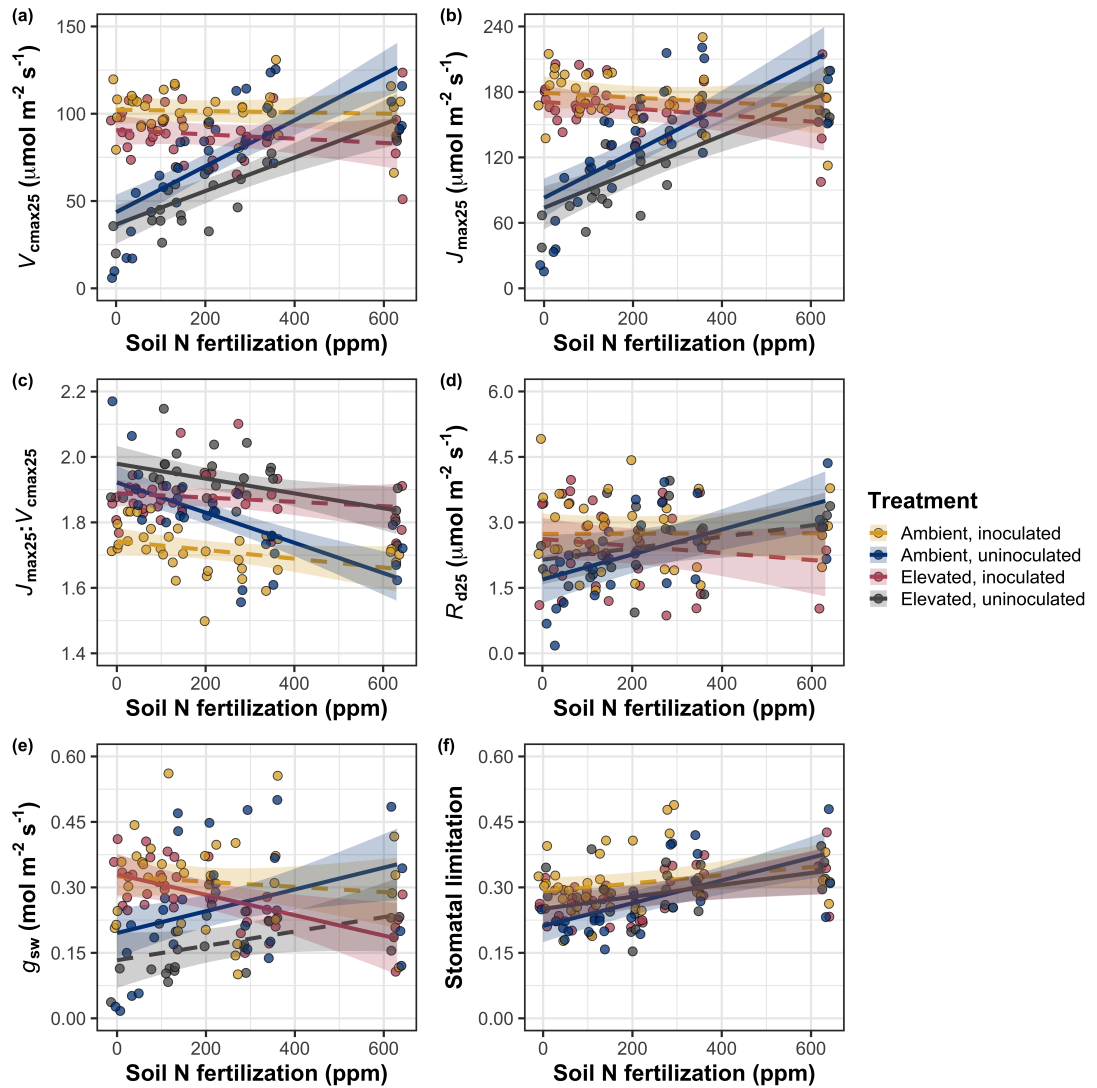


Figure 5.2. Effects of CO₂, fertilization, and inoculation on maximum rate of Rubisco carboxylation (a), the maximum rate of RuBP regeneration (b), and the ratio of the maximum rate of RuBP regeneration to the maximum rate of Rubisco carboxylation leaf mass per unit leaf area (c), dark respiration (d), stomatal conductance (e), and stomatal limitation (f). Soil nitrogen fertilization is represented on the x-axis in all panels. Colored points and trendlines are as explained in Figure 5.1.

2254 5.3.3 *Leaf nitrogen allocation*

2255 A relatively stronger downregulation in N_{area} than $V_{\text{cmax}25}$ and $J_{\text{max}25}$ resulted in
2256 an 20% and 29% respective stimulation in ρ_{rubisco} and ρ_{bioe} under elevated CO₂
2257 ($p<0.001$ in both cases; Table 5.3). There was no effect of CO₂ on ρ_{light} ($p=0.700$;
2258 Table 5.3), but the stimulation in ρ_{rubisco} and ρ_{bioe} resulted in a 21% stimulation
2259 of ρ_{photo} under elevated CO₂ ($p<0.001$; Table 5.3; Fig. 5.3a). The stimulation
2260 of ρ_{rubisco} , ρ_{bioe} , and ρ_{photo} under elevated CO₂ was not modified across the fer-
2261 tilization gradient (CO₂-by-fertilization interaction: $p_{\text{rubisco}}=0.269$, $p_{\text{bioe}}=0.298$,
2262 $p_{\text{photo}}=0.281$; Table 5.3). A marginal interaction between inoculation and CO₂ on
2263 ρ_{rubisco} and ρ_{photo} (CO₂-by-inoculation interaction: $p_{\text{rubisco}}=0.057$, $p_{\text{photo}}=0.055$;
2264 Table 5.3) indicated that the positive effect of inoculation on ρ_{rubisco} and ρ_{photo}
2265 ($p<0.001$ in both cases; Table 5.3) was only apparent under ambient CO₂ (Tukey:
2266 $p<0.001$ in both cases). Inoculation did not modify the stimulation of ρ_{bioe} un-
2267 der elevated CO₂ (CO₂-by-inoculation interaction: $p=0.122$; Table 5.3) or the
2268 null effect of CO₂ on ρ_{bioe} (CO₂-by-inoculation interaction: $p=0.298$; Table 5.3).
2269 An interaction between fertilization and inoculation on ρ_{rubisco} , ρ_{bioe} , and ρ_{photo}
2270 (fertilization-by-inoculation interaction: $p<0.001$ in all cases; Table 5.3) indicated
2271 that the negative effect of increasing fertilization on each trait ($p<0.001$ in all
2272 cases; Table 5.3) was only observed in inoculated pots (Tukey: $p<0.001$ in all
2273 cases). An additional interaction between fertilization and inoculation on ρ_{light}
2274 (fertilization-by-inoculation interaction: $p<0.001$; Table 5.3) indicated a negative
2275 effect of increasing fertilization on ρ_{light} in inoculated pots (Tukey: $p=0.041$), but
2276 a positive effect of increasing fertilization in uninoculated pots (Tukey: $p<0.001$).
2277 The stimulation in M_{area} under elevated CO₂ resulted in an 133% stimu-

2278 lation of $\rho_{\text{structure}}$ ($p<0.001$; Table 5.3; Fig 5.3b). An interaction between fertil-
2279 ization and CO₂ (CO₂-by-fertilization interaction: $p=0.039$; Table 5.3) indicated
2280 that the negative effect of increasing fertilization ($p<0.001$; Table 5.3) on $\rho_{\text{structure}}$
2281 was marginally stronger under ambient CO₂ (Tukey: $p=0.055$). A marginal inter-
2282 action between inoculation and CO₂ (CO₂-by-inoculation interaction: $p=0.057$;
2283 Table 5.3) indicated that the positive effect of inoculation on $\rho_{\text{structure}}$ ($p<0.001$;
2284 Table 5.3) was only observed under elevated CO₂ (Tukey: $p<0.001$), with no ap-
2285 parent inoculation effect observed under ambient CO₂ (Tukey: $p=0.513$). Finally,
2286 an interaction between fertilization and inoculation (fertilization-by-inoculation
2287 interaction: $p<0.001$; Table 5.3) indicated that, while increasing fertilization in-
2288 creased $\rho_{\text{structure}}$ ($p<0.001$; Table 5.3), this response was stronger in uninoculated
2289 pots (Tukey: $p=0.001$; Fig. 5.3b).

Table 5.3. Effects of soil nitrogen fertilization, inoculation, and CO₂ on the fraction of leaf nitrogen allocated to Rubisco (ρ_{rubisco} ; gN gN⁻¹), bioenergetics (ρ_{bioe} ; gN gN⁻¹), light harvesting proteins (ρ_{light} ; gN gN⁻¹), photosynthesis (ρ_{photo} ; gN gN⁻¹), and structure ($\rho_{\text{structure}}$; gN gN⁻¹)*

	ρ_{rubisco}			ρ_{bioe}			ρ_{light}			
	df	Coefficient	χ^2	p	Coefficient	χ^2	p	Coefficient	χ^2	p
(Intercept)	-	2.70E-01	-	-	5.26E-02	-	-	8.48E-03	-	-
CO ₂	1	1.42E-01	23.510	<0.001	3.00E-02	53.899	<0.001	2.03E-03	0.149	0.700
Inoculation (I)	1	1.83E-01	23.475	<0.001	2.80E-02	13.860	<0.001	2.04E-02	147.234	<0.001
Fertilization (N)	1	1.35E-04	16.609	<0.001	1.22E-05	26.827	<0.001	3.22E-05	19.378	<0.001
CO ₂ *I	1	-1.07E-01	3.629	0.057	-1.67E-02	2.390	0.122	-5.33E-03	0.684	0.408
CO ₂ *N	1	-2.16E-04	1.223	0.269	-3.59E-05	1.085	0.298	-7.01E-06	0.351	0.553
I*N	1	-4.26E-04	20.045	<0.001	-6.87E-05	15.458	<0.001	-4.37E-05	64.042	<0.001
CO ₂ *I*N	1	2.50E-04	3.327	0.068	4.08E-05	2.651	0.103	1.74E-05	3.735	0.053

	ρ_{photo}			$\rho_{\text{structure}}^a$			
	df	Coefficient	χ^2	p	Coefficient	χ^2	p
(Intercept)	-	3.32E-01	-	-	-2.93E+00	-	-
CO ₂	1	1.81E-01	27.651	<0.001	8.77E-01	229.571	<0.001
Inoculation (I)	1	2.31E-01	26.238	<0.001	-2.55E-01	13.872	<0.001
Fertilization (N)	1	1.76E-04	15.899	<0.001	-1.51E-03	38.128	<0.001
CO ₂ *I	1	-1.36E-01	3.671	0.055	-2.99E-01	3.622	0.057
CO ₂ *N	1	-2.72E-04	1.163	0.281	3.14E-04	4.266	0.039
I*N	1	-5.37E-04	21.355	<0.001	7.00E-04	11.025	0.001
CO ₂ *I*N	1	3.29E-04	4.009	0.045	4.52E-04	0.669	0.413

2290 *Significance determined using Type II Wald χ^2 tests ($\alpha=0.05$). P-values less than 0.05 are in bold, while p-values
 2291 between 0.05 and 0.1 are italicized. A superscript “a” is included after trait labels to indicate if models were fit with
 2292 natural log transformed response variable. Key: df=degrees of freedom; χ^2 =Wald Type II chi-square test statistic.

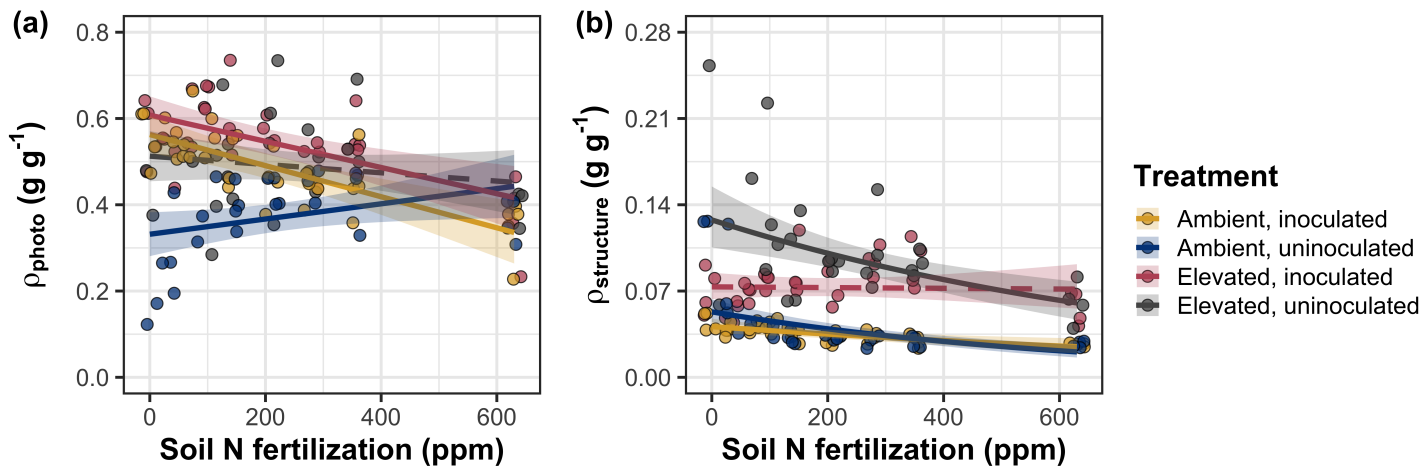


Figure 5.3. Effects of CO_2 , fertilization, and inoculation on the relative fraction of leaf nitrogen allocated to photosynthesis (a) and the fraction of leaf nitrogen allocated to structure (b). Soil nitrogen fertilization is represented on the x-axis in both panels. Colored points and trendlines are as explained in Figure 5.1.

2293 5.3.4 *Whole plant traits*

2294 Total leaf area and total biomass were 51% and 102% greater under elevated CO₂,
2295 respectively ($p<0.001$ in both cases; Table 5.4). The stimulation in total leaf area
2296 and total biomass under elevated CO₂ was enhanced by increasing fertilization
2297 (CO₂-by-fertilization interaction: $p<0.001$ in both cases; Table 5.4; Figs. 5.4a,
2298 5.4b) but was not modified across inoculation treatments (CO₂-by-inoculation
2299 interaction: $p_{total_leaf_area}=0.151$, $p_{total_biomass}=0.472$; Table 5.4). The positive
2300 effect of increasing fertilization on total leaf area and total biomass was modified by
2301 inoculation treatment (fertilization-by-inoculation interaction: $p<0.001$ in both
2302 cases; Table 5.4), indicating a stronger positive effect of increasing fertilization in
2303 uninoculated pots (Tukey: $p_{total_leaf_area}=0.002$, $p_{total_biomass}=0.001$, Figs. 5.4a,
2304 5.4b).

2305 A 62% stimulation in N_{cost} under elevated CO₂ was modified through a
2306 strong three-way interaction between CO₂, fertilization, and inoculation (CO₂-
2307 by-inoculation-by-fertilization interaction: $p<0.001$; Table 5.4; Fig. 5.4). This
2308 interaction revealed a general negative effect of increasing fertilization on N_{cost}
2309 ($p<0.001$; Table 5.4) that was observed in all treatment combinations (Tukey:
2310 $p<0.001$ in all cases) except for inoculated pots grown under elevated CO₂ (Tukey:
2311 $p=0.779$; Fig. 5.4c). This response also resulted in stronger negative effects of in-
2312 creasing fertilization on N_{cost} in uninoculated pots grown under elevated CO₂ than
2313 uninoculated pots grown under ambient CO₂ (Tukey: $p=0.001$) and inoculated
2314 pots grown under either ambient CO₂ (Tukey: $p<0.001$) or elevated CO₂ (Tukey:
2315 $p<0.001$), while uninoculated pots grown under ambient CO₂ had stronger nega-
2316 tive effects of increasing fertilization on N_{cost} than inoculated pots grown under

2317 elevated CO₂ (Tukey: $p=0.002$), but not inoculated pots grown under ambient
2318 CO₂ (Tukey: $p=0.216$; Fig. 5.4). The reduction in N_{cost} with increasing fertiliza-
2319 tion and in uninoculated pots were driven by a stronger positive effect of increasing
2320 fertilization on N_{wp} (denominator of N_{cost}) than C_{bg} (numerator of N_{cost}), while
2321 the stimulation in N_{cost} under elevated CO₂ was driven by a stronger positive
2322 effect of elevated CO₂ on C_{bg} than N_{wp} (Table 5.4).

Table 5.4. Effects of CO₂, fertilization, and inoculation on total leaf area (cm²), whole plant biomass (g), carbon costs to acquire nitrogen (N_{cost} ; gC gN⁻¹), belowground carbon biomass (C_{bg} ; gC), and whole plant nitrogen biomass (N_{wp} ; gN)*

	Total leaf area			Total biomass ^b			<i>N</i> _{cost}			
	df	Coefficient	χ^2	p	Coefficient	χ^2	p	Coefficient	χ^2	p
(Intercept)	-	8.78E+01	-	-	9.96E-01	-	-	8.67E+00	-	-
CO ₂	1	3.36E+01	69.291	<0.001	5.07E-01	131.477	<0.001	8.75E+00	88.189	<0.001
Inoculation (I)	1	1.88E+02	35.715	<0.001	7.96E-01	34.264	<0.001	-1.68E+00	136.343	<0.001
Fertilization (N)	1	9.35E-01	274.199	<0.001	3.14E-03	269.046	<0.001	-8.50E-03	80.501	<0.001
CO ₂ *I	1	6.44E+01	2.064	0.151	-7.69E-02	0.518	0.472	-8.38E+00	85.237	<0.001
CO ₂ *N	1	5.05E-01	18.655	<0.001	1.61E-03	16.877	<0.001	-9.17E-03	1.050	0.306
I*N	1	-3.84E-01	10.804	0.001	-1.45E-03	15.779	<0.001	4.20E-03	46.489	<0.001
CO ₂ *I*N	1	-2.97E-03	<0.001	0.990	-1.14E-04	0.023	0.880	1.32E-02	18.125	<0.001

	C_{bg}^{a}		N_{wp}^{b}				
	df	Coefficient	χ^2	p	Coefficient	χ^2	p
(Intercept)	-	-1.70E+00	-	-	1.24E-01	-	-
CO ₂	1	9.21E-01	84.134	<0.001	-3.41E-03	23.890	<0.001
Inoculation (I)	1	1.18E+00	41.030	<0.001	1.68E-01	134.460	<0.001
N fertilization (N)	1	3.38E-03	152.248	<0.001	6.69E-04	529.021	<0.001
CO ₂ * I	1	-6.18E-01	8.965	0.003	3.68E-02	1.190	0.275
CO ₂ * N	1	-3.66E-05	1.188	0.276	1.58E-04	5.915	0.015
I * N	1	-2.22E-03	22.648	<0.001	-3.20E-04	55.562	<0.001
CO ₂ * I * N	1	8.09E-04	1.109	0.292	-7.54E-05	0.620	0.431

2323 *Significance determined using Type II Wald χ^2 tests ($\alpha=0.05$). *P*-values less than 0.05 are in bold. Superscripts
2324 included after trait labels indicate if models were fit with natural log (^a) or square root (^b) transformed response
2325 variables. Key: df=degrees of freedom; χ^2 =Wald Type II chi-square test statistic.

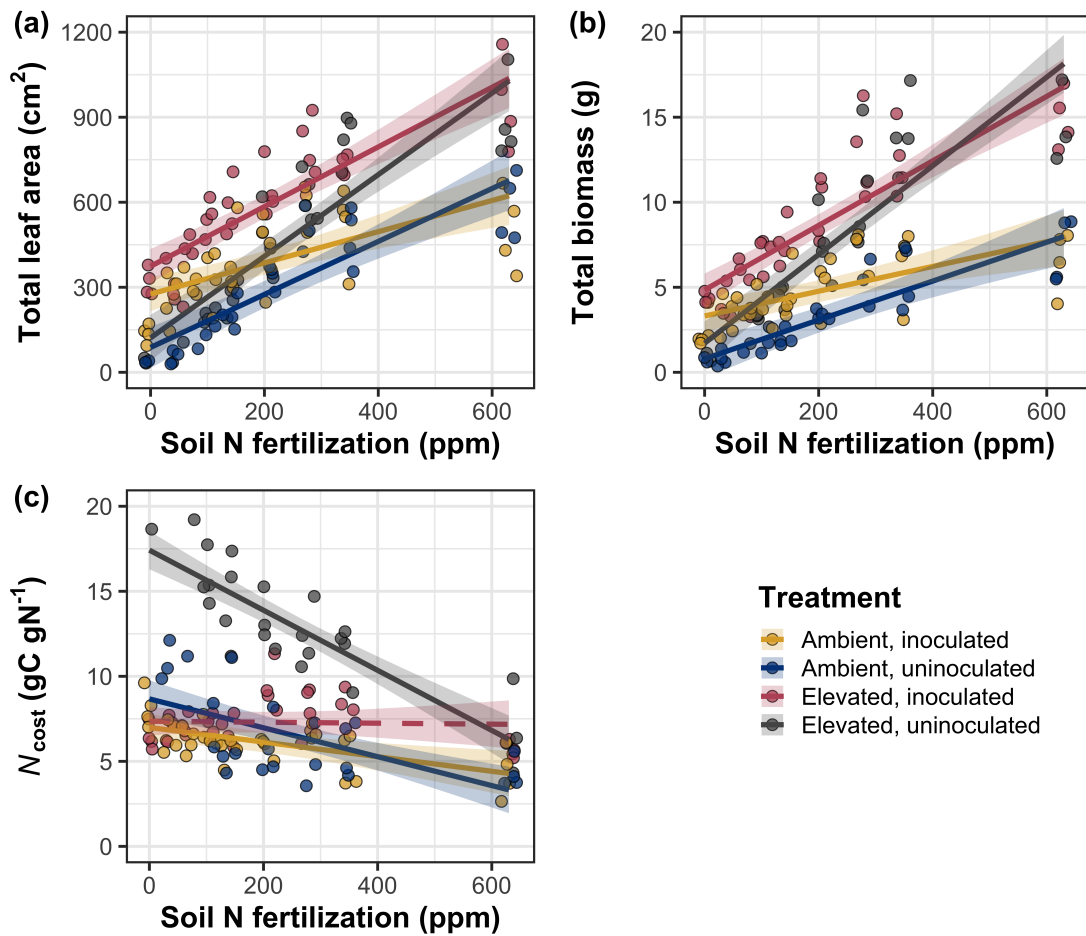


Figure 5.4. Effects of CO_2 , fertilization, and inoculation on total leaf area (a), total biomass (b), and structural carbon costs to acquire nitrogen (c). Soil nitrogen fertilization is represented on the x-axis in all panels. Colored points and trendlines are as explained in Figure 5.1.

2326 5.3.5 *Nitrogen fixation*

2327 Nodule biomass was stimulated by 30% under elevated CO₂ ($p<0.001$; Table 5.5),
2328 a pattern that was modified across the fertilization gradient (CO₂-by-fertilization
2329 interaction: $p=0.479$; Table 5.5), but not between inoculation treatments (CO₂-
2330 by-inoculation interaction: $p=0.404$; Table 5.5). Specifically, the negative effect
2331 of increasing fertilization on nodule biomass ($p<0.001$; Table 5.5) was stronger
2332 under elevated CO₂ (Tukey: $p<0.001$; Fig. 5.5a). An interaction between fertil-
2333 ization and inoculation (fertilization-by-inoculation interaction: $p<0.001$; Table
2334 5.5) indicated a stronger negative effect of increasing fertilization in inoculated
2335 pots (Tukey: $p<0.001$; Fig. 5.5a).

2336 There was no effect of CO₂ on nodule: root biomass ($p=0.767$; Table 5.5),
2337 although an interaction between CO₂ and inoculation (CO₂-by-inoculation in-
2338 teraction: $p<0.001$; Table 5.5) indicated that the positive effect of inoculation
2339 on nodule: root biomass ($p<0.001$; Table 5.5) was stronger under ambient CO₂
2340 (3129% increase; Tukey: $p<0.001$) than elevated CO₂ (379% increase; Tukey:
2341 $p<0.001$; Fig. 5.5b). The null effect of CO₂ on nodule: root biomass was consis-
2342 tently observed across the fertilization gradient (CO₂-by-fertilization interaction:
2343 $p=0.183$; Table 5.5; Fig. 5.5b). An interaction between fertilization and inocula-
2344 tion (fertilization-by-inoculation interaction: $p<0.001$; Table 5.5) indicated that
2345 the negative effect of increasing fertilization on nodule: root biomass ($p<0.001$;
2346 Table 5.5) was stronger in inoculated pots (Tukey: $p<0.001$; Fig. 5.5b).

2347 There was no effect of CO₂ on %N_{dfa} ($p=0.472$; Table 5.5), a pattern
2348 that was not modified by inoculation (CO₂-by-inoculation interaction: $p=0.156$;
2349 Table 5.5) or fertilization (CO₂-by-fertilization interaction: $p=0.099$; Table 5.5).

- 2350** An interaction between fertilization and inoculation (fertilization-by-inoculation
2351 interaction: $p<0.001$; Table 5.5) indicated that the negative effect of increasing
2352 fertilization on $\%N_{dfa}$ ($p<0.001$; Table 5.5) was only observed in inoculated pots
2353 (Tukey: $p<0.001$; Fig. 5.5c).

Table 5.5. Effects of CO₂, fertilization, and inoculation on root nodule biomass (g), plant investments in symbiotic nitrogen fixation (unitless), and percent nitrogen fixed from the atmosphere (%N_{dfa}; unitless)*

	Root nodule biomass ^b			Root nodule: root biomass ^b			%N _{dfa} ^b			
	df	Coefficient	χ^2	p	Coefficient	χ^2	p	Coefficient	χ^2	p
(Intercept)	-	9.41E-03	-	-	1.33E-02	-	-	7.48E-01	-	-
CO ₂	1	1.20E-01	19.258	<0.001	9.94E-02	0.087	0.768	-1.00E-01	0.518	0.472
Inoculation (I)	1	5.74E-01	755.020	<0.001	5.40E-01	903.691	<0.001	9.01E+00	955.570	<0.001
Fertilization (N)	1	7.71E-06	84.376	<0.001	-5.99E-06	258.099	<0.001	3.64E-04	292.938	<0.001
CO ₂ *I	1	-4.68E-02	0.950	0.330	-1.38E-01	20.614	<0.001	-1.44E-01	2.010	0.156
CO ₂ *N	1	-1.59E-04	2.106	0.147	-1.73E-04	1.773	0.183	-6.21E-05	2.716	0.099
I*N	1	-5.82E-04	44.622	<0.001	-7.45E-04	133.918	<0.001	-1.58E-02	231.290	<0.001
CO ₂ *I*N	1	7.26E-05	0.196	0.658	1.76E-04	2.359	0.125	2.77E-03	2.119	0.145

2354 *Significance determined using Type II Wald χ^2 tests ($\alpha=0.05$). P-values less than 0.05 are in bold, while p-values
 2355 between 0.05 and 0.1 are italicized. Superscript letters indicate model coefficients fit to square-root (^b) transformed
 2356 data. Key: df=degrees of freedom; χ^2 =Wald Type II chi-square test statistic.

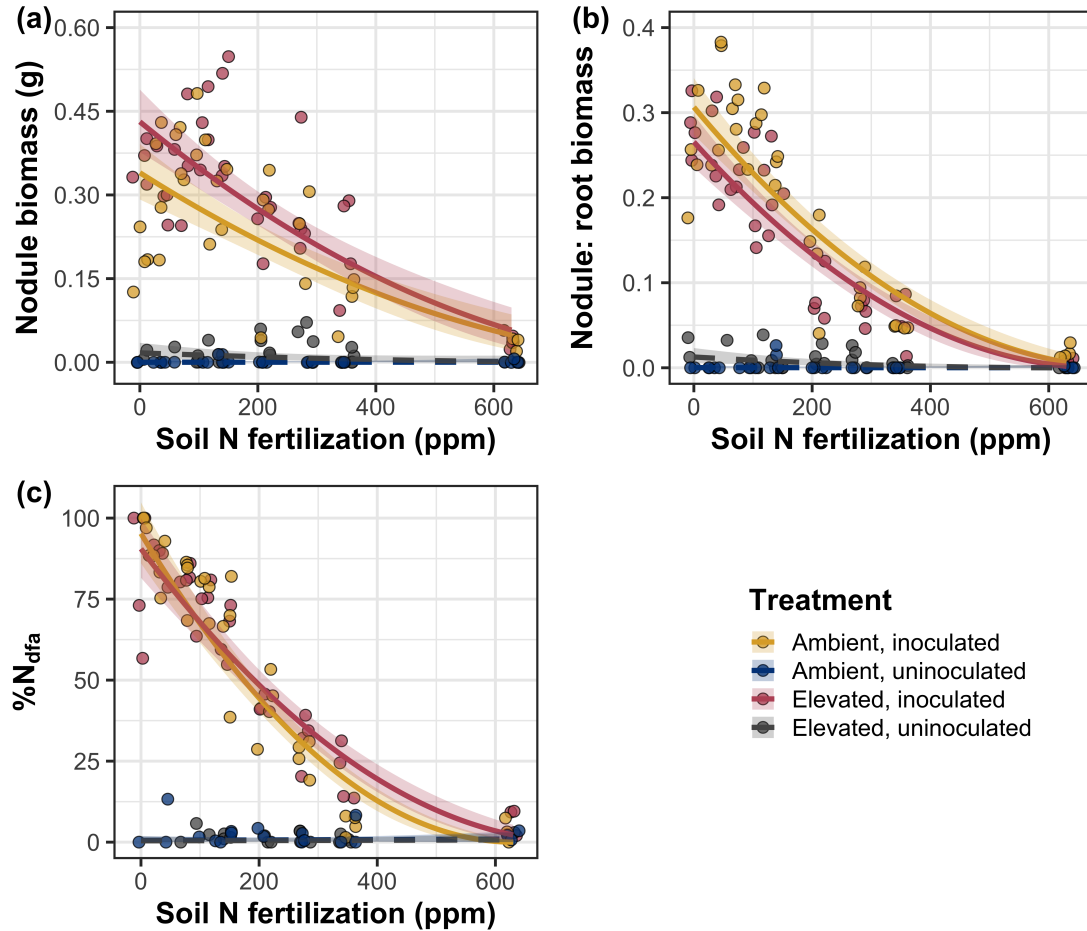


Figure 5.5. Effects of CO₂, fertilization, and inoculation on nodule biomass (a), nodule biomass: root biomass (b), and percent nitrogen fixed from the atmosphere (c). Soil nitrogen fertilization is represented on the x-axis. Colored points and trendlines are as explained in Figure 5.1. Curvilinear trendlines occur as a result of back-transforming models where response variables received either a natural log or square root transformation prior to fitting.

2357 5.4 Discussion

2358 In this study, I determined leaf and whole plant acclimation responses of 7-week *G.*
2359 *max* seedlings grown under two CO₂ concentrations, two inoculation treatments,
2360 and nine soil nitrogen fertilization treatments in a full-factorial growth chamber
2361 experiment. In support of hypotheses and patterns expected from theory, elevated
2362 CO₂ reduced N_{area} , V_{cmax25} , and J_{max25} . The relatively stronger downregulation in
2363 V_{cmax25} than J_{max25} under elevated CO₂ resulted in a stimulation in $J_{\text{max25}}:V_{\text{cmax25}}$
2364 under elevated CO₂. The downregulation of V_{cmax25} and J_{max25} under elevated
2365 CO₂ was similar across fertilization and inoculation treatments, indicating that
2366 the CO₂ responses were not associated with nitrogen limitation. Interestingly,
2367 results indicate that elevated CO₂ increased the fraction of leaf nitrogen allocated
2368 to photosynthesis and structure, leading to a stimulation in nitrogen use efficiency
2369 under elevated CO₂ despite the apparent downregulation in N_{area} , V_{cmax25} , and
2370 J_{max25} .

2371 The downregulation in leaf photosynthetic processes under elevated CO₂
2372 corresponded with a strong stimulation in total leaf area and total biomass. Strong
2373 stimulations in whole plant growth due to elevated CO₂ were generally enhanced
2374 with increasing fertilization and were negatively related to structural carbon costs
2375 to acquire nitrogen. Inoculation generally did not modify whole plant responses
2376 to elevated CO₂ across the fertilization gradient, likely due to a strong reduc-
2377 tion in root nodulation with increasing fertilization. However, strong positive
2378 effects of inoculation on whole plant growth were observed under low fertilization,
2379 consistent with hypotheses. Overall, observed leaf and whole plant acclimation
2380 responses to CO₂ support hypotheses and patterns expected from photosynthetic

2381 least-cost theory, showing that leaf acclimation responses to CO₂ were decoupled
2382 from soil nitrogen availability and ability to acquire nitrogen via symbiotic nitro-
2383 gen fixation. Instead, leaf and whole plant acclimation responses to CO₂ were
2384 driven by optimal resource investment to photosynthetic capacity, where optimal
2385 resource investment at the leaf level maximized nitrogen allocation to structures
2386 that support whole plant growth.

2387 5.4.1 *Soil nitrogen fertilization has divergent effects on leaf and whole plant*
2388 *acclimation responses to CO₂*

2389 Elevated CO₂ reduced N_{area} , V_{cmax25} , J_{max25} , and stomatal conductance by 29%,
2390 16%, 10%, and 20%, respectively. The larger downregulation of V_{cmax25} than
2391 J_{max25} led to an 8% stimulation in $J_{\text{max25}}:V_{\text{cmax25}}$, while the larger downregulation
2392 of N_{area} than V_{cmax25} resulted in a 21% stimulation in the fraction of leaf nitro-
2393 gen allocated to photosynthesis under elevated CO₂. These acclimation responses
2394 are directionally consistent with previous studies that have investigated or re-
2395 viewed leaf acclimation responses to CO₂ (Drake et al. 1997; Makino et al. 1997;
2396 Ainsworth et al. 2002; Ainsworth and Long 2005; Ainsworth and Rogers 2007;
2397 Smith and Dukes 2013; Smith and Keenan 2020; Poorter et al. 2022), and fol-
2398 low patterns expected from photosynthetic least-cost theory (Wright et al. 2003;
2399 Prentice et al. 2014; Smith et al. 2019; Smith and Keenan 2020). Together, the
2400 stimulation in $J_{\text{max25}}:V_{\text{cmax25}}$ and the fraction of leaf nitrogen allocated to pho-
2401 tosynthesis under elevated CO₂ provide strong support for the idea that leaves
2402 were downregulating V_{cmax25} in response to elevated CO₂ in order to optimally co-
2403 ordinate photosynthesis such that net photosynthesis rates approached becoming

2404 equally co-limited by Rubisco carboxylation and RuBP regeneration (Chen et al.
2405 1993; Maire et al. 2012) while optimizing resource use efficiency.

2406 Increasing fertilization and inoculation induced strong positive effects on
2407 N_{area} , $V_{\text{cmax}25}$, $J_{\text{max}25}$. The general positive response of N_{area} to increasing fertiliza-
2408 tion and in inoculated pots was enhanced under ambient CO₂, which, paired with
2409 the general downregulation of N_{area} under elevated CO₂, resulted in a stronger
2410 downregulation of N_{area} under elevated CO₂ with increasing fertilization and in
2411 inoculated pots. These patterns suggest that N_{area} responses to CO₂ were at least
2412 partially dependent on soil nitrogen fertilization and nitrogen acquisition strat-
2413 egy. However, the general stimulation in the fraction of leaf nitrogen allocated to
2414 Rubisco, bioenergetics, or photosynthesis under elevated CO₂ was not modified
2415 across the fertilization gradient and was only marginally enhanced in inoculated
2416 pots. These patterns suggest that the increased downregulation of N_{area} under
2417 elevated CO₂ with increasing fertilization was not necessarily associated with a
2418 change in relative investment to photosynthetic tissue, providing another line of
2419 evidence suggesting that leaf acclimation responses to CO₂ are decoupled from
2420 changes in soil nitrogen availability.

2421 Leaf acclimation responses to elevated CO₂ corresponded with a 62% and
2422 100% stimulation in total leaf area and total biomass, respectively. The stimula-
2423 tion in total leaf area and total biomass under elevated CO₂ corresponded with
2424 generally larger structural carbon costs to acquire nitrogen, a pattern driven by
2425 a stimulation in belowground carbon biomass and reduction in whole plant ni-
2426 trogen biomass. This result suggests that elevated CO₂ reduces plant nitrogen
2427 uptake efficiency, which does not explain why plants grown under elevated CO₂

2428 generally had higher biomass and total leaf area, unless growth stimulations un-
2429 der elevated CO₂ were driven by reductions in per-tissue nitrogen demand (Dong
2430 et al. 2022). Interestingly, strong negative effects of increasing fertilization on
2431 structural carbon costs to acquire nitrogen, which were generally similar between
2432 CO₂ concentrations, were driven by stronger increases in whole plant nitrogen
2433 biomass than belowground carbon biomass. This response allowed plants to in-
2434 crease nitrogen uptake efficiency with increasing fertilization, which could be the
2435 mechanism that drove the enhanced growth stimulation under elevated CO₂ with
2436 increasing fertilization.

2437 Interestingly, results indicate that the stimulation in total leaf area and
2438 whole plant growth under elevated CO₂ was not modified by inoculation despite
2439 an apparent general negative effect of inoculation on N_{cost} . This response could
2440 have been due to strong negative effect of increasing fertilization on nodulation,
2441 which may have caused the strong increase in the positive effect of elevated CO₂ on
2442 whole plant growth with increasing fertilization to mask any increase in the posi-
2443 tive effect of elevated CO₂ on whole plant growth due to inoculation. Reductions
2444 in nodulation with increasing fertilization are commonly observed patterns that
2445 have been inferred to be a response that allows species optimize nitrogen uptake
2446 efficiency as costs to acquire nitrogen via direct uptake become more similar (Gib-
2447 son and Harper 1985; Rastetter et al. 2001). In this study, pairwise comparisons
2448 indicated strong positive effects of inoculation on total leaf area and total biomass
2449 (158% increase in total leaf area, 119% increase in total biomass) under elevated
2450 CO₂ at 0 ppm N ($p < 0.05$ in both cases), but no observable inoculation effect on
2451 total leaf area or total biomass under elevated CO₂ at 350 ppm N or 630 ppm N

2452 ($p>0.05$ in both cases). While these responses did not generally differ from those
2453 observed under ambient CO₂, they do confirm the hypothesis that positive effects
2454 of inoculation on whole plant growth responses to elevated CO₂ would decrease
2455 with increasing fertilization.

2456 Combined, results reported here suggest that soil nitrogen availability plays
2457 divergent roles in shaping leaf and whole plant acclimation responses to CO₂. Leaf
2458 acclimation responses were generally decoupled from fertilization, while whole
2459 plant acclimation responses relied heavily on an increase in nitrogen uptake ef-
2460 ficiency and consequent reduction in costs of acquiring nitrogen associated with
2461 increasing fertilization. Whole plant responses to CO₂ indicated that fertilization
2462 may play a more important role in determining whole plant acclimation responses
2463 to CO₂ than nitrogen acquisition strategy, although any inoculation effect was
2464 likely masked by the strong reduction in root nodulation with increasing fertil-
2465 ization. These results suggest that plants acclimate to CO₂ in nitrogen-limited
2466 systems by minimizing the number of optimally coordinated leaves, and that
2467 downregulations in leaf nitrogen content under elevated CO₂ are not driven by
2468 changes in soil nitrogen availability as has been previously implied.

2469 5.4.2 *Implications for future model development*

2470 Many terrestrial biosphere models predict photosynthetic capacity through plant
2471 functional group-specific linear regressions between N_{area} and V_{cmax} (Rogers 2014;
2472 Rogers et al. 2017), which assumes that leaf nitrogen-photosynthesis relation-
2473 ships are constant across growing environments. These results build on previ-
2474 ous work suggesting that leaf nitrogen-photosynthesis relationships dynamically
2475 change across growing environments (Luo et al. 2021; Dong et al. 2022), showing

2476 that CO₂ concentration increases the fraction of leaf nitrogen content allocated to
2477 photosynthesis independent of fertilization or acquisition strategy. Additionally,
2478 increasing fertilization strongly decreased the fraction of leaf nitrogen allocated
2479 to photosynthesis, a response that was largely determined by acquisition strategy.
2480 Specifically, reductions in the fraction of leaf nitrogen allocated to photosynthesis
2481 with increasing fertilization were only observed in inoculated pots that had less
2482 finite access to nitrogen, suggesting that constant leaf nitrogen-photosynthesis
2483 relationships may only be apparent in environments where nitrogen is limiting.
2484 Terrestrial biosphere models that parameterize photosynthetic capacity through
2485 linear relationships between N_{area} and V_{cmax} (Rogers 2014; Rogers et al. 2017) may
2486 therefore be overestimating photosynthetic capacity in systems where nitrogen is
2487 not as limiting. Such models are also not capable of detecting stimulations in the
2488 fraction of leaf nitrogen allocated to photosynthesis with increasing CO₂ concen-
2489 tration. The inability of models to predict these responses likely contributes to the
2490 widespread divergence of model simulations under future environmental scenarios
2491 (Friedlingstein et al. 2014; Davies-Barnard et al. 2020), and should therefore be
2492 a target for resolving in future generations of terrestrial biosphere models.

2493 These results demonstrate that optimal resource investment to photosyn-
2494 thetic capacity defines leaf acclimation responses to elevated CO₂, and that these
2495 responses were independent of fertilization or inoculation treatment. Current
2496 model approaches for simulating photosynthetic responses to CO₂ generally invoke
2497 patterns expected from progressive nitrogen limitation, where the downregulation
2498 in N_{area} , and therefore photosynthetic capacity, due to elevated CO₂ is formu-
2499 lated as a function of progressive reductions in soil nitrogen availability. Results

2500 reported here contradict this formulation, suggesting that the leaf acclimation re-
2501 sponse is driven by optimal resource investment to photosynthetic capacity and
2502 is independent of soil resource supply. Optimality models that leverage prin-
2503 ciples from optimal coordination and photosynthetic least-cost theories (Wang
2504 et al. 2017; Stocker et al. 2020; Scott and Smith 2022) are capable of capturing
2505 such acclimation responses to CO₂ (Smith and Keenan 2020), suggesting that the
2506 implementation of these models may improve the simulation of photosynthetic
2507 processes in terrestrial biosphere models under increasing CO₂ concentrations.

2508 5.4.3 *Study limitations and future directions*

2509 There are two study limitations that must be addressed to contextualize patterns
2510 observed in this study. First, restricting the volume of belowground substrate
2511 via a potted experiment does not adequately replicate belowground environments
2512 of natural systems, and therefore may modify effects of soil resource availability
2513 and inoculation on plant nitrogen uptake. This limitation may be particularly
2514 relevant if pot size limits whole plant growth (Poorter et al. 2012). I attempted
2515 to minimize the extent of pot size limitation experienced in the first experimen-
2516 tal chapter while accounting for the expected stimulation in whole plant growth
2517 under elevated CO₂ by using 6-liter pots. Despite attempts to minimize growth
2518 limitation imposed by pot volume, fertilization and CO₂ treatments increased the
2519 biomass: pot volume ratio such that all treatment combinations to exceed 1 g L⁻¹
2520 biomass: pot volume under high fertilization (Table D3; Fig. D2). The 1 g L⁻¹
2521 biomass: pot volume recommendation from Poorter et al. (2012) was designated
2522 to avoid growth limitation imposed by pot volume. However, if pot size limita-

2523 tion indeed limited whole plant growth, then structural carbon costs to acquire
2524 nitrogen, belowground carbon biomass, whole plant nitrogen biomass, and whole
2525 plant biomass should each exhibit strong saturation points with increasing fertil-
2526 ization, which was not observed here. Importantly, leaf acclimation responses to
2527 CO₂ observed in this study are consistent with findings reported in (Smith and
2528 Keenan 2020), who used data from field manipulation experiments that did not
2529 have any belowground space limitation.

2530 Second, this study evaluated leaf and whole plant responses to CO₂ in 7-
2531 week seedlings. Given the long-term scale of the progressive nitrogen limitation
2532 hypothesis, patterns observed here should be validated in longer-term nitrogen
2533 manipulation experiments. Previous work in free air CO₂ enrichment experiments
2534 show some support for patterns expected from the progressive nitrogen limitation
2535 hypothesis (Reich et al. 2006; Norby et al. 2010), although results are not consis-
2536 tent across experimental sites (Finzi et al. 2006; Moore et al. 2006; Liang et al.
2537 2016). I found some support for patterns expected by the progressive nitrogen
2538 limitation hypothesis, namely the increase in plant nitrogen uptake under elevated
2539 CO₂ (Luo et al. 2004), though leaf acclimation responses to CO₂ were strongly
2540 indicative of optimal resource investment to photosynthetic capacity as expected
2541 from photosynthetic least-cost theory (Prentice et al. 2014; Smith et al. 2019;
2542 Smith and Keenan 2020).

2543 5.4.4 *Conclusions*

2544 This study provides strong evidence suggesting that leaf acclimation responses
2545 to elevated CO₂ did not vary with soil nitrogen fertilization or ability to acquire
2546 nitrogen through symbiotic nitrogen fixation. However, whole plant acclimation

2547 responses to CO₂ were dependent on fertilization, where increasing fertilization
2548 increased the positive effect of whole plant growth under elevated CO₂. Results
2549 also indicate that fertilization played a relatively more important role in modify-
2550 ing whole plant responses to CO₂ than inoculation with symbiotic nitrogen-fixing
2551 bacteria, perhaps due to a reduction in nodulation across the fertilization gra-
2552 dient. These patterns strongly support the hypothesis that leaf and whole plant
2553 acclimation responses are driven by optimal resource investment to photosynthetic
2554 capacity, and that leaf acclimation responses to CO₂ were not modified by changes
2555 in soil nitrogen availability. These results build on previous work suggesting that
2556 constant leaf nitrogen-photosynthesis relationships are dynamic and change across
2557 growing environments, calling the current formulation of photosynthetic processes
2558 used in many terrestrial biosphere models into question.

2559

Chapter 6

2560

Conclusions

2561 The experiments included in this dissertation test mechanisms that drive patterns
2562 expected from photosynthetic least-cost theory across various edaphic and climatic
2563 gradients. Specifically, I investigate environmental drivers of carbon costs to ac-
2564 quire nitrogen, tradeoffs between nitrogen and water use, and plant acclimation
2565 responses to CO₂. These experiments provide important empirical data needed to
2566 test assumptions made in optimality models that leverage photosynthetic least-
2567 cost frameworks, and are among the first manipulative experiments to show sup-
2568 port for patterns expected from theory. Below, I summarize main findings of each
2569 chapter, synthesize common patterns observed across experiments, and conclude
2570 with a few study ideas that I think will help refine our understanding of plant
2571 nutrient acquisition and allocation responses to environmental change leveraging
2572 patterns predicted by photosynthetic least-cost theory.

2573 In the first experimental chapter, I quantified carbon costs to acquire ni-
2574 trogen in a species capable of forming associations with symbiotic nitrogen-fixing
2575 bacteria (*Glycine max*) and a species not capable of forming such associations
2576 (*Gossypium hirsutum*) grown under four soil nitrogen fertilization treatments and
2577 four light availability treatments in a full factorial greenhouse experiment. Sup-
2578 porting hypotheses, increasing light availability increased carbon costs to acquire
2579 nitrogen in both species due to a larger increase in belowground carbon biomass
2580 than whole plant nitrogen biomass. In further support of hypotheses, increasing
2581 fertilization decreased carbon costs to acquire nitrogen due to a larger increase in

2582 whole plant nitrogen biomass than belowground carbon biomass. Root nodulation
2583 data indicated that *G. max* shifted relative carbon allocation from nitrogen fixa-
2584 tion to direct uptake with increasing fertilization, which may explain the reduced
2585 responsiveness of *G. max* carbon costs to acquire nitrogen across the fertilization
2586 gradient.

2587 Despite evidence that reductions in the response of *G. max* carbon costs
2588 to acquire nitrogen to increasing fertilization may have been driven by shifts away
2589 from nitrogen fixation with increasing fertilization, I urge caution in assigning
2590 causality to the differential response of carbon costs to acquire nitrogen between
2591 species. This is because *G. max* and *G. hirsutum* are not phylogenetically related
2592 and have different life histories. Differences in life history between the two species
2593 limit my ability to assess whether reductions in the negative effect of increasing
2594 fertilization on carbon costs to acquire nitrogen in *G. max* were driven by shifts
2595 to direct uptake with increasing fertilization. However, these patterns were later
2596 confirmed in the fourth experimental chapter, where similar weaker negative ef-
2597 fects of increasing fertilization on carbon costs to acquire nitrogen were observed
2598 in *G. max* that were inoculated with symbiotic nitrogen-fixing bacteria compared
2599 to *G. max* that were left uninoculated across a similar soil nitrogen fertilization
2600 gradient.

2601 In the second experimental chapter, I assessed whether changes in soil
2602 nitrogen availability or soil pH drove changes in nitrogen-water use tradeoffs pre-
2603 dicted by photosynthetic least-cost theory. I measured leaf traits of mature upper
2604 canopy deciduous trees growing in a nine-year nitrogen-by-sulfur field manipula-
2605 tion experiment, where experimental sulfur additions were added with intent to

2606 acidify plots. Following patterns expected from the theory, increasing soil nitrogen
2607 availability was associated with increased leaf nitrogen content, but not net photo-
2608 synthesis, resulting in an increase in photosynthetic nitrogen use efficiency. In
2609 further support of theory, increasing soil nitrogen availability exhibited slight, but
2610 nonsignificant, decreases in leaf $C_i:C_a$ and increases in measures of photosynthetic
2611 capacity. Perhaps the strongest evidence for the theory was a strong negative
2612 relationship between leaf nitrogen content and leaf $C_i:C_a$, of which increased with
2613 increasing soil nitrogen availability through a stronger increase in leaf nitrogen
2614 content than leaf $C_i:C_a$.

2615 I found no effect of soil pH on nitrogen-water use tradeoffs aside from a
2616 marginal reduction in net photosynthesis rates that marginally reduced photosyn-
2617hetic nitrogen use efficiency with increasing soil pH. Directionally, reductions in
2618 photosynthetic nitrogen use efficiency with increasing soil pH were expected per
2619 theory; however, this response was driven by no change in leaf nitrogen content
2620 and a reduction in net photosynthesis. Theory predicts that these tradeoffs should
2621 be driven by no change in net photosynthesis and an increase in leaf nitrogen con-
2622tent. The general null leaf response to changing soil pH may have been due to
2623 experimental treatments directly increased soil nitrogen availability and affected
2624 soil pH in opposite patterns, suggesting that soil nitrogen availability may be more
2625 important in dictating nitrogen-water use tradeoffs than soil pH per se.

2626 In the third experimental chapter, I quantified variance in leaf nitrogen
2627 content across a precipitation and soil resource availability gradient in Texan
2628 grasslands. Specifically, I measured area-based leaf nitrogen content, components
2629 of area-based leaf nitrogen content (leaf mass per unit leaf area, leaf nitrogen per

2630 unit dry biomass), leaf $C_i:C_a$, and the unit cost of acquiring nitrogen relative to
2631 water in 520 individuals comprising 57 species. I found that variance in area-
2632 based leaf nitrogen content was positively associated with increasing soil nitrogen
2633 availability, soil moisture, vapor pressure deficit, and was negatively related to
2634 increasing leaf $C_i:C_a$. Following patterns expected from theory, a path analysis
2635 revealed that the positive soil nitrogen-leaf nitrogen relationship was driven by a
2636 positive relationship between soil nitrogen availability and the unit cost of acquir-
2637 ing and using nitrogen relative to water, a positive relationship between the unit
2638 cost of acquiring and using nitrogen relative to water, and negative relationship
2639 between leaf $C_i:C_a$ and leaf mass per unit leaf area. Interestingly, there was no
2640 effect of $C_i:C_a$ on leaf nitrogen content per unit dry biomass, indicating that vari-
2641 ance in area-based leaf nitrogen content across the environmental gradient was
2642 driven by a change in leaf morphology and not leaf chemistry.

2643 In the fourth experimental chapter, I quantified leaf and whole plant accli-
2644 mation responses in *G. max* grown under two atmospheric CO₂ levels, with and
2645 without inoculation with *Bradyrhizobium japonicum*, and across nine nitrogen fer-
2646 tilization treatments in a full factorial growth chamber experiment. I found strong
2647 evidence that leaf nitrogen content, V_{cmax} , and J_{max} were each downregulated un-
2648 der elevated CO₂. A stronger downregulation in V_{cmax} than J_{max} and stronger
2649 downregulation in leaf nitrogen content than V_{cmax} or J_{max} provided strong sup-
2650 port suggesting that leaves were acclimating to elevated CO₂ by optimizing leaf
2651 photosynthetic resource use efficiency to achieve optimal coordination. In striking
2652 support of my hypotheses, I find strong evidence suggesting that leaf acclimation
2653 responses to elevated CO₂ were decoupled from soil nitrogen fertilization and in-

2654 oculation treatment, despite apparent strong increases in leaf nitrogen content,
2655 V_{cmax} , and J_{max} with increasing fertilization and in inoculated pots. These find-
2656 ings contrast the current formulation of photosynthetic processes in terrestrial
2657 biosphere models, where many models simulate downregulations in leaf nitrogen
2658 content under elevated CO₂ as a function of progressive nitrogen limitation.

2659 There are currently two iterations of optimality models that employ the
2660 use of patterns expected from photosynthetic least-cost theory, one for C₃ species
2661 (Wang et al. 2017; Smith et al. 2019; Stocker et al. 2020) and one more recently
2662 developed for C₄ species (Scott and Smith 2022). In both model variants, costs
2663 to acquire and use nitrogen relative to water are held constant using a global
2664 dataset of δ¹³C (Cornwell et al. 2018). Throughout experiments, I show strong
2665 evidence suggesting that costs to acquire and use nitrogen are dynamic and vary
2666 predictably across environmental gradients, and that changes in these costs scale
2667 to alter leaf nitrogen-water use tradeoffs and acclimation responses to changing
2668 environments in ways predicted through photosynthetic least-cost theory. Thus,
2669 while optimality model simulations show good agreement with measured data
2670 (Smith et al. 2019; Stocker et al. 2020), such models may not be capturing an
2671 important source of variability in leaf nitrogen-water use tradeoffs by holding costs
2672 of resource use constant across environmental gradients.

2673 First principles of photosynthetic least-cost theory suggest that, in a given
2674 environment, plants optimize photosynthesis rates by sacrificing inefficient use of
2675 a relatively more abundant (and less costly to acquire) resource for more efficient
2676 use of a relatively less abundant (and more costly to acquire) resource. Through-
2677 out experimental chapters, I show strong support for these patterns across ex-

2678 periments, where increasing soil nitrogen fertilization generally decreased the cost
2679 of acquiring nitrogen relative to water, a pattern that scaled to influence leaf
2680 nitrogen-water use tradeoffs. I did not find evidence to suggest that soil moisture
2681 influenced nitrogen-water use tradeoffs, though this was due to strong covariation
2682 between soil moisture and soil nitrogen availability. Overall, findings across exper-
2683 iments provide empirical validation of photosynthetic least-cost theory needed to
2684 further develop optimality models and eventually implement such models in ter-
2685 restrial biosphere model products. Many terrestrial biosphere model products do
2686 not include robust frameworks for simulating acclimation responses to changing
2687 environmental conditions, and empirical findings shown here provide some support
2688 that optimality models that leverage photosynthetic least-cost theory predictions
2689 may improve the ability of terrestrial biosphere models to accurately simulate
2690 photosynthetic processes.

2691 Many terrestrial biosphere models predict photosynthetic capacity through
2692 plant functional group-specific linear regressions between area-based leaf nitrogen
2693 content and V_{cmax} (Rogers 2014; Rogers et al. 2017), which assumes that leaf
2694 nitrogen-photosynthesis relationships are constant across growing environments.
2695 I found constant leaf nitrogen-photosynthesis relationships with increasing soil ni-
2696 trogen availability in the nitrogen-by-sulfur field manipulation experiment. How-
2697 ever, results from the CO₂-by-nitrogen-by-inoculation manipulation experiment
2698 indicated that leaf nitrogen-photosynthesis responses to soil nitrogen availability
2699 were dependent on whether nitrogen was limiting. Further investigation regard-
2700 ing the effect of soil nitrogen availability in modifying leaf nitrogen-photosynthesis
2701 relationships is warranted to better understand the generality of leaf nitrogen pho-

2702 tosynthesis relationships across environmental gradients. However, findings from
2703 these experiments suggest that representing photosynthetic processes through pos-
2704 itive relationships between soil nitrogen availability, leaf nitrogen, and photosyn-
2705 thetic capacity are likely contributing to erroneous errors in model simulations and
2706 may explain the high degree of divergence in simulated processes across terrestrial
2707 biosphere models (Friedlingstein et al. 2014; Davies-Barnard et al. 2020).

2708 The experiments included in this dissertation have provided a strong foun-
2709 dation for me to continue growing as a plant physiological ecologist. I envision
2710 five primary avenues for future research that build on the work presented here,
2711 which are briefly summarized below:

2712 1. Manipulative and environmental gradient experiments included here were
2713 designed to provide empirical data needed to test photosynthetic least-cost
2714 theory assumptions. While these results show promising patterns for pat-
2715 terns expected from photosynthetic least-cost theory, they do not necessarily
2716 address whether these patterns follow those simulated by optimality models
2717 that leverage photosynthetic least-cost principles. Thus, a clear future di-
2718 rection of these experiments would be to conduct model-data comparisons
2719 using data collected here (or similar experiments) to compare against opti-
2720 mality model simulations.

2721 2. Experiments included here explicitly quantify effects of symbiotic nitrogen
2722 fixation on carbon costs to acquire nitrogen, nitrogen-water use tradeoffs,
2723 and leaf nitrogen-photosynthesis relationships. However, carbon costs to ac-
2724 quire nitrogen also vary in species that associate with different mycorrhizal
2725 types (Brzostek et al. 2014; Terrer et al. 2018), and dominant mycorrhizal

2726 type in an ecosystem has been shown to determine net biogeochemical cycle
2727 dynamics in deciduous forests of the northeastern United States (Phillips
2728 et al. 2013). Thus, future work should consider conducting similar experi-
2729 ments while manipulating mycorrhizal association to better understand how
2730 microbial symbioses modify leaf and whole plant acclimation responses to
2731 changing environments.

2732 3. Recent work indicates a high degree of variance in symbiotic nitrogen fixa-
2733 tion rates across terrestrial biosphere models (Meyerholt et al. 2016; Davies-
2734 Barnard et al. 2020), perhaps due to nitrogen fixation rates that are im-
2735 plemented across terrestrial biosphere models as a function of temperature
2736 (Houlton et al. 2008). While energetic costs of nitrogen fixation are de-
2737 pendent on temperature, I show that structural carbon costs to acquire
2738 nitrogen via symbiotic nitrogen fixation are driven by factors that influence
2739 demand to acquire nitrogen (i.e. CO₂, light) and are modified by soil ni-
2740 tragen supply. The light-by-nitrogen greenhouse experiment was published
2741 in *Journal of Experimental Botany*, and a reviewer encouraged future work
2742 to include a model-data comparison comparing structural carbon costs to
2743 acquire nitrogen measured in the experiment to carbon costs to acquire ni-
2744 tragen simulated by the FUN biogeochemical model (Fisher et al. 2010;
2745 Brzostek et al. 2014; Allen et al. 2020). Conveniently, FUN calculates car-
2746 bon costs to acquire nitrogen following the same calculation used in the first
2747 and fourth experimental chapter. Conducting such a model-data comparison
2748 would be a useful step toward identifying biases in the FUN biogeochemi-
2749 cal model, which is currently coupled to several terrestrial biosphere models

2750 (Clark et al. 2011; Shi et al. 2016; Lawrence et al. 2019; Davies-Barnard
2751 et al. 2020).

2752 4. Carbon costs to acquire nitrogen relative to water were quantified at the
2753 leaf level as a function of $\delta^{13}\text{C}$ and vapor pressure deficit, while structural
2754 carbon costs to acquire nitrogen were quantified at the whole plant level
2755 as the ratio of belowground carbon allocation per unit whole plant nitro-
2756 gen biomass. As increasing soil nitrogen availability decreases both leaf and
2757 whole plant estimates of costs to acquire and use nitrogen, one might expect
2758 leaf and whole plant carbon cost to acquire nitrogen estimates to covary. Fu-
2759 ture work should consider investigating if leaf and whole plant estimates of
2760 carbon costs to acquire nitrogen covary and evaluate whether environmental
2761 conditions (or species acquisition strategy) modifies any of this possible co-
2762 variance. Strong covariance between leaf and whole plant costs of nitrogen
2763 acquisition could be a possible avenue to implement frameworks for allowing
2764 costs of nitrogen acquisition to vary in optimality models, as the FUN model
2765 calculates carbon costs of nitrogen acquisition at the whole plant level.

2766 5. While experiments included here target effects of soil nitrogen availability
2767 on carbon costs to acquire nitrogen and associated leaf nitrogen-water use
2768 tradeoffs, photosynthetic least-cost theory predicts that plants acclimate
2769 their photosynthetic processes by minimizing the summed cost of nutrient
2770 (not just nitrogen) and water use. Therefore, the theory would predict
2771 similar leaf acclimation responses across soil phosphorus or other nutrient
2772 availability gradients. Recent iterations of the FUN biogeochemical cycle
2773 includes a framework for determining the carbon and nitrogen cost of ac-

2774 quiring and using phosphorus, which similarly varies in species with different
2775 nutrient acquisition strategies (Allen et al. 2020). The implementation of
2776 this model in a terrestrial biosphere model (E3SM) was also recently shown
2777 to improve model performance of ecosystem nutrient limitation (Braghieri
2778 et al. 2022). As nitrogen and phosphorus commonly co-limit leaf photo-
2779 synthesis and primary productivity, extending experiments reported here to
2780 investigate carbon and nitrogen costs of phosphorus use, and whether these
2781 patterns scale to leaf nutrient-water use tradeoffs would be a useful next
2782 step in understanding extensions and limitations of photosynthetic least-
2783 cost theory.

2784 The experiments included in this dissertation and the proposed experiments sum-
2785 marized above provide a snapshot view of the things that I have learned through-
2786 out my time as a graduate student. I am excited to continue learning and growing
2787 as a plant ecophysiologicalist, ecologist, and scientist, and look forward to continuing
2788 along my journey of investigating nutrient acquisition and allocation responses to
2789 global change.

2790

References

- 2791** Abrams, M. D. and S. A. Mostoller (1995). Gas exchange, leaf structure and
2792 nitrogen in contrasting successional tree species growing in open and under-
2793 story sites during a drought. *Tree Physiology* 15(6), 361–370.
- 2794** Adams, M. A., T. L. Turnbull, J. I. Sprent, and N. Buchmann (2016). Legumes
2795 are different: Leaf nitrogen, photosynthesis, and water use efficiency. *Pro-
2796 ceedings of the National Academy of Sciences of the United States of Amer-
2797 ica* 113(15), 4098–4103.
- 2798** Ainsworth, E. A., P. A. Davey, C. J. Bernacchi, O. C. Dermody, E. A. Heaton,
2799 D. J. Moore, P. B. Morgan, S. L. Naidu, H. S. Y. Ra, X. G. Zhu, P. S. Curtis,
2800 and S. P. Long (2002). A meta-analysis of elevated [CO₂] effects on soybean
2801 (*Glycine max*) physiology, growth and yield. *Global Change Biology* 8(8),
2802 695–709.
- 2803** Ainsworth, E. A. and S. P. Long (2005). What have we learned from 15 years of
2804 free-air CO₂ enrichment (FACE)? A meta-analytic review of the responses
2805 of photosynthesis, canopy properties and plant production to rising CO₂.
2806 *New Phytologist* 165(2), 351–372.
- 2807** Ainsworth, E. A. and A. Rogers (2007). The response of photosynthesis and
2808 stomatal conductance to rising [CO₂]: mechanisms and environmental in-
2809 teractions. *Plant, Cell and Environment* 30(3), 258–270.
- 2810** Allen, K., J. B. Fisher, R. P. Phillips, J. S. Powers, and E. R. Brzostek (2020).
2811 Modeling the carbon cost of plant nitrogen and phosphorus uptake across
2812 temperate and tropical forests. *Frontiers in Forests and Global Change* 3,

- 2813** 1–12.
- 2814** Allison, S. D., C. I. Czimczik, and K. K. Treseder (2008). Microbial activity
2815 and soil respiration under nitrogen addition in Alaskan boreal forest. *Global
2816 Change Biology* 14(5), 1156–1168.
- 2817** Andersen, M. K., H. Hauggaard-Nielsen, P. Ambus, and E. S. Jensen (2005).
2818 Biomass production, symbiotic nitrogen fixation and inorganic N use in dual
2819 and tri-component annual intercrops. *Plant and Soil* 266(1-2), 273–287.
- 2820** Andrews, M., E. K. James, J. I. Sprent, R. M. Boddey, E. Gross, and F. B. dos
2821 Reis (2011). Nitrogen fixation in legumes and actinorhizal plants in natural
2822 ecosystems: Values obtained using ^{15}N natural abundance. *Plant Ecology
2823 and Diversity* 4(2-3), 117–130.
- 2824** Arndal, M. F., A. Tolver, K. S. Larsen, C. Beier, and I. K. Schmidt (2018). Fine
2825 root growth and vertical distribution in response to elevated CO₂, warming
2826 and drought in a mixed heathland–grassland. *Ecosystems* 21(1), 15–30.
- 2827** Arnone, J. A. (1997). Indices of plant N availability in an alpine grassland under
2828 elevated atmospheric CO₂. *Plant and Soil* 190(1), 61–66.
- 2829** Arora, V. K., A. Katavouta, R. G. Williams, C. D. Jones, V. Brovkin,
2830 P. Friedlingstein, J. Schwinger, L. Bopp, O. Boucher, P. Cadule, M. A.
2831 Chamberlain, J. R. Christian, C. Delire, R. A. Fisher, T. Hajima, T. Ilyina,
2832 E. Joetzjer, M. Kawamiya, C. D. Koven, J. P. Krasting, R. M. Law, D. M.
2833 Lawrence, A. Lenton, K. Lindsay, J. Pongratz, T. Raddatz, R. Séférian,
2834 K. Tachiiri, J. F. Tjiputra, A. Wiltshire, T. Wu, and T. Ziehn (2020).
2835 Carbon-concentration and carbon-climate feedbacks in CMIP6 models and
2836 their comparison to CMIP5 models. *Biogeosciences* 17(16), 4173–4222.

- 2837 Bae, K., T. J. Fahey, R. D. Yanai, and M. Fisk (2015). Soil nitrogen availability affects belowground carbon allocation and soil respiration in northern
2838 hardwood forests of New Hampshire. *Ecosystems* 18(7), 1179–1191.
- 2839
- 2840 Barber, S. A. (1962). A diffusion and mass-flow concept of soil nutrient availability. *Soil Science* 93(1), 39–49.
- 2841
- 2842 Barnes, J. D., L. Balaguer, E. Manrique, S. Elvira, and A. W. Davison (1992).
2843 A reappraisal of the use of DMSO for the extraction and determination
2844 of chlorophylls a and b in lichens and higher plants. *Environmental and
2845 Experimental Botany* 32(2), 85–100.
- 2846 Bates, D., M. Mächler, B. Bolker, and S. Walker (2015). Fitting linear mixed-
2847 effects models using lme4. *Journal of Statistical Software* 67(1), 1–48.
- 2848 Beaudette, D., J. Skovlin, S. Roeker, and A. Brown (2022). soilDB: Soil
2849 Database Interface.
- 2850 Bengtson, P., J. Barker, and S. J. Grayston (2012). Evidence of a strong cou-
2851 pling between root exudation, C and N availability, and stimulated SOM
2852 decomposition caused by rhizosphere priming effects. *Ecology and Evolu-
2853 tion* 2(8), 1843–1852.
- 2854 Bernacchi, C. J., E. L. Singsaas, C. Pimentel, A. R. Portis, and S. P. Long
2855 (2001). Improved temperature response functions for models of Rubisco-
2856 limited photosynthesis. *Plant, Cell and Environment* 24(2), 253–259.
- 2857 Bialic-Murphy, L., N. G. Smith, P. Voothuluru, R. M. McElderry, M. D.
2858 Roche, S. T. Cassidy, S. N. Kivlin, and S. Kalisz (2021). Invasion-induced
2859 root–fungal disruptions alter plant water and nitrogen economies. *Ecology*

- 2860** *Letters* 24(6), 1145–1156.
- 2861** Bloom, A. J., F. S. Chapin, and H. A. Mooney (1985). Resource limitation
2862 in plants - an economic analogy. *Annual Review of Ecology and Systemat-*
2863 *ics* 16(1), 363–392.
- 2864** Bloomfield, K. J., B. D. Stocker, T. F. Keenan, and I. C. Prentice (2023).
2865 Environmental controls on the light use efficiency of terrestrial gross primary
2866 production. *Global Change Biology* 29(4), 0–2.
- 2867** Bonan, G. B., M. D. Hartman, W. J. Parton, and W. R. Wieder (2013). Eval-
2868 uating litter decomposition in earth system models with long-term litter
2869 bag experiments: an example using the Community Land Model version 4
2870 (CLM4). *Global Change Biology* 19(3), 957–974.
- 2871** Bonan, G. B., P. J. Lawrence, K. W. Oleson, S. Levis, M. Jung, M. Reich-
2872 stein, D. M. Lawrence, and S. C. Swenson (2011). Improving canopy pro-
2873 cesses in the Community Land Model version 4 (CLM4) using global flux
2874 fields empirically inferred from FLUXNET data. *Journal of Geophysical Re-*
2875 *search* 116(G2), G02014.
- 2876** Booth, B. B. B., C. D. Jones, M. Collins, I. J. Totterdell, P. M. Cox, S. Sitch,
2877 C. Huntingford, R. A. Betts, G. R. Harris, and J. Lloyd (2012). High sen-
2878 sitivity of future global warming to land carbon cycle processes. *Environ-*
2879 *mental Research Letters* 7(2), 024002.
- 2880** Borer, E. T., W. S. Harpole, P. B. Adler, E. M. Lind, J. L. Orrock, E. W.
2881 Seabloom, and M. D. Smith (2014). Finding generality in ecology: A model
2882 for globally distributed experiments. *Methods in Ecology and Evolution* 5(1),
2883 65–73.

- 2884** Braghieri, R. K., J. B. Fisher, K. Allen, E. Brzostek, M. Shi, X. Yang, D. M.
2885 Ricciuto, R. A. Fisher, Q. Zhu, and R. P. Phillips (2022). Modeling global
2886 carbon costs of plant nitrogen and phosphorus acquisition. *Journal of Ad-*
2887 *vances in Modeling Earth Systems* 14(8), 1–23.
- 2888** Brix, H. (1971). Effects of nitrogen fertilization on photosynthesis and respira-
2889 tion in Douglas-fir. *Forest Science* 17(4), 407–414.
- 2890** Brzostek, E. R., J. B. Fisher, and R. P. Phillips (2014). Modeling the carbon
2891 cost of plant nitrogen acquisition: Mycorrhizal trade-offs and multipath
2892 resistance uptake improve predictions of retranslocation. *Journal of Geo-*
2893 *physical Research: Biogeosciences* 119, 1684–1697.
- 2894** Bubier, J. L., R. Smith, S. Juutinen, T. R. Moore, R. Minocha, S. Long, and
2895 S. Minocha (2011). Effects of nutrient addition on leaf chemistry, morphol-
2896 ogy, and photosynthetic capacity of three bog shrubs. *Oecologia* 167(2),
2897 355–368.
- 2898** Cernusak, L. A., N. Ubierna, K. Winter, J. A. M. Holtum, J. D. Marshall, and
2899 G. D. Farquhar (2013). Environmental and physiological determinants of
2900 carbon isotope discrimination in terrestrial plants. *New Phytologist* 200(4),
2901 950–965.
- 2902** Chen, J.-L., J. F. Reynolds, P. C. Harley, and J. D. Tenhunen (1993). Coor-
2903 dination theory of leaf nitrogen distribution in a canopy. *Oecologia* 93(1),
2904 63–69.
- 2905** Clark, D. B., L. M. Mercado, S. Sitch, C. D. Jones, N. Gedney, M. J. Best,
2906 M. Pryor, G. G. Rooney, R. L. H. Essery, E. Blyth, O. Boucher, R. J.
2907 Harding, C. Huntingford, and P. M. Cox (2011). The Joint UK Land Envi-

- 2908 ronment Simulator (JULES), model description. Part 2: Carbon fluxes and
2909 vegetation dynamics. *Geoscientific Model Development* 4(3), 701–722.
- 2910 Cornwell, W. K., J. H. C. Cornelissen, K. Amatangelo, E. Dorrepaal, V. T.
2911 Eviner, O. Godoy, S. E. Hobbie, B. Hoorens, H. Kurokawa, N. Pérez-
2912 Harguindeguy, H. M. Quested, L. S. Santiago, D. A. Wardle, I. J. Wright,
2913 R. Aerts, S. D. Allison, P. van Bodegom, V. Brovkin, A. Chatain, T. V.
2914 Callaghan, S. Díaz, E. Garnier, D. E. Gurvich, E. Kazakou, J. A. Klein,
2915 J. Read, P. B. Reich, N. A. Soudzilovskaia, M. V. Vaieretti, and M. Westoby
2916 (2008). Plant species traits are the predominant control on litter decompo-
2917 sition rates within biomes worldwide. *Ecology Letters* 11(10), 1065–1071.
- 2918 Cornwell, W. K., I. J. Wright, J. Turner, V. Maire, M. M. Barbour, L. A.
2919 Cernusak, T. E. Dawson, D. S. Ellsworth, G. D. Farquhar, H. Griffiths,
2920 C. Keitel, A. Knohl, P. B. Reich, D. G. Williams, R. Bhaskar, J. H. C. Cor-
2921 nelissen, A. Richards, S. Schmidt, F. Valladares, C. Körner, E.-D. Schulze,
2922 N. Buchmann, and L. S. Santiago (2018). Climate and soils together regulate
2923 photosynthetic carbon isotope discrimination within C₃ plants worldwide.
2924 *Global Ecology and Biogeography* 27(9), 1056–1067.
- 2925 Cramer, W. and I. C. Prentice (1988). Simulation of regional soil moisture
2926 deficits on a European scale. *Norsk Geografisk Tidsskrift - Norwegian Jour-*
2927 *nal of Geography* 42(2-3), 149–151.
- 2928 Curtis, P. S. (1996). A meta-analysis of leaf gas exchange and nitrogen in trees
2929 grown under elevated carbon dioxide. *Plant, Cell and Environment* 19(2),
2930 127–137.
- 2931 Daly, C., M. Halbleib, J. I. Smith, W. P. Gibson, M. K. Doggett, G. H. Taylor,

- 2932** J. Curtis, and P. P. Pasteris (2008). Physiographically sensitive mapping
2933 of climatological temperature and precipitation across the conterminous
2934 United States. *International Journal of Climatology* 28(15), 2031–2064.
- 2935** Davies-Barnard, T., J. Meyerholt, S. Zaehle, P. Friedlingstein, V. Brovkin,
2936 Y. Fan, R. A. Fisher, C. D. Jones, H. Lee, D. Peano, B. Smith, D. Wårlind,
2937 and A. J. Wiltshire (2020). Nitrogen cycling in CMIP6 land surface models:
2938 progress and limitations. *Biogeosciences* 17(20), 5129–5148.
- 2939** Davis, T. W., I. C. Prentice, B. D. Stocker, R. T. Thomas, R. J. Whitley,
2940 H. Wang, B. J. Evans, A. V. Gallego-Sala, M. T. Sykes, and W. Cramer
2941 (2017). Simple process-led algorithms for simulating habitats (SPLASH
2942 v.1.0): robust indices of radiation, evapotranspiration and plant-available
2943 moisture. *Geoscientific Model Development* 10, 689–708.
- 2944** Delaire, M., E. Frak, M. Sigogne, B. Adam, F. Beaujard, and X. Le Roux
2945 (2005). Sudden increase in atmospheric CO₂ concentration reveals strong
2946 coupling between shoot carbon uptake and root nutrient uptake in young
2947 walnut trees. *Tree Physiology* 25(2), 229–235.
- 2948** Doane, T. A. and W. R. Horwáth (2003). Spectrophotometric determination of
2949 nitrate with a single reagent. *Analytical Letters* 36(12), 2713–2722.
- 2950** Dong, N., I. C. Prentice, B. J. Evans, S. Caddy-Retalic, A. J. Lowe, and I. J.
2951 Wright (2017). Leaf nitrogen from first principles: field evidence for adaptive
2952 variation with climate. *Biogeosciences* 14(2), 481–495.
- 2953** Dong, N., I. C. Prentice, I. J. Wright, B. J. Evans, H. F. Togashi, S. Caddy-
2954 Retalic, F. A. McInerney, B. Sparrow, E. Leitch, and A. J. Lowe (2020).
2955 Components of leaf-trait variation along environmental gradients. *New Phy-*

- 2956** *tologist* 228(1), 82–94.
- 2957** Dong, N., I. C. Prentice, I. J. Wright, H. Wang, O. K. Atkin, K. J. Bloomfield,
- 2958** T. F. Domingues, S. M. Gleason, V. Maire, Y. Onoda, H. Poorter, and N. G.
- 2959** Smith (2022). Leaf nitrogen from the perspective of optimal plant function.
- 2960** *Journal of Ecology* 110(11), 2585–2602.
- 2961** Dong, N., I. J. Wright, J. M. Chen, X. Luo, H. Wang, T. F. Keenan, N. G.
- 2962** Smith, and I. C. Prentice (2022). Rising CO₂ and warming reduce global
- 2963** canopy demand for nitrogen. *New Phytologist* 235(5), 1692–1700.
- 2964** Dovrat, G., H. Bakhshian, T. Masci, and E. Sheffer (2020). The nitrogen eco-
- 2965** nomic spectrum of legume stoichiometry and fixation strategy. *New Phytol-*
- 2966** *ogist* 227(2), 365–375.
- 2967** Dovrat, G., T. Masci, H. Bakhshian, E. Mayzlish Gati, S. Golan, and E. Shef-
- 2968** fer (2018). Drought-adapted plants dramatically downregulate dinitrogen
- 2969** fixation: Evidences from Mediterranean legume shrubs. *Journal of Ecol-*
- 2970** *ogy* 106(4), 1534–1544.
- 2971** Drake, B. G., M. A. Gonzàlez-Meler, and S. P. Long (1997). More efficient
- 2972** plants: a consequence of rising atmospheric CO₂? *Annual Review of Plant*
- 2973** *Biology* 48, 609–639.
- 2974** Duursma, R. A. (2015). Plantecophys - An R package for analyzing and mod-
- 2975** elling leaf gas exchange data. *PLOS ONE* 10(11), e0143346.
- 2976** Eamus, D., N. Boulain, J. Cleverly, and D. D. Breshears (2013). Global change-
- 2977** type drought-induced tree mortality: Vapor pressure deficit is more impor-
- 2978** tant than temperature per se in causing decline in tree health. *Ecology and*

- 2979** *Evolution* 3(8), 2711–2729.
- 2980** Eastman, B. A., M. B. Adams, E. R. Brzostek, M. B. Burnham, J. E. Carrara,
- 2981** C. Kelly, B. E. McNeil, C. A. Walter, and W. T. Peterjohn (2021). Altered
- 2982** plant carbon partitioning enhanced forest ecosystem carbon storage after 25
- 2983** years of nitrogen additions. *New Phytologist* 230(4), 1435–1448.
- 2984** Ellsworth, D. S. and P. B. Reich (1996). Photosynthesis and leaf nitrogen in five
- 2985** Amazonian tree species during early secondary succession. *Ecology* 77(2),
- 2986** 581–594.
- 2987** Espelta, J. M., P. Cortés, M. Mangirón, and J. Retana (2005). Differences
- 2988** in biomass partitioning, leaf nitrogen content, and water use efficiency δ^{13}
- 2989** result in similar performance of seedlings of two Mediterranean oaks with
- 2990** contrasting leaf habit. *Ecoscience* 12(4), 447–454.
- 2991** Evans, J. R. (1989). Photosynthesis and nitrogen relationships in leaves of C₃
- 2992** plants. *Oecologia* 78(1), 9–19.
- 2993** Evans, J. R. and V. C. Clarke (2019). The nitrogen cost of photosynthesis.
- 2994** *Journal of Experimental Botany* 70(1), 7–15.
- 2995** Evans, J. R. and H. Poorter (2001). Photosynthetic acclimation of plants to
- 2996** growth irradiance: the relative importance of specific leaf area and nitrogen
- 2997** partitioning in maximizing carbon gain. *Plant, Cell and Environment* 24(8),
- 2998** 755–767.
- 2999** Evans, J. R. and J. R. Seemann (1989). The allocation of protein nitrogen in
- 3000** the photosynthetic apparatus: costs, consequences, and control. *Photosynthesis*
- 3001** 8, 183–205.

- 3002** Exbrayat, J.-F., A. A. Bloom, P. Falloon, A. Ito, T. L. Smallman, and
3003 M. Williams (2018). Reliability ensemble averaging of 21st century projec-
3004 tions of terrestrial net primary productivity reduces global and regional
3005 uncertainties. *Earth System Dynamics* 9(1), 153–165.
- 3006** Farquhar, G. D., J. R. Ehleringer, and K. T. Hubick (1989). Carbon isotope
3007 discrimination and photosynthesis. *Annual Review of Plant Physiology and*
3008 *Plant Molecular Biology* 40(1), 503–537.
- 3009** Farquhar, G. D. and T. D. Sharkey (1982). Stomatal conductance and photo-
3010 synthesis. *Annual Review of Plant Physiology* 33(1), 317–345.
- 3011** Farquhar, G. D., S. von Caemmerer, and J. A. Berry (1980). A biochemical
3012 model of photosynthetic CO₂ assimilation in leaves of C₃ species.
3013 *Planta* 149(1), 78–90.
- 3014** Fay, P. A., S. M. Prober, W. S. Harpole, J. M. H. Knops, J. D. Bakker, E. T.
3015 Borer, E. M. Lind, A. S. MacDougall, E. W. Seabloom, P. D. Wragg, P. B.
3016 Adler, D. M. Blumenthal, Y. M. Buckley, C. Chu, E. E. Cleland, S. L.
3017 Collins, K. F. Davies, G. Du, X. Feng, J. Firn, D. S. Gruner, N. Hagenah,
3018 Y. Hautier, R. W. Heckman, V. L. Jin, K. P. Kirkman, J. A. Klein, L. M.
3019 Ladwig, Q. Li, R. L. McCulley, B. A. Melbourne, C. E. Mitchell, J. L. Moore,
3020 J. W. Morgan, A. C. Risch, M. Schütz, C. J. Stevens, D. A. Wedin, and
3021 L. H. Yang (2015). Grassland productivity limited by multiple nutrients.
3022 *Nature Plants* 1(7), 15080.
- 3023** Feng, X. (1999). Trends in intrinsic water-use efficiency of natural trees for the
3024 past 100-200 years: A response to atmospheric CO₂ concentration. *Geochim-
ica et Cosmochimica Acta* 63(13-14), 1891–1903.

- 3026 Field, C. B. and H. A. Mooney (1986). The photosynthesis-nitrogen relationship
3027 in wild plants. In T. J. Givnish (Ed.), *On the Economy of Plant Form and*
3028 *Function*, pp. 25–55. Cambridge: Cambridge University Press.
- 3029 Finzi, A. C., D. J. P. Moore, E. H. DeLucia, J. Lichter, K. S. Hofmockel, R. B.
3030 Jackson, H. S. Kim, R. Matamala, H. R. McCarthy, R. Oren, J. S. Pippen,
3031 and W. H. Schlesinger (2006). Progressive nitrogen limitation of ecosystem
3032 processes under elevated CO₂ in a warm-temperate forest. *Ecology* 87(1),
3033 15–25.
- 3034 Firn, J., J. M. McGree, E. Harvey, H. Flores Moreno, M. Schutz, Y. M. Buckley,
3035 E. T. Borer, E. W. Seabloom, K. J. La Pierre, A. M. MacDougall, S. M.
3036 Prober, C. J. Stevens, L. L. Sullivan, E. Porter, E. Ladouceur, C. Allen,
3037 K. H. Moromizato, J. W. Morgan, W. S. Harpole, Y. Hautier, N. Eisen-
3038 hauer, J. P. Wright, P. B. Adler, C. A. Arnillas, J. D. Bakker, L. Biederman,
3039 A. A. D. Broadbent, C. S. Brown, M. N. Bugalho, M. C. Caldeira, E. E. Cle-
3040 land, A. Ebeling, P. A. Fay, N. Hagenah, A. R. Kleinhesselink, R. Mitchell,
3041 J. L. Moore, C. Nogueira, P. L. Peri, C. Roscher, M. D. Smith, P. D. Wragg,
3042 and A. C. Risch (2019). Leaf nutrients, not specific leaf area, are consistent
3043 indicators of elevated nutrient inputs. *Nature Ecology and Evolution* 3(3),
3044 400–406.
- 3045 Fisher, J. B., S. Sitch, Y. Malhi, R. A. Fisher, C. Huntingford, and S.-Y. Tan
3046 (2010). Carbon cost of plant nitrogen acquisition: A mechanistic, globally
3047 applicable model of plant nitrogen uptake, retranslocation, and fixation.
3048 *Global Biogeochemical Cycles* 24(1), 1–17.
- 3049 Fox, J. and S. Weisberg (2019). *An R companion to applied regression* (Third

- 3050** edit ed.). Thousand Oaks, California: Sage.
- 3051** Franklin, O., R. E. McMurtrie, C. M. Iversen, K. Y. Crous, A. C. Finzi, D. Tis-
- 3052** sue, D. S. Ellsworth, R. Oren, and R. J. Norby (2009). Forest fine-root
- 3053** production and nitrogen use under elevated CO₂: contrasting responses
- 3054** in evergreen and deciduous trees explained by a common principle. *Global*
- 3055** *Change Biology* 15(1), 132–144.
- 3056** Friedlingstein, P., M. Meinshausen, V. K. Arora, C. D. Jones, A. Anav, S. K.
- 3057** Liddicoat, and R. Knutti (2014). Uncertainties in CMIP5 climate projections
- 3058** due to carbon cycle feedbacks. *Journal of Climate* 27(2), 511–526.
- 3059** Friel, C. A. and M. L. Friesen (2019). Legumes modulate allocation to rhizobial
- 3060** nitrogen fixation in response to factorial light and nitrogen manipulation.
- 3061** *Frontiers in Plant Science* 10, 1316.
- 3062** Fujikake, H., A. Yamazaki, N. Ohtake, K. Sueoshi, S. Matsuhashi, T. Ito,
- 3063** C. Mizuniwa, T. Kume, S. Hoshimoto, N.-S. Ishioka, S. Watanabe, A. Osa,
- 3064** T. Sekine, H. Uchida, A. Tsuji, and T. Ohyama (2003). Quick and reversible
- 3065** inhibition of soybean root nodule growth by nitrate involves a decrease in
- 3066** sucrose supply to nodules. *Journal of Experimental Botany* 54(386), 1379–
- 3067** 1388.
- 3068** Ghannoum, O., J. R. Evans, and S. von Caemmerer (2011). Nitrogen and water
- 3069** use efficiency of C₄ plants. In A. S. Raghavendra and R. F. Sage (Eds.), *C₄*
- 3070** *Photosynthesis and Related CO₂ Concentrating Mechanisms*, Chapter 8, pp.
- 3071** 129–146. Springer.
- 3072** Ghimire, B., W. J. Riley, C. D. Koven, J. Kattge, A. Rogers, P. B. Reich, and
- 3073** I. J. Wright (2017). A global trait-based approach to estimate leaf nitro-

- 3074 gen functional allocation from observations:. *Ecological Applications* 27(5),
3075 1421–1434.
- 3076 Giardina, C. P., M. D. Coleman, J. E. Hancock, J. S. King, E. A. Lilleskov,
3077 W. M. Loya, K. S. Pregitzer, M. G. Ryan, and C. C. Trettin (2005). The
3078 response of belowground carbon allocation in forests to global change. In
3079 D. Binkley and O. Manyailo (Eds.), *Tree Species Effects on Soils: Implica-*
3080 *tions for Global Change* (Volume 55 ed.), Chapter Chapter 7, pp. 119–154.
3081 Berlin/Heidelberg: Springer-Verlag.
- 3082 Gibson, A. H. and J. E. Harper (1985). Nitrate effect on nodulation of soybean
3083 by *Bradyrhizobium japonicum*. *Crop Science* 25(3), 497–501.
- 3084 Gill, A. L. and A. C. Finzi (2016). Belowground carbon flux links biogeochemical
3085 cycles and resource-use efficiency at the global scale. *Ecology Letters* 19(12),
3086 1419–1428.
- 3087 Goll, D. S., V. Brovkin, B. R. Parida, C. H. Reick, J. Kattge, P. B. Reich, P. M.
3088 van Bodegom, and Ü. Niinemets (2012). Nutrient limitation reduces land
3089 carbon uptake in simulations with a model of combined carbon, nitrogen
3090 and phosphorus cycling. *Biogeosciences Discussions* 9(3), 3173–3232.
- 3091 Gregory, L. M., A. M. McClain, D. M. Kramer, J. D. Pardo, K. E. Smith, O. L.
3092 Tessmer, B. J. Walker, L. G. Ziccardi, and T. D. Sharkey (2021, oct). The
3093 triose phosphate utilization limitation of photosynthetic rate: Out of global
3094 models but important for leaf models. *Plant, Cell and Environment* 44(10),
3095 3223–3226.
- 3096 Grossiord, C., T. N. Buckley, L. A. Cernusak, K. A. Novick, B. Poulter, R. T. W.
3097 Siegwolf, J. S. Sperry, and N. G. McDowell (2020). Plant responses to rising

- 3098** vapor pressure deficit. *New Phytologist* 226(6), 1550–1566.
- 3099** Gulmon, S. L. and C. C. Chu (1981). The effects of light and nitrogen on photo-
- 3100** synthesis, leaf characteristics, and dry matter allocation in the chaparral
- 3101** shrub, *Diplacus aurantiacus*. *Oecologia* 49(2), 207–212.
- 3102** Gutschick, V. P. (1981). Evolved strategies in nitrogen acquisition by plants.
- 3103** *The American Naturalist* 118(5), 607–637.
- 3104** Hallik, L., Ü. Niinemets, and I. J. Wright (2009). Are species shade and drought
- 3105** tolerance reflected in leaf-level structural and functional differentiation in
- 3106** Northern Hemisphere temperate woody flora? *New Phytologist* 184(1), 257–
- 3107** 274.
- 3108** Harrison, M. T., E. J. Edwards, G. D. Farquhar, A. B. Nicotra, and J. R.
- 3109** Evans (2009). Nitrogen in cell walls of sclerophyllous leaves accounts for
- 3110** little of the variation in photosynthetic nitrogen-use efficiency. *Plant, Cell*
- 3111** and *Environment* 32(3), 259–270.
- 3112** Harrison, S. P., W. Cramer, O. Franklin, I. C. Prentice, H. Wang,
- 3113** Å. Brännström, H. de Boer, U. Dieckmann, J. Joshi, T. F. Keenan,
- 3114** A. Lavergne, S. Manzoni, G. Mengoli, C. Morfopoulos, J. Peñuelas,
- 3115** S. Pietsch, K. T. Rebel, Y. Ryu, N. G. Smith, B. D. Stocker, and I. J.
- 3116** Wright (2021). Eco-evolutionary optimality as a means to improve vegetation
- 3117** and land-surface models. *New Phytologist* 231(6), 2125–2141.
- 3118** Henneron, L., P. Kardol, D. A. Wardle, C. Cros, and S. Fontaine (2020). Rhizo-
- 3119** sphere control of soil nitrogen cycling: a key component of plant economic
- 3120** strategies. *New Phytologist* 228(4), 1269–1282.

- 3121** Hijmans, R. J. (2022). *terra: Spatial Data Analysis*.
- 3122** Hikosaka, K. and A. Shigeno (2009). The role of Rubisco and cell walls in the
3123 interspecific variation in photosynthetic capacity. *Oecologia* 160(3), 443–
3124 451.
- 3125** Hoagland, D. R. and D. I. Arnon (1950). The water culture method for growing
3126 plants without soil. *California Agricultural Experiment Station: 347* 347(2),
3127 1–32.
- 3128** Hobbie, E. A. (2006). Carbon allocation to ectomycorrhizal fungi correlates
3129 with belowground allocation in culture studies. *Ecology* 87(3), 563–569.
- 3130** Hobbie, E. A. and J. E. Hobbie (2008). Natural abundance of ^{15}N in nitrogen-
3131 limited forests and tundra can estimate nitrogen cycling through mycorrhizal
3132 fungi: a review. *Ecosystems* 11(5), 815–830.
- 3133** Hoek, T. A., K. Axelrod, T. Biancalani, E. A. Yurtsev, J. Liu, and J. Gore
3134 (2016). Resource availability modulates the cooperative and competitive na-
3135 nature of a microbial cross-feeding mutualism. *PLOS Biology* 14(8), e1002540.
- 3136** Höglberg, M. N., M. J. I. Briones, S. G. Keel, D. B. Metcalfe, C. Campbell, A. J.
3137 Midwood, B. Thornton, V. Hurry, S. Linder, T. Näsholm, and P. Höglberg
3138 (2010). Quantification of effects of season and nitrogen supply on tree below-
3139 ground carbon transfer to ectomycorrhizal fungi and other soil organisms in
3140 a boreal pine forest. *New Phytologist* 187(2), 485–493.
- 3141** Höglberg, P., M. N. Höglberg, S. G. Göttlicher, N. R. Betson, S. G. Keel, D. B.
3142 Metcalfe, C. Campbell, A. Schindlbacher, V. Hurry, T. Lundmark, S. Linder,
3143 and T. Näsholm (2008). High temporal resolution tracing of photosynthate

- 3144** carbon from the tree canopy to forest soil microorganisms. *New Phytologist* 177(1), 220–228.
- 3146** Houlton, B. Z., Y.-P. Wang, P. M. Vitousek, and C. B. Field (2008). A unifying framework for dinitrogen fixation in the terrestrial biosphere. *Nature* 454(7202), 327–330.
- 3149** Huber, M. L., R. A. Perkins, A. Laesecke, D. G. Friend, J. V. Sengers, M. J. Assael, I. N. Metaxa, E. Vogel, R. Mareš, and K. Miyagawa (2009). New international formulation for the viscosity of H₂O. *Journal of Physical and Chemical Reference Data* 38(2), 101–125.
- 3153** Hungate, B. A., J. S. Dukes, M. R. Shaw, Y. Luo, and C. B. Field (2003). Nitrogen and climate change. *Science* 302(5650), 1512–1513.
- 3155** IPCC (2021). *Climate Change 2021: The Physical Science Basis. Contribution of Working Group I to the Sixth Assessment Report of the Intergovernmental Panel on Climate Change*, Volume In Press. Cambridge, United Kingdom and New York, NY, USA: Cambridge University Press.
- 3159** Johnson, N. C., J. H. Graham, and F. A. Smith (1997). Functioning of mycorrhizal associations along the mutualism-parasitism continuum. *New Phytologist* 135(4), 575–585.
- 3162** Kachurina, O. M., H. Zhang, W. R. Raun, and E. G. Krenzer (2000). Simultaneous determination of soil aluminum, ammonium- and nitrate- nitrogen using 1 M potassium chloride. *Communications in Soil Science and Plant Analysis* 31(7-8), 893–903.
- 3166** Kaiser, C., M. R. Kilburn, P. L. Clode, L. Fuchslueger, M. Koranda, J. B. Cliff,

- 3167** Z. M. Solaiman, and D. V. Murphy (2015). Exploring the transfer of recent
3168 plant photosynthates to soil microbes: mycorrhizal pathway vs direct root
3169 exudation. *New Phytologist* 205(4), 1537–1551.
- 3170** Katabuchi, M. (2015). LeafArea: An R package for rapid digital analysis of leaf
3171 area. *Ecological Research* 30(6), 1073–1077.
- 3172** Kattge, J. and W. Knorr (2007). Temperature acclimation in a biochemical
3173 model of photosynthesis: a reanalysis of data from 36 species. *Plant, Cell*
3174 and *Environment* 30(9), 1176–1190.
- 3175** Kattge, J., W. Knorr, T. Raddatz, and C. Wirth (2009). Quantifying photosyn-
3176 thetic capacity and its relationship to leaf nitrogen content for global-scale
3177 terrestrial biosphere models. *Global Change Biology* 15(4), 976–991.
- 3178** Kayler, Z., A. Gessler, and N. Buchmann (2010). What is the speed of link
3179 between aboveground and belowground processes? *New Phytologist* 187(4),
3180 885–888.
- 3181** Kayler, Z., C. Keitel, K. Jansen, and A. Gessler (2017). Experimental evidence
3182 of two mechanisms coupling leaf-level C assimilation to rhizosphere CO₂
3183 release. *Environmental and Experimental Botany* 135, 21–26.
- 3184** Keeling, C. D., W. G. Mook, and P. P. Tans (1979, jan). Recent trends in the
3185 ¹³C:¹²C ratio of atmospheric carbon dioxide. *Nature* 277(5692), 121–123.
- 3186** Keeney, D. R. and D. W. Nelson (1983). Nitrogen—Inorganic Forms. In A. L.
3187 Page (Ed.), *Methods of Soil Analysis* (2nd ed.), Chapter 33, pp. 643–698.
3188 Madison, WI, USA: ASA and SSSA.
- 3189** Kenward, M. G. and J. H. Roger (1997). Small sample inference for fixed effects

- 3190 from restricted maximum likelihood. *Biometrics* 53(3), 983.
- 3191 Knapp, A. K., M. L. Avolio, C. Beier, C. J. W. Carroll, S. L. Collins, J. S.
- 3192 Dukes, L. H. Fraser, R. J. Griffin-Nolan, D. L. Hoover, A. Jentsch, M. E.
- 3193 Loik, R. P. Phillips, A. K. Post, O. E. Sala, I. J. Slette, L. Yahdjian, and
- 3194 M. D. Smith (2017). Pushing precipitation to the extremes in distributed
- 3195 experiments: recommendations for simulating wet and dry years. *Global*
- 3196 *Change Biology* 23(5), 1774–1782.
- 3197 Knorr, W. (2000). Annual and interannual CO₂ exchanges of the
- 3198 terrestrial biosphere: process-based simulations and uncertainties. *Global*
- 3199 *Ecology and Biogeography* 9(3), 225–252.
- 3200 Knorr, W. and M. Heimann (2001). Uncertainties in global terrestrial biosphere
- 3201 modeling: 1. A comprehensive sensitivity analysis with a new photosynthesis
- 3202 and energy balance scheme. *Global Biogeochemical Cycles* 15(1), 207–225.
- 3203 Kulmatiski, A., P. B. Adler, J. M. Stark, and A. T. Tredennick (2017). Water
- 3204 and nitrogen uptake are better associated with resource availability than
- 3205 root biomass. *Ecosphere* 8(3), e01738.
- 3206 Lavergne, A., D. Sandoval, V. J. Hare, H. Graven, and I. C. Prentice (2020).
- 3207 Impacts of soil water stress on the acclimated stomatal limitation of pho-
- 3208 tosynthesis: Insights from stable carbon isotope data. *Global Change Biol-*
- 3209 *ogy* 26(12), 7158–7172.
- 3210 Lawrence, D. M., R. A. Fisher, C. D. Koven, K. W. Oleson, S. C. Swen-
- 3211 son, G. B. Bonan, N. Collier, B. Ghimire, L. Kampenhout, D. Kennedy,
- 3212 E. Kluzek, P. J. Lawrence, F. Li, H. Li, D. L. Lombardozzi, W. J. Riley,
- 3213 W. J. Sacks, M. Shi, M. Vertenstein, W. R. Wieder, C. Xu, A. A. Ali,

- 3214** A. M. Badger, G. Bisht, M. Broeke, M. A. Brunke, S. P. Burns, J. Buzan,
3215 M. Clark, A. Craig, K. M. Dahlin, B. Drewniak, J. B. Fisher, M. Flanner,
3216 A. M. Fox, P. Gentine, F. M. Hoffman, G. Keppel-Aleks, R. Knox, S. Ku-
3217 mar, J. Lenaerts, L. R. Leung, W. H. Lipscomb, Y. Lu, A. Pandey, J. D.
3218 Pelletier, J. Perket, J. T. Randerson, D. M. Ricciuto, B. M. Sanderson,
3219 A. Slater, Z. M. Subin, J. Tang, R. Q. Thomas, M. Val Martin, and X. Zeng
3220 (2019). The Community Land Model Version 5: description of new features,
3221 benchmarking, and impact of forcing uncertainty. *Journal of Advances in*
3222 *Modeling Earth Systems* 11(12), 4245–4287.
- 3223** LeBauer, D. S. and K. K. Treseder (2008). Nitrogen limitation of net primary
3224 productivity. *Ecology* 89(2), 371–379.
- 3225** Lefcheck, J. S. (2016). piecewiseSEM: Piecewise structural equation modelling
3226 in r for ecology, evolution, and systematics. *Methods in Ecology and Evolu-*
3227 *tion* 7(5), 573–579.
- 3228** Lenth, R. (2019). emmeans: estimated marginal means, aka least-squares
3229 means.
- 3230** Li, W., H. Zhang, G. Huang, R. Liu, H. Wu, C. Zhao, and N. G. McDowell
3231 (2020). Effects of nitrogen enrichment on tree carbon allocation: A global
3232 synthesis. *Global Ecology and Biogeography* 29(3), 573–589.
- 3233** Liang, J., X. Qi, L. Souza, and Y. Luo (2016). Processes regulating progressive
3234 nitrogen limitation under elevated carbon dioxide: a meta-analysis. *Bioge-
osciences* 13(9), 2689–2699.
- 3235** Liang, X., T. Zhang, X. Lu, D. S. Ellsworth, H. BassiriRad, C. You, D. Wang,
3236 P. He, Q. Deng, H. Liu, J. Mo, and Q. Ye (2020). Global response patterns of
- 3237**

- 3238** plant photosynthesis to nitrogen addition: A meta-analysis. *Global Change*
3239 *Biology* 26(6), 3585–3600.
- 3240** López, J., D. A. Way, and W. Sadok (2021). Systemic effects of rising atmo-
3241 spheric vapor pressure deficit on plant physiology and productivity. *Global*
3242 *Change Biology* 27(9), 1704–1720.
- 3243** Lu, J., J. Yang, C. Keitel, L. Yin, P. Wang, W. Cheng, and F. A. Dijkstra
3244 (2022). Belowground carbon efficiency for nitrogen and phosphorus acqui-
3245 sition varies between *Lolium perenne* and *Trifolium repens* and depends on
3246 phosphorus fertilization. *Frontiers in Plant Science* 13, 1–9.
- 3247** Luo, X., T. F. Keenan, J. M. Chen, H. Croft, I. C. Prentice, N. G. Smith,
3248 A. P. Walker, H. Wang, R. Wang, C. Xu, and Y. Zhang (2021). Global
3249 variation in the fraction of leaf nitrogen allocated to photosynthesis. *Nature*
3250 *Communications* 12(1), 4866.
- 3251** Luo, Y., W. S. Currie, J. S. Dukes, A. C. Finzi, U. A. Hartwig, B. A. Hungate,
3252 R. E. McMurtrie, R. Oren, W. J. Parton, D. E. Pataki, R. M. Shaw, D. R.
3253 Zak, and C. B. Field (2004). Progressive nitrogen limitation of ecosystem
3254 responses to rising atmospheric carbon dioxide. *BioScience* 54(8), 731–739.
- 3255** Maire, V., P. Martre, J. Kattge, F. Gastal, G. Esser, S. Fontaine, and J.-F.
3256 Soussana (2012). The coordination of leaf photosynthesis links C and N
3257 fluxes in C₃ plant species. *PLoS ONE* 7(6), e38345.
- 3258** Makino, A. (2003). Rubisco and nitrogen relationships in rice: leaf photosyn-
3259 thesis and plant growth. *Soil Science and Plant Nutrition* 49(3), 319–327.
- 3260** Makino, A., M. Harada, T. Sato, H. Nakano, and T. Mae (1997). Growth and N

- 3261** Allocation in Rice Plants under CO₂ Enrichment. *Plant Physiology* 115(1),
3262 199–203.
- 3263** Markham, J. H. and C. Zekveld (2007). Nitrogen fixation makes biomass al-
3264 location to roots independent of soil nitrogen supply. *Canadian Journal of*
3265 *Botany* (9), 787–793.
- 3266** Marschner, H. and B. Dell (1994). Nutrient uptake in mycorrhizal symbiosis.
3267 *Plant and Soil* 159(1), 89–102.
- 3268** Matamala, R. and W. H. Schlesinger (2000). Effects of elevated atmospheric
3269 CO₂ on fine root production and activity in an intact temperate forest
3270 ecosystem. *Global Change Biology* 6(8), 967–979.
- 3271** Medlyn, B. E., E. Dreyer, D. S. Ellsworth, M. Forstreuter, P. C. Harley,
3272 M. U. F. Kirschbaum, X. Le Roux, P. Montpied, J. Strassmeyer, A. Wal-
3273 croft, K. Wang, and D. Loustau (2002). Temperature response of parameters
3274 of a biochemically based model of photosynthesis. II. A review of experimen-
3275 tal data. *Plant, Cell and Environment* 25(9), 1167–1179.
- 3276** Menge, D. N. L., S. A. Levin, and L. O. Hedin (2008). Evolutionary tradeoffs can
3277 select against nitrogen fixation and thereby maintain nitrogen limitation.
3278 *Proceedings of the National Academy of Sciences* 105(5), 1573–1578.
- 3279** Menne, M. J., I. Durre, R. S. Vose, B. E. Gleason, and T. G. Houston (2012).
3280 An overview of the global historical climatology network-daily database.
3281 *Journal of Atmospheric and Oceanic Technology* 29(7), 897–910.
- 3282** Meyerholt, J., K. Sickel, and S. Zaehle (2020). Ensemble projections elucidate
3283 effects of uncertainty in terrestrial nitrogen limitation on future carbon up-

- 3284 take. *Global Change Biology* 26(7), 3978–3996.
- 3285 Meyerholt, J., S. Zaehle, and M. J. Smith (2016). Variability of projected ter-
3286 restrial biosphere responses to elevated levels of atmospheric CO₂ due to
3287 uncertainty in biological nitrogen fixation. *Biogeosciences* 13(5), 1491–1518.
- 3288 Minocha, R., S. Long, A. H. Magill, J. D. Aber, and W. H. McDowell (2000).
3289 Foliar free polyamine and inorganic ion content in relation to soil and soil
3290 solution chemistry in two fertilized forest stands at the Harvard Forest,
3291 Massachusetts. *Plant and Soil* 222(1-2), 119–137.
- 3292 Moore, D. J., S. Aref, R. M. Ho, J. S. Pippen, J. G. Hamilton, and E. H. De
3293 Lucia (2006). Annual basal area increment and growth duration of Pinus
3294 taeda in response to eight years of free-air carbon dioxide enrichment. *Global
3295 Change Biology* 12(8), 1367–1377.
- 3296 Morgan, J. A., D. E. Pataki, C. Körner, H. Clark, S. J. Del Gross, J. M.
3297 Grünzweig, A. K. Knapp, A. R. Mosier, P. C. D. Newton, P. A. Niklaus,
3298 J. B. Nippert, R. S. Nowak, W. J. Parton, H. W. Polley, and M. R. Shaw
3299 (2004). Water relations in grassland and desert ecosystems exposed to ele-
3300 vated atmospheric CO₂. *Oecologia* 140(1), 11–25.
- 3301 Muñoz, N., X. Qi, M. W. Li, M. Xie, Y. Gao, M. Y. Cheung, F. L. Wong, and
3302 H.-M. Lam (2016). Improvement in nitrogen fixation capacity could be part
3303 of the domestication process in soybean. *Heredity* 117(2), 84–93.
- 3304 Nadelhoffer, K. J. and J. W. Raich (1992). Fine root production estimates and
3305 belowground carbon allocation in forest ecosystems. *Ecology* 73(4), 1139–
3306 1147.

- 3307 Niinemets, Ü. and J. D. Tenhunen (1997). A model separating leaf structural
3308 and physiological effects on carbon gain along light gradients for the shade-
3309 tolerant species *Acer saccharum*. *Plant, Cell and Environment* 20(7), 845–
3310 866.
- 3311 Norby, R. J., J. Ledford, C. D. Reilly, N. E. Miller, and E. G. O'Neill
3312 (2004). Fine-root production dominates response of a deciduous forest to
3313 atmospheric CO₂ enrichment. *Proceedings of the National Academy of Sci-
3314 ences* 101(26), 9689–9693.
- 3315 Norby, R. J., J. M. Warren, C. M. Iversen, B. E. Medlyn, and R. E. Mc-
3316 Murtrie (2010). CO₂ enhancement of forest productivity constrained by
3317 limited nitrogen availability. *Proceedings of the National Academy of Sci-
3318 ences* 107(45), 19368–19373.
- 3319 Novick, K. A., D. L. Ficklin, P. C. Stoy, C. A. Williams, G. Bohrer, A. C.
3320 Oishi, S. A. Papuga, P. D. Blanken, A. Noormets, B. N. Sulman, R. L.
3321 Scott, L. Wang, and R. P. Phillips (2016). The increasing importance of
3322 atmospheric demand for ecosystem water and carbon fluxes. *Nature Climate
3323 Change* 6(11), 1023–1027.
- 3324 Noyce, G. L., M. L. Kirwan, R. L. Rich, and J. P. Megonigal (2019). Asyn-
3325 chronous nitrogen supply and demand produce nonlinear plant allocation re-
3326 sponses to warming and elevated CO₂. *Proceedings of the National Academy
3327 of Sciences* 116(43), 21623–21628.
- 3328 Onoda, Y., K. Hikosaka, and T. Hirose (2004). Allocation of nitrogen to
3329 cell walls decreases photosynthetic nitrogen-use efficiency. *Functional Ecol-
3330 ogy* 18(3), 419–425.

- 3331** Onoda, Y., I. J. Wright, J. R. Evans, K. Hikosaka, K. Kitajima, Ü. Niinemets,
3332 H. Poorter, T. Tosens, and M. Westoby (2017). Physiological and structural
3333 trade-offs underlying the leaf economics spectrum. *New Phytologist* 214(4),
3334 1447–1463.
- 3335** Oren, R., J. S. Sperry, G. G. Katul, D. E. Pataki, B. E. Ewers, N. Phillips,
3336 and K. V. R. Schäfer (1999). Survey and synthesis of intra- and interspecific
3337 variation in stomatal sensitivity to vapor pressure deficit. *Plant, Cell and*
3338 *Environment* 22(12), 1515–1526.
- 3339** Oreskes, N., K. Shrader-Frechette, and K. Belitz (1994). Verification, vali-
3340 dation, and confirmation of numerical models in the Earth sciences. *Sci-
ence* 263(5147), 641–646.
- 3342** Paillassa, J., I. J. Wright, I. C. Prentice, S. Pepin, N. G. Smith, G. Ethier,
3343 A. C. Westerband, L. J. Lamarque, H. Wang, W. K. Cornwell, and V. Maire
3344 (2020). When and where soil is important to modify the carbon and water
3345 economy of leaves. *New Phytologist* 228(1), 121–135.
- 3346** Parvin, S., S. Uddin, S. Tausz Posch, R. Armstrong, and M. Tausz (2020). Car-
3347 bon sink strength of nodules but not other organs modulates photosynthesis
3348 of faba bean (*Vicia faba*) grown under elevated [CO₂] and different water
3349 supply. *New Phytologist* 227(1), 132–145.
- 3350** Paul, K. I., P. J. Polglase, A. M. O'Connell, J. C. Carlyle, P. J. Smethurst, and
3351 P. K. Khanna (2003). Defining the relation between soil water content and
3352 net nitrogen mineralization. *European Journal of Soil Science* 54(1), 39–48.
- 3353** Peng, Y., K. J. Bloomfield, L. A. Cernusak, T. F. Domingues, and I. C. Pre-
3354 nance (2021). Global climate and nutrient controls of photosynthetic capacity.

- 3355** *Communications Biology* 4(1), 462.
- 3356** Perkowski, E. A., E. F. Waring, and N. G. Smith (2021). Root mass carbon
3357 costs to acquire nitrogen are determined by nitrogen and light availability
3358 in two species with different nitrogen acquisition strategies. *Journal of*
3359 *Experimental Botany* 72(15), 5766–5776.
- 3360** Phillips, R. P., E. R. Brzostek, and M. G. Midgley (2013). The mycorrhizal-
3361 associated nutrient economy: a new framework for predicting carbon-
3362 nutrient couplings in temperate forests. *New Phytologist* 199(1), 41–51.
- 3363** Phillips, R. P., A. C. Finzi, and E. S. Bernhardt (2011). Enhanced root ex-
3364 udation induces microbial feedbacks to N cycling in a pine forest under
3365 long-term CO₂ fumigation. *Ecology Letters* 14(2), 187–194.
- 3366** Pinheiro, J. and D. Bates (2022). nlme: linear and nonlinear mixed effects
3367 models.
- 3368** Poggio, L., L. M. De Sousa, N. H. Batjes, G. B. M. Heuvelink, B. Kempen,
3369 E. Ribeiro, and D. Rossiter (2021). SoilGrids 2.0: Producing soil information
3370 for the globe with quantified spatial uncertainty. *Soil* 7(1), 217–240.
- 3371** Pons, T. L. and R. W. Pearcy (1994). Nitrogen reallocation and photosynthetic
3372 acclimation in response to partial shading in soybean plants. *Physiologia*
3373 *Plantarum* 92(4), 636–644.
- 3374** Poorter, H., J. Bühler, D. Van Dusschoten, J. Climent, and J. A. Postma (2012).
3375 Pot size matters: A meta-analysis of the effects of rooting volume on plant
3376 growth. *Functional Plant Biology* 39(11), 839–850.
- 3377** Poorter, H., O. Knopf, I. J. Wright, A. A. Temme, S. W. Hogewoning, A. Graf,

- 3378 L. A. Cernusak, and T. L. Pons (2022). A meta-analysis of responses of C₃
3379 plants to atmospheric CO₂: dose-response curves for 85 traits ranging from
3380 the molecular to the whole-plant level. *New Phytologist* 233(4), 1560–1596.
- 3381 Prentice, I. C., N. Dong, S. M. Gleason, V. Maire, and I. J. Wright (2014).
3382 Balancing the costs of carbon gain and water transport: testing a new theo-
3383 retical framework for plant functional ecology. *Ecology Letters* 17(1), 82–91.
- 3384 Prentice, I. C., X. Liang, B. E. Medlyn, and Y.-P. Wang (2015). Reliable, ro-
3385 bust and realistic: The three R's of next-generation land-surface modelling.
3386 *Atmospheric Chemistry and Physics* 15, 5987–6005.
- 3387 Priestley, C. H. B. and R. J. Taylor (1972). On the Assessment of Surface
3388 Heat Flux and Evaporation Using Large-Scale Parameters. *Monthly Weather
3389 Review* 100(2), 81–92.
- 3390 Querejeta, J. I., I. Prieto, C. Armas, F. Casanoves, J. S. Diémé, M. Diouf,
3391 H. Yossi, B. Kaya, F. I. Pugnaire, and G. M. Rusch (2022). Higher leaf
3392 nitrogen content is linked to tighter stomatal regulation of transpiration
3393 and more efficient water use across dryland trees. *New Phytologist* 235(4),
3394 1351–1364.
- 3395 R Core Team (2021). R: A language and environment for statistical computing.
- 3396 Raich, J. W., D. A. Clark, L. Schwendenmann, and T. E. Wood (2014). Above-
3397 ground tree growth varies with belowground carbon allocation in a tropical
3398 rainforest environment. *PLoS ONE* 9(6), e100275.
- 3399 Rastetter, E. B., P. M. Vitousek, C. B. Field, G. R. Shaver, D. Herbert, and
3400 G. I. Ågren (2001). Resource optimization and symbiotic nitrogen fixation.

- 3401** *Ecosystems* 4(4), 369–388.
- 3402** Reich, P. B. (2014). The world-wide 'fast-slow' plant economics spectrum: a
3403 traits manifesto. *Journal of Ecology* 102(2), 275–301.
- 3404** Reich, P. B., S. E. Hobbie, T. Lee, D. S. Ellsworth, J. B. West, D. Tilman,
3405 J. M. H. Knops, S. Naeem, and J. Trost (2006). Nitrogen limitation con-
3406 strains sustainability of ecosystem response to CO₂. *Nature* 440(7086), 922–
3407 925.
- 3408** Reichman, G. A., D. L. Grunes, and F. G. Viets (1966). Effect of soil moisture
3409 on ammonification and nitrification in two Northern Plains soils. *Soil Science
Society of America Journal* 30(3), 363–366.
- 3411** Rhine, E. D., R. L. Mulvaney, E. J. Pratt, and G. K. Sims (1998). Improving
3412 the Berthelot reaction for determining ammonium in soil extracts and water.
3413 *Soil Science Society of America Journal* 62(2), 473.
- 3414** Rogers, A. (2014). The use and misuse of V_{cmax} in Earth System Models. *Pho-*
3415 *tosynthesis Research* 119(1-2), 15–29.
- 3416** Rogers, A., B. E. Medlyn, J. S. Dukes, G. B. Bonan, S. Caemmerer, M. C.
3417 Dietze, J. Kattge, A. D. B. Leakey, L. M. Mercado, Ü. Niinemets, I. C.
3418 Prentice, S. P. Serbin, S. Sitch, D. A. Way, and S. Zaehle (2017). A roadmap
3419 for improving the representation of photosynthesis in Earth system models.
3420 *New Phytologist* 213(1), 22–42.
- 3421** Saathoff, A. J. and J. Welles (2021). Gas exchange measurements in the un-
3422 steady state. *Plant Cell and Environment* 44(11), 3509–3523.
- 3423** Sage, R. F. and R. W. Pearcy (1987). The nitrogen use efficiency of C₃ and C₄

- 3424** plants: I. Leaf nitrogen, growth, and biomass partitioning in *Chenopodium*
3425 *album* (L.) and *Amaranthus retroflexus* (L.). *Plant Physiology* 84(3), 954–
3426 958.
- 3427** Saleh, A. M., M. Abdel-Mawgoud, A. R. Hassan, T. H. Habeeb, R. S. Yehia,
3428 and H. AbdElgawad (2020). Global metabolic changes induced by arbuscular
3429 mycorrhizal fungi in oregano plants grown under ambient and elevated levels
3430 of atmospheric CO₂. *Plant Physiology and Biochemistry* 151, 255–263.
- 3431** Saxton, K. E. and W. J. Rawls (2006). Soil water characteristic estimates by
3432 texture and organic matter for hydrologic solutions. *Soil Science Society of*
3433 *America Journal* 70(5), 1569–1578.
- 3434** Schaefer, K., C. R. Schwalm, C. Williams, M. A. Arain, A. Barr, J. M. Chen,
3435 K. J. Davis, D. Dimitrov, T. W. Hilton, D. Y. Hollinger, E. Humphreys,
3436 B. Poulter, B. M. Racza, A. D. Richardson, A. Sahoo, P. Thornton, R. Var-
3437 gas, H. Verbeeck, R. Anderson, I. Baker, T. A. Black, P. Bolstad, J. Chen,
3438 P. S. Curtis, A. R. Desai, M. C. Dietze, D. Dragoni, C. M. Gough, R. F.
3439 Grant, L. Gu, A. K. Jain, C. Kucharik, B. E. Law, S. Liu, E. Lokipitiya,
3440 H. A. Margolis, R. Matamala, J. H. McCaughey, R. Monson, J. W. Munger,
3441 W. Oechel, C. Peng, D. T. Price, D. Ricciuto, W. J. Riley, N. Roulet,
3442 H. Tian, C. Tonitto, M. Torn, E. Weng, and X. Zhou (2012). A model-
3443 data comparison of gross primary productivity: Results from the North
3444 American Carbon Program site synthesis. *Journal of Geophysical Research:*
3445 *Biogeosciences* 117(G3), G03010.
- 3446** Schmitt, M. R. and G. E. Edwards (1981). Photosynthetic capacity and nitrogen
3447 use efficiency of maize, wheat, and rice: A comparison between C₃ and C₄

- 3448** photosynthesis. *Journal of Experimental Botany* 32(3), 459–466.
- 3449** Schneider, C. A., W. S. Rasband, and K. W. Eliceiri (2012). NIH Image to
- 3450** ImageJ: 25 years of image analysis. *Nature Methods* 9(7), 671–675.
- 3451** Scott, H. G. and N. G. Smith (2022). A Model of C₄ photosynthetic acclima-
- 3452** tion based on least-cost optimality theory suitable for Earth system model
- 3453** incorporation. *Journal of Advances in Modeling Earth Systems* 14(3), 1–16.
- 3454** Shi, M., J. B. Fisher, E. R. Brzostek, and R. P. Phillips (2016). Carbon cost
- 3455** of plant nitrogen acquisition: Global carbon cycle impact from an improved
- 3456** plant nitrogen cycle in the Community Land Model. *Global Change Biol-*
- 3457** *ogy* 22(3), 1299–1314.
- 3458** Shi, M., J. B. Fisher, R. P. Phillips, and E. R. Brzostek (2019). Neglecting
- 3459** plant–microbe symbioses leads to underestimation of modeled climate im-
- 3460** pacts. *Biogeosciences* 16(2), 457–465.
- 3461** Smith, B., D. Wärldin, A. Arneth, T. Hickler, P. Leadley, J. Siltberg, and
- 3462** S. Zaehle (2014). Implications of incorporating N cycling and N limitations
- 3463** on primary production in an individual-based dynamic vegetation model.
- 3464** *Biogeosciences* 11(7), 2027–2054.
- 3465** Smith, N. G. and J. S. Dukes (2013). Plant respiration and photosynthesis in
- 3466** global-scale models: incorporating acclimation to temperature and CO₂.
- 3467** *Global Change Biology* 19(1), 45–63.
- 3468** Smith, N. G. and J. S. Dukes (2018). Drivers of leaf carbon exchange capacity
- 3469** across biomes at the continental scale. *Ecology* 99(7), 1610–1620.
- 3470** Smith, N. G. and T. F. Keenan (2020). Mechanisms underlying leaf photosyn-

- 3471 thetic acclimation to warming and elevated CO₂ as inferred from least-cost
3472 optimality theory. *Global Change Biology* 26(9), 5202–5216.
- 3473 Smith, N. G., T. F. Keenan, I. C. Prentice, H. Wang, I. J. Wright, Ü. Niinemets,
3474 K. Y. Crous, T. F. Domingues, R. Guerrieri, F. oko Ishida, J. Kattge, E. L.
3475 Kruger, V. Maire, A. Rogers, S. P. Serbin, L. Tarvainen, H. F. Togashi,
3476 P. A. Townsend, M. Wang, L. K. Weerasinghe, and S.-X. Zhou (2019).
3477 Global photosynthetic capacity is optimized to the environment. *Ecology*
3478 *Letters* 22(3), 506–517.
- 3479 Smith, N. G., D. L. Lombardozzi, A. Tawfik, G. B. Bonan, and J. S. Dukes
3480 (2017). Biophysical consequences of photosynthetic temperature acclimation
3481 for climate. *Journal of Advances in Modeling Earth Systems* 9(1), 536–547.
- 3482 Smith, N. G., S. L. Malyshev, E. Shevliakova, J. Kattge, and J. S. Dukes
3483 (2016). Foliar temperature acclimation reduces simulated carbon sensitivity
3484 to climate. *Nature Climate Change* 6(4), 407–411.
- 3485 Smith, S. E. and D. J. Read (2008). *Mycorrhizal Symbiosis*. Academic Press.
- 3486 Soil Survey Staff (2022). Web Soil Survey.
- 3487 Soudzilovskaia, N. A., J. C. Douma, A. A. Akhmetzhanova, P. M. van Bode-
3488 gom, W. K. Cornwell, E. J. Moens, K. K. Treseder, and J. H. C. Cornelissen
3489 (2015). Global patterns of plant root colonization intensity by mycorrhizal
3490 fungi explained by climate and soil chemistry. *Global Ecology and Biogeogra-*
3491 *phy* 24(3), 371–382.
- 3492 Stark, J. M. and M. K. Firestone (1995). Mechanisms for soil moisture ef-
3493 fects on activity of nitrifying bacteria. *Applied and Environmental Microbi-*

- 3494** *ology* 61(1), 218–221.
- 3495** Stocker, B. D., H. Wang, N. G. Smith, S. P. Harrison, T. F. Keenan, D. San-
- 3496** doval, T. Davis, and I. C. Prentice (2020). P-model v1.0: An optimality-
- 3497** based light use efficiency model for simulating ecosystem gross primary pro-
- 3498** duction. *Geoscientific Model Development* 13(3), 1545–1581.
- 3499** Stocker, B. D., J. Zscheischler, T. F. Keenan, I. C. Prentice, J. Peñuelas, and
- 3500** S. I. Seneviratne (2018). Quantifying soil moisture impacts on light use
- 3501** efficiency across biomes. *New Phytologist* 218(4), 1430–1449.
- 3502** Sulman, B. N., D. T. Roman, K. Yi, L. Wang, R. P. Phillips, and K. A.
- 3503** Novick (2016). High atmospheric demand for water can limit forest car-
- 3504** bon uptake and transpiration as severely as dry soil. *Geophysical Research*
- 3505** *Letters* 43(18), 9686–9695.
- 3506** Sulman, B. N., E. Shevliakova, E. R. Brzostek, S. N. Kivlin, S. L. Malyshev,
- 3507** D. N. L. Menge, and X. Zhang (2019). Diverse mycorrhizal associations
- 3508** enhance terrestrial C storage in a global model. *Global Biogeochemical Cy-*
- 3509** *cles* 33(4), 501–523.
- 3510** Sweet, S. K., D. W. Wolfe, A. DeGaetano, and R. Benner (2017). Anatomy
- 3511** of the 2016 drought in the Northeastern United States: Implications for
- 3512** agriculture and water resources in humid climates. *Agricultural and Forest*
- 3513** *Meteorology* 247, 571–581.
- 3514** Taylor, B. N. and D. N. L. Menge (2018). Light regulates tropical symbiotic
- 3515** nitrogen fixation more strongly than soil nitrogen. *Nature Plants* 4(9), 655–
- 3516** 661.

- 3517** Terrer, C., S. Vicca, B. A. Hungate, R. P. Phillips, and I. C. Prentice (2016).
3518 Mycorrhizal association as a primary control of the CO₂ fertilization effect.
3519 *Science* 353(6294), 72–74.
- 3520** Terrer, C., S. Vicca, B. D. Stocker, B. A. Hungate, R. P. Phillips, P. B. Reich,
3521 A. C. Finzi, and I. C. Prentice (2018). Ecosystem responses to elevated CO₂
3522 governed by plant–soil interactions and the cost of nitrogen acquisition. *New*
3523 *Phytologist* 217(2), 507–522.
- 3524** Thieurmel, B. and A. Elmarhraoui (2019). suncalc: Compute sun position,
3525 sunlight phases, moon position, and lunar phase.
- 3526** Thomas, R. Q., E. N. J. Brookshire, and S. Gerber (2015). Nitrogen limita-
3527 tion on land: how can it occur in Earth system models? *Global Change*
3528 *Biology* 21(5), 1777–1793.
- 3529** Thomas, R. Q., S. Zaehle, P. H. Templer, and C. L. Goodale (2013). Global pat-
3530 terns of nitrogen limitation: confronting two global biogeochemical models
3531 with observations. *Global Change Biology* 19(10), 2986–2998.
- 3532** Thornton, P. E., J.-F. Lamarque, N. A. Rosenbloom, and N. M. Mahowald
3533 (2007). Influence of carbon-nitrogen cycle coupling on land model response
3534 to CO₂ fertilization and climate variability. *Global Biogeochemical Cy-*
3535 *cles* 21(4), GB4018.
- 3536** Tingey, D. T., D. L. Phillips, and M. G. Johnson (2000). Elevated CO₂ and
3537 conifer roots: effects on growth, life span and turnover. *New Phytolo-*
3538 *gist* 147(1), 87–103.
- 3539** Udvardi, M. and P. S. Poole (2013). Transport and metabolism in legume-

- 3540 rhizobia symbioses. *Annual Review of Plant Biology* 64, 781–805.
- 3541 USDA NRCS (2022). The PLANTS Database.
- 3542 Uselman, S. M., R. G. Qualls, and R. B. Thomas (2000). Effects of increased
3543 atmospheric CO₂, temperature, and soil N availability on root exudation
3544 of dissolved organic carbon by an N-fixing tree (*Robinia pseudoacacia* L.).
3545 *Plant and Soil* 222, 191–202.
- 3546 van Diepen, L. T. A., E. A. Lilleskov, K. S. Pregitzer, and R. M. Miller (2007).
3547 Decline of arbuscular mycorrhizal fungi in northern hardwood forests ex-
3548 posed to chronic nitrogen additions. *New Phytologist* 176(1), 175–183.
- 3549 Vance, C. P. and G. H. Heichel (1991). Carbon in N₂ fixation: Limitation or
3550 exquisite adaptation. *Annual Review of Plant Physiology and Plant Molec-*
3551 *ular Biology* 42(1), 373–392.
- 3552 Viet, H. D., J.-H. Kwak, K.-S. Lee, S.-S. Lim, M. Matsushima, S. X. Chang,
3553 K.-H. Lee, and W.-J. Choi (2013). Foliar chemistry and tree ring δ¹³C of
3554 *Pinus densiflora* in relation to tree growth along a soil pH gradient. *Plant*
3555 *and Soil* 363(1-2), 101–112.
- 3556 Vitousek, P. M., K. Cassman, C. C. Cleveland, T. Crews, C. B. Field, N. B.
3557 Grimm, R. W. Howarth, R. Marino, L. Martinelli, E. B. Rastetter, and
3558 J. I. Sprent (2002). Towards an ecological understanding of biological nitro-
3559 gen fixation. In *The Nitrogen Cycle at Regional to Global Scales*, pp. 1–45.
3560 Springer Netherlands.
- 3561 Vitousek, P. M. and R. W. Howarth (1991). Nitrogen limitation on land and in
3562 the sea: How can it occur? *Biogeochemistry* 13(2), 87–115.

- 3563** Vitousek, P. M., S. Porder, B. Z. Houlton, and O. A. Chadwick (2010).
3564 Terrestrial phosphorus limitation: mechanisms, implications, and nitrogen–phosphorus interactions. *Ecological Applications* 20(1), 5–15.
3565
- 3566** Walker, A. P., A. P. Beckerman, L. Gu, J. Kattge, L. A. Cernusak, T. F.
3567 Domingues, J. C. Scales, G. Wohlfahrt, S. D. Wullschleger, and F. I. Woodward
3568 (2014). The relationship of leaf photosynthetic traits - V_{cmax} and J_{max}
3569 - to leaf nitrogen, leaf phosphorus, and specific leaf area: a meta-analysis
3570 and modeling study. *Ecology and Evolution* 4(16), 3218–3235.
- 3571** Walker, A. P., A. L. Johnson, A. Rogers, J. Anderson, R. A. Bridges, R. A.
3572 Fisher, D. Lu, D. M. Ricciuto, S. P. Serbin, and M. Ye (2021). Multi-
3573 hypothesis comparison of Farquhar and Collatz photosynthesis models re-
3574 veals the unexpected influence of empirical assumptions at leaf and global
3575 scales. *Global Change Biology* 27(4), 804–822.
- 3576** Wang, H., I. C. Prentice, T. F. Keenan, T. W. Davis, I. J. Wright, W. K.
3577 Cornwell, B. J. Evans, and C. Peng (2017). Towards a universal model for
3578 carbon dioxide uptake by plants. *Nature Plants* 3(9), 734–741.
- 3579** Wang, H., I. C. Prentice, I. J. Wright, D. I. Warton, S. Qiao, X. Xu, J. Zhou,
3580 K. Kikuzawa, and N. C. Stenseth (2023). Leaf economics fundamentals ex-
3581 plained by optimality principles. *Science Advances* 9(3), eadd566.
- 3582** Wang, J., J. M. Knops, C. E. Brassil, and C. Mu (2017). Increased productivity
3583 in wet years drives a decline in ecosystem stability with nitrogen additions
3584 in arid grasslands. *Ecology* 98(7), 1779–1786.
- 3585** Wang, W., Y. Wang, G. Hoch, Z. Wang, and J. Gu (2018). Linkage of root mor-
3586 phology to anatomy with increasing nitrogen availability in six temperate

- 3587 tree species. *Plant and Soil* 425(1-2), 189–200.
- 3588 Weatherburn, M. W. (1967). Phenol-hypochlorite reaction for determination of
- 3589 ammonia. *Analytical Chemistry* 39(8), 971–974.
- 3590 Wellburn, A. R. (1994). The spectral determination of chlorophylls a and b, as
- 3591 well as total carotenoids, using various solvents with spectrophotometers of
- 3592 different resolution. *Journal of Plant Physiology* 144(3), 307–313.
- 3593 Wen, Z., P. J. White, J. Shen, and H. Lambers (2022). Linking root exuda-
- 3594 tion to belowground economic traits for resource acquisition. *New Phytolo-*
- 3595 *gist* 233(4), 1620–1635.
- 3596 Westerband, A. C., I. J. Wright, V. Maire, J. Paillassa, I. C. Prentice, O. K.
- 3597 Atkin, K. J. Bloomfield, L. A. Cernusak, N. Dong, S. M. Gleason, C. Guil-
- 3598 herme Pereira, H. Lambers, M. R. Leishman, Y. Malhi, and R. H. Nolan
- 3599 (2023). Coordination of photosynthetic traits across soil and climate gradi-
- 3600 ents. *Global Change Biology* 29(3), 1–29.
- 3601 Wieder, W. R., C. C. Cleveland, W. K. Smith, and K. Todd-Brown (2015).
- 3602 Future productivity and carbon storage limited by terrestrial nutrient avail-
- 3603 ability. *Nature Geoscience* 8(6), 441–444.
- 3604 Wieder, W. R., D. M. Lawrence, R. A. Fisher, G. B. Bonan, S. J. Cheng, C. L.
- 3605 Goodale, A. S. Grandy, C. D. Koven, D. L. Lombardozzi, K. W. Oleson,
- 3606 and R. Q. Thomas (2019). Beyond static benchmarking: using experimental
- 3607 manipulations to evaluate land model assumptions. *Global Biogeochemical*
- 3608 *Cycles* 33(10), 1289–1309.
- 3609 Wright, I. J., P. B. Reich, and M. Westoby (2003). Least-cost input mixtures

- 3610 of water and nitrogen for photosynthesis. *The American Naturalist* 161(1),
3611 98–111.
- 3612 Wright, I. J., P. B. Reich, M. Westoby, D. D. Ackerly, Z. Baruch, F. Bongers,
3613 J. Cavender-Bares, T. Chapin, J. H. C. Cornelissen, M. Diemer, J. Flexas,
3614 E. Garnier, P. K. Groom, J. Gulias, K. Hikosaka, B. B. Lamont, T. Lee,
3615 W. Lee, C. Lusk, J. J. Midgley, M.-L. Navas, Ü. Niinemets, J. Oleksyn,
3616 N. Osada, H. Poorter, P. Poot, L. Prior, V. I. Pyankov, C. Roumet, S. C.
3617 Thomas, M. G. Tjoelker, E. J. Veneklaas, and R. Villar (2004). The world-
3618 wide leaf economics spectrum. *Nature* 428(6985), 821–827.
- 3619 Xu-Ri and I. C. Prentice (2017). Modelling the demand for new nitrogen fixation
3620 by terrestrial ecosystems. *Biogeosciences* 14(7), 2003–2017.
- 3621 Yahdjian, L., L. A. Gherardi, and O. E. Sala (2011). Nitrogen limitation in
3622 arid-subhumid ecosystems: A meta-analysis of fertilization studies. *Journal
3623 of Arid Environments* 75(8), 675–680.
- 3624 Yuan, W., Y. Zheng, S. Piao, P. Ciais, D. Lombardozzi, Y. Wang, Y. Ryu,
3625 G. Chen, W. Dong, Z. Hu, A. K. Jain, C. Jiang, E. Kato, S. Li, S. Lienert,
3626 S. Liu, J. E. Nabel, Z. Qin, T. Quine, S. Sitch, W. K. Smith, F. Wang,
3627 C. Wu, Z. Xiao, and S. Yang (2019). Increased atmospheric vapor pressure
3628 deficit reduces global vegetation growth. *Science Advances* 5(8), 1–12.
- 3629 Zaehle, S., B. E. Medlyn, M. G. De Kauwe, A. P. Walker, M. C. Dietze, T. Hick-
3630 ler, Y. Luo, Y. P. Wang, B. El-Masri, P. Thornton, A. Jain, S. Wang,
3631 D. Warlind, E. Weng, W. Parton, C. M. Iversen, A. Gallet-Budynek, H. Mc-
3632 carthy, A. C. Finzi, P. J. Hanson, I. C. Prentice, R. Oren, and R. J. Norby
3633 (2014). Evaluation of 11 terrestrial carbon-nitrogen cycle models against

- 3634** observations from two temperate Free-Air CO₂ Enrichment studies. *New*
3635 *Phytologist* 202(3), 803–822.
- 3636** Zaehle, S., S. Sitch, B. Smith, and F. Hatterman (2005). Effects of parame-
3637 ter uncertainties on the modeling of terrestrial biosphere dynamics. *Global*
3638 *Biogeochemical Cycles* 19(3), GB3020.
- 3639** Zhu, Q., W. J. Riley, J. Tang, N. Collier, F. M. Hoffman, X. Yang, and G. Bisht
3640 (2019). Representing nitrogen, phosphorus, and carbon interactions in the
3641 E3SM land model: development and global benchmarking. *Journal of Ad-*
3642 *vances in Modeling Earth Systems* 11(7), 2238–2258.
- 3643** Ziegler, C., M. E. Dusenge, B. Nyirambangutse, E. Zibera, G. Wallin, and
3644 J. Uddling (2020). Contrasting dependencies of photosynthetic capacity on
3645 leaf nitrogen in early- and late-successional tropical montane tree species.
3646 *Frontiers in Plant Science* 11, 1–12.
- 3647** Ziehn, T., J. Kattge, W. Knorr, and M. Scholze (2011). Improving the pre-
3648 dictability of global CO₂ assimilation rates under climate change. *Geophys-*
3649 *ical Research Letters* 38(10), L10404.

3650 Appendix A: Supplemental material for "Structural carbon costs to
3651 acquire nitrogen are determined by nitrogen and light availability in
3652 two species with different nitrogen acquisition strategies"

Table A1. Summary table containing volumes of compounds used to create modified Hoagland's solutions for each soil nitrogen fertilization treatment. All volumes are expressed as milliliters per liter (mL/L)

Compound	0 ppm N	70 ppm N	210 ppm N	630 ppm N
1 M NH ₄ H ₂ PO ₄	0	0.33	1	1
2 M KNO ₃	0	0.67	2	2
2 M Ca(NO ₃) ₂	0	0.67	2	2
1 M NH ₄ NO ₃	0	0.33	1	0
8 M NH ₄ NO ₃	0	0	0	2
1 M KH ₂ PO ₄	1	0.67	0	0
1 M KCl	4	1.33	0	0
1 M CaCO ₃	4	3	0	0
2 M MgSO ₄	1	1	1	1
10% Fe-EDTA	1	1	1	1
Trace Elements	1	1	1	1

Table A2. Analysis of variance results exploring species-specific effects of light availability, nitrogen fertilization, and their interactions on the ratio of whole plant biomass to pot volume (g L⁻¹)*

	df	Coefficient	χ^2	p
<i>G. hirsutum</i>				
Intercept		0.740	-	-
Light (L)	1	-4.23E-03	189.581	<0.001
Nitrogen (N)	1	7.86E-04	17.927	<0.001
L*N	1	-6.61E-06	4.709	0.030
<i>G. max</i>				
Intercept		-0.233	-	-
Light (L)	1	-1.12E-02	69.500	<0.001
Nitrogen (N)	1	8.29E-04	40.297	<0.001
L*N	1	-8.51E-06	5.548	0.019

3653 *Significance determined using Wald's χ^2 tests ($p=0.05$). P-values less than 0.05
3654 are in bold and p-values between 0.05 and 0.1 are italicized. Negative coefficients
3655 for light treatments indicate a positive effect of increasing light availability on
3656 all response variables, as light availability is treated as percent shade cover in all
3657 linear mixed-effects models.

Table A3. Slopes of the regression line describing the relationship between each dependent variable and nitrogen fertilization at each light level*

Shade cover	Slope
<i>G. hirsutum</i>	
0%	8.29E-04^a
30%	5.74E-04^a
50%	4.03E-04^a
80%	1.48E-04 ^a
<i>G. max</i>	
0%	7.86E-04
30%	5.87E-04
50%	4.55E-04
80%	<i>2.57E-05</i>

3658 *Slopes represent estimated marginal mean slopes from linear mixed-effects models described in the Methods. Slopes
3659 were calculated using the ‘emmeans’ R package (Lenth 2019). Superscripts indicate slopes fit to natural-log (^a) or
3660 square root (^b) transformed data. Slopes statistically different from zero (Tukey: $p < 0.05$) are indicated in bold.
3661 Marginally significant slopes (Tukey: $0.05 < p < 0.1$) are italicized.

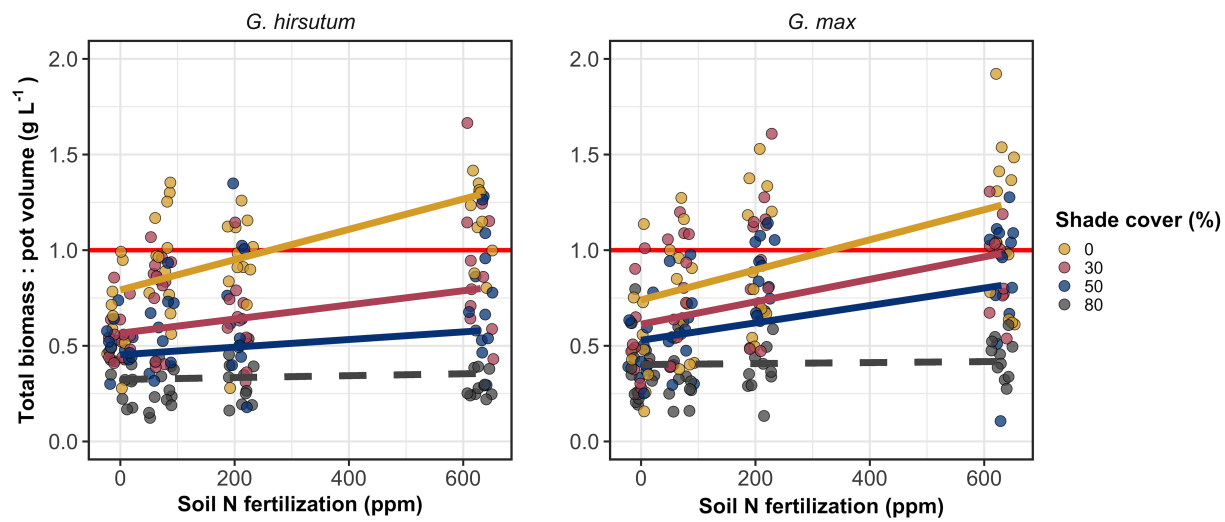


Figure A1. Effects of shade cover and nitrogen fertilization on the ratio of plant biomass to rooting volume in *G. hirsutum* (left panel) and *G. max* (right panel). The red horizontal line indicates the recommended 1 g L^{-1} threshold for BVR recommended by Poorter et al. (2012) to avoid pot size-induced growth limitation. Nitrogen fertilization treatments are represented on the x-axis. Shade cover treatments are represented through colored points and trendlines. Points are jittered for visibility. Yellow points and trendlines represent the 0% shade cover treatment, blue points and trendlines represent the 30% shade cover treatment, green points and trendlines represent the 50% shade cover treatment, and purple points and trendlines represent the 80% shade cover treatment. Solid trendlines indicate slopes that are significantly different from zero (Tukey: $p < 0.05$), while dashed trendlines indicate slopes that are not statistically different from zero.

3662 Appendix B: Supplemental material for "Soil nitrogen availability
3663 modifies leaf nitrogen economies in mature temperate deciduous
3664 forests: a direct test of photosynthetic least-cost theory"

Table B1. Sample sizes of each species, abbreviated by their USDA NRCS PLANTS database code, within each plot at each site*

	ACRU	ACSA	FAGR	FRAM	QURU	N_{plot}
Bald Hill						
+N; +S	0	6	1	0	1	8
+N; -S	1	2	2	0	1	6
-N; +S	2	2	0	0	2	6
-N; -S	2	3	3	0	2	10
Carter Creek						
+N; +S	0	6	1	2	0	9
+N; -S	0	4	0	2	0	6
-N; +S	0	5	1	4	0	10
-N; -S	0	7	0	0	0	7
Mount Pleasant						
+N; +S	3	2	1	0	3	9
+N; -S	0	5	4	1	0	10
-N; +S	1	2	4	0	0	7
-N; -S	3	3	1	2	1	10
N_{spp}	12	47	18	11	10	98

3665 *Plots within each site are represented based on nitrogen and sulfur addition
3666 status. The final column on the right depicts total sample size per plot in each
3667 site (N_{plot}) and the final row on the bottom represents cumulative species sample
3668 size across all plots and all sites (N_{spp}). Key: ACRU=*A. rubrum*; ACSA=*A.*
3669 *saccharum*; FAGR=*F. grandifolia*; FRAM=*F. americana*; QURU=*Q. rubra*

Table B2. Analysis of variance results exploring the linear effect of leaf temperature on net photosynthesis rate (A_{net} ; $\mu\text{mol m}^{-2} \text{s}^{-1}$) and stomatal conductance (g_{sw} ; $\mu\text{mol m}^{-2} \text{s}^{-1}$) measured at $400 \mu\text{mol mol}^{-1} \text{CO}_2$

	df	A_{net}		g_{sw}	
		χ^2	p	χ^2	p
Leaf temperature	1	1.287	0.257	1.716	0.190

3670 *Results detail linear mixed effects model where temperature was regressed against
3671 net photosynthesis or stomatal conductance, with site and species designated as
3672 random intercept terms. Significance was determined using Type II Wald χ^2 tests
3673 ($\alpha=0.05$).

Table B3. Second order log-polynomial regression coefficients that described the effect of leaf temperature on net photosynthesis (A_{net} ; $\mu\text{mol m}^{-2} \text{s}^{-1}$) and stomatal conductance (g_s ; $\mu\text{mol m}^{-2} \text{s}^{-1}$) measured at $400 \mu\text{mol mol}^{-1} \text{CO}_2$ *

	a	b	c
A_{net}	9.422	-0.573	0.010
g_s	-0.170	-0.186	0.003

3674 *Net photosynthesis and stomatal conductance values were fit to the log-polynomial
3675 equation $\log(y) = a + bx + cx^2$, where x is leaf temperature in °C.

Table B4. Mean, standard error, and 95% confidence interval ranges of soil nitrogen availability estimates across all measured plots. All units are expressed as $\mu\text{g N g}^{-1}$ resin d^{-1}

Site	Treatment	Mean	SE	Lower 95% CI	Upper 95% CI
Bald Hill	Ammonium sulfate	27.11	6.14	15.08	39.13
Bald Hill	Control	14.41	5.02	4.56	24.26
Bald Hill	Sodium nitrate	20.65	3.15	14.46	26.83
Bald Hill	Sulfur	6.33	2.19	2.04	10.62
Carter Creek	Ammonium sulfate	26.94	5.36	16.43	37.44
Carter Creek	Control	19.87	1.92	16.10	23.64
Carter Creek	Sodium nitrate	15.51	4.16	7.36	23.65
Carter Creek	Sulfur	5.50	1.40	2.75	8.25
Mount Pleasant	Ammonium sulfate	8.02	2.31	3.49	12.56
Mount Pleasant	Control	2.00	0.57	0.89	3.11
Mount Pleasant	Sodium nitrate	2.52	0.68	1.19	3.85
Mount Pleasant	Sulfur	2.42	0.39	1.66	3.17

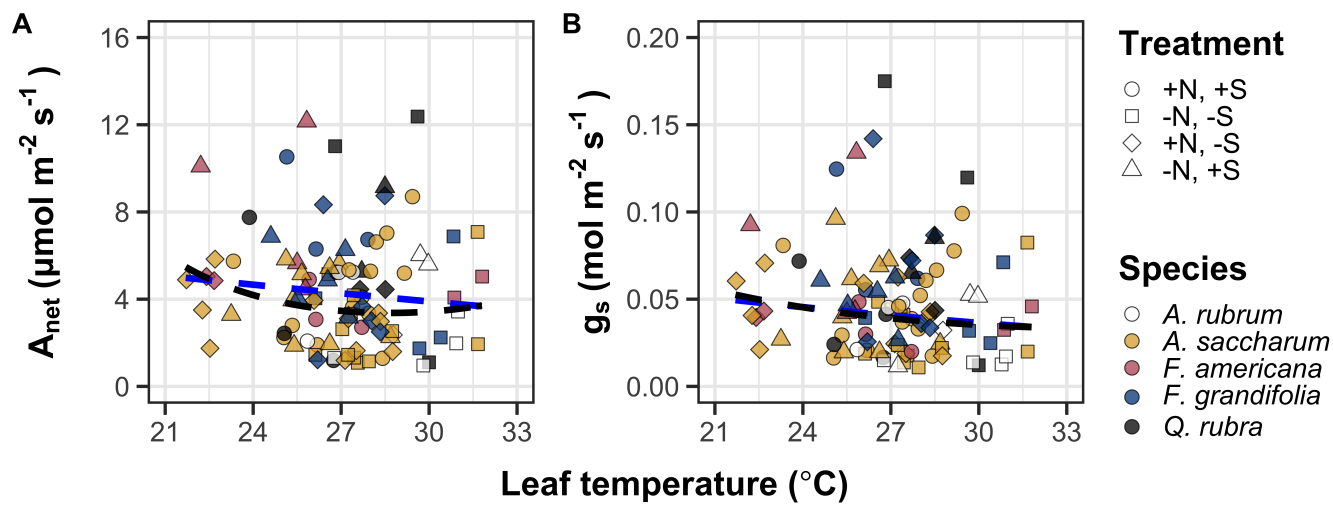


Figure B1. Effects of leaf temperature on net photosynthesis rate (A) and stomatal conductance (B) values when measured at $400 \mu\text{mol mol}^{-1} \text{CO}_2$. Leaf temperature is represented on the x-axis, while species are represented as colored points. Colored points and shapes are as explained in Figure 3.1. The dashed blue trendline describes the linear relationship between leaf temperature and each response variable, while the dashed black trendline describes the same relationship with a log-polynomial regression equation.

**3676 Appendix C: Supplemental material for "The relative cost of resource
3677 use for photosynthesis drives variance in leaf nitrogen content across a
3678 climate and soil resource availability gradient"**

3679 C.1 Calculations for soil water holding capacity

3680 Water holding capacity (θ_{WHC} ; mm) was calculated as a function of the volumetric
3681 soil water storage at field capacity (W_{FC} ; m³ m⁻³), and the volumetric soil water
3682 storage at wilting point (W_{PWP} ; m³ m⁻³):

$$\theta_{WHC} = (W_{FC} - W_{PWP})(1 - f_{gravel}) * \min(z_{bedrock}, z_{max}) \quad (\text{C4.1})$$

3683 where f_{gravel} (%) is the fraction of gravel content in soil, $z_{bedrock}$ (mm) is the
3684 distance to bedrock, and z_{max} (mm) is the maximum allowable distance to bedrock,
3685 set to 2000mm. W_{FC} is calculated as:

$$\theta_{FC} = k_{fc} + (1.283 * (k_{fc})^2 - 0.374 * k_{fc} - 0.015) \quad (\text{C4.2})$$

3686 where

$$\begin{aligned} k_{fc} = & -0.251 * f_{sand} + 0.195 * f_{clay} + 0.011 * f_{OM} \\ & + 0.006 * (f_{sand} * f_{OM}) - 0.027 * (f_{clay} \\ & * f_{OM}) + 0.452 * (f_{sand} * f_{clay}) + 0.299 \end{aligned} \quad (\text{C4.3})$$

3687 W_{PWP} is calculated as:

$$W_{PWP} = k_{pwp} + (0.14 * k_{pwp} - 0.02) \quad (\text{C4.4})$$

3688 where

$$\begin{aligned} k_{pwp} = & -0.024 * f_{sand} + 0.487 * f_{clay} + 0.006 * f_{OM} \\ & + 0.005 * (f_{sand} * f_{OM}) - 0.013 * (f_{clay} \\ & * f_{OM}) + 0.068 * (f_{sand} * f_{clay}) + 0.031 \end{aligned} \quad (\text{C4.5})$$

3689 In Equations C4.4 and C4.5, f_{sand} (%) is the fraction of sand content in soil
3690 (%), f_{clay} (%) is the fraction of clay content in soil (%), and f_{OM} is the fraction of
3691 organic matter in soil (%). Organic matter in the soil was calculated by converting
3692 soil organic carbon data extracted from SoilGrids 2.0 to soil organic matter using
3693 the van Bemmelen factor (1.724 conversion factor).

Table C1. List of sampled species and their plant functional group assignment

Symbol	Species	Photo. pathway	Growth duration	Growth habit	N-fixer?	Plant functional group	Number sampled
ACAN11	<i>Acaciella angustissima</i>	c3	perennial	forb	yes	c3_legume	3
AMAR2	<i>Ambrosia artemisiifolia</i>	c3	annual	forb	no	c3_nonlegume	25
AMPS	<i>Ambrosia psilostachya</i>	c3	perennial	forb	no	c3_nonlegume	32
ARAL3	<i>Argemone albiflora</i>	c3	annual	forb	no	c3_nonlegume	3
ARPU9	<i>Aristida purpurea</i>	c4	perennial	graminoid	no	c4_nonlegume	2
ASAS	<i>Asclepias asperula</i>	c3	perennial	forb	no	c3_nonlegume	3
ASLA4	<i>Asclepias latifolia</i>	c3	perennial	forb	no	c3_nonlegume	3
ASSY	<i>Asclepias syriaca</i>	c3	perennial	forb	no	c3_nonlegume	18
BOIS	<i>Bothriochloa ischaemum</i>	c4	perennial	graminoid	no	c4_nonlegume	6
BOSA	<i>Bothriochloa saccharoides</i>	c4	perennial	graminoid	no	c4_nonlegume	6
CAPL3	<i>Carex planostachys</i>	c4	perennial	graminoid	no	c4_nonlegume	3
CAREX	<i>Carex</i> spp.	c4	perennial	graminoid	no	c4_nonlegume	16
CHFE3	<i>Chamaesyce fendleri</i>	c3	perennial	forb	no	c3_nonlegume	2
CHPI8	<i>Chrysopsis pilosa</i>	c3	annual	forb	no	c3_nonlegume	3
COCO13	<i>Conoclinium coelestinum</i>	c3	perennial	forb	no	c3_nonlegume	3
COER	<i>Commelina erecta</i>	c3	perennial	forb	no	c3_nonlegume	3
CRGLL	<i>Croton glandulosus</i>	c3	annual	forb	no	c3_nonlegume	22
CYDA	<i>Cynodon dactylon</i>	c4	perennial	graminoid	no	c4_nonlegume	15
DIAN	<i>Dichanthium annulatum</i>	c4	perennial	graminoid	no	c4_nonlegume	8
ENPE4	<i>Engelmannia peristenia</i>	c3	perennial	forb	no	c3_nonlegume	6
EUMA8	<i>Euphorbia marginata</i>	c3	annual	forb	no	c3_nonlegume	6
GAPU	<i>Gaillardia pulchella</i>	c3	annual	forb	no	c3_nonlegume	16
GLGO	<i>Glandularia gooddngii</i>	c3	perennial	forb	no	c3_nonlegume	2
HEAN3	<i>Helianthus annuus</i>	c3	annual	forb	no	c3_nonlegume	6

Table C2. List of sampled species and their plant functional group assignment (cont.)

Symbol	Species	Photo. pathway	Growth duration	Growth habit	N-fixer?	Plant functional group	Number sampled
HECA8	<i>Heterotheca canescens</i>	c3	perennial	forb	no	c3_nonlegume	2
HETE3	<i>Heliotropium tenellum</i>	c3	annual	forb	no	c3_nonlegume	3
IVAX	<i>Iva axillaris</i>	c3	perennial	forb	no	c3_nonlegume	4
LIAT	<i>Lilaeopsis attenuata</i>	c3	perennial	forb	no	c3_nonlegume	3
LIPU	<i>Liatris punctata</i>	c3	perennial	forb	no	c3_nonlegume	3
LOPE	<i>Lolium perenne</i>	c3	perennial	graminoid	no	c3_nonlegume	9
MIQU2	<i>Mimosa quadrivalvis</i>	c3	perennial	forb	yes	c3_legume	15
NALE3	<i>Nassella leucotricha</i>	c3	perennial	graminoid	no	c3_nonlegume	19
OECU2	<i>Oenothera curtiflora</i>	c3	annual	forb	no	c3_nonlegume	3
OENOT	<i>Oenothera</i> spp.	c3	annual	forb	no	c3_nonlegume	1
PAVI2	<i>Panicum virgatum</i>	c4	perennial	graminoid	no	c4_nonlegume	12
RACO3	<i>Ratibida columnifera</i>	c3	perennial	forb	no	c3_nonlegume	40
RHSET	<i>Rhynchosia senna</i>	c3	perennial	forb	yes	c3_legume	1
RUHI2	<i>Rudbeckia hirta</i>	c3	perennial	forb	no	c3_nonlegume	3
RUNU	<i>Ruellia nudiflora</i>	c3	perennial	forb	no	c3_nonlegume	15
RUTR	<i>Rubus trivialis</i>	c3	perennial	vine	no	c3_nonlegume	3
SAFA2	<i>Salvia farinacea</i>	c3	perennial	forb	no	c3_nonlegume	7
SCHIZ4	<i>Schizachyrium</i> spp.	c4	perennial	graminoid	no	c4_nonlegume	8
SCSC	<i>Schizachyrium scoparium</i>	c4	perennial	graminoid	no	c4_nonlegume	3
SODI	<i>Solanum dimidiatum</i>	c3	perennial	forb	no	c3_nonlegume	1
SOEL	<i>Solanum elaeagnifolium</i>	c3	perennial	forb	no	c3_nonlegume	53
SOHA	<i>Sorghum halapense</i>	c4	perennial	graminoid	no	c4_nonlegume	38
STTE3	<i>Stillingia texana</i>	c3	perennial	forb	no	c3_nonlegume	3
VEOC	<i>Verbesina occidentalis</i>	c3	perennial	forb	no	c3_nonlegume	3
VEST	<i>Verbena stricta</i>	c3	perennial	forb	no	c3_nonlegume	3

Table C3. Model selection results for soil moisture and vapor pressure deficit. Soil moisture was used in a bivariate regression against log-transformed β , while vapor pressure deficit was used in bivariate regressions against leaf $C_l:C_a$

Day	Soil moisture		VPD	
	AICc	RMSE	AICc	RMSE
1	1431.77	0.8400	-772.71	0.0853
2	1431.76	0.8400	-775.47	0.0849
3	1431.78	0.8400	-770.86	0.0854
4	1431.79	0.8401	-793.49	0.0839
5	1431.79	0.8401	-771.66	0.0853
6	1431.78	0.8401	-771.66	0.0853
7	1431.78	0.8401	-771.05	0.0854
8	1431.76	0.8401	-770.94	0.0854
9	1431.75	0.8401	-770.11	0.0854
10	1431.74	0.8401	-770.08	0.0855
15	1431.54	0.8401	-768.64	0.0856
20	1431.40	0.8401	-769.77	0.0855
30	1431.23	0.8400	-772.18	0.0853
60	1429.84	0.8391	-779.06	0.0848
90	1429.14	0.8385	-773.99	0.0852

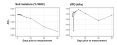


Figure C1. Model selection results exploring relevant timescales for soil moisture (left panel) and vapor pressure deficit (right panel). The x-axis indicates the number of days before each site visit and the y-axis notes the corrected Akaike Information Criterion value. The timescale with the lowest AICc value, and therefore most relevant timescale to include in statistical models, is noted as a red point.

**3694 Appendix D: Supplemental material for "Optimal resource investment
 3695 to photosynthetic capacity maximizes nutrient allocation to whole
 3696 plant growth under elevated CO₂"**

Table D1. Summary table containing volumes of compounds used to create modified Hoagland's solutions for each soil nitrogen fertilization treatment. All volumes are expressed as milliliters per liter (mL/L)

Compound	0 ppm N	35 ppm N	70 ppm N	105 ppm N	140 ppm N
1 M NH ₄ H ₂ PO ₄	0	0.165	0.33	0.5	0.67
2 M KNO ₃	0	0.335	0.67	1	1.33
2 M Ca(NO ₃) ₂	0	0.335	0.67	1	1.33
1 M NH ₄ NO ₃	0	0.165	0.33	0.5	0.67
8 M NH ₄ NO ₃	0	0	0	0	0
1 M KH ₂ PO ₄	1	0.85	0.67	0.5	0.33
1 M KCl	3	2.45	2	1.5	1
1 M CaCO ₃	4	3.33	2.67	2	1.33
2 M MgSO ₄	1	1	1	1	1
10% Fe-EDTA	1	1	1	1	1
Trace elements	1	1	1	1	1

Compound	210 ppm N	280 ppm N	350 ppm N	630 ppm N
1 M NH ₄ H ₂ PO ₄	1	1	1	1
2 M KNO ₃	2	2	2	2
2 M Ca(NO ₃) ₂	2	2	2	2
1 M NH ₄ NO ₃	1	3.5	0	0
8 M NH ₄ NO ₃	0	0	0.75	2
1 M KH ₂ PO ₄	0	0	0	0
1 M KCl	0	0	0	0
1 M CaCO ₃	0	0	0	0
2 M MgSO ₄	1	1	1	1
10% Fe-EDTA	1	1	1	1
Trace elements	1	1	1	1

Table D2. Summary of the daily growth chamber growing condition program

Time	Air temperature (°C)	Light (%)
09:00	21	25
09:45		50
10:30	25	75
11:15		100
22:45	21	75
23:30		50
00:15	17	25
01:00		0

Table D3. Effects of CO₂, fertilization, and inoculation on whole plant biomass: pot volume (BVR; g L⁻¹)*

	df	Coefficient	χ^2	p
(Intercept)	-	1.33E-01	-	-
CO ₂	1	1.53E-01	146.004	<0.001
Inoculation (I)	1	4.19E-01	19.320	<0.001
Fertilization (N)	1	1.90E-03	279.387	<0.001
CO ₂ *I	1	1.03E-01	0.007	0.934
CO ₂ *N	1	2.44E-03	49.725	<0.001
I*N	1	-6.90E-04	9.006	0.003
CO ₂ *I*N	1	-4.95E-04	0.640	0.424

3697 *Significance determined using Type II Wald χ^2 tests ($\alpha=0.05$). P-values less
3698 than 0.05 are in bold. Key: df=degrees of freedom; χ^2 =Wald Type II chi-square
3699 test statistic.

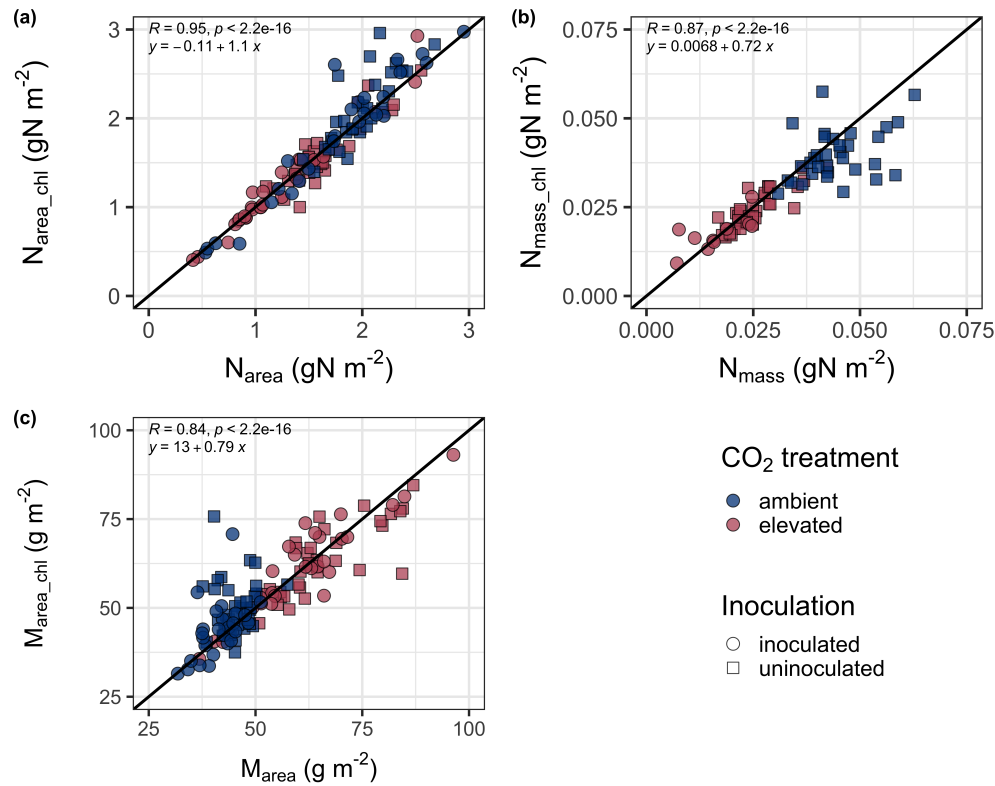


Figure D1. Relationships between area-based leaf nitrogen content (a), mass-based leaf nitrogen content (b), and leaf mass per unit leaf area (c) measured on the focal leaf used to generate A_{net}/C_i curves (x-axis) and leaf nitrogen content measured on the leaf used for chlorophyll extractions (y-axis). Blue points refer to leaves grown under ambient CO₂ and red points refer leaves grown under elevated CO₂. Square points indicate uninoculated pots and circular points indicate inoculated pots. Pearson's correlation coefficient, associated *p*-values, and the line of the regression line that described each bivariate are included in the top left corner of each plot. The solid black line visualizes the trend given a 1:1 bivariate relationship.

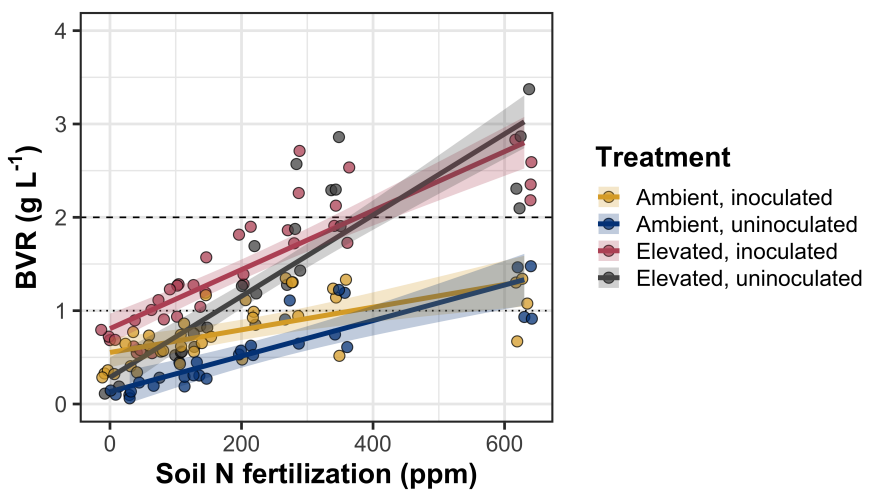


Figure D2. Effects of CO₂, fertilization, and inoculation on the ratio of whole plant biomass to pot volume. Soil nitrogen fertilization is represented on the x-axis in all panels. Yellow points and trendlines indicate inoculated individuals grown under ambient CO₂, blue points and trendlines indicate uninoculated individuals grown under ambient CO₂, red points and trendlines indicate inoculated individuals grown under elevated CO₂, and grey points indicate uninoculated individuals grown under elevated CO₂. Solid trendlines indicate regression slopes that are different from zero ($p<0.05$). The dotted horizontal line indicates the point where biomass:pot volume exceeds 1 g L⁻¹, and the dashed line indicates the point where biomass:pot volume exceeds 2 g L⁻¹.